Bone tissue regeneration using human dental pulp stromal cells isolated from extracted wisdom teeth on 3D printed scaffolds

Rasha Farouk Albannaa

BDS, MSc (Clin) Oral Surgery, LDS RCS

Acknowledgements

To Almighty God, the most kind and merciful. I can't thank you enough.

To my beloved Iraq, I pray to see you a better place one day. I am nothing but a little candle on the road

To my beloved parents, the reason for my existence. This effort is all yours. I will do my best always to make you proud of me.

To the love of my life. The best friend I ever had, my husband, Fahad. What an adventure we had together those five years! They were full of happy moments, hard work and sometimes lots of pain. But do you know what? We made it! I am so proud of what we could achieve together. You were always strong when I gave up. Your unlimited love, support and compassion are what keeps me going.

To my supervisor, Dr Xuebin Yang. I know I was a headache sometimes, but you were always patient and supportive. Many thanks for all your efforts.

To my supervisor Prof Jennifer Kirkham. You are such a wonderful person; not only because of your superb knowledge and magnificent scientific guide but also because you always care and support. I was honoured to be your student.

To my supervisor Dr Julie Burke. I am truly grateful for you. Despite being away, you were always there when I needed you. Thanks a lot.

To my beloved brothers Omar and Mohammed. I am blessed to have you.

To my dear friends, Zainab Noori, Aseel Al-Jabouri, Hanaa AlKharobi, Basmah Sameer and Aishah Alhodhodi. I shared all the moments with you, the good ones and the hard ones. Thanks for all your love and support.

To my little angels, Rasha and Yusuf. Thank you for being so patient with mummy and daddy those years. In the hard times, your laughs wiped all my burdens away.

To the colleagues who gave me great support; Dr Liam Lawlor, Dr Robert W. Davis, Dr Ali Marie and Dr Hasanain Al-Khafaji. I am so grateful for you.

Many thanks to my sponsor, the Higher Committee of Education Development in Iraq (HCED).

Thanks to people in Division of Oral Biology who helped me through the PhD journey; Mrs Jackie Hudson, Mr Gregory Baugh, Dr Sarah Myers and Dr Mathew Tomlinson.

To anyone who provided any help, thank you.

To the little mice that gave their lives for this work, thank you.

Abstract

The need to regenerate bone remains a significant healthcare challenge both now and in the future to meet the needs of an ageing population. The research carried out in this thesis aimed to investigate the potential of using a combination of human dental pulp stromal cells (hDPSCs), and different architectures of 3D printed polylactic acid (PLA) scaffolds with/without self-assembling peptide P_{11}-4 (SAP) for bone tissue engineering (BTE) *in vitro* and *in vivo.*

To evaluate hDPSCs multi-potential, considering donor variability, the cells were isolated from the dental pulp of upper/lower third molars from 3 different donors and characterised via trilineage differentiation (osteogenic, chondrogenic and adipogenic) approach. To investigate the effect of the architecture of 3D printed PLA scaffolds on cell attachment and bone matrix formation *in vitro* and *in vivo,* hDPSCs were statically seeded on 3D printed PLA scaffolds with fibres angled at either 45° or 90° and cultured in osteo-inductive medium for up to 5 weeks *in vitro.* At different time points, the constructs were examined using SEM, EDS, live/dead markers, histology and immunohistochemistry (IHC). For *in vivo* evaluation, the constructs were sealed within diffusion chambers (DCs), which were then implanted intraperitoneally in nude mice for a further eight weeks prior to retrieval and examination with SEM, histology and IHC. Based on the results from these experiments, 3D printed PLA scaffolds (45°) were infiltrated with SAP P_{11}-4 to evaluate the potential of this novel combination for enhancing BTE *in vitro* and *in vivo*. HDPSCs were pre-mixed with SAP and seeded on PLA 45° scaffolds or scaffolds were directly seeded with hDPSCs alone. Constructs were then cultured in osteo-inductive medium for up to 5 weeks *in vitro* and examined using SEM, live/ dead markers, histology and IHC at different time points. For *in vivo* evaluation, 3D printed PLA 45° scaffolds were seeded with hDPSCs with/without SAP

P$_{11}$-4 and sealed within DCs, which were implanted in nude mice for up to 8 weeks prior to retrieval and examination with SEM, histology and IHC. HDPSCs isolated from all donors showed marked morphological changes and positively expressed different markers for osteogenic, chondrogenic and adipogenic differentiation after monolayer culture in different induction media *in vitro*. PLA 45° scaffolds showed greater hDPSCs attachment, macro-pores bridging/ closure and expression of IHC osteogenic markers *in vitro* with higher accumulation of mineral deposits *in vivo* compared to the PLA 90° scaffold group. PLA 45° /SAP P$_{11}$-4 constructs showed greater hDPSC attachment, neo-tissue formation and enhanced expression of IHC osteogenic markers both *in vitro* and *in vivo* compared to the PLA 45° scaffold alone group.

The outcomes of this study verified the multilineage plasticity of hDPSCs. The data also demonstrated the significant effect of 3D printed PLA scaffold fibre geometry on hDPSCs osteogenic behaviour, suggesting that PLA 45° 3D printed scaffold layout is the design of choice for bone tissue engineering. In addition, incorporating SAP P$_{11}$-4 into 3D printed PLA scaffolds further enhanced hDPSCs attachment and osteogenesis both *in vitro* and *in vivo*, illustrating the complementary benefits from both technologies into one scaffold entity and the promising use of this novel combination for bone tissue regeneration in the future.

Table of Contents

xi

List of Tables

List of Figures

List of abbreviations

Abbreviation	Term
2D	Two dimensional
3D	Three dimensional
AB	Alcian blue
ALP	Alkaline phosphatase
Al-R	Alizarin red
AM	Additive manufacturing
BMPs	Bone morphogenic proteins
BMSCs	Bone marrow stem cells
BSE	Back-scattered emission
BTE	Bone tissue engineering
CFU-F	Colony forming unit
CJD	Creutzfeldt-Jakob disease
CMFDA	Chloro methyl fluorescein di acetate
Col-I	Collagen type I
DAB	Di-Amino-Benzidine
DC	Diffusion chambers
Dex	Dexamethasone
dH$_2$O	Distilled water
DMSO	Di-methyl-sulfoxide
DPX	Di-butyl-phthalate Polystyrene Xylene
DREC	Dental Research Ethics Committee

ECM	Extracellular matrix
EDS	Energy-dispersive X-ray spectroscopy
EDTA	Ethylene diamine tetraacetic acid
EHD-1	Ethidium homodimer-1
FCS	Foetal calf serum
FDA	Food and Drug Administration
FDM	Fused deposition modelling
FGF	Fibroblast growth factors
GBR	Guided Bone Regeneration
GelMA	Methacrylated gelatine
GF	Growth factors
GMP	Good Manufacturing Practice
GRAS	Generally recognised as safe
H -E	Haematoxylin-Eosin
HA	Hydroxyapatite
HCM	Haemocytometer chamber
hDPSCs	Human dental pulp stromal cells
HPLC	High-Performance Liquid Chromatography
HPMA	N-(2-hydroxypropyl) methacrylamide
IGFs	Insulin-like growth factors
IHC	Immunohistochemistry
ISCT	International Society of Cellular Therapy
IVC	Individually Ventilated Cage
LAsc	L- ascorbic acid

MCE	Mixed cellulose ester
MSCs	Mesenchymal stem cells
NBF	Neutral buffer formalin
NBF	Neutral buffered formalin
NP-40	Nonyl phenoxy-polyethoxylethanol
OCN	Osteopontin
OPN	Osteopontin
P	Passage
PBS	Phosphate buffer saline
PCL	Poly-caprolactone
PDGF	Platelet-derived growth factor
PES	Polyethersulfone
PGA	Polyglycolic acid
PLA	Poly Lactic Acid
PLGA	Polylactic – glycolic acid
pNPP	p-nitrophenyle phosphate substrate
qPCR	Polymerase chain reaction
rcf	Relative centrifuge force
RGD	Arginine–glycine–aspartic acid
RP	Rapid prototyping
SAPs	Self-assembling peptides
SD	Standard deviation
SEM	Scanning electron microscopy
SEM	Scanning electron microscopy

SFF	Solid free form fabrication
SHEDs	Human exfoliated teeth primary teeth
SLS	Selective laser sintering
SR	Sirius red
TC	Tissue culture
TE	Tissue Engineering
TE*	Tris EDTA buffer
TGF-β	Transforming growth factor β
UV	Ultraviolet
VEGF	Vascular endothelial growth factors
VG	Van Geissen
VK	Von Kossa
α-MEM	Minimal essential medium

CHAPTER ONE

General introduction and literature review

Chapter 1.   General introduction and literature review

1.1.   General introduction

Trauma and disease have always been part of human life. Although bone is usually less frequently injured than soft tissue; it also has the potential to be damaged due to trauma or pathologies such as tumours or infections. Alternatively, bone removal can also be a consequence of surgical procedures, including biopsies and autograft harvesting (Brydone *et al.*, 2010, Lanza *et al.*, 2011). Despite the fact that bone is a dynamic tissue that has considerable potential for healing, management of larger bone defects is still a challenging issue in clinical practice (Calori *et al.*, 2011, Djouad *et al.*, 2012).

There are many conventional methods for management of bone defects, including the use of different grafts, synthetic biomaterials or guided bone tissue regeneration techniques (Rodella *et al.*, 2011, Dimitriou *et al.*, 2012). However, each of these has its own pitfalls in clinical practice. Over the last two decades, tissue-engineered bone has attracted much attention as an alternative method for bone replacement with possible promising outcomes (Giannoudis *et al*, 2005, Nishi *et al*, 2012). Human dental pulp stromal cells (hDPSCs) used as a stem cell source were found to have the potential for mineralised tissue formation both *in vitro* and *in vivo* when cultured with appropriate environmental osteogenic cues (Laino *et al*, 2006, Zhang *et al*, 2006). They are also easily accessible and have a higher growth rate compared to other stem cell sources. For that reason, hDPSCs could potentially be a good candidate as cell source for bone regeneration research.

Polymers, whether natural or synthetic, have been extensively used for fabrication of scaffolds for bone tissue engineering (BTE). Polylactic acid (PLA) is a synthetic polymer that had been widely used as a bone scaffold as it is biocompatible and

biodegradable with good mechanical properties to support cellular growth (Serra *et al*, 2013a, Sharma *et al*, 2014). Furthermore, having the option of 3D printing, polymer scaffolds could be further modified or tailored across a wide range of mechanical and physical properties to meet the physiological needs of the engineered tissue (Wahl *et al*, 2007, Liu *et al*, 2008, Serra *et al*, 2013a, Liu *et al*, 2014). Different modalities were suggested in the literature to improve further PLA scaffold inert surface (Zhu *et al*., 2004, Rasal *et al*., 2010, Serra *et al*., 2013a). One such modification included incorporation of a nano phase material such as self-assembling peptides (SAPs) into the scaffold structure to provide closer simulation of the natural bone nano-physiological environment to which cells would favourably attach, grow, osteo-differentiate and mineralise their extra cellular matrix (Firth *et al*, 2006, Nisbet & Williams, 2012).

1.2.   Bone biology

1.2.1.   Macroscopic bone structure

Bone is a specialised connective tissue that has well-documented mechanical functions, including establishing body rigidity and shape, protection of vital body structures like the brain, heart and lungs and providing support for body motion. It also acts as a reservoir for body minerals (Sikavitsas *et al*., 2001, Junqueira *et al*., 2003, Datta *et al*., 2008, Nanci, 2017). Macroscopically, bones are classified into 3 groups based on general shape; short (like vertebral bodies), flat (like skull and sternum) and long bones (like tibia and femur) (Buckwalter *et al*., 1995, Nanci, 2017).

Generally, bones in the adult skeleton consist of a compact outer layer called cortical bone (80% of bone volume) surrounded by a dense connective tissue periosteum, and an inner cancellous (spongy or trabecular) bone representing the remaining 20% of bone volume (Buckwalter *et al*., 1995). The latter is composed of a medullary central

cavity that is usually filled by bone marrow substance rich with a vascular and nerve supply and intersected by a network of bone trabeculae (Buckwalter *et al.*, 1995, Sikavitsas *et al.*, 2001, Berkovitz, 2017, Nanci, 2017). The proportion of cortical\cancellous bone is variable among different bones of the body and relates to the physiological needs that each particular bone requires. Cortical bone provides higher mechanical strength, while cancellous bone provides higher elasticity (Buckwalter *et al.*, 1995)

1.2.2. Microscopic bone structure

Histologically, bone's basic metabolic unit is called the **osteon**, which is composed of cylindrical, concentrically arranged lamellar structures that run parallel to the long axis of the bone. A central **Haversian canal** can be seen in each osteon housing capillaries and nerve fibres within. Adjoining Haversian canals are linked together with lateral channels termed as **Volkmann canals**. This unique array of interconnected canals gives the bone its rich internal network responsible for its profuse blood and nerve supply (Buckwalter *et al.*, 1995, McCauley and Somerman, 2012, Berkovitz, 2017, Nanci, 2017). Figure (1-1) illustrates bone macro and microstructure.
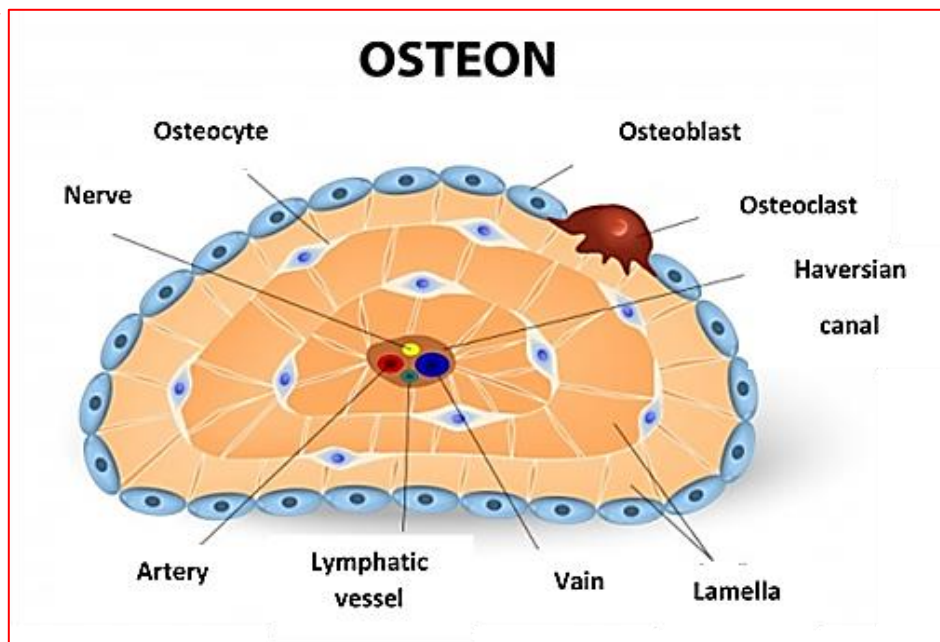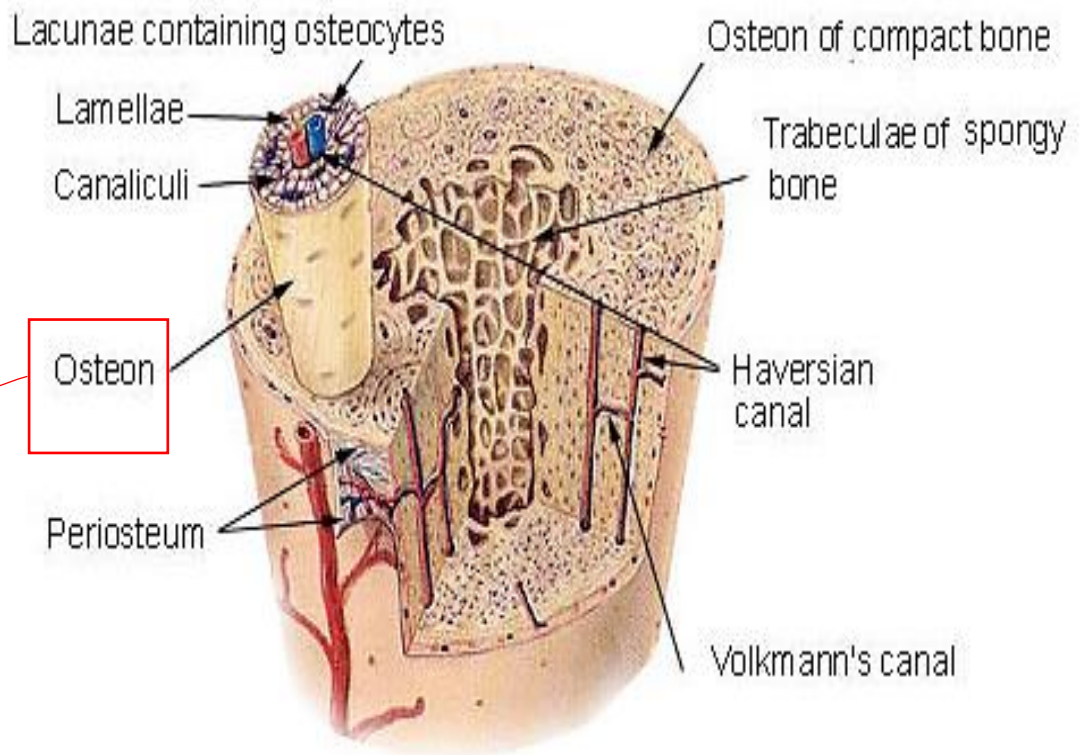
Figure 1-1: Illustration of bone macro and micro anatomical structures. Images from Wikipedia the free encyclopaedia, free to copy and reuse under the GNU Free Documentation License.

1.2.3. Bone cells

The highly organised composition of bone tissue echoes the cellular activity involved in its formation. Two main families of cells are involved in synthesis, repair and resorption of bone tissue. **Osteogenic** cells belong to the mesenchymal stem cell lineage and are the ones responsible for bone formation and maintenance, including osteoprogenitor cells, pre-osteoblasts and osteoblasts. Osteocytes and bone lining cells are derived from osteoblast, as will be discussed later in this section. In contrast, **osteoclasts** are part of the haemopoietic system and are involved in bone resorption (Berkovitz, 2017, Nanci, 2017).

Bone is a highly dynamic tissue that is subject to a continuous deposition- resorption process termed as "remodelling" (Berkovitz, 2017). This mechanism gives bone the potential to repair itself and to adapt to the forces exerted on it (Datta *et al.*, 2008). Bone remodelling is gained by a concurrent, mutual interaction between bone-forming osteoblasts and bone-resorbing osteoclasts that usually occurs at the bone surface. For that reason, osteoblasts and osteoclasts are anatomically present on the superficial layer of the forming bone (Figure 1-1, osteon).

Osteoblasts are specialized, mononuclear, spindle-shaped fibroblast-like cells that exist as a row on the exterior of the newly formed bone, creating a barrier that regulates ion reflux into and out of bone (Nanci, 2017). When active, osteoblasts become more cuboidal and are seen to have a dark, basophilic cytoplasm due to the copious amount of endoplasmic reticulum found within the cell (image illustrated in Table 1-1) (Berkovitz, 2017). Osteoblasts are mainly responsible for the secretion of collagenous and non-collagenous organic bone matrix proteins, as well as other signalling growth factors and cytokines that help in the regulation of cellular function and increasing the rate of bone formation and repair. These include bone morphogenic

proteins (BMPs), transforming growth factor β (TGF-β), platelet-derived growth factor and insulin-like growth factors (IGFs) (Anusaksathien and Giannobile, 2002, Berkovitz, 2017). Osteoblasts also help in the regulation of bone metabolism by possessing receptors for hormones like parathyroid hormone and vitamin D (Junqueira *et al.*, 2003, Datta *et al.*, 2008, Berkovitz, 2017, Nanci, 2017).

During bone formation, some osteoblasts become trapped within the matrix they produce; they are then called **osteocytes** which are considered to be mature bone cells. Osteocytes are enclosed in special spaces within the matrix called **osteocytic lacunae**. Radiating narrow extensions from these lacunae can be seen containing the osteocytes processes; these are the **canaliculi** (Fig. 1-1, osteon)**.** These act as connecting channels with the adjacent osteocytes and with the osteoblasts on the surface (Berkovitz, 2017, Nanci, 2017). This puts the osteocytes in the ideal situation to detect mechanical and biochemical stimulation within the local environment and transmit a response to the bone surface where the cells responsible for bone remodelling can respond accordingly (Marks *et al.*, 1988, Buckwalter *et al.*, 1995, Junqueira *et al.*, 2003, Nanci, 2017). When there is no more bone to be formed, osteoblasts significantly flatter in shape and become less involved in extracellular matrix (ECM) production. At this stage, these cells are termed **bone lining cells** and represent most of the adult skeleton coverage (Nanci, 2017).

Osteoclasts are giant, multinucleated cells seen on bone surfaces occupying hollowed depressions that they have created. Those cells are mainly responsible for bone resorption (Datta *et al.*, 2008). They have unique morphological characteristics, where the cell membrane close to the bone surface has a ruffled border, and the opposing side facing body tissues has a round, smooth surface (image illustrated in Table 1-1). During bone resorption, the ruffled border helps the osteoclasts to adhere to the

mineralised bone matrix and create a sealed micro-environment, where they pump out protons from this surface to dissolve bone mineral via low pH; in addition, acid phosphatase and lysosomal enzymes are released to degrade bone tissue (Arnett, 2003). Meanwhile, the ruffled surface helps in endocytosis of the bone degradation bi-products, which are then transported in special vesicles to be released extracellularly along the osteoclast smooth- surface side membrane, leaving a concave cavity on bone surface (Marks *et al.*, 1988, Nanci, 2017). Table 1-1 summarises the key points about the main bone cell types.

Table 1‑1: Summary for main bone cell types, illustrating their morphology, location and key function. (Images referenced to https://slideplayer.com/slide/10599283/36/images/13/ copyright to © 2013 Pearson Education, Inc)[1].

Cell type	Cell illustration	Location	Key function
Mesenchymal Stem cell		Periosteum, endosteum and bone marrow spaces	Develop into osteoblasts
Osteoblast (active state)		Periosteum and growing portions of bone	Synthesize bone matrix, bone formation and growth
Osteocyte		Entrapped in matrix	Maintain mineral concentration of matrix, mechanosensory cells of bone
Osteoclast		Periosteum, at sites of old, injured, or unneeded bone	Bone resorption
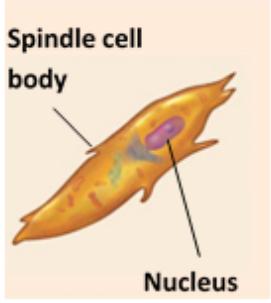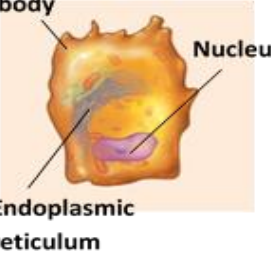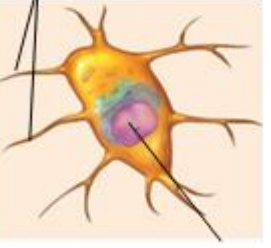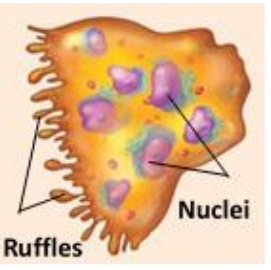
1.2.4. Bone extracellular matrix

Like other connective tissues, bone cells are not the major component of bone's weight, rather it is composed of the ECM produced by the osteoblasts that will then be mineralised to form calcified bone tissue.

By weight, bone is composed of approximately 33% organic matrix. This, in turn, consists of approximately 90% collagenous and 10% non-collagenous proteins (Marks *et al.*, 1988, Buckwalter *et al.*, 1995, Kim *et al.*, 2013, Nanci, 2017). This organic ECM is infused by the inorganic minerals which represent the remaining 67% of the bone weight and is mainly made up of calcium-phosphate in the form of hydroxyapatite ($Ca_{10}[PO_4]_6[OH]_2$) (Buckwalter *et al.*, 1995, Salmon *et al.*, 2013, Alford *et al.*, 2015, Nanci, 2017). The mineralised inorganic portion of bone tissue is responsible for bone rigidity and hardness, while the organic matrix of the ECM delivers the flexibility to the tissue (Alford *et al.*, 2015).

1.2.4.1. Collagenous bone matrix proteins

Collagens are the most dominant proteins in the human body. More than twenty different collagen types have been described, forming the ECM of different body tissues (Prockop and Kivirikko, 1995). In bone tissue, the two major types of collagens present are type I and type III, with collagen type I being the most abundant (85%), acting as the main organic scaffold for bone formation. Collagen type III, however, can be seen majorly within the walls of blood vessels and nerves and only to a limited extent is detected throughout the matrix (Scott, 1995, Gundberg, 2003).

Collagen type I is a member of the fibrillar collagen family. Immediately after secretion, the triple helical tropocollagen molecules spontaneously self-assemble under physiological conditions into fibrils that have a diameter of a few hundred

nanometres; with a series of successively arranged gap and overlap zones between the constituent monomer units, giving them their characteristic barcode (cross banded) appearance (Fratzl, 2003) (Figure 1-2 A). These gap zones of the collagen fibrils were believed to be associated with the formation of the initial crystals in the bone matrix, providing a scaffold for bio-mineralisation (Jackson, 1957). Collagen fibrils then assemble with each other to form larger collagen fibres (Weiner and Wagner, 1998) (Figure 1-2 B).
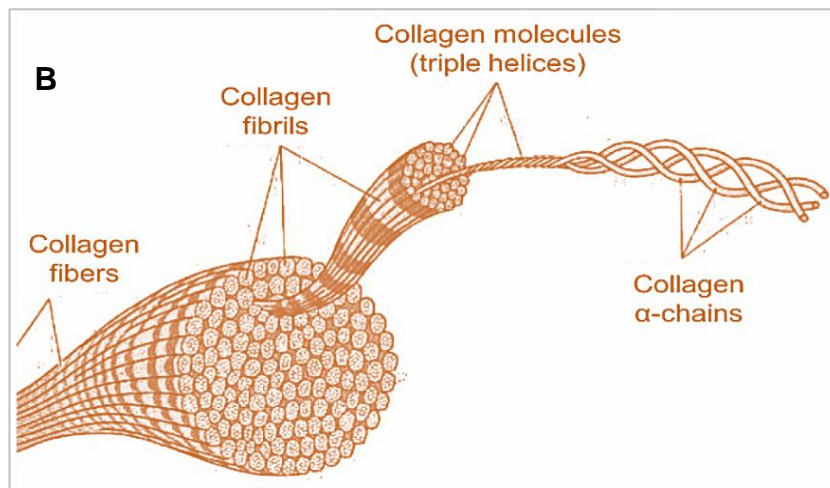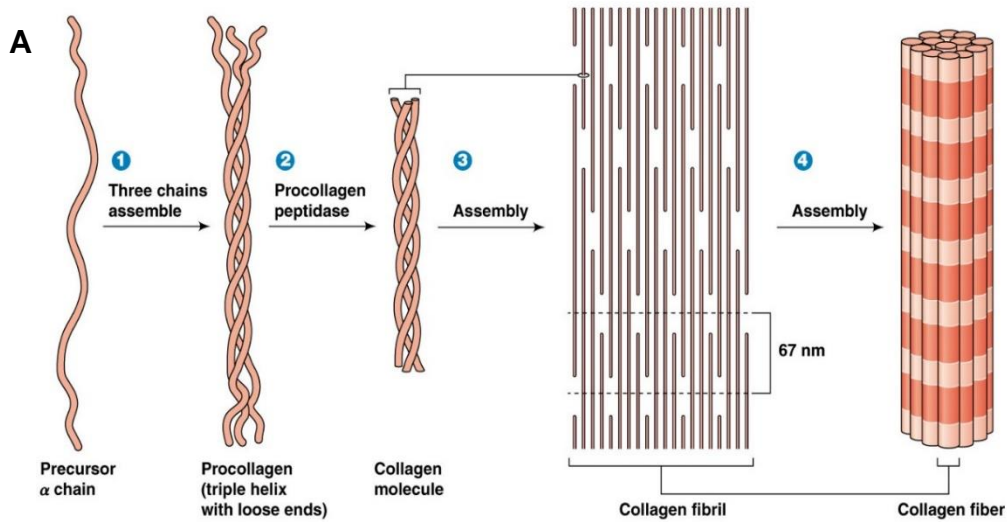
Figure 1-2: Collagen type I fibre structure. A: Collagen fibril structure, showing the successively arranged gap and overlap zones (Travascio, 2016) [2]. B: Hierarchical assembly of collagen fibre (Daniels *et al.*, 2007)

1.2.4.2. Non-collagenous bone matrix proteins

Apart from collagen type I, active osteoblasts produce other types of ECM proteins referred to as "non-collagenous proteins" (Cowles *et al.*, 1998). These proteins are believed to be found surrounding collagen type I and associated with different functions, including cell adhesion, growth, proliferation, migration and regulation of mineralisation, in addition to growth factor storage and regulation (Boskey, 1989, Gundberg, 2003). Table (1-2) below illustrates the main non-collagenous matrix proteins with their functions.

Table 1‑2: Main non-collagenous bone matrix proteins and their function

Non- collagenous matrix protein type	Function	References
Alkaline phosphatase (ALP)	• A co-enzyme that is found within vesicles in the extracellular membrane of osteoblasts. • Coded by the *ALPL* gene which is considered to be an early osteoblast marker. • Aids in the hydrolysis of organic phosphate to increase its local concentration, thus facilitating calcium phosphate precipitation. • Has a role in the transport of calcium and phosphate. • Thought to promote matrix crystal formation by removing nucleation inhibitors.	Register *et al.* (1986), Marks *et al.* (1988), Bellows *et al.* (1991), Sikavitsas *et al.* (2001)
Proteoglycans I and II	• Also known as biglycan and decorin, respectively. • Their gene expression has been associated with osteoblast proliferation and matrix mineralisation. • Thought to have an effect on collagen fibrillar growth.	Sikavitsas *et al.* (2001), Waddington *et al.* (2003)
Osteonectin	• A glycoprotein that binds to calcium, hydroxyapatite, and collagen, suggesting that it is a nucleator for matrix mineralisation	Cowles *et al.* (1998), Sikavitsas *et al.* (2001)
Fibronectin	• An extracellular protein mainly involved in cellular attachment	Sikavitsas *et al.* (2001)

Osteopontin (OPN)	• An acidic sialoprotein that it is implicated in general cell attachment to the bone matrix • Mediates osteoblast response to mechanical stimuli • Plays a role in promoting osteoclast migration thus contributes to bone remodelling • Controls mineralisation by inhibiting crystallisation	Cowles *et al.* (1998), Denhardt *et al.* (2001), Sikavitsas *et al.* (2001)
Bone sialoprotein	• Believed to initiate mineralisation; found to be a potent and specific nucleator of hydroxyapatite.	Hunter and Goldberg (1993)
Osteocalcin (OCN)	• Vitamin K- dependant, calcium-binding extracellular matrix proteins • The second most abundant extracellular protein in bone, frequently used as a biochemical marker for bone formation. • Suggested to have an important role in the regulation of mineralisation and bone remodelling.	Hauschka *et al.* (1989), Ducy *et al.* (1997), Sikavitsas *et al.* (2001), Gundberg (2003).

1.3. Mechanisms of bone formation and mineralisation

Bone development generally takes place through one of two main pathways; either endochondral (cartilaginous) or intramembranous ossification. Endochondral ossification is the process of bone formation from an initial cartilage precursor phase that eventually ossifies into mineralised bone (Dai and Rabie, 2007). This is typically involved during growth and fractures healing of long and short bones (Sikavitsas *et al.*, 2001).

Conversely, intramembranous ossification does not involve a cartilaginous stage as the formed connective tissue ossifies directly (Einhorn, 1998). Osteoblasts secrete an osteoid matrix, consisting mainly of type I collagen fibrils, into small appendages which then expand and merge to form bone trabeculae (Reddi, 1981). Flat bones generally develop and heal via intramembranous ossification (Buckwalter *et al.*, 1995).

Some references suggested a third type of bone development, termed as appositional bone formation, in which osteoblasts attach to existing bone and start to lay down bone matrix in layers on its surface. This usually occurs in cases of bone enlargement and during remodelling (Sikavitsas *et al.*, 2001).

Mineralisation of bone collagen fibrils is a highly organised process. The first mineral appears in the gap zone regions within collagen fibrils (as was discussed previously in *1.2.4.1*) (Fratzl, 2003). Non mineralised overlap regions of the fibrils initially separate the mineralised gap zones. Increasing numbers of mineralised gap zones within collagen fibrils leads to progressive mineralisation of the matrix until the mineral deposits eventually occupy all of the available gaps within the fibrils (Buckwalter *et al.*, 1995). Once triggered, mineralisation usually proceeds quite quickly. Interestingly, around 60% of the final mineral forms within hours (Buckwalter *et al.*, 1995). After this initial phase, mineral deposition gradually continues over time, increasing bone density.

Continuous changes take place in non-collagenous matrix proteins during mineralisation to control the process. However, collagen concentration remains relatively stable (Sikavitsas *et al.*, 2001). With advanced mineralisation, water and non-collagenous protein concentrations decrease as the mineral concentration increases, accompanied by continuous organisation of the matrix and maturation of bone crystals that will eventually replace the initial "woven bone" with lamellar bone, thus giving the bone its increased stiffness (Buckwalter *et al.*, 1995).

1.4. Events of bone healing

Traumatic bone fractures are the most common cause of bone injury, followed by other causes such as bone pathologies, infections, immune-relatedd conditions and osteoporosis (Brydone *et al.*, 2010). Unlike other tissues, the bone does not form scar tissue to heal the injury but rather responds by regenerative procedures where its original function and morphology are restored (McKibbin, 1978).

Bone fracture healing occurs in one of two ways depending on the size of the defect. Primary intention bone healing occurs when there is no bone loss encountered, and the 2 edges of the fracture could be directly juxtaposed against each other with no gaps. Healing in this type would be exclusively cortical (Tosounidis *et al.*, 2009).

The other type of bone healing is referred to as secondary intention or indirect healing when a large gap defect is formed between bone edges that need to be bridged with the formation of a woven bone callus. In this type, the healing process could involve a combination of both endochondral and intramembranous bone formation (Kalfas, 2001).

In general, bone healing takes place through 3 essential stages (Kalfas, 2001). This begins with an initial inflammatory phase which starts immediately after injury by haematoma formation, followed by chemotaxis of inflammatory cells (macrophages,

lymphocytes, monocytes and neutrophils) via the bloodstream to the site of injury that is mediated by the local cytokines released in the traumatised area. These cells help to scavenge necrotic debris and induce ECM production and angiogenesis. By the end of this stage, fibroblasts invade and stabilise the formed haematoma by granulation tissue formation, with the establishment of new local blood circulation (Bolander, 1992, Kalfas, 2001).

The second stage is the reparative phase. During this stage, the newly formed granulation tissue becomes more organised with the fibroblastic stroma which will support cellular growth and vasculature. In endochondral ossification, fibroblasts develop into chondroblasts, which form hyaline cartilage before ossification, while in intramembranous bone formation there is no intervening cartilaginous phase (Buckwalter *et al.*, 1995). Late in this stage, active osteoblasts start to lay down a collagen matrix followed by woven bone, which will then start to gradually mineralise, leading to callus formation around the fracture ends. This callus is relatively soft, it requires about 4-6 weeks of immobilisation or external fixation to support the fracture site until the callus becomes sufficiently supported by the bridging of woven bone between the fracture's ends (McKibbin, 1978).

The final stage of fracture healing is the remodelling phase, during which woven bone is replaced with lamellar bone, then reshaped to eventually restore bone original structure, function and mechanical integrity. This phase continues over many months to completion (Tosounidis *et al.*, 2009).

1.5. Current approaches in the management of bone defects and their limitations

The increased public expectations towards better function and aesthetics for defect restoration have escalated demands to develop new techniques to restore bone

defects with optimal healing outcomes. Many strategies have been adopted in current surgical practice to deal with bone defects that result from trauma or pathology; among these are bone grafts, guided tissue regeneration, distraction osteogenesis and tissue engineering (Ward *et al.*, 2010, Bernabe *et al.*, 2012).

1.5.1. Bone grafting

Bone is one of the top two most frequently transplanted tissues in the human body (Calori *et al.*, 2011, Li *et al.*, 2014). It is used to fill spaces, provide support and enhance biological repair of a defect area. Annually, about 2.2 million bone grafting procedures are performed worldwide (Sandhu and Nair, 2009, Saiz *et al.*, 2013).

1.5.1.1. Autografts

In this type of graft, the tissue is harvested from a healthy donor site to restore a remote defect area in the same individual. Autografts are considered to be the gold standard in bone replacement, being non-immunogenic and osteo-inductive, as well as being rapidly re-vascularised with the aid of growth factors present in natural bone (Solheim *et al*, 2001, Mathoulin *et al*, 2010). However, the harvesting method for autografts is potentially invasive as it creates an extra defect site for the patient. This would possibly require longer operation times, increase the risk for donor site complications and morbidity, and involve additional postoperative discomfort (Calori *et al*, 2011, Djouad *et al*, 2012). In addition, the available donor sites may not provide sufficient bone to restore the defect area, especially in children and the elderly; as well as the unlikely possibility of obtaining the specific shape and size that matches the defect area. It is also important to mention that cancellous bone grafts will be subjected to rapid resorption, especially in larger bone defects (Gugala *et al.*, 2007, Ward *et al.*, 2010, Nishi *et al.*, 2012).

1.5.1.2. Allografts

Allografts involve a different donor-recipient inter-individual transfer of tissues (different individuals of the same species) to restore a defect area. This type of graft includes a high risk of developing immunogenic reactions. As an attempt to reduce this, autografts are usually processed after harvesting using irradiation or freeze-drying in an attempt to reduce immunogenicity before use. This adds an extra cost for the patient upon their application. Also, allografts can increase the risk of blood-born infections between the donor and the recipient, such as hepatitis B and HIV viruses (Liu *et al*, 2011).

1.5.1.3. Xenografts

Grafts from animal origin (xenografts) are also available as another treatment option for bone replacement; it involves the use of graft material between 2 different species (Rodella *et al*, 2011). The most common are bovine-derived products (Oltramari *et al*, 2007). These include inorganic apatite crystals or bovine collagen (Rodella *et al*, 2011). Although it has been proved that these grafts have an osteo-conductive property; they have many clinical disadvantages. Residual mineral crystals can remain in the graft site up for up to three years which can delay healing. There is also a hazard of immunogenicity, allergenic reactions and transmission of inter-species diseases like Creutzfeldt-Jakob disease (CJD) or Bovine Spongiform Encephalopathy (Hallman, 2001, Wenz *et al*, 2001, Fontana *et al*, 2008, Rodella *et al*, 2011).

1.5.2. Bio-inspired approaches for bone repair

The limitations of the conventional graft sources available for the treatment of bone defects has directed intense research work over the past two decades towards finding alternative graft biomaterials; either to act as fillers or to enhance the biological repair

mechanisms at the defected site. These materials can present in several forms, each with a different mechanism of action (Gugala *et al*, 2007).

1.5.2.1. Osteo-conductive synthetic graft biomaterials

The use of synthetic graft material can provide a scaffold for new bone ingrowth and have the potential to osteo-integrate with natural bone boundaries (Cook *et al*, 1998). Many examples of such materials are commercially available; these include hydroxyapatite crystals, bioglass ceramics and tricalcium phosphate (Hasegawa *et al*, 2007, Rodella *et al*, 2011). In clinical practice, the main disadvantages of these materials include low resorption rate, difficult manipulation and occasional inflammatory foreign body reactions (Giannoudis *et al*, 2005). Also, the lack of osteo-inductive potential can delay healing (Nishi *et al*, 2012).

1.5.2.2. Osteogenic and osteo-inductive biomaterials

These include materials that can be osteogenic *per se* (such as bone marrow aspirates and concentrates of plasma) or materials that can induce pre-existing cells to form new bone (growth factors, cytokines and proteins) (Gugala *et al*., 2007). Even though these materials can produce satisfactory results in bone healing; they have many practical disadvantages. The cost-effectiveness is a concern as these materials require high concentrations to be effective in clinical practice. In addition, they generally lack physical strength, which is essential for bone support during the healing phase (Gugala *et al*, 2007).

1.5.3. Guided bone regeneration (GBR)

GBR techniques involve enclosing the bone defect with a membrane, preventing migration of soft tissue into the defect gap and maintaining space for new bone to regenerate (Hardwick *et al*, 1995). GBR is widely used in bone reconstruction, either alone or in combination with grafts and biomaterials. However, it has many limitations

depending on the type of membrane used. Non-absorbable (like cellulose acetate filters) membranes require a second surgery for membrane removal and increase the possibility for secondary infection., In contrast, absorbable membranes like collagen membranes , can collapse during the healing process with some can induce foreign body reaction upon degradation (Schmidmaier, *et al*, 2006, Rodella *et al*, 2011, Dimitriou *et al*, 2012).

1.5.4. Distraction osteogenesis

Distraction osteogenesis is the process of gradual, controlled tension applied to elongate newly formed bone that fills the gap between two separated bone segments. It has the unique advantage of simultaneous gradual expansion of the related soft tissue involved (nerves, blood vessels, skin and mucosa) that are also required to restore the whole defect as one unit. This method has many applications, especially in maxillofacial surgery, as in the management of facial deformities, mandibular lengthening and alveolar reconstruction (Samchukov *et al*, 1998, Gaggl *et al*, 1999a, Gaggl *et al*, 1999b, Hidding *et al*, 1999, Hegab and Shuman, 2012) However, it holds many potential complications. It is a prolonged procedure as the new bone regenerates at a slow rate. In addition, a high risk of contamination and infection is likely; adding to that the significant pain associated with bone transport process (Swennen *et al*, 2001, Gugala *et al*, 2007, Mahajan, 2013).

1.6. Tissue engineering (TE)

Tissue engineering (TE) is a multidisciplinary field that involves a combination of biology, chemistry, physics, engineering and medicine. It is based on the concept of using a patient's own cells to fabricate *ex-vivo* autografts in order to restore a tissue defect or a body function without the risk of rejection (Placzek *et al*, 2008, Schenke-Layland, 2011, Schenke-Layland and Narem, 2011, Petrovic *et al*, 2012).

22

TE is considered to be a relatively young science. There is controversy about the exact time of its foundation. Placzek *et al.* (2008) reported that there was evidence that TE had started in the late 1950s, being a part of other experimental trials. First trials to form cartilage tissue were introduced in the late 1970s. However, the term "tissue engineering" in its organised form as an individual discipline was introduced in the late 1980s by Langer and Vacanti in Boston, USA. They published their first article about the basics of TE in 1993. Afterwards, the past three decades have witnessed a rapid development of TE in respect to research work and potential medical applications (Langer and Vacanti, 1993, Vacanti, 2006, Placzek *et al*, 2008, Petrovic *et al*, 2012).

1.6.1. Basic elements of bone TE

TE requires four fundamental elements: stem cells, scaffolds, growth factors and mechanical stimulation (Berthiaume *et al*, 2011; Petrovic *et al*, 2012). For any bone to heal, these four basic components, together described as the "diamond concept" should interact (Giannoudis *et al*, 2007). This is when osteogenic cells differentiate in an osteo-conductive matrix in the presence of appropriate osteo-inductive cues and suitable mechanical stimulation (Giannoudis *et al*, 2007; Brydone *et al*, 2010).

1.6.2. Stem Cells

"Stemness" of cells is defined by a set of properties, including self-renewal capacity, multilineage differentiation potential and colony formation *in vitro* (Robey, 2000; Suchánek *et al*, 2009; Tomlinson *et al*, 2015).

In general, human stem cells can be derived either from embryonic or adult tissues. **Human embryonic stem cells** were proved to have pluripotent capacity to differentiate into all types of human tissues when properly induced, with

unlimited proliferative ability in their undifferentiated state (Drukker *et al*., 2006). However, their use in research and clinical therapies is limited, as many ethical issues have been raised about the violation of human dignity and privacy and damaging human embryos for the sake of tissue regeneration (Gershon, 2003). Contrariwise, **human adult mesenchymal stem cells (MSCs)** are present in every postnatal tissue of the human body. Their function is to restore damaged tissues by giving birth to new cells similar to the cells of origin. MSCs have been isolated from many tissues such as bone marrow, brain, skin, adipose tissue and hair follicles. Recently, MSCs have also been also isolated from dental tissues, including periodontal ligament, exfoliated deciduous teeth and dental pulp (Gronthos *et al*, 2002; Jones and Yang, 2011).

1.6.2.1. Non dental stem cell sources for bone tissue regeneration

The main non dental MSC sources that were recruited for BTE are bone marrow stem cells and adipose-derived stem cells. Both have been used for the regeneration of bone tissue and described in the previous literature (Zuk *et al*., 2001, Caplan, 2005, Levi and Longaker, 2011). However, harvesting methods for bone marrow are considered to be invasive and usually associated with donor site morbidity, pain and increased risk of infection (Huang *et al*., 2009). In addition, the total number of cells obtained is estimated to be the lowest among the known sources of MSCs, with slower *in vitro* culture growth rate (Huang *et al*., 2009, Orbay *et al*., 2012). Alternatively, adipose tissue is easier to access and contains higher numbers of stem cell populations than bone marrow (Wagner *et al*., 2005). Despite that, their use for BTE is controversial, as it was reported that they have inferior osteogenic differentiation potential compared to bone marrow cells (Im *et al*., 2005, Niemeyer *et al*., 2010, Jones and Yang, 2011).

1.6.2.2. Dental stem cell sources for bone tissue regeneration

The tooth is a complex organ composed of soft and hard tissues. For that reason, a number of distinct and interdependent tooth-associated precursor cell populations have been identified (Jo *et al.*, 2007). Stem cells were isolated from five well-defined dental tissues, including dental pulp stem cells from the pulp stroma of permanent teeth (hDPSCs); pulp stem cells of human exfoliated teeth primary teeth (SHEDs); periodontal ligament stem cells; stem cells from the apical papilla, and dental follicle progenitor cells (Gronthos *et al.*, 2000, Elluru *et al.*, 2012). All have been used previously for tissue regeneration research (Jo *et al.*, 2007, Huang *et al.*, 2009, La Noce *et al.*, 2014). Nevertheless, conflicting outcomes could be found in the literature for comparisons of these dental stem cell sources regarding cell growth rate and osteogenic commitment. This is more likely to be related to lack of standardisation of donor age, cell seeding densities, culture time, passage number of the cells and inter-donor variability among experiments. (Koyama *et al.*, 2009, Verma *et al.*, 2014, Potdar and Jethmalani, 2015). As dental pulp stem cells basically act as a reservoir to replace odontoblasts destroyed due to trauma or caries, so *in vivo* dentine regeneration is an innate property of their own (Téclès *et al.*, 2005). The molecular and biological similarities between dentine and bone, along with the easy accessibility of hDPSCs made it a promising stem cell source to be recruited for BTE (Graziano *et al.*, 2008). This was evidenced in literature with the successful use of hDPSCs as a model to study bone formation (Yang *et al.*, 2009, El-Gendy, 2010, Mangano *et al.*, 2010, Yang *et al.*, 2012) and their involvement in a number of bone regeneration clinical trials (d'Aquino *et al.*, 2009, Giuliani *et al.*, 2013).

Several studies had been conducted to compare hDPSCs and SHEDs as dental pulp stem cell source for regenerative medicine; with many of them reporting the superiority of SHEDs with respect to higher proliferation rate and higher capacity for osteogenic differentiation compared to hDPSCs (Miura *et al.*, 2003, Seo *et al.*, 2008, Daltoe *et al.*, 2014, Yazid *et al.*, 2018). This was mainly explained by the younger pulp tissue source with increased stem cell activity potential (Gronthos *et al.*, 2000; Miura *et al*, 2003). In most cases, however, these studies used patients' age as a reference with little information on the varying degrees of root resorption among those exfoliated teeth (Miura *et al.*, 2003, Miyagi *et al.*, 2010). Resorption of deciduous teeth is a genetically programmed, physiological phenomenon that leads to apoptosis of cementoblasts and consequently promotes osteoclastogenesis (Bolan and de Carvalho Rocha, 2007). The course of this process was found to cause observable changes of pulp tissue characteristics such as reduced vascular component, increased metabolic activity of the pulp tissue and cellular changes such as the reduction of odontoblasts and the increase in inflammatory, clastic cells as well as mononuclear precursors (Yildirim *et al.*, 2008, Bönecker *et al.*, 2009, Monteiro *et al.*, 2009). Furthermore, possible pulp tissue contamination was seen resulting from open-end resorbed roots and/or coronal carious lesions that are commonly seen in exfoliated deciduous teeth (Pilbauerová and Suchánek, 2018). In a significant study conducted by Bernardi *et al.* (2011), it was found that SHEDs isolated from exfoliated deciduous teeth at varying level of root resorption showed significant variability in growth rates and expression of stem cells markers.

1.6.2.3. Adult human dental pulp stromal cells

The human dental pulp is the connective tissue that occupies the core part of all teeth, providing the blood and nerve supply essential for their vitality. Histologically, it is composed of connective tissue, containing a mixed cell population surrounded by fibrovascular stroma (Oliveira *et al.*, 2003). Cells within dental pulp include fibroblasts, lymphocytes, macrophages, nerve cells, pericytes, endothelial cells and undifferentiated mesenchymal stem cells (Oliveira *et al.*, 2003); these cells will therefore be present in human dental pulp primary cultures, referred to in this project as "human dental pulp stromal cells" (hDPSCs).

Soon after being first described by Gronthos and colleagues, hDPSCs attracted much attention for being easily accessible, rich with MSCs and having higher proliferation rates compared to cells from other sources when cultured under the same conditions (Gronthos *et al.*, 2000). HDPSCs were found to have the ability to differentiate into odontoblasts, chondrocytes, adipocytes and neural-like cells under appropriate environmental stimulants. Furthermore, these cells could survive after years of cryopreservation and still be able to differentiate into pre-osteoblasts, providing a potential source of stem cell banking for autologous grafts for various applications in orthopaedics and cranio-maxillofacial surgery (Laino *et al.*, 2006, Zhang *et al.*, 2006, El-Sayed and Mohamed, 2012).

Adult hDPSCs have been successfully obtained from extracted permanent premolars, third molars and supernumerary teeth (Zhang *et al.*, 2006, Huang *et al.*, 2008, Lee *et al.*, 2011). Isolating these cells from the pulp tissue of third molar (wisdom) teeth enfolds many advantages. Although many factors, such as gender, race, and habitation, are related with the incidence of impacted third

molars, it has been demonstrated that 70% of the population has at least one impacted third molar in their dentition (Zhang *et al.*, 2006, Koyama *et al.*, 2009). These teeth are often routinely removed from young, healthy individuals due to issues related to discrepancies in size between the dental arch and the teeth; ending up discarded with clinical waste (Nakajima *et al.*, 2018). For that reason, these teeth provide a widely available source for hDPSCs (Zhang *et al.*, 2006, Petrovic and Stefanovic, 2009, Kawashima, 2012). Moreover, despite the fact that third molar tooth germs begin development around the sixth year of life, the root formation is often still incomplete at the age of 18 (Tirino *et al.*, 2012). Being the last tooth type to develop within the adult dental arch, third molars theoretically have the "youngest" pulp tissue, with increased chances of a considerable amount of undifferentiated stem cells still present that could be recruited for tissue regeneration purposes (Zhang *et al.*, 2006).

Two main methods for hDPSCs isolation from pulp have been described in the literature, **culture explant** (tissue outgrowth) and **enzyme digestion**. The first method involves aseptic scooping of the pulp tissue out of the extracted teeth, then chopping it into 1-2 mm explants that are left to grow in culture (Huang *et al.*, 2006, Tirino *et al.*, 2012). In the second method, the excavated dental pulp tissue is finely minced then digested to produce a cell suspension using enzyme digestion medium containing collagenase type I and dispase (Gronthos *et al.*, 2000, Huang *et al.*, 2006, Tirino *et al.*, 2012, La Noce *et al.*, 2014). Enzyme digestion has been generally preferred over the explant method for the advantages of resulting faster cell proliferation, a higher number of cells produced, reliability of obtaining distinct cell types within the culture and the increased number of formed fibroblast-like colonies in culture within shorter

culture period (Tsukamoto *et al.*, 1992, Couble *et al.*, 2000). Characterisation of hDPSCs is discussed in **Chapter 4** of this thesis.

1.6.3.   Growth factors (GFs)

GFs are a group of signalling proteins that are naturally excreted in the body to regulate a wide range of cellular activities. They are used in BTE to induce different functions, including cellular growth, osteo-induction, angiogenesis, extracellular matrix maturation and mineralisation (Brydone *et al*, 2010; Fisher *et al*, 2013). Table 1-3 summarises the most important GFs involved in bone regeneration with their functions.

Table 1-3: Growth factors associated with bone regeneration and their functions

Growth Factor	Function	Reference
Bone morphogenic proteins (BMP)	• A super-family of more than 20 cytokines. • BMPs play a major role in committing pluripotent mesenchymal stem /stromal cells to the osteoblastic lineage • Stimulate the proliferation of both chondrocytes and osteoblasts and cause increased matrix production by each cell type. • Induce bone nodule formation and expression of osteoblastic markers *in vitro.*	Buckwalter *et al.* (1995), Sikavitsas *et al.* (2001), Dimitriou *et al.* (2005), Hughes *et al.* (2006)
Fibroblast growth factors (FGF)	• Play a role in angiogenesis • Play a role in mesenchymal cell mitogenesis. • Increase osteoblast proliferation *in vitro,* however, they inhibit osteoblast differentiation in terms of collagen I synthesis and *ALP* expression • May also influence bone development through their angiogenic properties	Sikavitsas *et al.* (2001), Dimitriou *et al.* (2005), Hughes *et al.* (2006)
Insulin-like growth factors (IGF)	• A family of growth factors that stimulates proliferation of osteoblasts and chondrocytes as well as inducing matrix secretion by both cell types.	Buckwalter *et al.* (1995), Sikavitsas *et al.* (2001), Dimitriou *et al.* (2005), Hughes *et al.* (2006)

Platelet-derived growth factor (PDGF)	• Secreted by platelets during the early phases of fracture healing • Stimulates proliferation of chondrocytes and osteoblasts. However, in different concentrations, it has also been implicated in bone resorption • Has a chemotactic and mitogenic effect on MSCs. • Plays a vasculogenic role in wound healing	Dimitriou *et al.* (2005), Hughes *et al.* (2006)
Transforming growth factor-β (TGF-β)	• Plays a role in cell proliferation, differentiation and the production of extracellular matrix. • Induces differentiation of MSCs to chondrocytes • May also induce chondrocyte and osteoblast proliferation. • Seen to enhance bone resorption at high concentrations.	Buckwalter *et al.* (1995), Sikavitsas *et al.* (2001), Dimitriou *et al.* (2005), Hughes *et al.* (2006)
Vascular endothelial growth factors (VEGF)	• A group of potent stimulators of endothelial cell proliferation. • Also expressed during bone formation and endochondral ossification. • External administration of VEGF was found to enhances fracture repair	Street *et al.* (2002), Dimitriou *et al.* (2005)

1.6.4. Mechanical stimulation

Recently, mechanical stimulation had been included as the fourth element in TE (Giannoudis *et al*, 2007; Ji *et al*, 2014), especially for dynamic tissues that are subjected to continuous environmental loads like bone. This would naturally drive the remodelling process according to the functional needs of the area (Sikavitsas *et al.*, 2001). Achieving this could be challenging using static *in vitro* cultures, but in addition to biochemical stimulation and selection of an ideal scaffold material, the utilisation of mechanical loading on the seeded cells would permit better optimisation of their performance as bone-forming cells (Salgado *et al.*, 2004). Recently, studies involving tissues that are naturally subjected to continuous loads such as bone, cartilage and ligaments have adopted different types of bioreactors in *in vitro* models of BTE, thus aiming to simulate the natural physiological forces imposed on these tissues and attempting to discover the effect on cellular growth and differentiation (Martin *et al*, 2004; Ji *et al*, 2014). Bioreactors can be spinning flasks, rotating bioreactors or perfusion systems (Sikavitsas *et al.*, 2002). They primarily aim to create dynamic culture systems which have been proven to produce uniform cell distribution, uniform perfusion and exchange of nutrients and gases, in addition to providing good cellular penetration and speeding up the growth process (Bancroft *et al.*, 2003, Salgado *et al.*, 2004, El Haj and Cartmell, 2010).

1.6.5. Scaffolds

Scaffolds are a fundamental requirement for the treatment of critical size bone defects, as one of the major considerations is to bridge the physical gap at the defect area. They provide a template for cells' attachment, growth and differentiation; and also act as a reservoir for nutrients and signalling growth factors.

Moreover, they have an essential role as a matrix for neovascularisation and of extracellular matrix formation (Kleinman *et al.*, 2003, Rozario and DeSimone, 2010, Ward *et al.*, 2010, Petrovic *et al.*, 2012, Mobini and Ayoub, 2016).

The ideal scaffold material for BTE should be biocompatible, time-biodegradable, osteo-inductive and osteo-conductive. Also, it should have a highly inter-connected porous structure to allow cellular infiltration, vascularisation and nutrients and waste product diffusion throughout the cellular construct. In addition, scaffold material should be strong enough to transduce mechanical load and support cells during growth and differentiation (Hasegawa *et al.*, 2007, Bose *et al.*, 2012).

A great deal of effort has been made over the years to develop novel scaffolds for BTE, using different materials in different fabrication techniques. Several categories of scaffold materials have been used for BTE; the main ones to mention are metallic scaffolds, ceramics, polymers (naturals or synthetic) or their combinations (Novosel *et al.*, 2011, Liu *et al.*, 2013, Sharma *et al.*, 2014).

1.6.5.1.   Metal scaffolds

Solid metals and their alloys have wide applications in the construction of implants replacing hard human tissues. Titanium and its alloys were proven to be highly reliable biomaterials for orthopaedic and maxillofacial bone reconstruction due to their excellent biocompatibility, good corrosion resistance and high mechanical strength (Oh *et al.*, 2003, Takemoto *et al.*, 2005, Frosch and Stürmer, 2006, Dabrowski *et al.*, 2010). However, the main disadvantages of metallic scaffolds are the lack of biodegradation, possibility of metal ion release and stiffness that is much higher than that of bone tissue; which can loosen the implant with time by creating a stress shielding effect at the bone tissue/implant interface (Dabrowski *et al.*, 2010, Novosel *et al.*, 2011, Bose *et al.*, 2012, Sharma

33

et al., 2014). In addition, metal implants show low bonding ability to the surrounding bone due to their solid structure. This led to an increase in recent research work on developing metal scaffolds with highly interconnected porous structures to improve cellular ingrowth through the porous implant, creating more appropriate scaffolds for BTE (Wang *et al.*, 2008, Dabrowski *et al.*, 2010).

1.6.5.2. Bio-ceramic scaffolds

Bone is a highly mineralised tissue, so one of the bone scaffold materials that might be expected to be used would be bio-ceramics (Mobini and Ayoub, 2016). These are inorganic, mineralised biomaterials of different categories, such as hydroxyapatite, other calcium phosphates and bioactive glass, all of which have very well documented applications as bone substitutes in orthopaedic surgery (Sarkar and Banerjee, 2010, Asa'ad *et al.*, 2016, Mobini and Ayoub, 2016). Bioceramics are drawing great attention in bone regeneration because they are unlimitedly available, biocompatible, osteo-conductive, potentially osteo-inductive and close in nature to the native bone inorganic components (LeGeros, 2002, Woodard *et al.*, 2007, Blokhuis and Arts, 2011, Asa'ad *et al.*, 2016). However, bioceramics are mostly non-absorbable, extremely brittle materials with low mouldability, which makes it very difficult to shape the material to match the defected area. In addition, their generally poor mechanical properties limit their use to non-stress bearing areas (Kim *et al.*, 2005, Asa'ad *et al.*, 2016). However, combining bioceramics with other mechanically strong biomaterials, like polyesters or metals, greatly improves their mechanical properties and mouldability for ultimate utilisation in BTE (Zhang *et al.*, 2013, Długoń *et al.*, 2014, Asa'ad *et al.*, 2016).

1.6.5.3. Polymer scaffolds

Polymer scaffolds may be either natural or synthetic. Commonly used natural polymers for BTE are collagen, fibrin, alginate, silk, hyaluronic acid, and chitosan (Bose *et al.*, 2012, Liu *et al.*, 2013). Natural polymers are highly biodegradable, biocompatible and naturally support cellular attachment, but their main disadvantages are lack of mechanical strength and limited control of their porosity and degradability upon manufacturing. For BTE, they are often used combined with other materials, like bioceramics, in order to overcome these problems (Yang *et al.*, 2004a, Novosel *et al.*, 2011, Sharma *et al.*, 2014). Due to these limitations, synthetic polymers are gaining much attention as scaffold materials for being mechanically strong, having excellent manufacturing control over wide range of porosities, flexibility and degradability characteristics that can be consistently reproduced (Novosel *et al.*, 2011, Bose *et al.*, 2012, Liu *et al.*, 2013, Serra *et al.*, 2013a). Popular synthetic polymers for BTE are polylactic acid (PLA), polyglycolic acid (PGA), polylactic – glycolic acid (PLGA) and polycaprolactone (PCL) (Bose *et al.*, 2012, Liu *et al.*, 2013, Sharma *et al.*, 2014).

1.7. PLA scaffolds for BTE

1.7.1. General Properties of PLA polymer

Polylactic acid (PLA) has been extensively researched and employed as a biodegradable polyester, replacing the conventional petrochemical-based polymers in industrial applications. It has since become a principal biomaterial in the medical field (Lopes *et al.*, 2012, Farah *et al.*, 2016).

PLA is a clear, colourless, aliphatic polyester that is produced by polymerisation of lactic acid monomers (Lopes *et al.*, 2012). It has many advantages compared to

other biopolymers. Firstly, it is an environmentally friendly material, regarding its sources and fate after degradation (Farah *et al.*, 2016). Lactic acid is a renewable, naturally occurring organic acid which is a fermentation product of sugars obtained from corn, wheat, or rice. Even though it has been reported that PLA acidic degradation products could have toxic effect on viable cells, this polymer degrades by non-enzymatic hydrolysis when implanted in living systems like the human body, producing nontoxic, natural metabolites that are eventually converted to carbon dioxide and water via the citric acid cycle. These final products will either be exhaled or excreted (Neumann, 2009). Additionally, the rate of formation of these acidic by-products can be significantly reduced by adjusting the rate of PLA degradation rate upon manufacturing (Liu and Ma, 2004, Neumann, 2009, Serra *et al.*, 2013a, Farah *et al.*, 2016). For that reason, PLA was approved by the Food and Drug Administration (FDA) as generally recognised as safe (GRAS) for direct contact with biological fluids; and since, it has been increasingly employed in biomedical applications and research (Liu and Ma, 2004, Gupta *et al.*, 2007, Farah *et al.*, 2016). PLA had been used for decades as a degradable surgical suture, for the fabrication of biodegradable mini-plates and screws for fracture fixation surgeries and for the fabrication of facial reconstruction prosthetic implants (Gupta *et al.*, 2007, Neumann, 2009, Lopes *et al.*, 2012, Farah *et al.*, 2016).

Another advantage of PLA compared to other biopolymers is its superior thermal handling with different processing techniques, including injection, moulding, film-forming, and fibre spinning (Auras *et al.*, 2004). This can give the polymer a wide range of physical designs and characteristics for various applications in the biomedical field (Farah *et al.*, 2016).

Tissue engineering is a recent area of research where PLA is being applied. It has proven to be a highly favourable scaffold material for skeletal tissue engineering (including bone, cartilage and tendons) for being mechanically strong and having excellent manufacturing control over a wide range of porosity and degradability characteristics (Drumright *et al.,* 2000, Gupta *et al.,* 2007, Lopes *et al.*, 2012). It can provide the desired scaffold properties by simple fine-tuning of its physical-chemical structure at a reasonably low cost (Cheng *et al.*, 2009, Lopes *et al.*, 2012).

1.7.1.1. PLA degradation rate

PLA by nature has a slower degradation rate compared to other synthetic polymers. Being more hydrophobic reduces its molecular affinity to water, leading to a slower hydrolysis rate. This leads to a long *in vivo* lifetime, which in some cases could take years to fully degrade in a biological setting resulting in inflammation and infection (Ma, 2004, Farah *et al.*, 2016). The time required for hydrolytic fragmentation of PLA depends on many factors that could be environmental, such as temperature, pH, availability of water and mechanical strain; or material-related represented by the configuration of PLA (including its molecular weight and degree of crystallinity). Tuning of such properties can influence and control PLA degradation rate (Lopes *et al.*, 2012).

Molecular weight has a significant effect on how PLA retains its mechanical strength over time in the presence of moisture. High molecular weight PLA has resorption rates that can be up to 8 years. Therefore, producing a lower molecular weight PLA is desirable for use in BTE applications as it reduces its degradation time to the limit required for supporting bone tissue during the healing phase (Lopes *et al.*, 2012, Neumann, 2009).

Crystallinity is an indication of the extent of crystalline regions in the polymer relative to its amorphous content. Polymers with highly crystalline regions are degraded more slowly due to the fact that hydrolytic degradation usually begins in the amorphous regions (Neumann, 2009). PLA properties could be controlled through the use of special catalysts aiming to adjust the stereochemistry of its crystals to meet the desired degradation speed in the presence of water (Farah *et al.*, 2016).

1.7.1.2. Methods of porous PLA 3D scaffold fabrication and their limitations

Various conventional techniques have been used for the fabrication of PLA 3D scaffolds for BTE. **Salt leaching** involves placing salt crystals, like sodium chloride, into a mould then adding the melted polymer to occupy the spaces in between. After the polymer is hardened, the salt is washed out by a solvent such as water or alcohol. After all salt crystals have leached out, a hard, porous polymer will be left (Lee *et al.*, 2005b, Loh and Choong, 2013). The pore size of the formed scaffold can be controlled by changing the amount and size of the salt particles used (Ma, 2004). This technique involves minimal polymer use and waste compared to other available techniques (Loh and Choong, 2013, Ma, 2004).

Gas foaming is a different technique that utilises gas as the porogen. A PLA disc is formed by compression moulding under high temperatures, and then a high-pressure carbon dioxide gas is applied through the discs for a few days to foam up the polymer. This method eliminates the need for chemical solvents and the leaching step, thus reducing the overall fabrication time (Loh and Choong, 2013, Schugens *et al.*, 1996).

Another method for 3D PLA fabrication is **phase separation**, by which PLA dissolved in the solvent is placed in a mould then rapidly cooled to freeze the solvent. The solvent is then removed by freeze-drying, leaving behind numerous pores within the polymer (Schugens *et al.*, 1996).

Electrospinning is another method that offers an alternative option of 3D construction where the polymer solution is ejected from a tip of a capillary tube as a jet towards a collecting target in the presence of a voltage difference. When the surface tension of the solution is exceeded by the applied voltage, the jet fibres will dry and elongate toward the collector due to electric forces, eventually depositing as a uniform mesh of nanometre-sized fibres on the conductive substrate. This is a simple and inexpensive technique that can generate high porosity with increased scaffold surface area for better cell attachment (Loh and Choong, 2013, Li *et al.*, 2014).

The main limitations of the current conventional techniques include the inability to control reproducible pore size, distribution and geometry within the scaffold. It is also impossible to design the interconnections between the pores themselves, which has a crucial effect on how deep the cells can migrate inside the scaffold and how efficient vascularisation in different areas within the scaffold would be achieved (Sachlos and Czernuszka, 2003, Liu and Ma, 2004, Novosel *et al.*, 2011). Another limitation is the use of toxic solvents, which if not completely eliminated, could cause cellular death (Yeong *et al.*, 2004). Furthermore, the involvement of extreme temperature or pressure application during the fabrication process will rule out the ability to incorporate bioactive molecules within the scaffolds (Mikos and Temenoff, 2000). These limitations contributed to the introduction of scaffold 3D printing techniques which are computer-controlled.

This would provide more precise control over macro scaffold shape as well as internal structure geometry that would greatly enhance cellular attachment, growth and differentiation (Liu *et al.*, 2008, Serra *et al.*, 2013a, Li *et al.*, 2014, Holmes *et al.*, 2015).

1.7.1.3.　PLA scaffold 3D printing

The beginnings of contemporary 3D printing can be tracked back to the 1980s, then rapidly advanced within the last 30 years for different biomedical applications (Bandyopadhyay *et al.*, 2015). 3D printing, which could also be termed as additive manufacturing (AM), rapid prototyping (RP), or solid freeform fabrication (SFF), is a family of technologies that constructs three-dimensional physical objects based on two-dimensional computerised data. The 3D object is fabricated by the sequential deposition of material layers in a progressive pattern that is determined by the computer software and designed by the user (Serra *et al.*, 2013b, Gross *et al.*, 2014, Colasante *et al.*, 2016). The use of this technique could be applied to a wide variety of materials including polymers, ceramics and metals; giving rise to an unlimited range of geometrical designs that could be utilised for unlimited applications (Colasante *et al.*, 2016).

One major consideration of 3D printing technology is the right material choice, which is critical for achieving the ultimate mechanical properties and functional performance of the final 3D printed scaffold (Serra *et al.*, 2013a, Asa'ad *et al.*, 2016). PLA has excellent thermoplastic potential compared to other polymers and can be processed using different 3D printing techniques into fibres and films (Lopes *et al.*, 2012). 3D printing in turn aids in generating highly precise structures with better resolution than that obtained with other available conventional methods of fabrication. This improvement in resolution is achieved

by controlling the right tuning of temperature printing parameters throughout the printing process (Xiong *et al.*, 2002, Melchels *et al.*, 2009, Serra *et al.*, 2013b). However, choosing the right printing technique of a PLA scaffold will assure achieving high-quality 3D structures without impairing the material properties (Serra *et al.*, 2013b). Below are the main available techniques for PLA scaffold 3D printing:

3D Plotting/direct ink writing is a technique where strands of viscous material in solution form are extruded according to a predesigned pattern. The strands are deposited, under specific pressure, at a layer by constant layer rate. This process could be applied across a range of polymer viscosities and it allows for the addition of drugs and biomolecules such as proteins as well as living cells to the polymer due to the mild processing conditions (Bose *et al.*, 2013, Bandyopadhyay *et al.*, 2015).

Selective laser sintering (SLS) is another method in which a material powder bed is prepared through layer by layer deposition. Each layer is then sintered, either partially or entirely, based on the pre-determined computer design using a laser-based heat source. In this process, the powder bed acts as support, so there is no need for additional support during fabrication. (Williams *et al.*, 2005, Pereira *et al.*, 2012).

Fused deposition modelling (FDM) is a process that involves extrusion of strands of the heated polymer through a nozzle according to the computer prepared design. It is an easily applied technique that does not require a platform for secondary material support (Bose *et al.*, 2003, Bose *et al.*, 2013, Bandyopadhyay *et al.*, 2015).

The above techniques in the 3D fabrication of PLA scaffolds share some main advantages and drawbacks. They can generate reproducible, complex PLA scaffolds with geometrical designs customised to match the tissue defect. Also, they provide excellent control over material composition and can produce scaffolds with superior strength\ porosity ratio compared to available conventional techniques (as was discussed in *1.7.1.2*.). However, these techniques are generally of the higher cost compared to conventional techniques; and are still considered to provide relatively limited resolution in terms of nanoscale printing details (Bose *et al.*, 2003, Bose *et al.*, 2013).

1.7.1.4. 3D printed PLA scaffold applications in bone tissue regeneration research

3D printed PLA scaffolds have been extensively used for *in vitro* BTE applications, investigating different aspects of fabrication and design. Several studies have been carried out to determine the optimal scaffold printing layout that best simulates the natural bone environment. This aspect of interest will be covered in more detail in *Chapter 5* of this thesis.

Another field that was extensively investigated in the literature is the control of PLA surface properties. PLA as a material is relatively hydrophobic, with a static water contact angle of approximately 80°. This can dramatically affect cell affinity to its surface (Rasal *et al.*, 2010). In addition, PLA polymer lacks reactive side-chain motifs on its surface which makes it chemically inert (Burg *et al.*, 1999, Farah *et al.*, 2016).

Different techniques were adopted to modify PLA wettability and tailor the functional groups at the material surface, thus aiming to improve its surface interaction with cells and proteins; these include:

Bulk modifications: Some techniques involved modification of the PLA material bulk, which involves blending PLA with other biomaterials such as chitosan, collagen or even other polymers that are more hydrophilic (poly ethylene glycol for example) to enhance its hydrophilicity (Ke *et al.*, 2003, Yang *et al.*, 2004b, Wan *et al.*, 2006). However, the relatively slow degradation rate of PLA can limit the action of these techniques (Rasal *et al.*, 2010).

Surface modification modalities: These were proven to be highly effective in enhancing PLA scaffolds' surface wettability, surface topography and roughness to allow better attachment of cells to the scaffolds' surfaces (Rasal *et al.*, 2010, Serra *et al.*, 2013a). PLA material on its own usually has a smooth flat surface. Roughening of PLA surfaces enhances the diffusion rates of growth factors and oxygen and nutrient supply between the cells and the scaffold (Cheung *et al.*, 2007).

PLA surface modification can be achieved either by creating permanent changes to its surface or by direct non-permanent surface coating (Rasal *et al.*, 2010). Permanent treatments can be carried out through chemical conjugation of biocompatible macromolecules like gelatin, chitosan, or collagen onto the PLA surface (Zhu *et al.*, 2004) or by UV photo-treatment which relies on PLA photo-activation followed by grafting of other molecules to create surface reactive groups (Ma *et al.*, 2000). Alternatively, direct surface modification of the materials a convenient and straightforward protocol that can be done by the coating of the PLA surface with various substances. Examples of these include extracellular matrix proteins (such as fibronectin, collagen or laminin) which is one of the simplest surface modification methods. These proteins have a natural ability to foster cell adhesion. Therefore, coating polymer surfaces with these bioactive

factors before further treatment can significantly improve its biocompatibility providing an adhesive interface between the scaffold surface and cells that resembles the native cellular environment (Wang *et al.*, 2005). Plasma treatment is another method where the desired mixture of positive ions and electrons (like nitrogen, oxygen or helium) are introduced onto the surface of the polymer to modify the surface property of scaffolds with complex shapes without changing the bulk properties, thus aiming to improve polymer hydrophilicity and cellular affinity and reduce cell loss during cell seeding (Rasal *et al.*, 2010, Jacobs *et al.*, 2012, de Valence *et al.*, 2013).

1.7.1.5. Pre-clinical and clinical applications of 3D printed synthetic polymers in bone reconstruction

Many pre-clinical studies using animal models and clinical trials on human patients have been conducted using 3D printed synthetic polymers to reconstruct various bone defects. *In vivo* applications mainly involved restoring dento-maxillofacial bone defects. Examples of these are dental socket preservation after tooth extraction and reconstruction of the mandibular condyle and orbital bone defects in combination with bone marrow stem cells (BMSCs) (Rohner *et al.*, 2003, Xu *et al.*, 2010, Farré-Guasch *et al.*, 2015, Asa'ad *et al.*, 2016).

In clinical reconstructive surgery, 3D printing offers clinicians an exclusive opportunity to fabricate constructs that are precisely tailored to the individual therapeutic and anatomical needs for each patient in a rapid delivery time compared to conventional techniques (Marro *et al.*, 2016, Schubert *et al.*, 2013). This can be achieved by integrating computer-aided design with patient-specific 2D imaging data (X-rays, MRI or CT scans) to create a computer model that will be eventually materialised into a customised 3D scaffold construct for that

individual (Chia and Wu, 2015, Winder and Bibb, 2005). In the same context, 3D printed polymer models have also been used as an indirect aid in clinical applications of maxillofacial reconstruction. 3D printed PLA models were effectively constructed to be used for pre-operative surgical planning. Surgeons are now able to visualise a detailed physical model of the operation area that was 3D printed according to data obtained from the patient's own computer-based scan images. This provides the opportunity to thoroughly examine, plan and even practice the reconstruction procedure prior to the actual operation which offers higher success outcomes and reduces the chance of unexpected complications (Klein *et al.*, 2013, Keyhan *et al.*, 2016). Likewise, 3D printed models were used as templates to measure and harvest bone grafts from donor sites more precisely. This greatly improved graft adaptation and aesthetic outcome and significantly minimised operation time (Mehra *et al.*, 2011). Some clinical trials have also reported on the utilisation of 3D printed polymeric scaffolds for bone defects reconstruction of vertebral body, zygomatic and alveolar bones (Lee *et al.*, 2005a, Li *et al.*, 2011, Ogden *et al.*, 2014).

1.8. Smart scaffolds

"Smart scaffolds" refers to biomaterials to which rationally designed "biomimetic" properties are applied in an attempt to simulate the natural extracellular matrix environment to enhance cell function and cell-material interaction (Rosso *et al.*, 2005). Recently, one example of a smart material that has been designed and put forward to be used in BTE is self- assembling peptides technology (Gazit, 2007). These materials are produced from specific polypeptide sequences, with the possibility to modify the sequence of amino acids within them so that they can smartly and spontaneously accomplish certain biological functions such as the incorporation of RGD sequences

45

to enhance cellular attachment, or *de novo* nucleation of hydroxyapatite crystals in response to specific environmental triggers (Firth *et al.*, 2006, Kirkham *et al.*, 2007). In the following section, the focus will be placed on the self-assembling peptides fibrillar networks that were first developed in the University of Leeds to be used as smart scaffolds for BTE.

1.8.1. Self-assembling peptides

Self-assembly has been defined as the spontaneous organisation of individual components into well-defined structures without external intervention (Zhang *et al.*, 2002). It is a key property of peptide molecules because of the common peptide backbone (Davies *et al.*, 2006). There are a number of different nanostructures that can be produced through peptide self-assembly, two of the most common secondary structures found within proteins throughout nature are the α-helix and the β-sheet (Pauling *et al.*, 1951). It is the latter structure that Leeds self-assembling peptides technology was designed around (Aggeli *et al.*, 1997) (Figure 1-3).
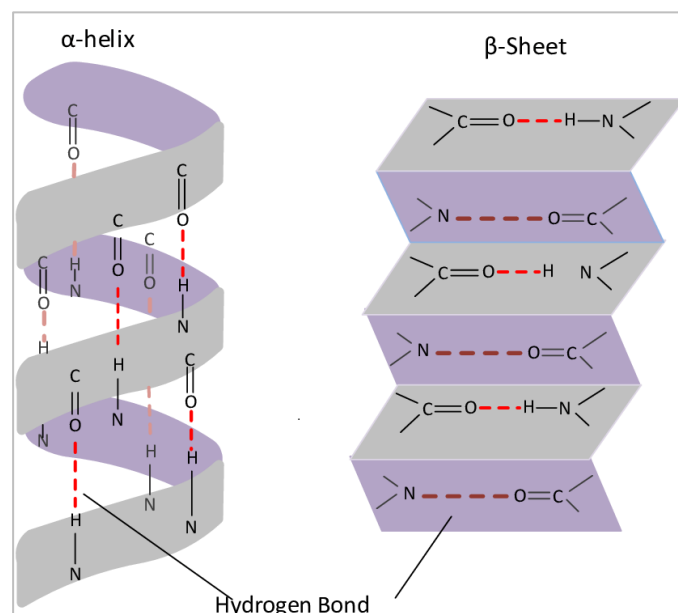
Figure 1-3: α-helix and the (anti-parallel) β-sheet secondary structures (Whitford, 2013)

Aggeli and colleagues designed a family of 11[-mer] peptides, with varying overall charge, hydrophobicity and polarity that can self-assemble in response to different physico-chemical triggers to produce hydrogels (Aggeli *et al.*, 2001). They will be referred to as "SAPs" throughout this thesis. These peptides were engineered in such a way as to be adaptable for biomedical use. When placed in conditions of physiological pH, temperature and ionic strength, certain SAPs will assemble from monomer state to form a transparent, thermostable, self-supporting gel (Aggeli *et al.*, 1997). The main forces responsible for peptide monomer self-assembly into β-sheet structures in SAPs are the intermolecular hydrogen bonding between the participating peptide backbones and the non-covalent intramolecular interactions of the side chains (Kirkham *et al.*, 2007). SAPs can form many different types of polymeric structures, the most common of which is the hierarchy of structure (tape,

ribbon, fibril, fibre) (Aggeli *et al.*, 2001) (Figure 1-4).SAPs hierarchical self-assembly is a concentration dependent process, as a threshold peptide monomer concentration must be present for the gel to form (Davies *et al.*, 2006). This assembly process is reversible, where the material can trans-change between liquid monomer to gel state in response to certain triggering factors, allowing SAPs to be

Peptide monomers have different 'faces' due to differing side-chains

FLUID

+ trigger

Hierarchical self-assembly

Tapes also have different 'sides'

Tapes aggregate together via hydrophobic faces to form ribbons

GEL

Ribbons stack together to form fibrils

Fibrils can aggregate to yield fibres
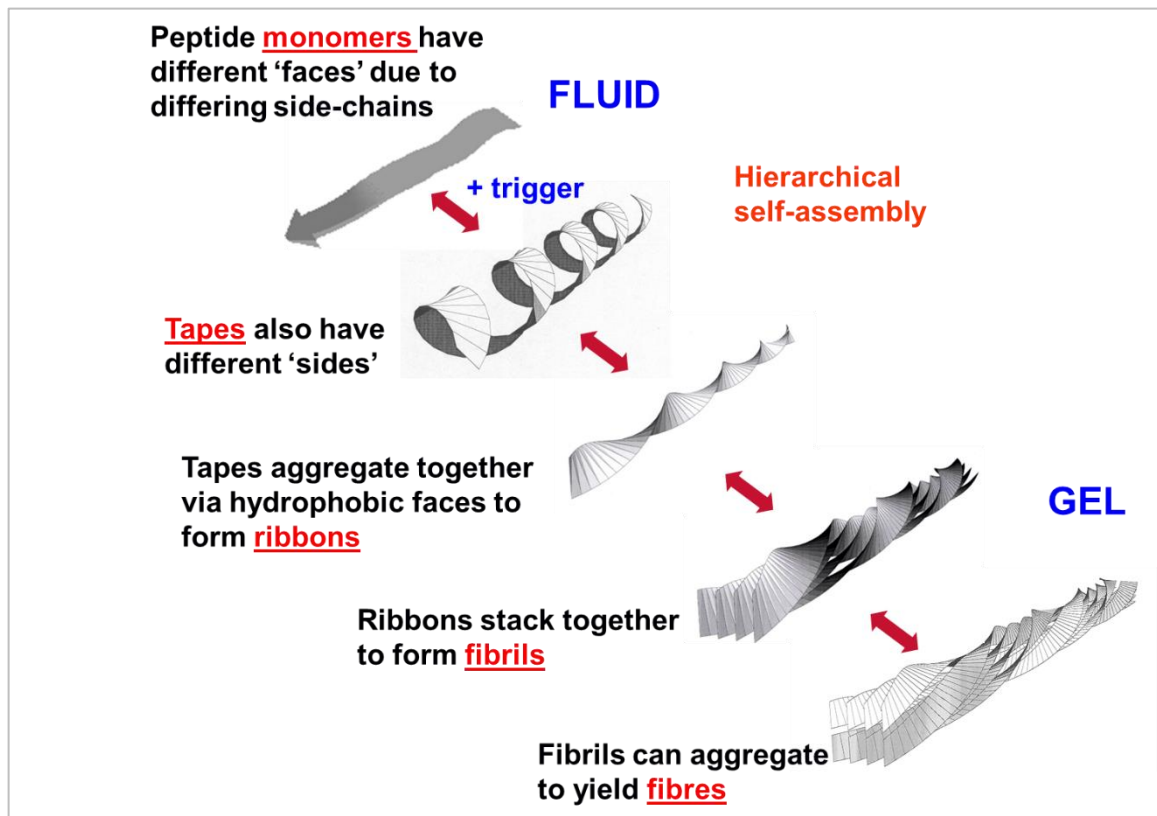
Figure 1-4: Hierarchical self-assembly of SAPs monomer from monomer fluid to gel (image modified from (Aggeli *et al.*, 2001), used with kind permission of Prof Jennifer Kirkham)

applied in liquid monomeric form and then to gel *in situ* at the target site (Maude *et al.*, 2013). It has been observed that converting the gel to monomer can be achieved by switching the pH, heating to temperature >70 °C or changing ionic solution strength. Peptides can re-assemble again into gels on cooling to room temperature or on re-adjustment of pH (Carrick *et al.*, 2007).

The 11 amino acid long SAP P_{11}-4 (primary sequence COQQRFEWEFEQQ) has been previously shown to produce fibrillar networks mimicking the biological

48

macromolecules found in the extracellular matrices of the mammalian skeleton which are known to control the mineralisation of hard tissues (Kirkham *et al.*, 2007). It was designed to spontaneously assemble at pH ≤ 2 to form a self-supporting hydrogel in a concentration-dependent manner (Davies *et al.*, 2006). The fibrils formed by SAP P_{11}-4 have an overall net charge of -2 at physiological pH (Davies *et al.*, 2006). The sites of a negative charge, through molecular dynamics simulations, were found to approximately match the dimension of calcium ions in the hydroxyapatite crystal (Thomson *et al.*, 2014). These negatively charged regions on the SAP P_{11}-4 surface are thought to act as a nucleating template for hydroxyapatite crystal formation (Kirkham *et al.*, 2007).

Rationally designed SAPs represent a promising technology to be used for tissue engineering applications. They can be designed to assemble into gel scaffolds *in situ* at the environments in which they are placed; as they can be injected in their monomeric form and triggered to assemble into gel following a change in pH or surrounding ionic concentration (Aggeli, *et al.*, 1997). They offer an easy to manipulate, highly uniform reproducible scaffold structure formed with full control of gel formation dynamics, degradation rates and mechanical properties. Furthermore, their side chains could be modified to provide an ideal environment for anchorage-dependent cells (Ravichandran *et al.*, 2014). The highly hydrated nature of the material allows for rapid diffusion of nutrients and metabolites for the incorporated cells; with low amounts of dry mass and they thus cause minimal irritation to living systems with negligible production of degradation products (Fedorovich *et al.*, 2007).

Moreover, their advantages as a nanophase material are revolutionary as a scaffold material, as will be discussed in detail in **Chapter 6**. Based upon its proven ability

to nucleate hydroxyapatite mineral *de novo,* SAP P_{11}-4 has already shown significant outcomes in hard tissue regeneration applications, being already licensed for clinical use and available commercially as a regenerative treatment for early dental caries, management of dentin hypersensitivity and enamel erosion (Brunton *et al.*, 2013, Ravichandran *et al.*, 2014, Ceci *et al.*, 2016, Schlee *et al.*, 2018, Whitworth, 2018, Jablonski-Momeni *et al.*, 2019). It also holds a promising potential to be used as a scaffold for BTE with the possibility to enhance the bone matrix mineralisation process; as was demonstrated by a number of previous studies (Burke, 2011, Saha *et al.*, 2019).

1.9. Addressing relevant gaps in research

Based on what has been reviewed above, the current literature clearly recognised the shortcomings of the conventional clinical methods used for managing bone defects, with no single option being able to convincingly demonstrate its efficiency when compared to others. This is true even for autografts, which are considered to be the gold standard for bone replacement, as was discussed earlier in (*1.5*). The revolutionary introduction of TE for skeletal tissue regeneration and the intensive research work produced in the field within the last two decades has made this technology more promising and formed its role in future clinical applications (Nishi et al., 2012).

HDPSCs have attracted much attention as a stem cell source for BTE, offering the advantages of being more accessible, richer with MSCs and having higher proliferation rates compared to other cell sources (like bone marrow derived stem cells) when cultured under similar conditions (Gronthos *et al.*, 2002). Several studies have shown that hDPSCs were successfully used for bone TE studies both *in vitro* and *in vivo* (Zhang *et al*, 2006; d'Aquino *et al*, 2008; Morad *et al*, 2013).

Another important consideration in developing strategies for bone TE is the choice of scaffold material and the geometry of its internal structure (Knychala et al., 2013, Li et al., 2014). Synthetic polymers PLA are mechanically strong and have excellent manufacturer control over a wide range of porosity and degradability characteristics (Ma, 2004; Serra et al, 2014). Scaffold internal geometry is strongly related to the techniques used for its fabrication (Ma, 2004). Having the option of 3D printing would aid in overcoming the limitations of conventional scaffold fabrication techniques (as was discussed earlier in *1.7.1.2*) and give the opportunity to generate reproducible pore size, distribution, and geometry within PLA scaffold and control the interconnections between the pores themselves, which has a crucial effect on how deep the cells can migrate inside the scaffold, and how efficient vascularisation in different areas within the scaffold can be achieved (Sachlos and Czernuszka, 2003 , Novosel et al., 2011). In the literature, different designs of 3D printed PLA scaffolds have been suggested to support skeletal tissue (Hutmacher et al., 2001, Yilgor et al., 2008, Lee et al., 2012). However, each of those fibre printing layouts generated variable pore sizes and geometries which can have direct effects on cells attachment and tissue ingrowth within the scaffold both *in vitro* and *in vivo* (Domingos et al., 2013). For this reason, the selection of the optimum 3D printing layout for PLA polymer scaffolds is one important factor to be investigated for improved bone regeneration outcomes. To the author's best knowledge, no previous research could be found in the literature to investigate the effect of 3D printed PLA fibre geometry on hDPSCs attachment, growth and osteogenic differentiation.

Finding an efficient technique to enhance PLA inert surface chemistry is another research area that has been investigated; with different methods suggested in the literature to achieve this aim (those were discussed earlier in *1.7.1.4*). Incorporating

SAPs into PLA scaffolds could contribute to this aspect, as these hydrogels have the ability of spontaneous assembly into well-organised 3D fibres and thus can serve as a synthetic analogue for extracellular matrix, which can hypothetically enhance cellular attachment, growth, differentiation (Hosseinkhani, 2006, Horii *et al*, 2007, Semino, 2008, Nisbet *et al*, 2012). SAP P_{11}-4 is a member of biomimetic SAPs family that has already been approved for clinical use in enamel regeneration (Brunton *et al*., 2013) for its unique potential to drive *de novo* mineral nucleation (Kirkham et al., 2007). This property can offer significant advantage when employed for bone regeneration, as it can hypothetically enhance neo matrix mineralisation. A great deal of work towards that was carried out by Burke *et al* (2011) and Saha *et al* (2019), as results of both studies were promising with respect of successful use of SAP P_{11}-4 as a scaffold for *in vivo* bone repair. However, these studies addressed the mechanical weakness of SAP gel scaffold as an issue which needs to be improved. In addition, Saha's group study debated the benefits of adding hDPSCs as a cellular component to SAP P_{11}-4 scaffold on the overall bone defect healing outcome. Incorporating SAP P_{11}-4 gel within a rigid 3D printed PLA framework seems to be a tempting novel approach to be investigated as a scaffold for BTE, proposing a solution to enhance SAP hydrogel mechanical properties. To the author best knowledge, this had not been evaluated in previous research. Moreover, including hDPSCs within the proposed PLA/ SAP P_{11}-4 scaffold would be another aspect to be looked into in more details to assess the novel scaffold effect on these cells' growth and osteogenic differentiation both *in vitro* and *in vivo*.

CHAPTER TWO

Aims and objectives

Chapter 2. Aims and objectives

2.1. Aims

This long-term aim of the research to which this thesis has contributed was to regenerate bone using 3D printed scaffolds. The **specific aim of this thesis** was to investigate, both *in vitro* and *in vivo,* the use of hDPSCs combined with 3D printed PLA scaffolds of different architectures with/ without self-assembling peptides (SAPs) as constructs for bone tissue engineering applications.

2.2. Objectives

- To isolate hDPSCs from human dental pulp tissue collected from the freshly extracted third molars of three donors; followed by their expansion in monolayers and cryopreservation.

- To characterise the isolated hDPSCs using trilineage differentiation (osteogenic, chondrogenic and adipogenic) methods *in vitro*.

- To evaluate the effect(s) of PLA 3D scaffold architecture on hDPSCs attachment, growth and osteo-differentiation *in vitro*

- To evaluate the bone regeneration potential of hDPSCs-3D printed PLA constructs *in vivo* using a diffusion chamber model implanted in CD1 immune-deficient nude mice.

- To investigate the effect(s) of combining SAP P_{11}-4 with the selected 3D printed PLA scaffold on hDPSCs attachment, growth and osteogenesis both *in vitro* and *in vivo*.

CHAPTER THREE

General materials and methods

Chapter 3. General materials and methods

This chapter includes the general materials and methods that were used throughout the project. Any other specific methods will be described in the appropriate chapter.

3.1. General materials

Reagents including phosphate-buffered saline (PBS) (calcium and magnesium free), alpha modified minimal essential medium (α-MEM) and foetal calf serum (FCS), L-glutamine, penicillin / streptomycin antibiotic mix and trypsin-EDTA were purchased from Lonza, Slough, UK.

All centrifuge tubes, Eppendorfs, stripetts and tissue culture (TC) vessels (surface treated flasks, plates and flat bottom well plates) were from Corning, Flintshire, UK unless stated otherwise.

3.2. Different compositions of the prepared medium used in hDPSCs cell culture throughout the project

All of the medium types used frequently in this project are described in (Table 3-1) below along with their components.

Table 3‑1: Definition of mediums used frequently in the project with any additional components

Medium name	Description
Plain medium	α-MEM medium alone without additives
Basal medium	α-MEM medium with 10% FCS, 1% L-glutamine and 1% penicillin/ streptomycin antibiotic
Cryopreservation medium	Medium used to cryopreserve hDPSCs, containing comprising of 50% FCS, 40% basal medium and 10% dimethyl sulfoxide (DMSO) (Millipore, Darmstadt, Germany).
Osteo-inductive medium	Medium used to induce hDPSCs through osteogenic cues, comprising of α-MEM with 10% FCS, 1% L-glutamine, 1% penicillin/ streptomycin, 100 µM L- ascorbic acid (LAsc) (Sigma-Aldrich, Gillingham, UK) and 10 nM dexamethasone (Dex) (Sigma-Aldrich, Gillingham, UK)
Digestive medium	Medium used for digestion of isolated dental pulp tissue prior to primary culture, comprising of plain medium with 3 mg / mL of collagenase- I and 4 mg / mL of dispase (both from Gibco Life Technologies, Loughborough, UK).

3.3. *In vitro* isolation and expansion of hDPSCs

3.3.1. Isolation of hDPSCs from sound human third molars

After approval from the Dental Research Ethics Committee (DREC No: 101114/RA/150), third molar teeth were collected from Leeds' Dental School Tissue Bank to be used for dental pulp stromal cell isolation and characterisation. Teeth from

five donors (3 females, 2 males with an age range of 18-25) were used as a source of hDPSCs throughout the project.

The freshly extracted teeth were stored in a sealed container at -2° C in the cold room (without a medium to avoid pulp contamination) to be used for hDPSCs isolation within a maximum of 48 hours after the extraction to ensure pulp cells vitality. Cell isolation via enzymatic digestion was performed as described previously (Tirino *et al.*, 2012). Immediately before cell isolation, the tooth surface was decontaminated with 70% ethanol for 30 seconds, then soaked in plain medium to avoid dehydration. The tooth surface was then carefully scraped clean using a sterile surgical blade to remove any remnants of gingival and periodontal tissues attached to the outside of the tooth. The tooth was then placed inside three layers of sterile surgical gloves and cracked using a vice. The tooth, still inside the glove, was then taken inside a class II tissue culture hood where all of the remaining steps were performed. The crushed tooth material was emptied into a large, sterile petri dish and the pulp tissue carefully detached from the surrounding tooth fragments and washed with the plain medium before being placed in a second sterile petri dish soaked with plain medium to maintain hydration. About 2-3 mm of the apical part of the pulp tissue was excised and discarded; then the remaining pulp tissue was chopped as fine as possible with a large surgical blade and placed in a small Eppendorf tube with 1 mL of digestive medium (described in *3.2)*. All the Eppendorfs were then placed within a MACSmix™ Tube Rotator (Miltenyi Biotec, Bergisch Gladbach, Germany) and incubated at 37° C, 5% CO_2 for 45-60 minutes to ensure maximum pulp tissue digestion. Samples were then centrifuged at 1.2 relative centrifuge force (rcf) for 5 minutes to obtain a cell pellet. The supernatant was carefully aspirated, and the cell pellets were re-suspended in a T25 flask with 7 mL of the basal medium then incubated in 37° C, 5% CO_2 and checked daily for cellular

attachment and growth and any possible fungal infection. The isolated cells reached around 80-90% confluence within 4-6 days, during which time the medium was changed regularly every three days. When the cells were almost confluent, the cells were passaged into P1, 3 T75 flasks, as described in *3.3.2*. Figure (3-1) highlights the hDPSCs isolation steps.

3.3.2. Cell detachment and passage

When the cells across the flask had reached about 80-90% confluence, the cell monolayer was washed twice with 10 mL of PBS and incubated with trypsin- EDTA (ethylene diamine tetraacetic acid) (Lonza, Slough, UK) at 37° C for 5 minutes (5 mL for cells in a T75 flask). Cell detachment was checked under the microscope. When the cells were fully detached, the trypsin solution was deactivated by adding 5 mL of basal medium to the upright-held flask. This procedure will be termed "trypsinisation" throughout the project (Harrison and Allen, 1979). The flask contents were then transferred to a 15 mL universal centrifuge tube and centrifuged at 1.2 rcf for 5 minutes

1. Extracted wisdom tooth from tissue bank

2. The tooth was cracked to isolate dental pulp tissue

3. Pulp tissue was isolated in sterile conditions

4. Pulp tissue was finely minced

5. Minced pulp tissue was placed in cell mixer for 1 hour with digestion medium to be enzymatically digested

6. Isolated hDPSCs were seeded in T25 flask to grow
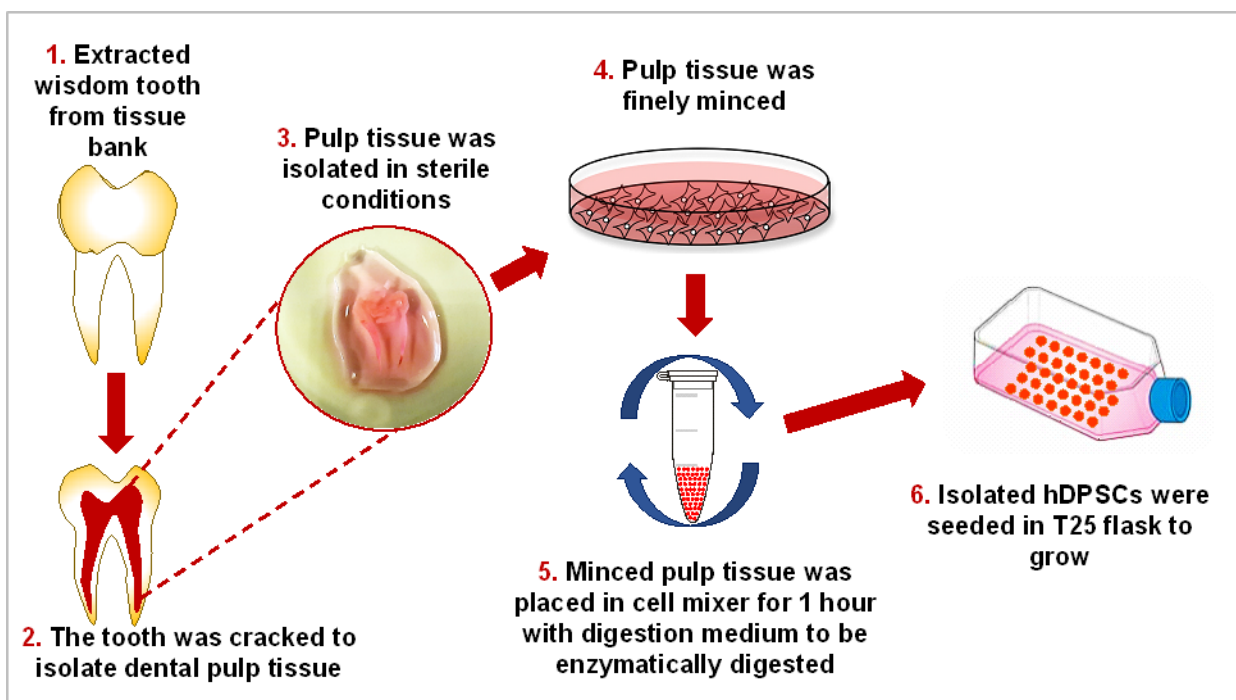
Figure 3-1: Diagram showing the hDPSCs isolation procedure

to obtain a cell pellet. After aspiration of the supernatant, the cell pellet was re-suspended in 2 mL fresh basal medium and aliquoted to several new TC flasks (T25, T75 or T175) according to the cell density required for each particular experiment. The total volume of medium in the new flask (after addition of cell suspension) was topped up with basal medium to be maintained at 7 mL, 15 mL or 25 mL in T25, T75 and T175 flasks respectively. The cell suspension was mixed well, encouraging cells to spread evenly on the bottom of the flask. The flasks were then incubated at 37° C, 5% CO_2 and not less than 90% humidity. The medium was regularly changed twice per week until the cells had reached the required level of confluence.

3.3.3. Cryopreservation of hDPSCs

Where cells were not immediately required for experimental use, they were cryopreserved (Tirino *et al.*, 2012). Briefly, when the cells across the flask had reached 80-90% confluency, the culture medium was aspirated from each flask, the cells were gently washed twice with 10 mL PBS, trypsinised and centrifuged as described previously (*3.2.2*). Each cell pellet was re-suspended in 1.5 mL cryopreservation medium (see *3.2.*). Cell samples were then placed in 2 mL cryovials (Star Lab, Blake lands, UK), and placed in a "Mr Frosty" freezing container (Nalgene ®, Neots, UK) with 100% isopropyl alcohol to be stored at -80° C short term (up to 6 months) until used for experiments. For cell samples that were stored for longer terms, the containers were transferred to the main lab liquid nitrogen cryostore tank with -130 ° C freezing temperature.

3.3.4. Resuscitation of cryopreserved hDPSCs

Whenever required for experimental work, cryovials containing hDPSCs (prepared previously as described in *3.3.3*. above) were taken out of the -80° C deep freezer (or

liquid nitrogen cryostore) and thawed in a water bath at 37° C for about 1 minute. The vial content was transferred into a 15 mL universal centrifuge tube and topped up with 1 × PBS to 5 mL at room temperature. A cell pellet was obtained by centrifuging the sample at 1.2 rcf for 5 minutes. The supernatant was then aspirated, and the cell pellet was re-suspended in fresh basal medium. The cell suspension was then transferred into a TC flask (T25, T75 or T175 as required) with fresh medium (5 mL, 15 mL or 25 mL respectively) and incubated at 37° C, in 5% CO_2 and at not less than 90% humidity. The medium was changed the next day to remove any floating dead cells, then changed regularly twice per week until the cells reach the desired confluence.

3.3.5. Seeding hDPSCs at different densities

After trypsinisation, the cells were re-suspended in 4 mL of the fresh basal medium then the cell number within the suspension was counted using 20 μL of the cell suspension, loaded into a haemocytometer chamber (HCM) (Hawksley, Sussex, UK). The number of cells/mL was calculated as follows, taking into account any dilution factor wherever required (Hughes and Mehmet, 2003, Camacho-Fernández et al., 2018):

$$\text{No. of cells per mL} = \left(\frac{\text{Cell count by HCM}}{4}\right) \times 10000$$

The volume of cell suspension needed to seed cells at the required density was calculated as follows:

$$\text{Volume of cell suspension} = \frac{\text{Required cell density X vessel surface area}}{\text{No. of cells per mL}}$$

HDPSCs were then seeded at specific densities into different TC flasks and well plates as required by each experiment. For 3D scaffolds, the required seeding density was calculated by setting the number of cells per 1 mL of cell suspension that was required to be seeded onto individual scaffold sample.

3.3.6. Osteogenic induction of hDPSCs

Osteogenic induction of hDPSCs (either in monolayer or for 3D culture), was carried out by first seeding the cells in the TC vessel with a basal medium. When the cells across the flask had reached about 80%-90% confluence, the basal medium was replaced with osteo-inductive medium (L-ascorbic acid (LAsc) and dexamethasone (Dex) used in the medium was from Sigma-Aldrich, Gillingham, UK). The osteo-inductive medium was changed regularly twice per week. G_{292} human osteosarcoma cells (European collection of cell cultures, ECCAC, clone A141B1, passage 22) were used as a positive control whenever required in these experiments using the same cell culture as used for hDPSCs. G_{292} cells were seeded on 6 and 24 well plates ($5x10^3$ cell/mL density) and maintained in the basal medium until fully confluent. At this point they were washed twice with 0.5 mL PBS/ well, fixed with 98% ethanol for 20 minutes then air-dried and stored in a cold room at -2° C until required.

3.3.7. *In vitro* culture of hDPSCs on 3D scaffolds

Scaffold material used throughout this project was 3D printed polylactic acid (PLA), obtained as part of a collaboration with Dr Chaozong Liu and his team (John Scales Centres for Biomedical Engineering, Institute of Orthopaedics and Musculo-Skeletal Science, Stanmore, London). PLA scaffolds were fabricated using a 3D printer that utilises fused deposition modelling (FDM) technology by heating and extruding thermoplastic filament in overlapping layers into 7x7x3 mm^3 discs. Two groups, each with different PLA fibre layouts (0\90° and 0\45°\90°\135°) were provided; both with

0.5 mm PLA filament diameter. After printing, PLA scaffolds were subjected to 10 minutes of nitrogen plasma processing to improve their surface wettability.

3.3.7.1. Scaffold sterilisation and surface conditioning

PLA discs were divided into two halves using a scalpel blade. The scaffolds were sterilised inside a TC hood with direct exposure to UV light from a TC hood steriliser for 15 minutes on each side. A small black dot was placed on the bottom of each scaffold using a permanent marker pen to define seeding direction. Scaffolds were immersed in a plain α-MEM medium at -2° C overnight prior to cell seeding to increase surface wetness. Scaffolds used as negative controls were immersed in plain α-MEM medium without serum.

3.3.7.2. Fluorescence labelling of hDPSCs with CMFDA live marker

In order to make cells visible when attached to the scaffolds, the cells were fluorescently labelled with a live marker before proceeding to the scaffold seeding process. Depending on the number of cells required for a particular experiment, an appropriate flask size was selected and seeded with hDPSCs at the required cell density, then incubated at 37° C, in 5% CO_2 and at not less than 90% humidity until 80-90% confluence was attained (as described in *3.3.2*) prior to scaffold seeding to be ready for cell labelling at the day of the experiment. For live-cell labelling, 50 μg CMFDA (chloromethyl fluorescein diacetate) cell tracker powder (Life Technologies, Waltham, USA) was dissolved in 10 μL of DMSO and kept protected from light. Five mL of plain medium was added and mixed well with the dissolved CMFDA cell tracker to prepare the labelling medium. The existing medium was aspirated from the flask containing confluent cells, and the cell monolayer was washed twice with 10 mL PBS. For a T75 flask, 5 mL of the labelling medium prepared as described above was added

to cover the monolayer. The flask was then protected from light and incubated at 37° C, 5% CO_2 for 45 minutes, after which the labelling medium was aspirated and replaced with 5 mL of plain medium. Th flask was then re-incubated while protected from light for a further 45 minutes to wash off the excess background fluorescent labelling. The washing medium was then aspirated, and the labelled cells were then ready to be seeded on to a 3D scaffold.

3.3.7.3. Static seeding of fluorescence labelled hDPSCs on 3D scaffolds

Static seeding of hDPSCs on PLA scaffolds was generally performed as described previously in the literature (Vunjak-Novakovic and Radisic, 2004, Villalona *et al*., 2010). After labelling hDPSCs with CMFDA life marker as described in *3.3.7* above, the labelled cells were detached and re-suspended in 2 mL of plain medium (as described in *3.3.2)*. Cell counting with HCM was carried out as described in *3.3.5,* after which the required volume of cell suspension was aspirated and diluted with plain medium to obtain $2x10^5$ cells \ mL\ sample. One millilitre of the final cell suspension was carefully added over the surface of each scaffold, which was placed at the bottom of a 5 mL sterile tube. The tube caps were replaced and ¼ - circle loosened to allow for gaseous exchange, followed by incubation at 37° C with 5% CO_2 for at least 4 hours before checking cellular attachment on scaffolds.

For monitoring hDPSCs' viability on scaffolds after culture, a live-dead labelling medium was prepared. To prepare this medium, 5 mL of CMFDA-containing medium was prepared as described in *section 3.3.7.2* above to be used for live-cell labelling. To label dead cell, ethidium homodimer-1 (EHD-1) (Life Technologies, Waltham, USA) dead marker was added (40 µL of EHD1 liquid) to the prepared 5 mL CMFDA-containing medium. The constructs requiring live-dead labelling were placed in a 24 well-plate and immersed with 0.5 mL\ sample of labelling medium, then incubated

(protected from light), at 37° C, 5% CO_2 for 45 minutes. The following procedure was exactly the same as that applied for live-cell labelling as described earlier in this section.

3.3.8. Sample imaging methods

3.3.8.1. Stereomicroscopy

A light stereomicroscope (VM-4F, Olympus Hamburg, Germany) was used to image well plates, and 3D samples under low magnification (x1, x4) wherever required.

3.3.8.2. Fluorescence imaging of seeded scaffolds

The fluorescence-labelled samples were imaged via the Zeiss fluorescence inverted microscope (Axio-Vert A1, Oberkochen, Germany) using ZEN 2 blue digital software for image processing (Carl Zeiss microscopy, Göttingen, Germany).

3.3.8.3. Scanning electron microscopy (SEM) and energy-dispersive X-ray spectroscopy (EDS) analysis

Whenever SEM and\or EDS were required, the samples were washed with 1x PBS, then fixed in 10% neutral buffer formalin (NBF) before being kept in the cold room ready for imaging. Samples were washed twice in PBS immediately before putting into the SEM. A low-vacuum, environmental SEM fitted with a -20° C cold stage sample-holder (Hitachi, Tokyo, Japan) was used, in back-scattered emission (BSE) X-ray mode with 20.0 kV voltage. Applying similar SEM settings to those mentioned above, QUANTAX EDS for SEM (Bruker, Massachusetts, USA) elemental analysis was used whenever required. To do so, the "Stage> Analyse" function on the SEM software was selected to redirect sample analysis to the EDS function, where parameters such as selective element spectrum, elemental image mapping and element atomic ratio quantification could be applied.

3.4. Experimental work using animal models

3.4.1. Preparation of diffusion chambers

Diffusion chambers (DCs) are devices for implantation *in vivo* that are used to isolate tissue-engineered implanted constructs from the cells of the animal host, allowing only nutrients and waste exchange through the chamber's membranes (Ashton *et al.*, 1980). For the projects described in this thesis, all *in vivo* experiments used a modification of a DC method previously described in the literature (Breivik *et al.*, 1971, Ashton *et al.*, 1980, Yang *et al.*, 2003, Yang *et al.*, 2004). A custom-made DC comprising of coloured plastic autoclavable rings (8x4 mm) that were sealed with two 13 mm diameter, mixed cellulose ester (MCE) hydrophilic membrane 0.22 μm filters (Millipore^{TM,} Darmstadt, Germany) were used. One side of the ring was first sealed with the filter membrane using cyanoacrylate superglue (Loctite, Farnell, UK). The excess membrane was trimmed out with a scalpel blade after the glue had set and the resulting one-end-sealed DCs were then UV sterilised for 15 minutes on each side. On the day of *in vivo* surgery, each chamber was filled with plain α-MEM medium, and the prepared constructs were inserted inside. The open end of the DC was then sealed with the second filter membrane, again using superglue. Different colour rings were used to permit different construct groups to be identified. When the glue had dried, the excess membrane was trimmed, and the chambers with the constructs *in situ* were transferred to the surgical theatre in parafilm-sealed well plates filled with plain α-MEM medium ready to be implanted into the animal hosts. Figure (3-2) illustrates the DC preparation procedure.
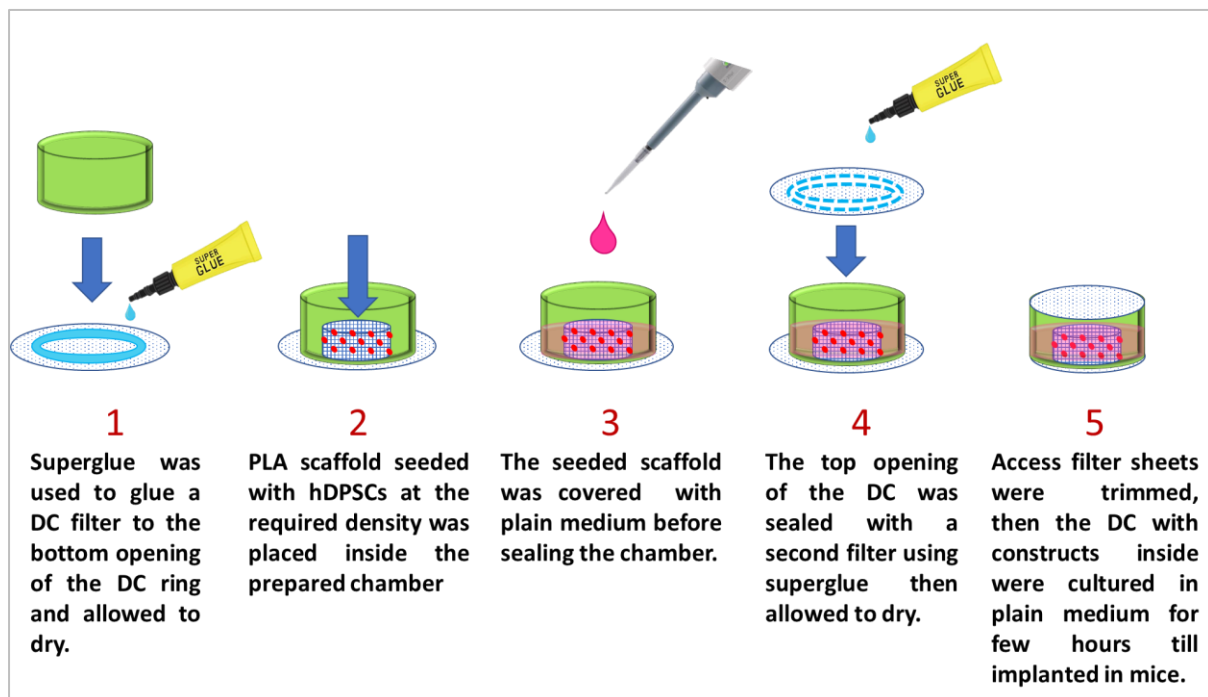
Figure 3-2: A diagram illustrating preparation steps of diffusion chambers prior to implantation intraperitoneally in nude mice

3.4.2. Diffusion Chamber intra-peritoneal implantation in CD1 nude mice

All animal work throughout this project was conducted under a Home Office personal licence (IAD815DD7) and a project licence (PPL70/8549). Diffusion chambers were prepared as described above (***section 3.3.1***). The animal model selected for these *in vivo* experiments were male CD1 nude mice, 8 weeks of age and of approx. 25 ± 3 g in weight. A randomised sample grouping chart was generated using Excel to ensure random implantation of samples within the individual animals. The mice were anesthetised using liquid isoflurane (Zoetis – Iso Flo), 100% w/w inhalation vapour was supplied using a special vaporizer (Vet Tech Solutions Ltd) with the mice in an inhalation chamber. The primary dose of isoflurane in the inhalation chamber was 5 L/min for induction; the animals were then maintained at 2.5 L/min using a close-fit gas mask during the surgery (Figure 3-3 A). The oxygen supply was maintained throughout the procedure at a flow rate of 5 L/min. A midline abdominal skin incision

(1-1.5 cm) was made on the animal's ventral surface using a scalpel blade no. 15 (Figure 3-3 B). Careful traction of the underlying peritoneal wall was maintained using artery forceps. A small hole was then made in the wall, taking care not to damage the organs underneath. The initial hole was then enlarged carefully using scissors (Figure 3-3 C). Two DCs per animal were carefully slid into each side of the peritoneal cavity (Figure 3-3 D). The peritoneal wall was sutured using absorbable coated 5/0 vicryl sutures. In comparison, the outer skin was closed using non-absorbable 5/0 polyamide sutures (both supplied from Ethilon, Miller Medical Supplies, Newport, UK) (Figure 3-3 E and F). The animals' ears were punched for identification, and an analgesic (Vetergisic, CeVa, Amersham, UK) 0.3 mg/ mL was then given intraperitoneally to each animal. When the procedure was completed, the animals were moved to pre-warmed recovery chambers until fully recovered from anaesthesia. They were then housed in an Individually Ventilated Cage (IVC) system, checked daily for any possible gross complications by the facility technicians' team and twice per week by the operator up to the time of euthanasia. At different time points, the animals were sacrificed by the Home Office approved Schedule 1 method.
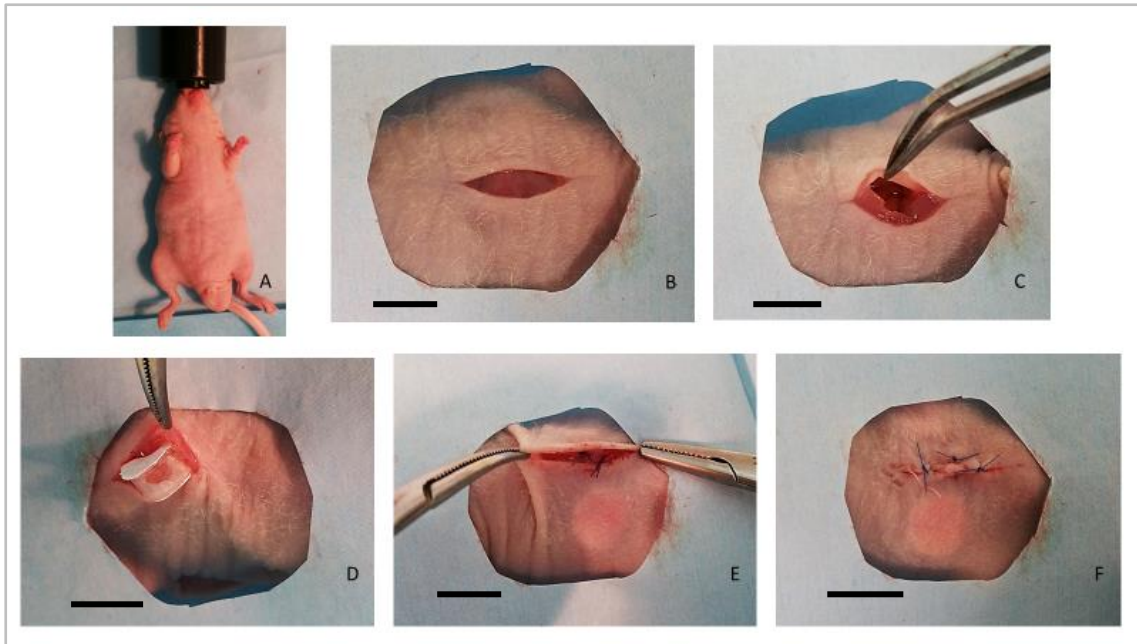
Figure 3-3: Implantation of DC in CD1 mice. A: Isoflurane face mask adapted to mouse nasal protrusion. B: Mid-midline 1-1.5 cm ventral skin incision. C: Cutting through and undermining the underlying peritoneal wall. D: Sliding the DC inside the mouse peritoneal cavity. E: Suturing peritoneal wall with absorbable 5/0 vicryl suture. F: Suturing skin incision using 5/0 non- absorbable polyamide suture (scale bar = 1 cm).

3.5. Histological characterisation of HDPSCs under different conditions

All histological protocols used throughout this project were performed following procedures that were previously optimised by the histology technical team in the Division of Oral Biology, Leeds School of Dentistry, or using protocols provided by the manufacturer that will be referred to wherever applied. All procedures, including fixation, processing, embedding, sectioning, staining, microscopy and photography, were applied and carried out by the author.

3.5.1. Preparation of 3D scaffolds for histology

3.5.1.1. Sample fixation, processing, embedding and sectioning

Histological processing, embedding and sectioning described below were first performed by the author on PLA scaffolds alone to optimize the procedures before applying them on the cultured constructs. For the 3D constructs with hDPSCs, the

samples were fixed with 10% neutral buffered formalin (NBF) for 24 hours at room temperature at the selected time point, then processed using a Shandon Excelsior ES tissue processor (Thermo Scientific, Loughborough, UK) (using an overnight processing cycle. Construct samples were taken thorough the following steps:

- NBF 10% 30 minutes x2

- Ethanol 70% for 1 hour x1

- Ethanol 90% for 1 hour x1

- Ethanol 100% for 1 hour x4

- Pure xylene for 1 hour x3

- Paraffin wax immersion for 1hour and 20 minutes x3

After processing was completed, the samples were embedded in paraffin wax to be sectioned using a Leica RM 2135 rotary microtome (Leica biosystems, Nußloch-Germany) to produce 5 μm thick sections. The sections were then mounted on to histology-grade glass slides (Thermo-Fisher Scientific, Loughborough, UK) from a water bath at 40° C, dried on a hot plate for 15 minutes and then placed in an incubator at 37° C overnight before histological staining.

3.5.1.2. Taking sections to water (section rehydration)

After mounting the sample sections on microscopy slides, the sections needed to be completely cleared of wax before being rehydrated again to be ready to receive the histological stains. This is termed as "taking sections to water". It was achieved by first dewaxing the slides with xylene for 5 minutes, then clearing them with a second xylene immersion for a further 5 minutes. Afterwards, the sections were moved to 2 successive absolute ethanol immersions of 5 minutes each before being taken to the tap water wash tub.

3.5.2. Staining of histological samples

3.5.2.1. Haematoxylin and Eosin (H-E) staining

This is a non-specific histological staining method that is used to examine the general structure of tissues. Haematoxylin stains nuclei violet, while eosin stains cytoplasmic material and matrix background different shades of pink. After taking sections to water, they were immersed in Harris' haematoxylin (Surgipath, Linford Wood, UK) solution for 4 minutes, then washed under running water. Afterwards, the sections were dipped 3 times in 1% acid alcohol (concentrated hydrochloric acid in 70% ethanol) and then washed under running water. Then the samples were immersed in Scott's tap water (Surgipath, Linford Wood, UK) for 2 minutes and washed again under running tap water before being placed in aqueous eosin (Surgipath, Linford Wood, UK) for 4 minutes. The sections were then washed in water, taken to 2 successive immersions in absolute alcohol for 5 minutes each, cleared with xylene for a further 5 minutes and finally mounted with a coverslip using Di-butyl-phthalate Polystyrene Xylene (DPX) non-aqueous mounting solution (Agar Scientific, Essex, UK).

3.5.2.2. Wiegert haematoxylin- Alcian blue- Sirius red stains

A combination of stains was used as part of the evaluation of the newly formed extracellular matrix within the cultured constructs. Wiegert haematoxylin was used to stain nuclei, along with Alcian blue (AB), which is mainly used to visualise proteoglycans that are usually associated with the chondrogenic activity. Sirius red (SR) stain is generally used to detect the presence of collagen. The protocols used for the application of those stains were according to manufacturer instructions for each.

The Wiegert haematoxylin stain used here consisted of two ready-made reagent solutions, A (methanol haematoxylin) and B (iron III chloride 6 H_2O) (Polysciences inc., Bergstraße, Germany). The working stain was prepared fresh each time by mixing

equal volumes of solutions A and B. After taking sections to water; they were immersed in Wiegert stain for 10 minutes, then washed thoroughly under running water before being immersed in AB stain (8GX AB in acetic acid solution, TCS Biosciences, Buckinghamshire, UK) all as supplied by the manufacturer, for another 10 minutes. After washing in running tap water, the sections were then stained with different stains according to the specific experiment.

An SR staining kit (Polysciences inc., Bergstraße, Germany) was used. This involved staining sections in 3 solutions successively; solution A (phospho-molybdic acid hydrate) for 3 minutes, solution B (picrosirius direct red stain) for 60 minutes, and solution C (1 M hydrochloric acid) for 3 minutes, all as supplied by the manufacturer. The sections were then washed, dehydrated with two changes of absolute ethanol (5 minutes each), then finally cleared with xylene before being mounted with DPX.

3.5.2.3. Van Giessen and Safranin red stains

These are general counterstains that are used to stain the matrix background in different shades of red. After sections were taken to water and following application of any nuclear or other special stains, the sections were washed in tap water and placed in either Van Geissen (VG) stain (for collagen) (Dorn & Hart Microedge, Loxley, UK) or Safranin red stain (Sigma-Aldrich, Gillingham, UK) (usually used for detection of cartilage formation, here it was used as a general background stain) for 5 minutes. The slides were finally dehydrated, cleared and mounted with DPX for future examination.

3.5.2.4. Alkaline phosphatase (ALP) staining

ALP staining was used to detect the activity of alkaline phosphatase enzyme, which is considered as an early marker for osteogenesis and was applied directly to both monolayer and 3D cultures. ALP stain working solution (10 mL) was prepared by

72

adding 0.4 mL of naphthol AS-MX phosphate (Sigma-Aldrich, Gillingham, UK) to 9.6 mL of distilled water (dH$_2$O). Then 4.2 mg of Fast Violet stain powder (Sigma-Aldrich, Gillingham, UK) was added to the solution immediately before staining. After samples were washed twice with PBS and fixed with 98% ethanol (in the case of monolayers) or 10% NBF (in the case of 3D cultures) for 20 minutes, ALP stain working solution was added to cover the sample of interest. Samples were then incubated at 37°C in the dark for 30-60 minutes (checking the colour change every 5-10 minutes). The reaction was stopped by washing the samples with dH$_2$O.

3.5.2.5. Alizarin red staining

This stain (Al-R) is used to detect calcium deposits within samples, which are visualised as red-stained areas when positive. In this project, this stain was applied directly on to hDPSCs monolayers only, using the manufacturer's protocol. Monolayer samples were washed twice with 1x PBS and fixed with 98% ethanol for 20 minutes, then Al-R ready-made solution (Millipore, Darmstadt, Germany) was added to each sample (500 μL/well for a 24 well plate, 1 mL/ well for 6 well plate). Samples were all then incubated at room temperature for 15 minutes and washed with several changes of dH$_2$O over 5 minutes.

3.5.2.6. Von Kossa (VK) staining

VK is used to indirectly detect the presence of phosphate-containing mineral deposition within the samples, seen under a light microscope as a black or dark brown colour. In this project, both cell monolayers and histological sections were stained using this procedure. In both cases, the samples were immersed in 10% silver nitrate solution (Von Kossa stain kit, Atom Scientific, Cheshire, UK) for up to 60 minutes in a UV light chamber, then washed twice with dH$_2$O before being incubated in 5% sodium thiosulphate for 5 minutes to remove any unreacted silver (as described by the

manufacturer). When counterstaining was required, monolayers were stained with Van-Geisson, safranin red or Harris' haematoxylin for 5 minutes (please see ***3.5.2.1.*** and ***3.5.2.3***) then washed in dH_2O and left to air dry; while for histology slides, any of the above-mentioned counterstains were also applied for 5 minutes then washed in dH_2O prior to dehydration, clearing and mounting with DPX (please see ***3.5.2.1***.).

3.6.   Immunohistochemistry (IHC) staining

Similar methods of sample fixation, histological processing and sectioning were used for the preparation of slides for IHC as described for general histology (please see ***3.5.1.1***) but with some modifications. Attention was paid not to fix samples for more than 24 hours in 10% NBF to avoid antigen masking. Extra adhesive slides (Leica Pink X-tra slides, Breckland, UK) were used to mount the sections to ensure maximum survival of the sample on the slides after IHC staining. It was also important not to place samples directly on to the hot plate to avoid antigen denaturation by heat.

Three primary antibodies were optimised for use in the characterisation of osteogenic differentiation within the samples wherever required throughout these experiments. Suitable sections for use as positive controls were selected according to the manufacturer's recommendations for each antibody. These were then used for the optimisation of the antibodies. Full details about the antibodies used can be seen in (Table 3-2) below:

Table 3‑2: Antibodies used in this project

Antibody	Brand and catalogue number	Species reactive against	Positive control	Optimised antibody dilution
Monoclonal mouse anti-Collagen – I (Col-I) antibody (Primary antibody)	Abcam (ab6308)	Rat, rabbit, cow, cat, dog, human, pig, monkey, rhesus monkey and deer	Human dental pulp	1: 150
Monoclonal, mouse anti-human anti-osteopontin (OPN) antibody (Primary antibody)	Santa-Cruz (sc-73631)	Rat, human	Rat femur	1: 100
Monoclonal, mouse anti-osteocalcin (OCN) antibody (Primary antibody)	Abcam (ab13420)	Rat, sheep, rabbit, goat, chicken, cow, dog, human and pig	Sheep bone marrow	1:500
Goat anti-rabbit/ mouse immunoglobulins (Secondary antibody)	DAKO Envision kit (K4065)	Rabbit, mouse	-	Ready from kit

The first step for IHC staining was to block exogenous peroxidase within the rehydrated sections with 3% v/v H_2O_2 in methanol for 20 minutes to eliminate any undesired background staining. The samples were then washed in PBS for 5 minutes. Different techniques were checked for the efficiency of antigen retrieval with the three antibodies used. These included:

- Boiling the sections with 0.01 M of citrate buffer in a microwave for 30 seconds, then letting them cool down fully at room temperature.

- Immersing sections in 0.1% chymotrypsin in 0.1% calcium chloride solution for 20 minutes at 37° C in pH 7.8.

- No antigen retrieval.

Both citrate buffer and chymotrypsin methods resulted in negative IHC staining in positive control sections, while the samples without antigen retrieval showed positive stains in different areas within all the positive controls for the 3 osteogenic marker antibodies used.

The sections were first loaded on to Shandon Sequenza immunostaining cassettes (Thermo-fisher scientific, Loughborough, UK) to facilitate further processing. Normal goat serum (NGS) (Agilent Technology- UK) 20% v/v in PBS was applied to the sections for 30 minutes before they were then incubated with the primary antibody. The optimised antibody solutions were then added to the sections, incubated overnight in the cold room at 4° C and then washed twice in PBS. One drop per slide of secondary antibody polymer-HRP (EnVision® + Dual Link System-HRP, Glostrup, Denmark) was then added on to each section and incubated at room temperature for 30 minutes before being washed twice in PBS. Di-Amino-Benzidine (DAB) substrate stain (Abcam, Cambridge, UK) was used to detect antibody activity in each sample by incubating the washed sections for a further 10 minutes. The slides were then

demounted from the cassettes, washed with water, counterstained with Harris'
haematoxylin for 45 seconds, washed under running tap water, dehydrated, cleared
and mounted in DPX on adhesive slides for future examination.

3.7.   Data statistical analysis

All statistical data analyses related to this thesis were performed using T-test applied
by Microsoft Excel 2016 and SPSS – IBM software version 21. Statistical significance
was tested against p-value of 0.05.

CHAPTER FOUR

In vitro characterisation of human dental pulp stromal cells (hDPSCs)

Chapter 4. *In vitro* characterisation of human dental pulp stromal cells (hDPSCs)

4.1. Introduction

Stem cells are characterised by their ability to self-renew and be induced via different cues to differentiate into multiple types of specialised cells (Pereira *et al.*, 1995, Sanchez-Ramos *et al.*, 2000). In their native tissues, their main functions are tissue development, homeostasis and repair in case of damage or disease (Suchanek *et al.*, 2009). Rationally, any tissue that is able to repair itself must contain a reservoir of progenitor and/or stem cells that can contribute to the renewal and/or replenishment of cells in that tissue, including dental pulp (Petrovic and Stefanovic, 2009). However, there is no unique, unequivocal evidence to date to explicitly detect MSCs' possible existence or exact anatomical location within dental pulp stromal tissue (Baksh *et al.*, 2004, Marquez-Curtis *et al.*, 2015). Different approaches have been adopted to demonstrate MSCs' putative existence within pulp stroma; the gold standard of which was suggested to be based on their tendency to adhere to the plastic surface of culture vessels using colony forming unit-fibroblast (CFU-F) assay (Baksh *et al.*, 2004). However, this method has a number of limitations, including inter-protocol variations (Pamphilon *et al.*, 2013) and confounding issues associated with MSCs cross similarities with other cells present within the dental pulp (regarding their ability to adhere to plastic and form colonies *in vitro*) like stromal fibroblasts and pericytes enfolding endothelial cells in micro blood vessels (Dominici *et al.*, 2006, Hematti, 2012, Lv *et al.*, 2014, Marquez-Curtis *et al.*, 2015). Stem cell characterisation could also be verified by positive detection of stem cell surface markers (like STRO-1, CD73 and CD90) along with the negative expression of haemopoietic stem cells markers (like CD34 and CD45) (Dominici *et al.*, 2006, Zhang

et al., 2006, La Noce *et al.*, 2014). Thes attempts to identify MSCs via expression of variably suggested surface markers; however, are still indefinite. To date, there is no single definitive marker to be relied on for their detection, so a list of markers need to be collectively analysed as a reference for MSCs' existence in a culture, making it a time consuming and expensive option compared to other methods (Dominici *et al.*, 2006, Marquez-Curtis *et al.*, 2015). Moreover, the isolation of MSCs based on surface marker expression is quite laborious, not to mention the need for prolonged *in vitro* culture expansion required to obtain sufficient cell numbers for such investigations to be accomplished; this, in turn, can increase the risk of culture ageing and alteration of cellular genetic profile (Dominici *et al.*, 2006, Bueno and Glowacki, 2009, Alsulaimani *et al.*, 2016). In addition, these tests analyse samples in the form of cell suspensions or cell lysates, making information on tissue architecture and cell-cell interactions unavailable (Jahan-Tigh *et al.*, 2012).

Another commonly used method for detecting stem cell existence is to look at their multilineage differentiation capability via different cues under inductive culture conditions (Zhang *et al.*, 2006, Alraies, 2013, Nuti *et al.*, 2016). In a position statement of the International Society of Cellular Therapy (ISCT), this method was described as "the biological property that most uniquely identifies MSCs" with the advantages of being feasible for all investigators due to the relatively similar and reproducible protocols published in the literature and kits being commercially available (Dominici *et al.*, 2006). In addition, this method gives the advantages of a minimal need for expansion of cells in monolayer culture, with the ability to visually monitor changes in cellular morphology and tissue architecture of the same culture at different time points without the need to use culture-destructive methods (Zhang *et al.*, 2006, Mor-Yossef Moldovan *et al.*, 2019).

As the presence and quantity of stem cells within the primary pulp cell cultures used in this study are known to be highly variable between different donors, there was a need to evaluate hDPSCs plasticity from the different donors recruited to this study prior to using the cells in subsequent bone regeneration experiments.

4.2. Aims

The aim of this chapter was to evaluate hDPSCs multilineage differentiation capability *in vitro* using osteogenic, chondrogenic and adipogenic cues in order to provide evidence for the presence of stem cells within the total stromal cell population in the human dental pulp tissue of each of the different donors and to ensure hDPSCs donor quality before being included in formal experiments

4.3. Materials and methods

HDPSCs were isolated from 3 different donors and passaged as previously described in *3.3.1* and *3.3.2.*

4.3.1. Induction of hDPSCs osteogenic differentiation in monolayer culture

The overall culture method for induction of hDPSCs osteogenic differentiation was described in *3.3.6*.

4.3.1.1. Preparation of hDPSCs osteo-induced culture

After resuscitation from the cryo-store (please see *3.3.4*), passage 3 (P3) hDPSCs from 3 different donors were seeded at a density of $3x10^4$ into 24 well plates (as described in *3.3.5*). When the cells had reached 80-90% confluence, 2 groups of samples were generated for each donor; a control group that continued to receive basal medium and an osteo-induced group where the basal medium was replaced with an osteo-inductive one (as described in *3.2)*. Three technical replicates were prepared for each group

(n=3), and 2 sets of 24 well plates were prepared from each donor to be used for ALP staining and quantitative assays. Another 2 sets of 6 well plates were prepared for each donor and each group at a similar density as above (n=3 per group) to be used for Alizarin red (Al-R) and Von Kossa (VK) staining as described below. The medium for all plates was changed twice per week.

4.3.1.2. ALP staining

ALP is a known early marker for osteogenesis. Staining for ALP was therefore used as an indication of hDPSCs osteogenic differentiation. At 14 days of culture, 1 set of 24 well plates/donor was fixed for ALP staining **(**full method of fixation and stain as described in ***3.5.2.4)***. A G_{292} positive control group in 24 well plates (please see ***3.3.6***) (n=3) was included to monitor any possible technical errors.

4.3.1.3. Quantitative evaluation of hDPSCs osteogenic differentiation *in vitro* via alkaline phosphatase specific activity (ALPSA) assay

4.3.1.3.1. Preparation of cells for quantitative assays

At 14 days of osteo-inductive culture, 300 µL of 0.1% Triton X-100 (Fisher Scientific, Pittsburgh, USA) was added to each well containing the hDPSCs monolayers (24 well plate/donor). Each whole plate was sealed by parafilm, then frozen/thawed for 2-3 time to ensure full cell lysis. The bottom of each well was then carefully scraped using a cell scraper, and the cell lysate was mixed well with a pipette to ensure homogenisation.

4.3.1.3.2. PicoGreen® DNA quantification assay

The PicoGreen® assay measures total DNA content as an indirect measurement of cell numbers within a culture. A stock solution of 10 mg/mL DNA was prepared by adding 10.47 mg of DNA acid sodium salt (from herring testes, Sigma-Aldrich, Gillingham, UK) to 1047 µL Tris EDTA buffer (TE*) 1%, pH 7.4 (Sigma-Aldrich, Gillingham, UK). The resulting solution was incubated for 60 minutes at 37° C, with periodic shaking every 10 minutes to ensure full dissolution. This solution was then filtered using syringe driven polyethersulfone (PES) membrane sterile filters (0.22 µm pore size, Millipore, Darmstadt, Germany), and its final concentration was checked using a Nano-drop spectrophotometer (Thermo Scientific ND1000, Loughborough, UK) at a wavelength of 260-280 nm. Then the concentration was adjusted using TE* buffer to achieve the 10 mg/mL DNA stock. A series of dilutions of the DNA stock solution to the standards with final DNA concentrations of 1 ng/ mL, 10 ng/ mL, 50 ng/ mL, 100 ng/ mL, 200 ng/ mL, 500 ng/ mL and 1 µg/ mL. TE* alone was used as the blank (n=3). Ten microliters of cell lysate from each well (prepared in *4.3.1.3.1* above) were added into flat-bottom 96 well plates (n=3), TE* was then added to each well-containing cell lysate to top up the volume to 100 uL\well. One hundred microliters of working PicoGreen® reagent (Life Technologies, Waltham, USA) (1:200 concentration diluted in TE*) was added to each well, and the plate was incubated at room temperature for 3-5 minutes, protected from direct light. The fluorometric analysis was carried out using the Varioskan Flash multimode microplate reader (model 3001, Thermo Scientific,

Loughborough, UK) at wavelengths of 480 nm excitation and 520 nm emission. The final DNA concentration for each sample was obtained by generating an equation from the resultant standard curve.

4.3.1.3.3. Determination of alkaline phosphatase (ALP) activity

Ten microliters of cell lysate from each well (as described in *4.3.1.3.2* above) were added into flat-bottom 96 well plates (n=3). p-Nitrophenyl phosphate substrate (pNPP) (Sigma-Aldrich, Gillingham, UK) was used as a blank solution and six dilutions of Tergitol with NP-40 solution (nonyl phenoxy-polyethoxylethanol) in 70% H_2O (Sigma Aldrich, Gillingham, UK) (10, 50, 100, 200, 300, 400 nM respectively). It was used as the calibration standards (100 µL/ well). For each sample of cell lysate, 90 µL of pNPP was added, and the plate was incubated at 37° C for 30-60 minutes, protected from light. The reaction in all wells was then stopped by adding 100 µL NaOH (1 M) and the time taken for the whole reaction was recorded. The spectrophotometric analysis was carried out using a Varioskan Flash multimode microplate reader at 405 nm wavelength. The standard curve generated, as described above, was used to work out the ALP concentration for each sample. Total ALP activity (nmol/min/well) was obtained by calculating the ALP concentration in the well for the given lysate volume of the sample at a given time, all multiplied by the total volume in that well.

4.3.1.3.4. Determination of alkaline phosphatase specific activity (ALPSA)

In order to take in to account any differences in cell numbers in each of the samples, the total ALPA was normalised to the total DNA content in the same well:

$$\text{ALPSA} = \frac{\text{Total ALP activity per well nmol per hour}}{\text{Total DNA content per well (µg)}}$$

4.3.2. Detection of mineral deposits within the newly formed matrix using Alizarin red (Al-R) and Von Kossa (VK) histological stains

In order to detect any mineral deposit within the extracellular matrix produced by hDPSCs cells were stained using Al-R and VK, as described below.

HDPSCs (P3) from the 3 donors (*4.3.1.1)* were seeded (3×10^4 cell/ mL) into two sets of 6 well plates per donor (n=3). All of the cells were first cultured in the basal medium until they had reached 80-90% confluence (*3.3.6*), then in osteo-inductive medium for 21 days, with the medium being changed regularly twice a week. The samples were fixed (*3.5.2.4)*, then one 6 well plate/ donor was stained with Al-R stain (*3.5.2.5*), and the other was stained with VK stain (*3.5.2.6*). The samples were examined after staining both by visual inspection and under the microscope.

4.3.3. Induction of chondrogenic differentiation of hDPSCs *in vitro* using micro-mass culture

4.3.3.1. Preparation and culture of cell pellets

StemMax™ ChondroDiff medium (Miltenyi Biotec, Surrey, UK) was used to promote chondrogenic differentiation of hDPSCs *in vitro;* this will be referred to as " chondro-inductive medium" throughout the chapter. When using this medium for the first time, it was thawed completely, mixed with 1% penicillin/ streptomycin to avoid bacterial

contamination then pre-dispensed into 1 mL aliquots that were stored at -20 ° C until use. HDPSCs (P3) from 3 different donors were used after their resuscitation from cryostorage into T175 flasks (**3.3.4)** and incubated at 37° C, 5% CO_2 and not less than 90% humidity in basal medium for 2-3 days until 80-90% confluent. The cells were then trypsinised and counted for micro-mass pellets preparation **(3.3.2. and 3.3.5)**.

Three technical replicates were prepared from each donor by aliquoting the cell suspension into three 15 mL centrifuge tubes per donor at a density of 2.5×10^5 cell/ sample. A negative control group (n=3) that did not receive chondro-inductive medium was also prepared from hDPSCs at a similar passage and cell density to the experimental groups. All samples were centrifuged at 1.2 relative centrifuge force (rcf) for 5 minutes to obtain cell pellets. The resulting supernatant was then aspirated carefully, and 1 mL samples of ChondroDiff medium was carefully placed on to each experimental group pellet. The control group received 1 mL of basal medium for each sample. All of the tubes were then loosely capped to allow for gaseous exchange, then incubated at 37° C, 5 % CO_2 and not less than 90 % humidity for 21 days (as recommended by manufacturer's protocol), with the medium been regularly changed twice per week.

4.3.3.2. Use of Alcian blue (AB)- Van Geisen (VG) stains for histological detection of chondrogenic differentiation *in vitro*

At day 21 of cell culture, the medium was aspirated from all samples, and the micro-mass pellets that had formed were washed carefully twice with 0.5 mL/ sample of PBS. All of the samples were then fixed with 0.5 mL of 10 % NBF for 24 hours and washed twice with 0.5 mL/ sample of PBS. A drop of undiluted eosin stain was then placed over each pellet and maintained for 1

min to ease visualisation and handling of the micro-mass. Each pellet was then carefully taken out from its tube and placed in a specimen small biopsy bag (31 × 43 mm) (Thermo Scientific- Shandon, Loughborough, UK) before being placed in the tissue processor plastic cassette to reduce the risk of small specimen loss during processing. All of the samples were then tissue processed and then sectioned (see *3.5.1.1*) ready for histological staining. Wiegert haematoxylin-AB (see *3.5.2.2.*) with VG counterstain (described *3.5.2.3.*) were used to evaluate any possible cartilaginous formation within the pellet micro-masses.

4.3.4. Induction of adipogenic differentiation of hDPSCs *in vitro*

4.3.4.1. Preparation and adipo-inductive culture of hDPSCs

StemMax™ AdipoDiff medium (Miltenyi Biotec, Surrey, UK) was used to promote adipogenic differentiation of hDPSCs *in vitro; ;* this will be referred to as " adipo-inductive medium" throughout the chapter. When using this medium for the first time, it was thawed completely, mixed with 1% penicillin/ streptomycin to inhibit bacterial contamination and then pre-aliquoted in to1 mL aliquots that were stored at -20 °C until use. The cell seeding protocol used was according to the StemMax™ AdipoDiff medium manufacturer manual. HDPSCs (P3) from 3 different donors were used for these adipogenic differentiation experiments. After resuscitation from cryostorage (see *3.3.4.),* hDPSCs were resuspended in StemMax™ AdipoDiff medium and seeded into 4- chambered cell culture slides (Falcon™, Loughborough, UK) at a density of $5x10^4$ cell/ mL/ chamber. Three technical replicates were prepared for each donor, using a separate chamber slide. A further group of hDPSCs (P3, n=3) was similarly

prepared and cultured in basal medium to be used as a negative control. A positive control group of P7 adipose-derived stromal cells (ADSCs) (STEMPRO® Human Adipose-Derived Stem Cells, Thermo-Fisher Scientific, Loughborough, UK) (n=3). These cells were also cultured in a 4-chamber slide at a density of $5x10^4$ cell/ mL/ chamber in basal medium to be used for Oil red-O stain evaluation as described below. All of the chambers were then incubated at 37° C, 5% CO_2 and not less than 90% humidity for 21 days (as recommended by the manufacturer's protocol). The medium was regularly changed twice per week for all of the prepared samples.

4.3.4.2. Detection of adipogenic differentiation using cell morphology and Oil red-O staining

Careful monitoring for any possible alterations in hDPSCs cell morphology within the samples in the adipo-inductive medium was maintained throughout the 21 days of culture, with parallel comparisons with control cells. Detection of intracellular lipid droplet formation was performed at the end of the culture time (3 weeks). All of the chambers were washed twice with 0.5 mL PBS/ chamber. According to manufacturer protocol, the cell monolayers that had formed in each chamber were fixed by adding 0.5 mL of chilled absolute methanol to each chamber and incubating for 5 minutes at room temperature. Afterwards, the methanol was completely aspirated, and the monolayers were washed twice with 0.5 mL deionised water per chamber.

Oil red-O stain in isopropanol (0.5% w/v) (New Comer Supply, Middleton, UK) was used to detect any possible intra- and extracellular lipid droplets

formed within the hDPSCs samples after adipogenic induction. A fresh working solution was prepared by adding 3 mL Oil red- O staining reagent to 2 mL dH_2O, then filtering the solution through filter paper before use. Half a millilitre of Oil red-O working stain solution was then added to each slide chamber, and all of the chamber slides were placed on a plate shaker (Millipore™ SD1P005V05, Loughborough, UK) and slowly mixed on a shaker with the stain solution for 20 minutes at room temperature. The stain solution was then aspirated and washed with dH_2O, before carefully detaching the chamber walls from the slide using the plastic instrument provided with the chamber slides kit. The slides were then dehydrated and mounted with DPX as described earlier in *3.5.1.2*.

4.4. Results

4.4.1. Osteogenic differentiation potential of hDPSCs *in vitro*

4.4.1.1. ALP staining of hDPSCs from 3 different donors

After 14 days of culturing hDPSCs *in vitro* in osteo-inductive medium, the ALP staining intensity in osteo-induced hDPSCs from all 3 donors was stronger compared to both the corresponding negative controls (cultured in basal medium) and the G_{292} cells positive control group that had been cultured for the same time periods. However, HDPSC cultures from different donors showed variable positive stain intensity (Figure 4-1).
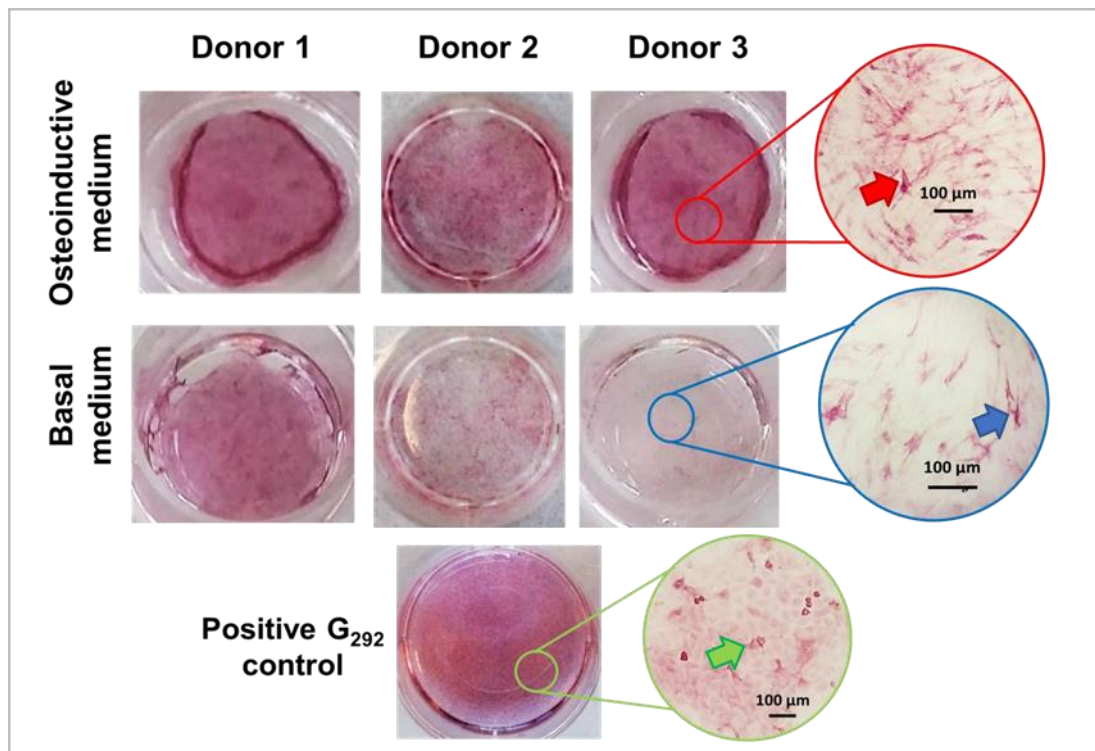
Figure 4-1: ALP staining of hDPSCs monolayers from 3 donors after 14 days of culture in osteo-inductive and basal media. The red colour indicates positive ALP staining, arrows show individual cells. Strongest staining was detected for all 3 donors within the osteo-inductive medium group (top row) compared to the corresponding basal medium negative controls (middle row) and G_{292} positive control (bottom row) groups when examined macroscopically. Microscopically, there were more ALP positive cells within osteo-induced hDPSCs monolayers (red arrow) compared to those seen in basal medium controls (blue arrow) and G292 cells (green arrow).

4.4.1.2. DNA concentration quantified using PicoGreen® biochemical assay

After 14 days in osteo-inductive culture, hDPSCs monolayers showed significantly higher DNA concentration compared to the basal medium control group, in 2 out of the 3 donors ($p<0.05$) (Figure 4-2).
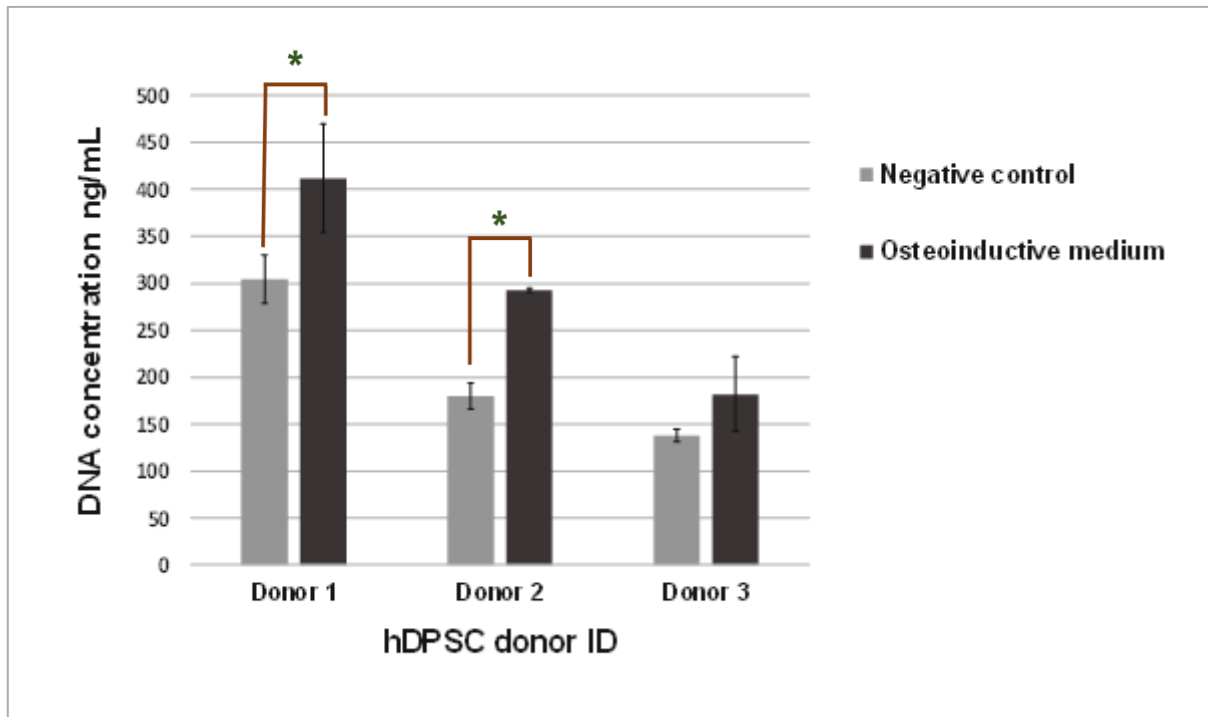
Figure 4-2: DNA concentration of hDPSCs monolayers from 3 donors after 14 days of culture (mean ±SD, n=3). Osteo-induced hDPSCs showed higher DNA concentration compared to the corresponding basal medium negative controls for all 3 donors, with results for donors 1 and 2 being statistically significant. *p<0.05.

4.4.1.3. ALPSA of hDPSCs in osteo-inductive culture

After normalising ALP activity to the total DNA content of each culture, the ALPSA results showed that for all 3 donors, hDPSCs cultured in osteo-inductive medium had significantly higher ALPSA compared to that of the basal medium negative control group from the same donors after 14 days in culture ($p<0.05$) (Figure 4-3).
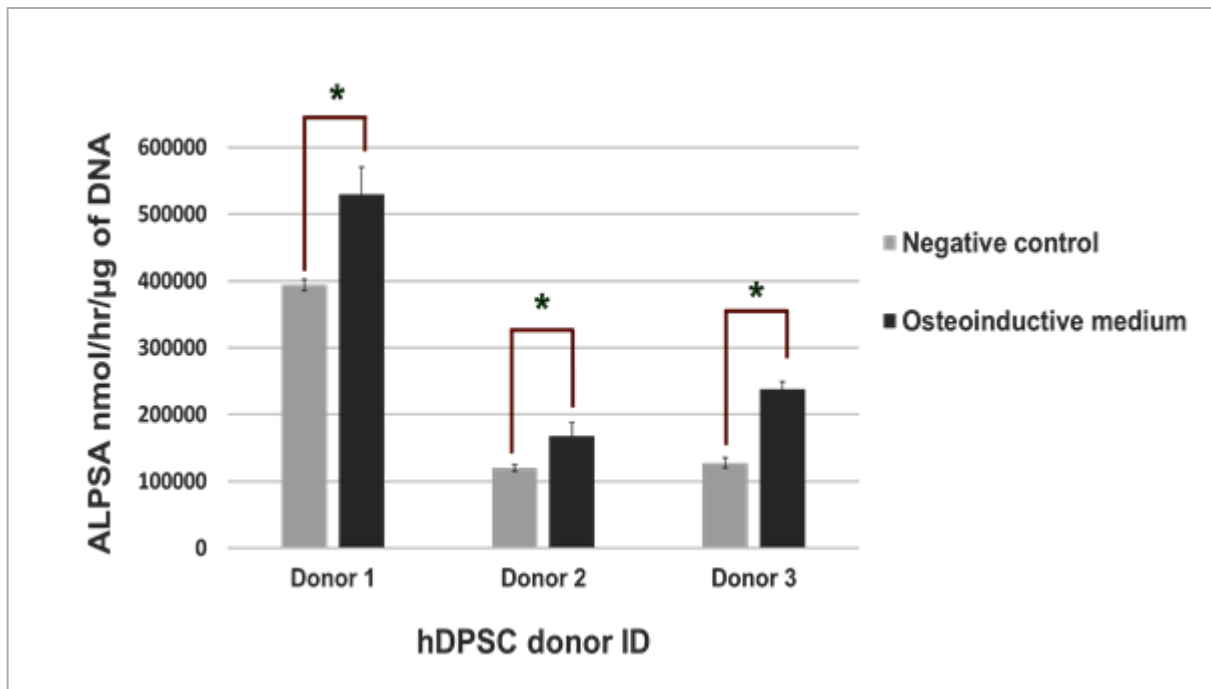
Figure 4-3: ALPSA of hDPSCs monolayers from 3 donors after 14 days of culture (mean ± SD, n=3). Osteo-induced cells showed higher ALPSA compared to their corresponding basal medium negative controls, which was statistically significant for cells from all 3 donors. * p<0.05.

4.4.1.4. Extracellular matrix mineralisation by hDPSCs in osteo-inductive culture *in vitro*

4.4.1.4.1. Alizarin red (Al-R) stain

After 21 days in culture, Al-R staining showed different staining intensities between hDPSCs in osteo-inductive culture compared to controls when viewed macroscopically. Osteo-induced hDPSCs cultures showed strong red staining macroscopically, with microscopic detection of multiple bright red nodules scattered all through the monolayers in all the 3 donors. In comparison, in the negative control group (hDPSCs from paired donors cultured in basal medium for the same time period), hDPSCs from all 3 donors showed faint staining when viewed macroscopically. No obvious red-stained nodules were detected within the control group monolayers when viewed microscopically (Figure 4-4).
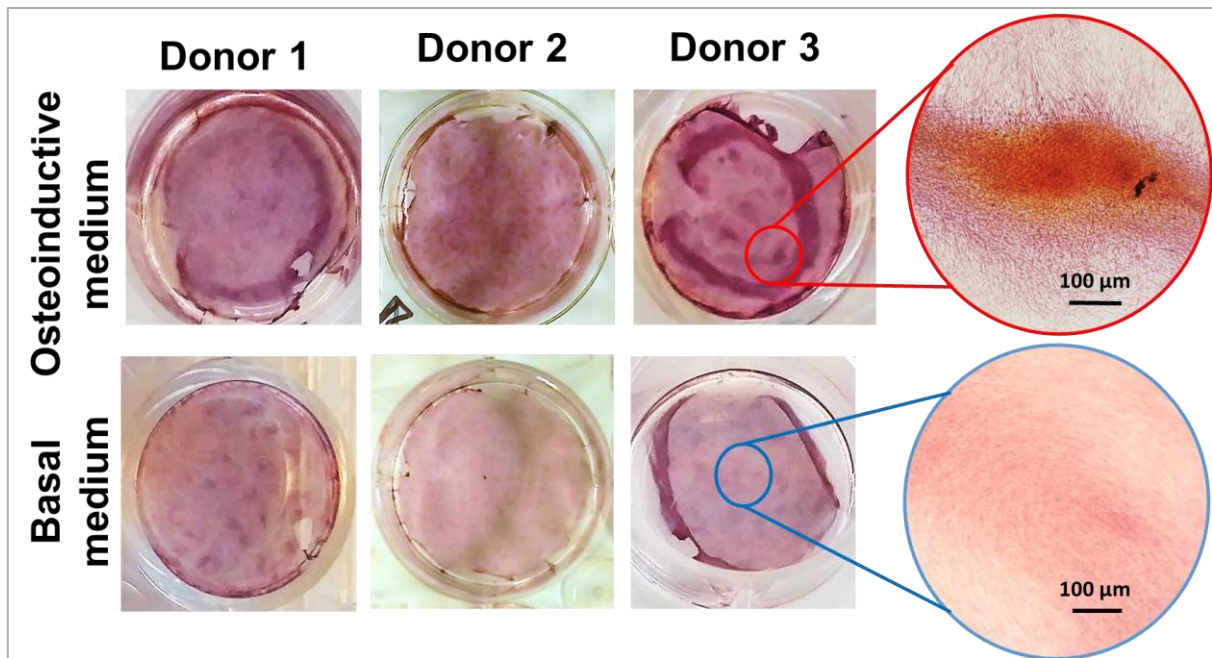
Figure 4-4: Al-R stain for hDPSCs monolayers from 3 donors after 21 days of culture. Positive Al-R staining was seen as red colour within the monolayers. Strong positive staining could be detected in osteo-induced monolayers from all 3 donors (top row) compared to the faint pink colour seen in the corresponding negative controls cultured in basal medium (bottom row) when examined macroscopically. Microscopically, obvious bright red stained nodules could be seen scattered within the monolayer sheets of osteo-induced hDPSCs (red labelling) while none could be seen in basal medium controls (blue labelling).

4.4.1.4.2. Von Kossa (VK) stain

Macroscopic examination of VK staining after 21 days of culture in osteo-inductive medium showed that the hDPSCs monolayers from 2 out of 3 donors appeared to have stronger dark brown staining compared to that of the corresponding negative control group cultured in basal medium. Microscopically, densely distributed, large black presumed mineral deposits could be seen within the neo matrix of the osteo-induced monolayers, in contrast to the negative control group, where only scanty black deposits, which were of obviously smaller sizes, could be detected within the monolayer sheets (Figure 4-5).
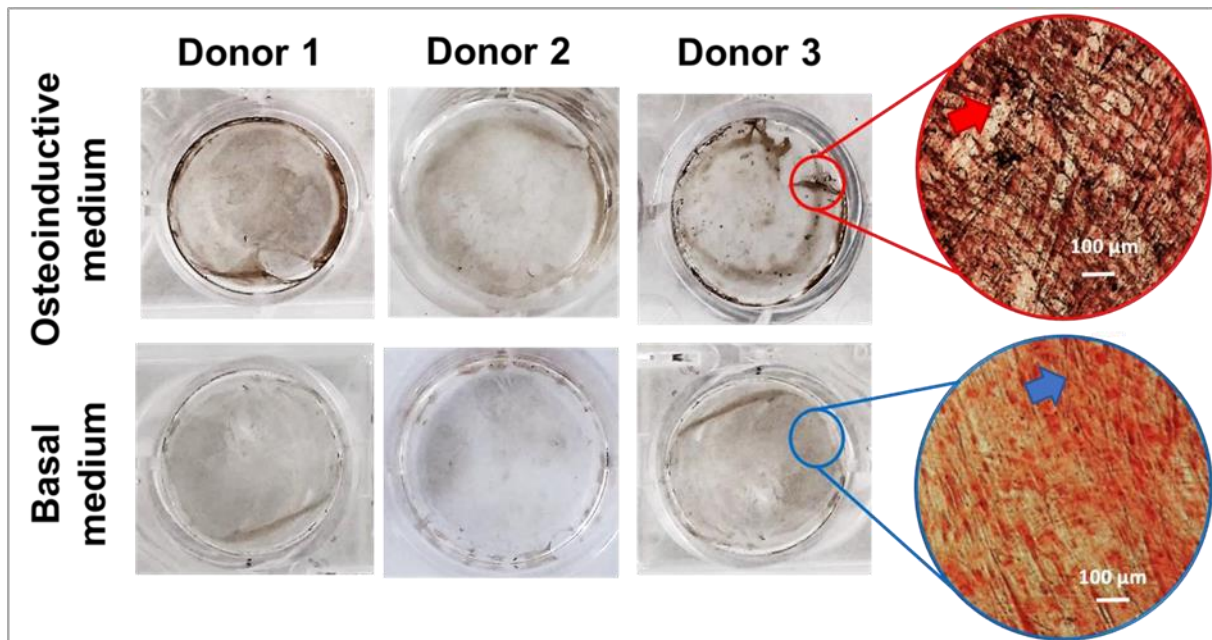
Figure 4-5: VK staining of hDPSCs monolayers from 3 donors after 21 days of culture. Positive VK staining was seen as black- dark brown colour within the monolayers. Strong positive staining could be detected in monolayers from donors 1 and 3 within the osteo-induced medium group (top row) compared to the faint colour seen in the corresponding negative controls that were cultured in basal medium (bottom row) when examined macroscopically. Microscopically, obvious black, heavily stained mineral deposits could be seen within the osteo-induced hDPSCs monolayer sheets (red arrow) while few of these that were minute in size (blue arrow) could be seen under high magnification in the corresponding basal medium controls.

4.4.2. Chondrogenic differentiation potential of hDPSCs *in vitro* detected by Alcian blue (AB) and Van Geissen (VG) stains

After 21 days of chondro-inductive culture, hDPSCs from all 3 donors appeared to have successfully formed solid pellet spheres of about 1 mm diameter that were fully detached from the walls of the tube in which they were incubated. In contrast, hDPSCs cultured in basal medium only (the control group) failed to form consistent pellets for cells from all 3 donors within the same period. In the latter case, the cultured cells looked like a loosely packed layer at the bottom of the tube that was easily disturbed upon trying to remove it for histology. AB staining for all of the pellets retrieved from chondro-inductive medium showed strongly positive blue-green staining over large

94

areas within each micro-mass, though to a different extent in samples from each of the 3 donors. The remaining areas within the pellets were stained different shades of red-pink with the VG stain, and these areas were mainly seen towards the periphery of the micro-masses. Under higher magnification, small round lacunae-like spaces were detected scattered within the neo-tissue, with the blue AB positive staining mainly concentrated around those lacunae-like spaces which were more obvious towards the centre of the pellet (Figure 4-6).
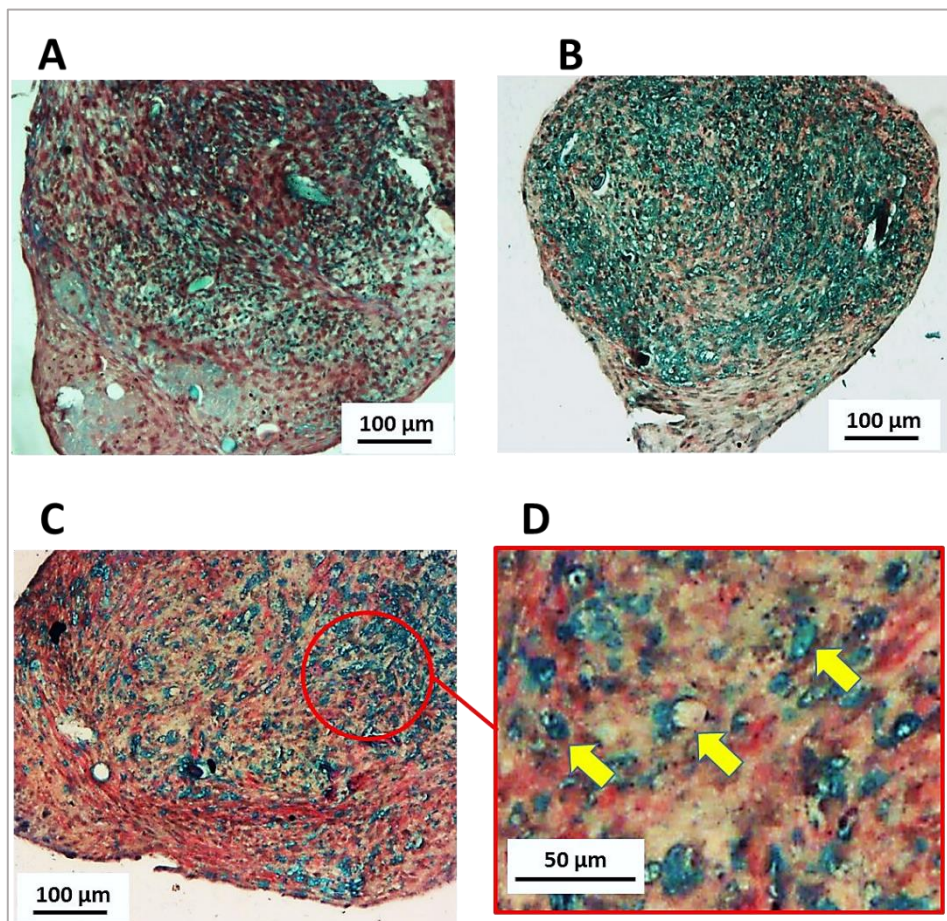
Figure 4-6: AB-VG histological staining of sections through micro-mass pellets of hDPSCs of 3 donors after 21 weeks of chondro-inductive culture. A, B and C: Pellets from hDPSCs from 3 donors under low magnification. AB positive staining (blue green) was positive to different extents for cells from different donors. D: Higher magnification showing lacunae-like structures (arrows) seen at the centre of each pellet within the zones of positive AB staining. Control samples cultured in basal medium for the same time period did not form micro-masses.

4.4.3. Adipogenic differentiation potential of hDPSCs *in vitro* detected by morphological changes and Oil red-O stain

HDPSCs from 3 different donors were cultured in the presence of adipo-inductive cues as described previously for up to 3 weeks. The hDPSCs in adipo-inductive culture revealed marked alterations in cell morphology with time in culture compared to the hDPSCs from the same donors in the negative control group that were cultured in basal medium only. Cells from different donors showed different changes in hDPSCs morphology throughout the period of adipo-induction. However, a general trend in cell shape change could be recognised (Figure 4-7). At the end of the first week in adipo-inductive culture, the majority of hDPSCs appeared to have a broader cell body and cellular projections, with an obvious enlargement of nuclei compared with the hDPSCs in basal medium. Towards the end of the second week in adipogenic culture, some cells were seen to have a flat, broad cell body with multiple stellate-like cytoplasmic processes with a central round nucleus. At the end of week 3 in adipogenic culture, many hDPSCs had assumed increased cell size, with a rounded morphology as the cell processes started to disappear, with the nuclei being obviously larger and eccentric and with a prominent nucleolus that could be clearly seen. Multiple small droplet-like structures could be seen within the cytoplasm of the cells post adipo-induction, though these differed in extent for cells from different donors. Non-induced hDPSCs in the basal medium control group remained typically fibroblast-like and spindle-shaped at the end of the third week in culture. Oil red-O staining of the samples at day 21 in adipo-inductive culture showed obvious red staining for the drop-like cytoplasmic structures within

the hDPSCs for cells from all 3 donors. This stain could not be detected within

the cells of the negative control group (Figure 4-8).
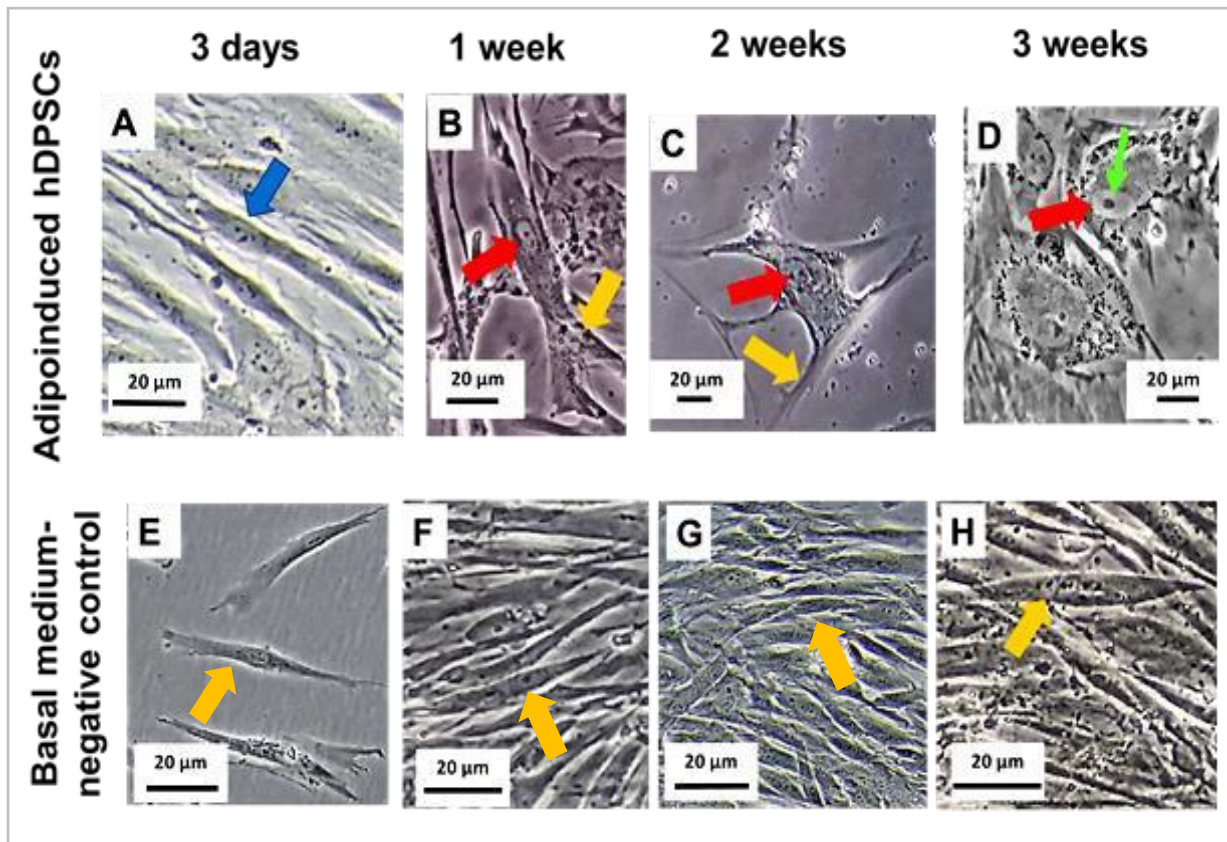
Figure 4-7: Typical morphological changes of hDPSCs from over 3 weeks of adipo-induction compared with negative controls cultured in basal medium for the same time periods. A: hDPSCs showed fibroblast- like morphology (blue arrow) in the first 3 days in adipo-inductive culture. B and C: Within the 1st and 2nd weeks respectively, the cells started to demonstrate broader cell bodies, enlarged nuclei (red arrows) and formation of cytoplasmic processes (yellow arrows). D: Towards the end of the 3rd week, the induced cells had rounder cell bodies with large eccentric nucleus (red arrow) that had a prominent nucleolus (green arrow). Disappearance of cytoplasmic processes could be noticed. E, F, G and H: Negative control hDPSCs cultured in basal medium showed no obvious changes in morphology over the 3 weeks of culture, as cells preserved their spindle fibroblast- like shape (yellow arrows).
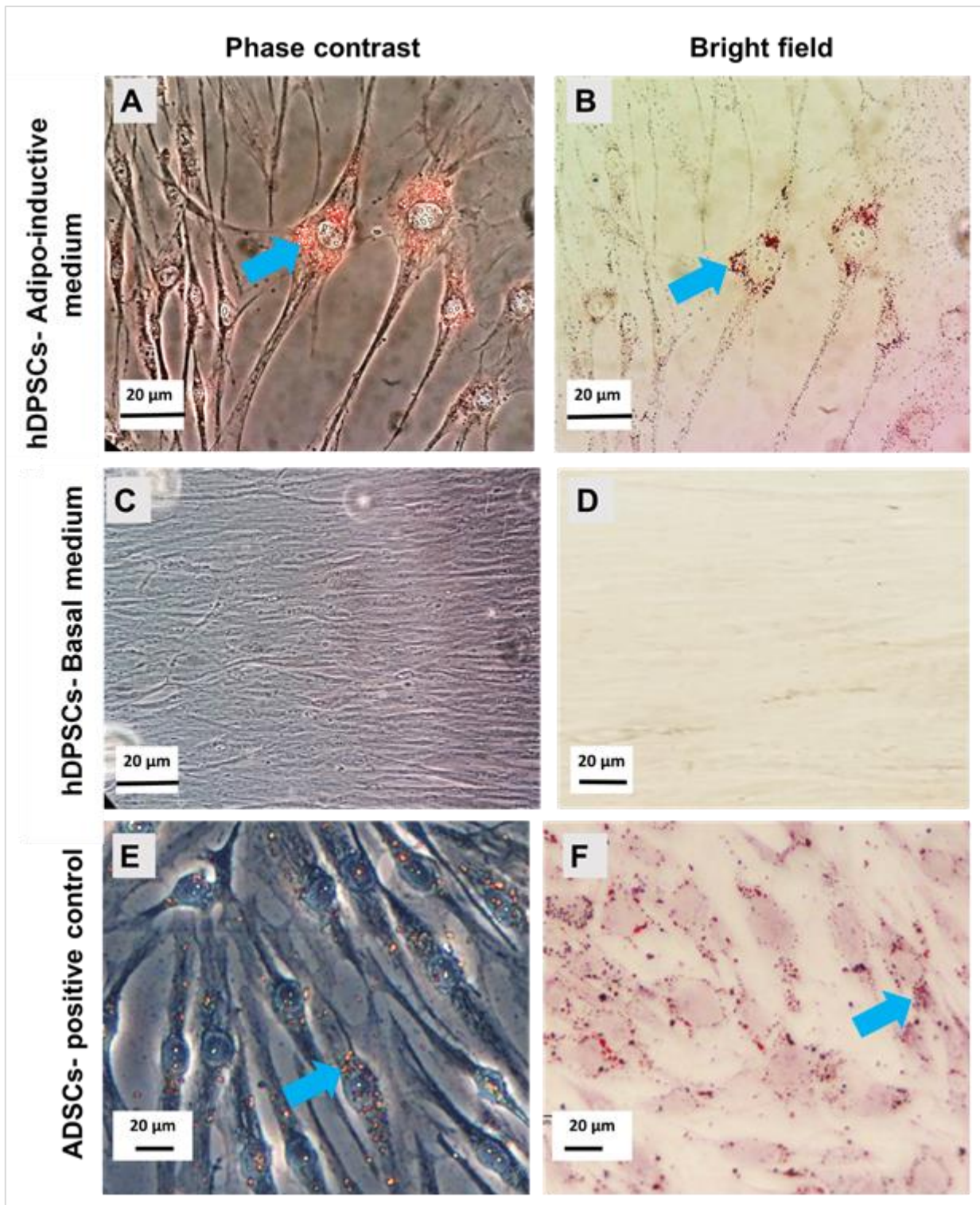
Figure 4-8: Oil red-O staining at day 21 for adipo-induced hDPSCs and respective control groups. A and B: Adipo-induced hDPSCs showing positively stained accumulated droplets (red) within their cellular cytoplasm (arrows). C and D: Negative control group cultured in basal medium showing no stain. E and F: Positive control group of ADSCs showing positively stained intracellular lipid droplets (arrows) similar to those seen for adipo-induced hDPSCs.

4.5. Discussion

Dental pulp stroma contains heterogeneous subpopulations of stem cells (Dominici *et al.*, 2006, Zhang *et al.*, 2006, La Noce *et al.*, 2014). It was suggested that sorting stem cells in high purity via stem cell surface markers could possibly provide a better cell source for therapeutic purposes compared to unsorted cells (Itaya *et al*, 2009). However, positive cells to stem cell markers are usually found in low numbers in primary culture, thus require extensive *in vitro,* increasing the risk of culture ageing (Itaya *et al*, 2009, Iwata *et al* 2010). In addition, from a practical point of view, the use of unsorted stromal cells is less time-consuming with minimal culture expansion required prior to application in tissue engineering applications compared to cell selection procedures (Dominici *et al.*, 2006, Marquez-Curtis *et al.*, 2015). Yan *et al* (2014) reported that there were no differences measured between the expanded sorted periodontal ligament stem cells and the unsorted stromal cells in terms of proliferation, CFU, and mineralization capacity. For that reason, heterogenous hDPSCs rather than sorted dental pulp stem cells were used in this project.

Results of this chapter showed that hDPSCs could be successfully induced along osteogenic, chondrogenic and adipogenic lineages *in vitro*. Several studies in the literature have provided evidence that hDPSCs possess multilineage differentiation potential when induced through different cues *in vitro* (Jo *et al.*, 2007, Nuti *et al.*, 2016, Zhou *et al.*, 2018, Zhu *et al.*, 2018). However, many of these studies used freshly isolated hDPSCs for the purpose of multilineage potential evaluation and thus did not take into account the self-renewal capability of hDPSCs after cryopreservation. This was in contrast to the work reported here in this thesis, where cryopreserved hDPSCs proved their self-renewal ability after resuscitation. The approach of using cryopreserved cell sample for multilineage capacity assessment in evidencing

hDPSCs self-renewal was also suggested by a number of previously conducted studies (Papaccio *et al.*, 2006, Zhang *et al.*, 2006).

It is important to consider the fact that there is still a wide debate in the literature regarding proving the multilineage properties of MSCs from different tissue sources, arguing that the plasticity detected in primary cultures may have resulted from the pre-existing differentiated cells in that tissue (Zhang *et al.*, 2006). This unlikely to be the case for hDPSCs, where odontoblasts and nerve cells are the most commonly differentiated cell types available in dental pulp tissue; while adipocytes are only occasionally found and no cartilage cells are normally resident (Takebe *et al.*, 2017). This supports the hypothesis that stem cell populations within hDPSCs can differentiate into pathways beyond their original tissue source.

4.5.1. Donor variability

Due to the likelihood of inter-donor response variations for primary human cells upon culture (Dalby *et al.*, 2007), there was a need to use 3 different donors in the current study to verify hDPSCs multi-potency. Several studies reported variable growth and/ or differentiation rates of stem cells from different donors when induced under similar culture conditions into different lineages (Phinney *et al.*, 1999, Siegel *et al.*, 2013, Beane *et al.*, 2014, Detela *et al.*, 2018, Kang *et al.*, 2018, Kim *et al.*, 2018, Mohamed-Ahmed *et al.*, 2018). This could be attributed to the variability of age, gender, disease status and/or cellular genetic profile among different donors which could probably affect the stem cell properties of the culture (Siegel *et al.*, 2013, Detela *et al.*, 2018, Kim *et al.*, 2018). In the current study, although hDPSCs positively expressed the induced lineages to a variable level between donors, satisfactory reproducibility of results for each of the 3 evaluated differentiation lineages could be seen among the different donors, supporting the robustness of the protocols used and the consistency

of the final observations (Dalby *et al.*, 2007). In addition, the donors used here were of similar age range which would increase the standardisation of the obtained outcomes.

Assessment of donor variability is quite essential to standardise stem cells' characteristics from different donors before their application in clinical trials (Dominici *et al.*, 2006, Pamphilon *et al.*, 2013). In addition, evaluation of donor-specific growth profile analysis prior to cell therapy would aid to predict culture performance and accomplishment of clinically sufficient yields (Detela *et al.*, 2018). The use of those cells might require tuning of cell density or culture expansion time on a donor-by-donor basis to provide more robust tissue formation for clinical applications (Kim *et al.*, 2018).

4.5.2. Osteogenic differentiation potential of hDPSCs *in vitro*

The results of the current study showed that hDPSCs monolayers from the pulps of 3 different donors had the potential to show positive osteogenic differentiation when cultured in osteo-inductive medium *in vitro*. This is consistent with several studies in the literature showing similar outcomes (Zhang *et al.*, 2006, Jo *et al.*, 2007, d'Aquino *et al.*, 2008, d'Aquino *et al.*, 2009, Mangano *et al.*, 2010). Different recipes for osteo-inductive medium have been suggested in the literature, but the standard formula for multipotent stem cell osteo-induction involves treating the confluent monolayer with a cocktail of dexamethasone (Dex), ascorbic acid and β-glycerophosphate (Alraies, 2013, Langenbach and Handschel, 2013). Due to variability in cellular differentiation state and the osteogenic potential among different donors, much argument can be found in the literature in respect of the optimal concentration of each of these constituents, with Dex being the most controversial (Langenbach and Handschel, 2013). As a supplement in osteo-inductive medium, Dex was found to play an important role in enhancing osteogenic differentiation and alkaline phosphatase

activity, which has a significant role in extracellular matrix mineralisation (Rickard *et al*, 1994; Ishida and Heersche, 1998; Miura *et al*, 2003; Jorgensen *et al*, 2004; Chadipiralla *et al*, 2010; Vater *et al*, 2011; Tomlinson *et al*, 2015). However, Dex has been used across a range of different concentrations in the relevant studies; commonly 10 or 100 nM (Eijken *et al*, 2006; Chadipiralla *et al*, 2010). Results reported in this thesis clearly demonstrate that adding Dex to osteogenic medium at 10 nM was associated with a significant increase in ALP staining and ALPSA for monolayer cultures of hDPSCs in all the 3 donors, hence promoting osteogenesis. The choice of this particular Dex concentration of 10 nM was made in accordance with the outcome of a preliminary experiment carried out to optimise Dex concentrations for hDPSCs osteo-induction *in vitro* (data not shown). This value is consistent with several other studies that recommended the use of 10 nM Dex to induce MSC osteogenesis (Walsh *et al*, 2001; Khanna-Jain *et al*, 2010; Vater *et al*, 2011; Khanna-Jain 2012). These studies argued that higher doses of Dex (around 100 nM) were found to have an inhibitory effect on bone formation *in vivo*, as well as hindering cellular proliferation by inhibiting collagen synthesis. In this chapter, quantification of total DNA content showed that addition of Dex at 10 nM had no apparent inhibitory effect on hDPSCs growth, especially with the synergistic effect of L-ascorbic acid in the medium that is known to enhance collagen synthesis and cellular proliferation (Gundle and Beresford, 1995; Vater *et al*, 2011). It was also reported that Dex used at 10 nM concentration is more analogous to physiological levels of cortisol, the natural corticosteroid in the human body (Langenbach and Handschel, 2013). However, Eijken *et al* (2006) pointed to the fact that impediment of bone formation can be detected at therapeutic doses of corticosteroid in a dose-period related manner that would not necessarily be the same *in vitro*.

Mineralisation of the extracellular matrix is considered to be the ultimate evidence for advanced cellular differentiation into hard tissue *in vitro* (Hoemann *et al*, 2009). As mentioned earlier, Dex is one conventional additive to the osteo-inductive medium that can promote matrix mineralisation when used in appropriate doses. Since matrix mineralisation usually involves both calcium and phosphate, it is important to detect the co-presence of both minerals to verify any matrix mineralisation process (Gregory *et al*, 2004; Hoemann *et al*, 2009). The results of this chapter showed that osteo-induced hDPSCs produced monolayers that stained strongly with Alizarin red and Von Kossa stains compared to the basal medium control group, suggesting an increase in both calcium and phosphate deposition within the cultured monolayers which might be contributed to the extracellular matrix mineralisation by hDPSCs. This agrees with the findings of Coelho and Fernandes (2000) and Hoemann *et al* (2009). In the current study, it was preferred not to add β-glycerophosphate to the culture medium. Despite being the source of phosphate needed to produce hydroxyapatite mineral, it was reported by many previous studies that it is likely to result in false-positive mineralisation detection outcomes (Langenbach and Handschel, 2013). When cells that are incapable of osteogenic differentiation have been cultured in the presence of β-glycerophosphate, especially at high concentrations, they can produce dystrophic mineralisation or non-apatitic mineralisation; being falsely detected as osteo-specific deposits by Alizarin Red or Von Kossa stains caused by creating mineralisation nuclei independent of the matrix or even by exceeding the solubility threshold (Bonewald *et al.*, 2003). This is quite critical in studies setting out to test multi-potency of primary cell cultures, because if positive results for adipogenic and chondrogenic differentiation were also observed for the same cells, it could lead to false assumption of stemness in that culture (Langenbach and Handschel, 2013).

4.5.3. Chondrogenic differentiation potential of hDPSCs *in vitro*

In the presence of an appropriately supportive biochemical environment, chondrogenic differentiation of MSCs can be obtained by culturing the cells under high-density culture conditions, favouring cell-cell interactions that simulate pre-cartilage condensation events during embryonic development (Latinoamericano, 2010, Zhang *et al.*, 2010, Ullah *et al.*, 2012). Following its description for use with bone marrow stem cell chondrogenesis by Johnstone *et al.* (1998), 3D pellet culture was shown to be a highly reliable method that has been extensively used to demonstrate MSCs chondrogenic potential *in vitro*. The method also uses a defined medium containing essential growth factors that are required for chondrogenesis, transforming growth factor-ß (Johnstone *et al.*, 1998, Pelttari *et al.*, 2008, Latinoamericano, 2010) being one of the most importance. A number of phenotypic characteristics could be recognised in cells undergoing chondrogenic differentiation. Fibroblast-like MSCs gradually change their morphology within the cultured aggregates to eventually present a flat, chondrocyte-like appearance with cartilage- typical lacuna structure; accompanied by synthesis of a characteristic extracellular matrix of cartilage, containing proteoglycan and type II collagen (Latinoamericano, 2010, Reich *et al.*, 2012, Khajeh *et al.*, 2018). The results of the current chapter confirmed the potential of hDPSCs to undergo chondrogenic differentiation. Histological examination of the pellets formed by chondro-induced hDPSCs from the pulps of all 3 donors after 21 days revealed the formation of numerous lacunae-like structures, with strong positive AB staining throughout the newly formed matrix, being more obvious in the areas surrounding these lacunae suggesting the formation of a glycosaminoglycan-rich matrix (Dehne *et al.*, 2009, Reich *et al.*, 2012). These findings agree with the results of several other studies in the literature regarding successful chondro-induction of

hDPSCs *in vitro* (Zhang *et al.*, 2006, Wei *et al.*, 2007, Dai *et al.*, 2012, Vasandan *et al.*, 2014, Nuti *et al.*, 2016, Khajeh *et al.*, 2018). Further confirmation of the results reported for this thesis could have been carried out using IHC with antibodies against collagen type II, but this was precluded by limited time availability.

4.5.4. Adipogenic differentiation potential of hDPSCs *in vitro*

The final trilineage differentiation pathway that was investigated for hDPSCs in this study was that of adipogenesis. A conflict could be seen in the literature regarding hDPSCs ability to differentiate through the adipogenic cue. In a study conducted by Zhang *et al.* (2006), hDPSCs failed to show morphological changes after adipo-induction and were negative to Oil red-O stain after 3 weeks in adipo-inductive culture. Other studies, however, proved the ability of hDPSCs to be successfully induced in response to adipogenic cues *in vitro* (Gronthos *et al.*, 2002, Jo *et al.*, 2007, Alraies, 2013, Marquez-Curtis *et al.*, 2015, Nuti *et al.*, 2016). This controversy could be attributed to donor variability and/or different adipo-inductive medium components used among different studies (Zhang *et al.*, 2006). Mor-Yossef Moldovan *et al.* (2019) summarised the morphological changes that fibroblast-like MSCs gradually undergo adipogenic transformation in a series of events; these are increased cell size, rounding of the cell body, reduction of cytoplasmic projection areas, nucleus eccentricity, and finally, intracellular lipid droplet accumulation by the end of the culture period. The results reported in this chapter clearly demonstrated the detection of similar events in the adipo-induced hDPSCs cultures from pulps from each of the 3 donors in a time-related manner (please see figures 4-7 and 4-8 in **section 4.4.3.** of this chapter). Although the commercial, ready-made adipo-inductive medium that was used in the current study seemed to be effective in *in vitro* adipo-induction of hDPSCs, its exact composition is unknown. It is likely to contain some of the essential medium

constituents required for induction of adipogenesis that are described in the literature, including high concentrations of dexamethasone which induces transcription of the adipogenic process, insulin which accelerates triglyceride accumulation (Cui *et al.*, 1997, Kubo *et al.*, 2000, Alraies, 2013) and other ingredients might include indomethacin and gentamycin (Zhang *et al.*, 2006, Nuti *et al.*, 2016).

4.6.   Conclusions

This study successfully demonstrated the plasticity of hDPSCs evidenced with their multilineage potential of the 3 different donors used; as they all could be induced, to variable extent, into osteogenic, chondrogenic and adipogenic lineages given the appropriate inductive medium. This provided confidence in the use of hDPSCs from those donors for the subsequent work carried out in this thesis. In addition, it gives a kind of support to the hypothetical presence of undifferentiated mesenchymal stem cells within the primary cell culture obtained from dental pulp tissue of the tested donors. Such evaluation of donor-specific growth and differentiation cellular profile analysis prior to cell therapy is quite important prior to cell therapy as it will help to predict culture performance before clinical use.

CHAPTER FIVE

Effect of different architecture of 3D printed polylactic acid (PLA) scaffold on hDPSCs attachment, growth and differentiation *in vitro* and *in vivo*

Chapter 5. Effect of different architecture of 3D printed polylactic acid (PLA) scaffold on hDPSCs attachment, growth and differentiation *in vitro* and *in vivo*

5.1. Introduction

Polylactic acid (PLA) scaffolds have attracted much attention as possible materials for bone tissue engineering (BTE) applications because PLA polymer was proven to be biocompatible, mechanically strong and have excellent manufacturing control over a wide range of porosities, flexibility and degradability characteristics that can be reproduced to a consistent quality (Serra *et al.*, 2013; Novosel *et al.*, 2011; Bose *et al.*, 2012; Liu *et al.*, 2013). Since its approval by the FDA, PLA has become a principal material in biomedical applications (Lopes *et al.*, 2012; Farah *et al.*, 2016).

Different techniques such as salt leaching, phase separation or gas foaming have been used for the fabrication of PLA scaffolds for BTE. However, several drawbacks are encountered using these techniques to construct a scaffold. They are quite limited in granting precise control of internal scaffold configuration such as pore size and geometry, as well as the 3D distribution of pores (Loh and Choong, 2013; Li *et al.*, 2014). Moreover, fabricating complex 3D architectures using these conventional techniques is rather challenging, requiring extra processing steps using custom made moulds (Gibson, 2006). Also, the use of organic solvents during the fabrication process is another issue, requiring complete removal of residual solvents prior to their use with living cells (Hutmacher *et al.*, 2001).

The introduction of 3D printing has contributed significantly to the potential of using PLA as a scaffold for BTE. It has offered the possibility of customising scaffolds to defect area needs, producing complex 3D shapes with precise, reproducible control over internal scaffold geometry and interconnectivity; aiming to improve the 3D culture environment and cellular response (Colasante *et al.*, 2016).

Different architectural designs of 3D printed PLA scaffolds have been suggested in the literature to support skeletal tissue regeneration, all provide necessary porosity and pore interconnectivity to ensure sufficient oxygen and nutrient perfusion accesses the colonising cells (Hutmacher *et al.*, 2001; Yilgor *et al.*, 2008; Lee, J.S. *et al.*, 2012). However, different PLA fibre printing layouts have generated a variety of pore sizes, geometries and internal structures among the proposed models and these factors are known to have effects on cellular adhesion, migration and tissue ingrowth within the scaffold both *in vitro* and *in vivo* (Domingos *et al.*, 2013). For this reason, there is a need to investigate different PLA scaffold 3D printing layouts and evaluate the influence of their geometry on their biological performance as scaffolds for BTE in living systems.

5.2.   Aims of the chapter

This chapter aimed to investigate the effect of different geometrical designs of 3D printed PLA scaffolds on hDPSCs attachment, growth and osteogenic differentiation both *in vitro* and *in vivo*.

5.3. Materials and methods

5.3.1. Evaluation of scaffold geometrical structure and morphology using stereomicroscopy and Image-J software

Two 3D printed PLA designs were used in this thesis (these will be referred to as "PLA 90°" and "PLA 45°" throughout the thesis). Initial evaluation of the geometric design of PLA scaffold groups was performed by examining and imaging the scaffolds using stereomicroscopy (please see *3.3.9.1*). Pore dimensions, PLA fibre orientation and angles within the two PLA designs were measured using Image-J (1.42 Q) software (Figure 5-1).
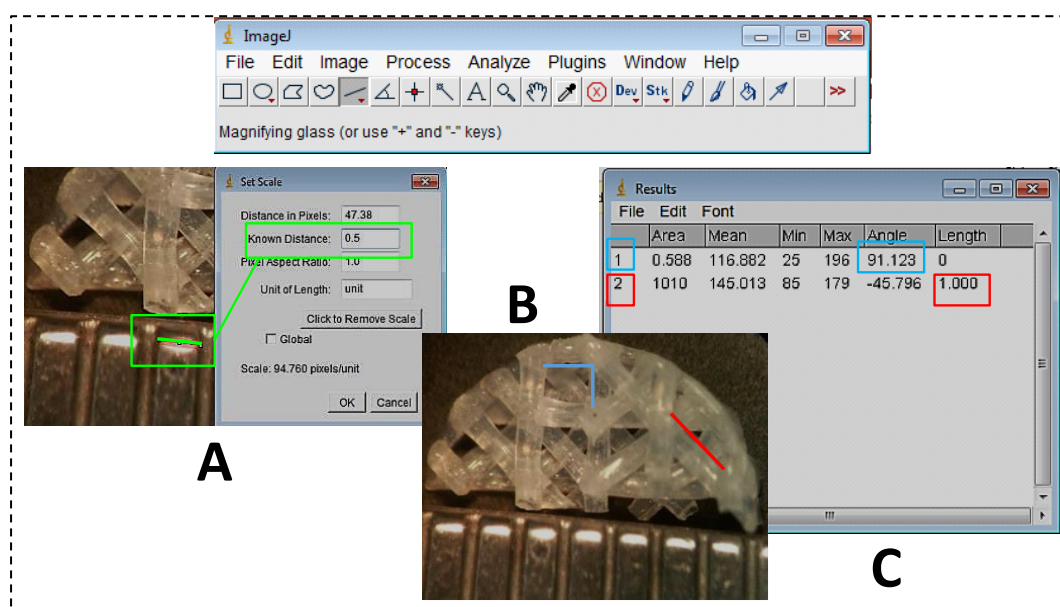
Figure 5-1: Analysis of 3D printed PLA scaffold geometry using Image-J software. A: After selecting the desired stereomicroscope image, a scale was calibrated using a known dimension reference on the image (green line representing 0.5 mm on a ruler). B: Desired angles (blue label) and/ or lines (red label) were selected on the image to analyse. C: Results output for the measured items in B (angle measure labelled blue and line measure labelled red)

5.3.2. Static seeding of hDPSCs on 3D printed PLA scaffolds

The PLA scaffolds were UV sterilised as described earlier (*3.3.7.1*). Two PLA groups were included consisting of 6 scaffolds each with two different geometrical designs,

PLA 45° and PLA 90°. All the scaffolds were then statically seeded with P4 hDPSCs at a density of 2×10^5 cell/ sample (as described in ***3.3.7.1***) and incubated in 37° C for 4 hours. HDPSCs from all the 3 donors were used for these experiments, aiming to include cells with passages ≤ 5 to reduce the possible effects of primary culture ageing (Park *et al.*, 2005, Turinetto *et al.*, 2016). Different time points were selected for different investigations; with each time point optimised to best detect and/or monitor hDPSCs ongoing growth and expression of variable osteogenic differentiation markers throughout the 5 weeks of *in vitro* culture.

5.3.3. Evaluation of hDPSCs attachment on 3D printed PLA scaffolds using fluorescent microscopy and cell counting

After 4 hours of seeding, all PLA constructs from both 45° and 90° groups were imaged using fluorescent microscopy to investigate the level of cellular attachment (please see ***3.3.8***). Afterwards, the number of unattached cells remaining in the medium was counted using an HCM for 3 scaffolds from each PLA group (please see ***3.3.5***) and the number of attached cells on each scaffold was indirectly quantified by using the initial cell seeding number and then subtracting the number of unattached cells left in the medium after seeding was complete. All PLA constructs were then cultured in an osteo-inductive medium for further 5 weeks, with medium changed twice a week.

5.3.4. Evaluation of hDPSCs pore bridging and closure on 3D printed PLA scaffolds using SEM imaging

After 3 weeks in osteo-inductive culture, 1 construct from each PLA group was washed and fixed as described in (***3.3.9.3).*** Cellular bridging across PLA fibres and pore closure with newly formed matrix were evaluated on both PLA 45° and PLA 90° using SEM imaging ***(3.3.9.3).***

5.3.5. Evaluation of hDPSCs viability and growth on 3D printed PLA scaffolds using CMFDA-EHD1 live/ dead markers

After 4 weeks in osteo-inductive culture, hDPSCs within 3 PLA scaffolds of both groups were labelled with CMFDA-EHD1 (live/dead) fluorescent markers for assessment of hDPSCs viability and cellular growth on both PLA scaffold groups (please see *3.3.8*).

5.3.6. Detection of extracellular mineral deposits within 3D printed PLA constructs using SEM imaging and EDS analysis

One live/dead labelled sample from each PLA group (prepared as described in *section 5.3.5.*) was fixed and examined using SEM for investigation of the presence of mineral deposits within PLA constructs' new matrix (please see the full procedure in *3.3.9.3*). EDS line scan elemental analysis was performed under high magnification (2000x) on 3 selected areas of what appeared to be mineral deposits within each construct to quantify calcium (Ca) and phosphorus (P) atomic weight percentage, with scan readings for 3 deposit-free areas to act as negative controls (full EDS procedure description can be seen in *3.3.9.3*). The crystals selected for EDS scanning were selected with a relatively similar size range (10x2 µm ±2) to increase elemental analysis consistency.

5.3.7. Histological evaluation of hDPSCs on 3D printed PLA scaffolds *in vitro*

After 3 weeks in osteo-inductive culture (from section *5.3.4*), the PLA constructs were fixed and stained for ALP activity (as described in *3.5.2.4*). The stained samples were examined and imaged using a stereomicroscope (please see *3.3.9.1*). Histological examination of hDPSCs on both PLA 45° and 90° scaffolds (n=3) was carried out after 5 weeks of osteo-inductive culture. Slides were stained with a combination of Von Kossa- haematoxylin-safranin red stains (full details could be seen in *3.5.2.3* and

3.5.2.6) to evaluate cellular growth, new tissue formation and mineral depositions within the extracellular matrix.

5.3.8. IHC evaluation of osteogenic differentiation of hDPSCs on 3D printed PLA constructs *in vitro*

To assess osteogenic differentiation of hDPSCs within PLA constructs, fixed PLA samples after 5 weeks in osteo-inductive culture (from ***6.2.7***) were evaluated via IHC to detect any reactivity with antibodies directed against 3 main osteogenic markers: Col-I, OPN and OCN. Full details of the IHC procedure and antibodies used are explained earlier in (***3.6***).

5.3.9. Seeding hDPSCs on 3D printed PLA scaffolds for diffusion chamber (DC) implantation *in vivo*

Six scaffolds of each 3D printed PLA design were statically seeded with hDPSCs (P4, $2x10^5$ cells/sample, described in ***3.3.7.2***). Three scaffolds from each group were cultured in plain α-MEM medium overnight, each placed in a DC and immediately implanted intraperitoneally in CD1 nude mice for up to 8 weeks (please see ***3.4.1*** and ***3.4.2***). The remaining PLA constructs from both 45° and 90° groups (n=3) were cultured in osteo-inductive culture *in vitro* for 8 weeks before being implanted in DCs for a further 8 weeks *in vivo*. All the samples above were then retrieved from the animals after their sacrifice according to schedule 1 regulations and fixed as described earlier (full details could be seen in ***3.6***).

5.3.10. Evaluation of neo-matrix formation and mineralisation within 3D printed PLA constructs *in vivo* using SEM imaging

The fixed *in vivo* constructs from ***5.3.9*** above were examined using SEM to evaluate neo-matrix formation and detect any mineral deposits within the newly formed ECM (please see ***3.3.7.3.3***).

5.3.11. Histological and IHC evaluation of newly formed tissue within 3D printed PLA constructs *in vivo*

The fixed *in vivo* constructs from **5.3.10** above were then processed for histology and IHC. Histological samples were stained using Alcian blue-Sirius red (AB-SR) stain to examine any new tissue formation and with Von Kossa stain to evaluate any extracellular matrix mineralisation (please see **3.5.2.2** and **3.5.2.6**). IHC samples were checked for reactivity against anti-Col-I, anti-OPN and anti-OCN antibodies to evaluate osteogenic differentiation (please see **3.6)**.

5.4. Results

5.4.1. Geometrical morphology and pore size of 3D printed PLA scaffolds

Stereomicroscopy showed two main differences between the two PLA designs used; those were fibre stacking orientation and pore size. PLA 90° comprised of 8 layers of 3D printed fibres, laid perpendicular to each other (0°\90° stacking angles), forming uniformly sized, square-shaped macropores of 800 µm side length and at 90° angles when seen from the top of the scaffold. PLA layers in this design were arranged in the same orientation, so the square macro pores went all the way through the whole scaffold thickness (Figure 5-2).

PLA 45° scaffolds had a more complex geometrical design, within which the 8 layers of 3D printed fibres were stacked at 4 distinct angles on top of each other (0°/45°/90°/135°), creating 3 different shapes and sizes of pores throughout the scaffold layers from surface to bottom   (i) parallelogram-shaped pores of 500 µm x1000 µm dimensions with 45°/135° internal angles, (ii) square pores of 500 µm side length and 90° angles and (iii) a third smaller series, 300 µm x 300 µm, of square pores with a 90° internal angle. A duplicate set of PLA fibres lay in a similar manner with the remaining 4 layers down to the bottom of the scaffold. As PLA fibre layers rotated by 45° on top of each other in an offset manner, no pores could be seen permeating through the entire scaffold depth. This circumstance will be described throughout the thesis by the term "offset pores" (Figure 5-2). All of the listed details for PLA 45° design are illustrated in (Figure 5-3). Table 5-1 summarises the scaffolds' measurements taken using image- J software.

Table 5-1: Summary of geometrical parameters of 3D printed PLA 90° and PLA 45° scaffolds measured using image-J software

Scaffold type	Top view pore size (µm)	Top view pore shape	Fibre stacking Angle	Pore surface area (mm²)	Number of stacked layers	Overall 3D pore geometrical shape
PLA 90° (Figure 5-2)	800x 800	Square	0/90°	640	8	Cubic
PLA 45° (Figure 5-3B)	• 500x 1000 • 500x 500 • 300x 300	• Parallelogram • Square • Square	0°/45°/ 90°/ 135°	• 500 • 250 • 90	8	Polygonal
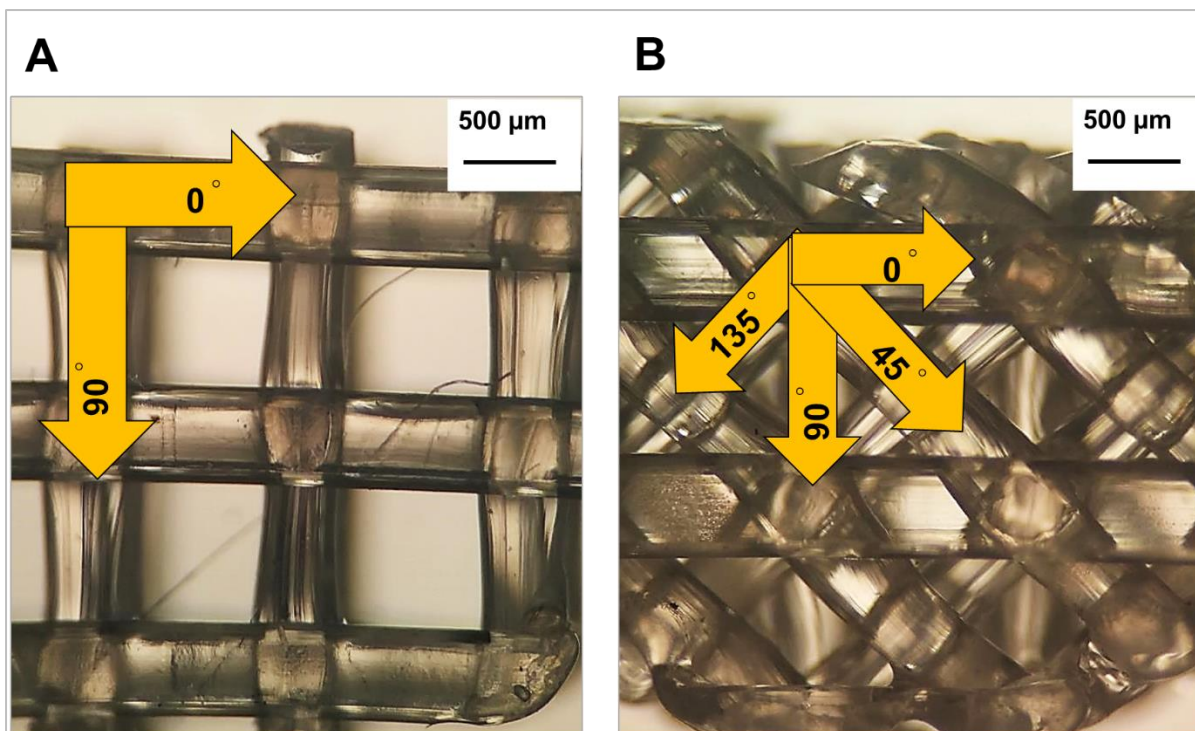
Figure 5-2: General layout of PLA 90° and PLA 45° 3D printed scaffolds viewed in the stereomicroscope. A: PLA 90° design. The fibres were printed with 0° / 90° stacking angles. All layers of fibres were stacked exactly on top of each other, forming equal square macro pores that go through the entire scaffold thickness. B: PLA 45° design. Fibre layers were arranged in 0° / 45° /90° /135° stacking angles forming three types of offset pores (as detailed below).
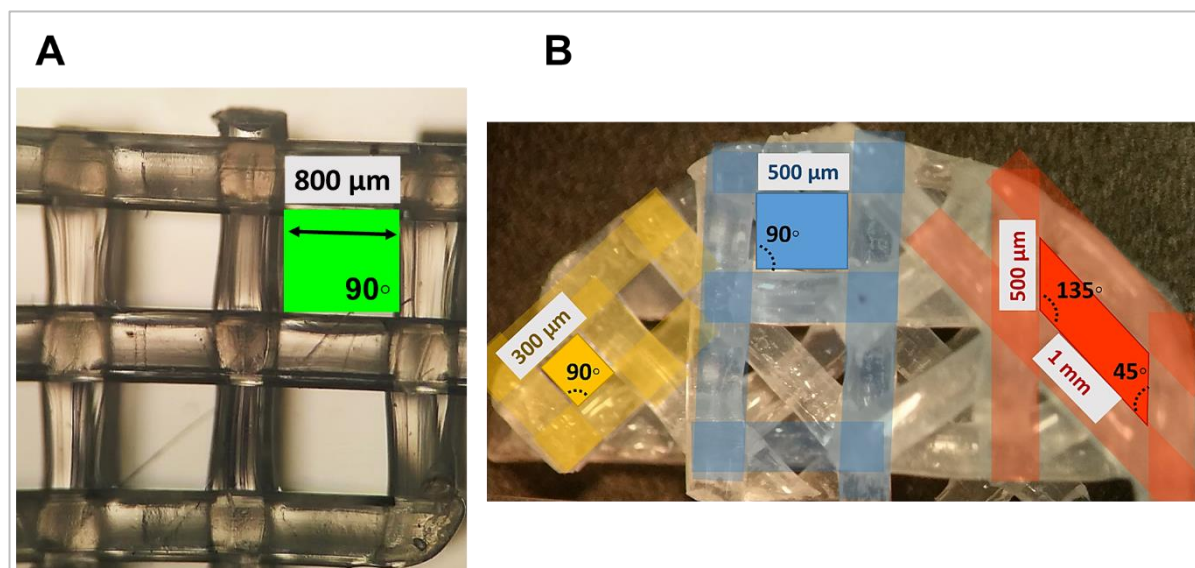
Figure 5-3 : Pore dimension and surface geometry of the 3D printed PLA scaffolds. A: PLA 90° showing square macro pores of 800 * 800 dimensions. B: Dissected PLA 45° showing 3 different shapes of pores; 500 μm * 1000 μm parallelogram (labelled red), 500* 500 μm large square (labelled blue) and 300 * 300 μm small square (labelled yellow). The angles within the pores are shown on the figure.

5.4.2. Effect of PLA fibre angle on hDPSCs attachment

Fluorescence imaging showed that cells were plentifully attached to all constructs of both PLA angle groups 4 hours after seeding, with some cells already appearing to have spread (Figure 5-4). However, quantification of the attached cell number revealed that PLA 45° scaffolds had significantly higher cellular attachment compared to the PLA 90° group ($p < 0.001$) (Figure 5-5).
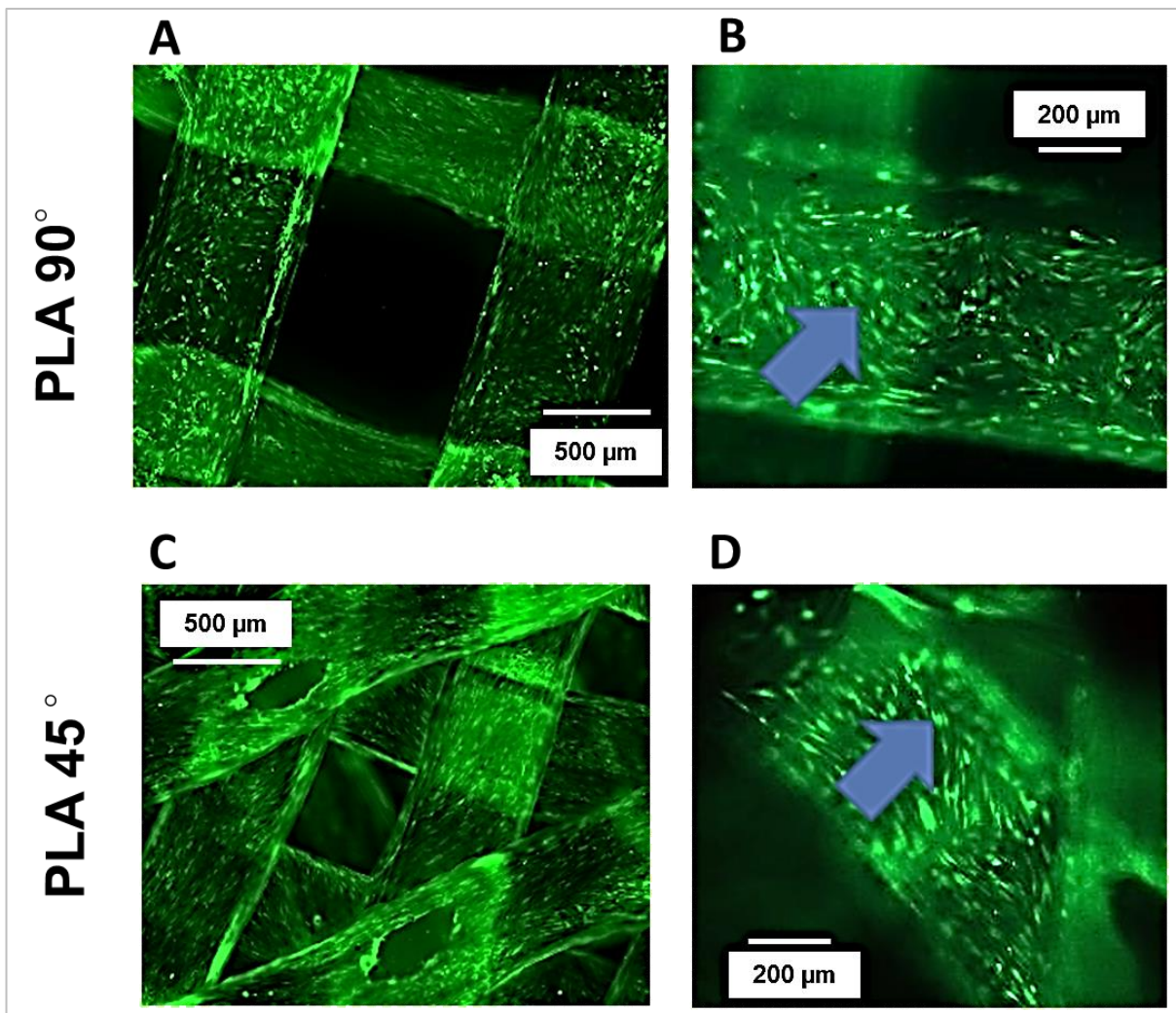
Figure 5-4: Fluorescent imaging of CMFDA labelled, live hDPSCs 4 hours after seeding. Plenty of cells could be seen attached to all scaffold groups regardless of fibre angle (arrows). A: PLA 90° constructs at low magnification. B: PLA 90° constructs at high magnification C: PLA 45° constructs at low magnification. D: PLA 45° constructs at high magnification.
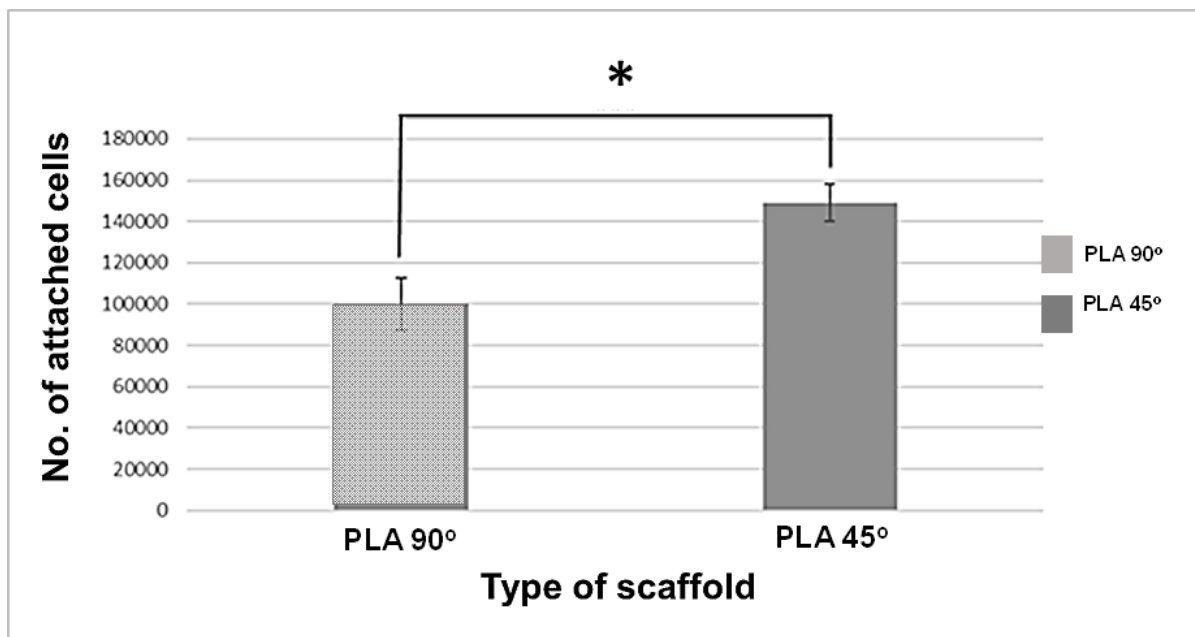
Figure 5-5: Number of hDPSCs attached to PLA 90° and 45° scaffolds 4 hours after seeding (n=3, mean ± SD). Cellular attachment on PLA 45° was greater compared to PLA 90° (* p<0.001).

5.4.3. Effect of PLA fibre angle on hDPSCs fibre bridging and pore closure

SEM imaging after 3 weeks of osteo-inductive culture showed that a limited amount of cellular bridging was present in the PLA group 90° and most of the macropores remained open (Figure 5-6 A and D**).** In comparison, in the PLA 45° group, almost all macropores were fully closed with newly formed cell sheets, which appeared as dense layers infiltrating most of the pores on the scaffold surface and the underlying scaffold layers (Figure5-6 B and E). Dense cellular bridging could be clearly seen at the corners formed by the PLA fibre intersections in PLA 45° constructs, while limited cells bridged the 90° corners within the PLA 90° group (Figure 5-6 C and F).
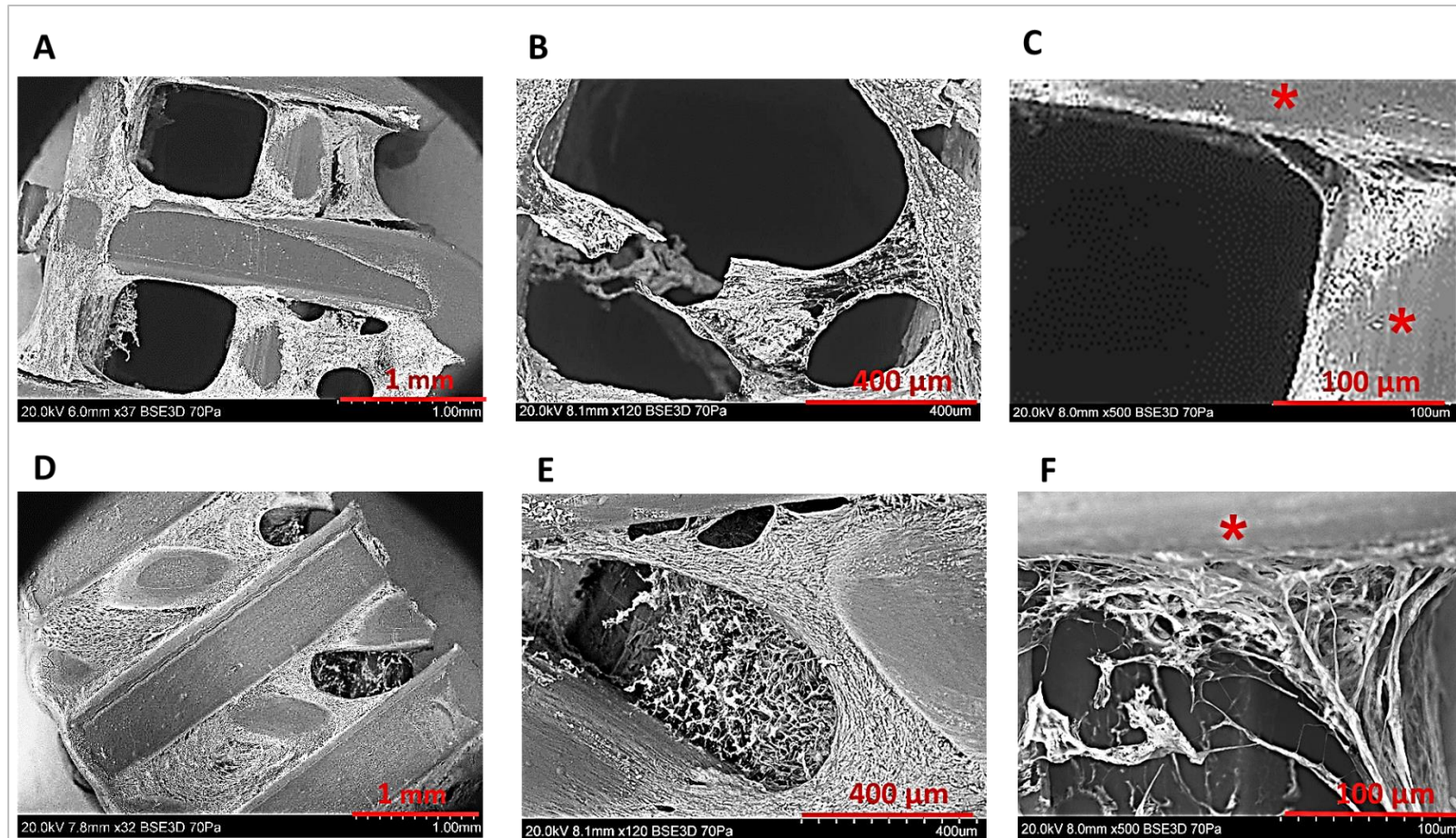
Figure 5-6: SEM imaging showing hDPSCs cellular bridge formation and matrix deposition after 3 weeks of 3D printed PLA constructs culture in osteo-inductive medium *in vitro*. A: Limited cellular bridging seen on PLA 90°. B: The centre of the macro pore appeared to be empty throughout the whole PLA 90° scaffold thickness. C: Limited cells bridged the corners within PLA 90°group (red stars represent PLA fibres). D: Almost full closure of PLA 45° scaffold surface pores was observed. E: Layered cell sheets were seen bridging deeper pores within the PLA 45° scaffold. F: Dense cellular bridging could be seen at the corners formed by PLA fibre intersection in PLA 45° constructs (red star represents PLA fibre).

5.4.4. Effect of PLA fibre angle on hDPSCs viability and growth

After 4 weeks of osteo-inductive culture, most hDPSCs showed high levels of viability in both PLA groups regardless of fibre angle, with few scattered dead cells within the newly formed cell sheets (Figure 5-7 A, B, D and E). Dense sheets of newly formed tissue could be seen in all of PLA scaffolds from both groups, covering almost the entire scaffold surface at the top and bottom. Interestingly, side view examination of the constructs showed that some central pores within PLA 90° constructs were still voided. At the same time, full closure of all scaffold spaces was evident within the PLA 45° constructs (Figure 5-7 C and F).
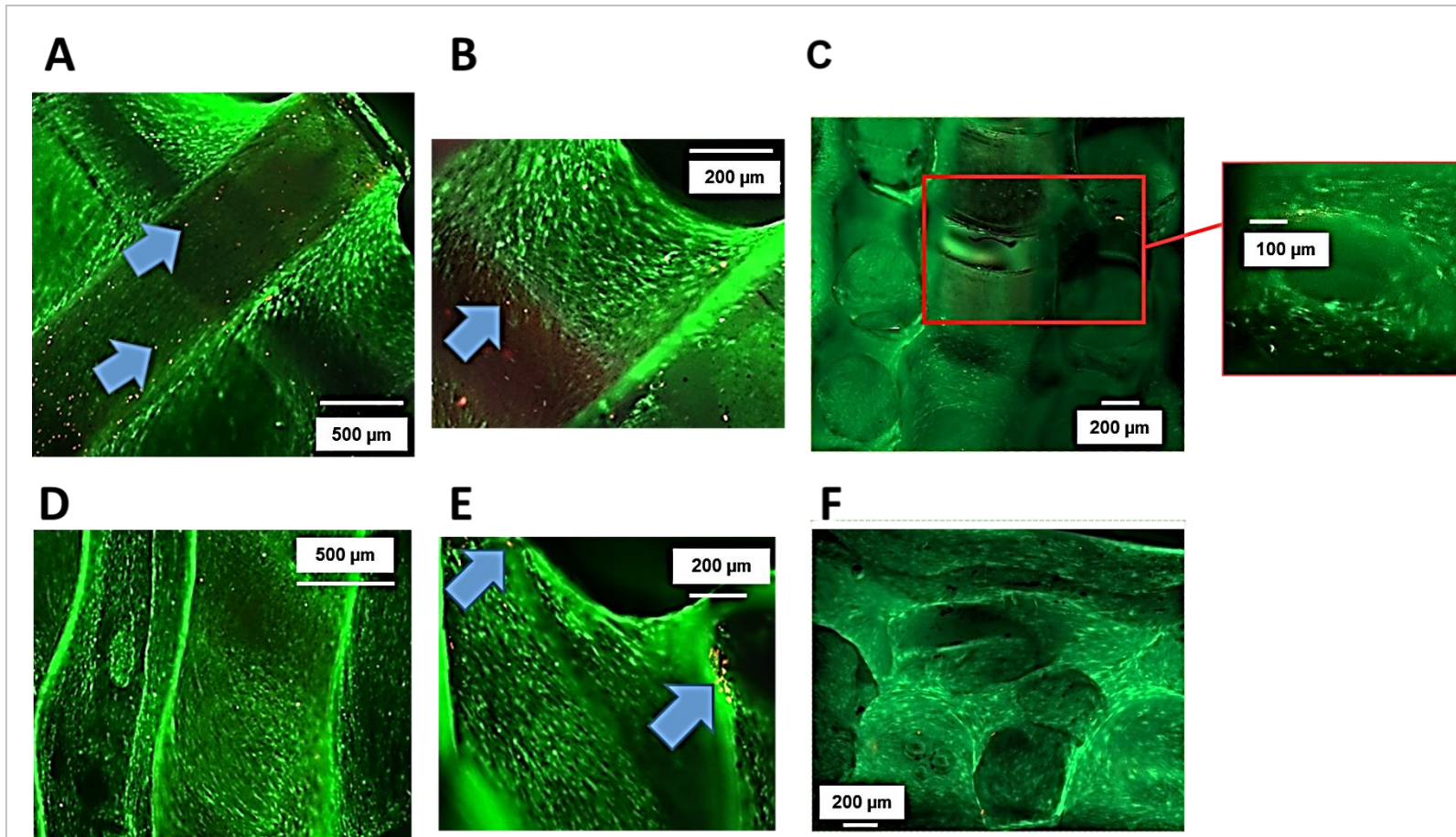
Figure 5-7: Fluorescent images showing live/dead hDPSCs (CMFDA/ EHD1 labelling) on 3D printed PLA scaffolds after 4 weeks in osteo-inductive culture *in vitro*, with thick sheets of viable hDPSCs (coloured green) in both groups regardless of fibre angle. Occasional dead cells (red dots labelled with arrows) were also detected within cell sheets in both groups. A: PLA 90° construct at low magnification (top view). B: PLA 90° construct at higher magnification (top view). C: Side view of the PLA 90° construct where open pores were seen as no cellular bridging across the centre of some pores was detected (red box). PLA 45° construct at low magnification (top view). D: PLA 45° construct at low magnification (top view). E: PLA 45° construct at higher magnification (top view). F: All spaces seemed to be covered with cell sheets within the PLA 45° construct when examined laterally.

5.4.5. Effect of PLA fibre angle on potential mineralisation within the newly formed matrix *in vitro*

5.4.5.1. SEM imaging

SEM imaging of the samples at 4 weeks after culture showed dense cell sheets with the presence of rod-like, apparently crystalline, deposits of different sizes scattered as clusters in different regions of the constructs in both PLA groups (Figure 5-9 A and D). Some of these deposits were seen enclosed within well-defined spaces in the newly formed extracellular matrix (Figure 5-8).
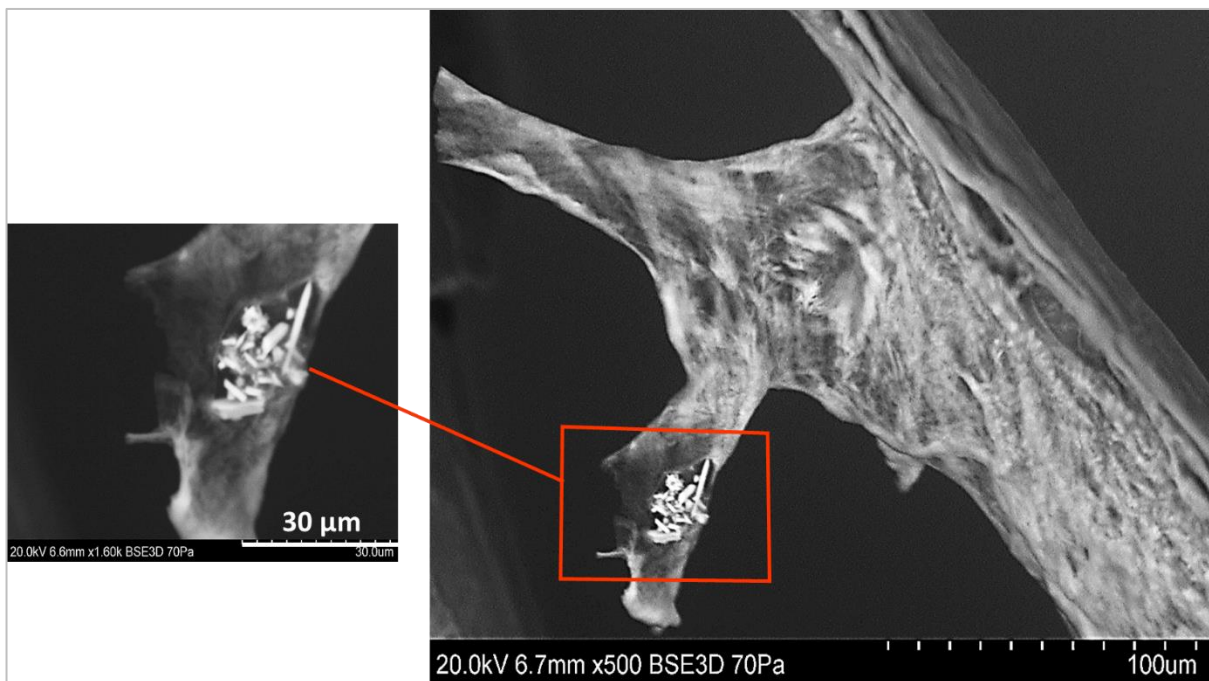
Figure 5-8: SEM of PLA 90° construct after 4 weeks in osteo-inductive culture. A cluster of rod-like mineralised deposits embedded in a well- defined space within the newly formed matrix (red labelling)

5.4.5.2. EDS analysis

EDS line scan elemental quantification for a selected crystal deposit from *5.4.5.1.* above (n=3) detected the presence of carbon (C), oxygen (O), nitrogen (N), Ca and P in different percentages in all the examined areas. No significant difference was detected in Ca and P percentages between deposits found in both PLA groups (Figure 5-10). However, Ca and P percentages deposits in both groups were significantly higher compared to those of the negative control readings ($p<0.05$ each) (Figure 5-11). Ca/P ratios were found to be 1.7 and 1.9 for PLA 90° and PLA 45° respectively (n=3, mean ± SD) with no significant difference between them ($p>0.05$) (Figure 5-12).
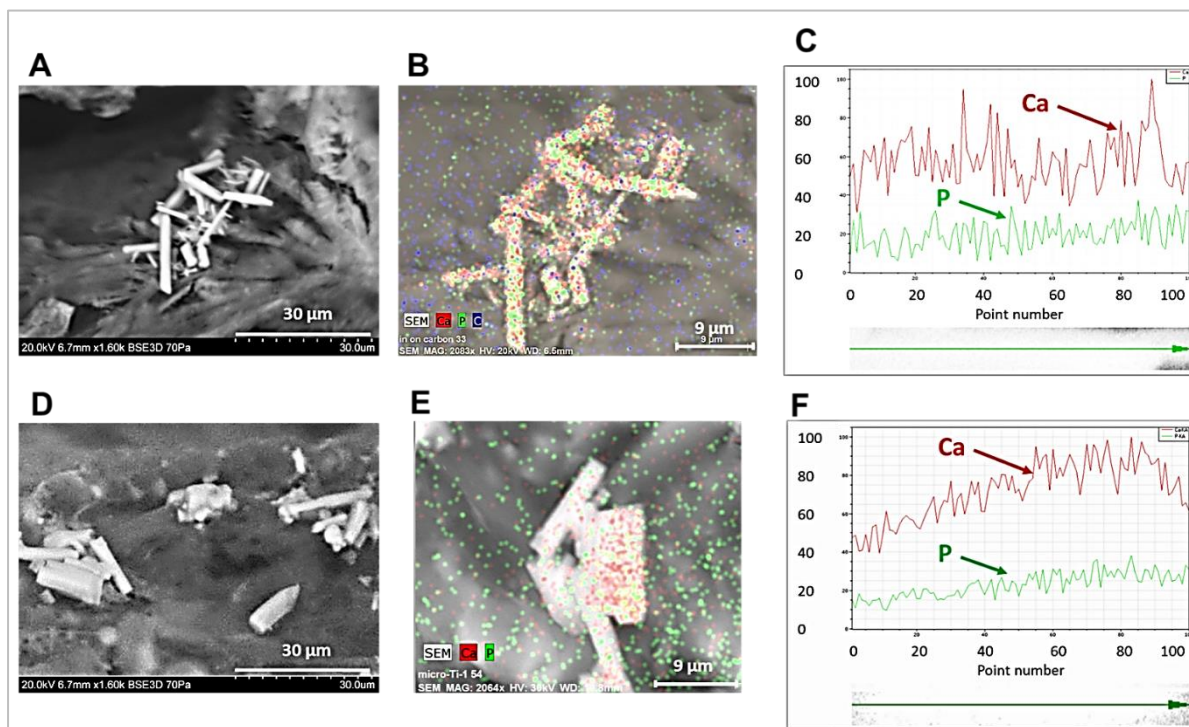
Figure 5-9: SEM with EDS elemental mapping for mineral deposits detected within 3D printed PLA constructs after 4 weeks in osteo-inductive culture. A: Rod like crystal deposits in PLA 90° constructs. B: EDS elemental mapping for crystals seen in (A) under high magnification showing high distribution of Ca (red channel) and P (green channel) within the deposit areas compared to the surrounding regions. C: Spectrum levels of Ca (red arrow) and P (green arrow) in PLA 90° deposits. D: Crystal deposits in PLA 45° constructs. E: Higher magnification of deposits in (D) showing abundant Ca (red channel) and P (green channel) within the crystal deposition areas. F: Spectrum levels of Ca (red arrow) and P (green arrow) in PLA 45° deposits.
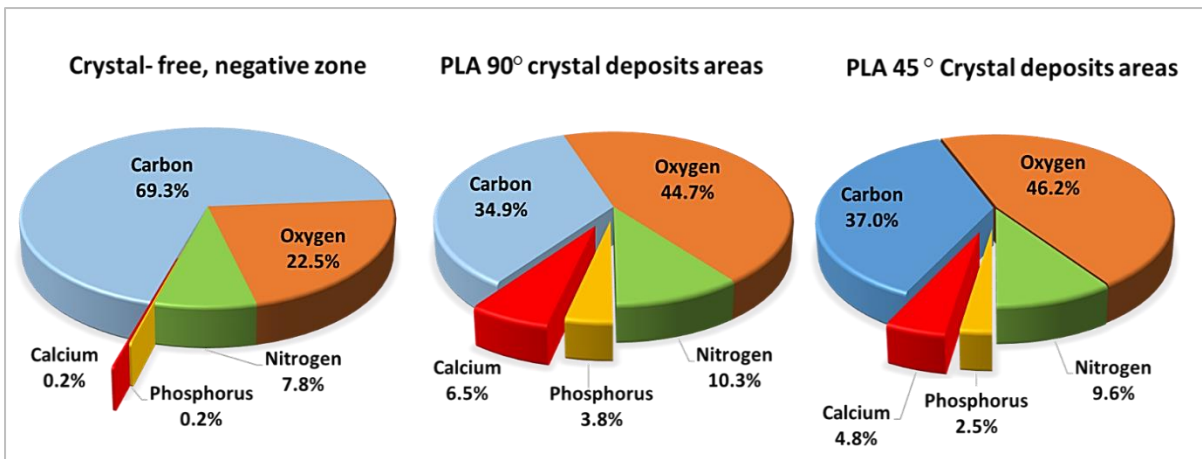
Figure 5-10: Pie chart showing EDS line scan elements quantification (atomic weight percentage) for areas of crystal deposits under high magnification on 3D printed PLA scaffolds (n=3) after 4 weeks of osteo-inductive culture in vitro.
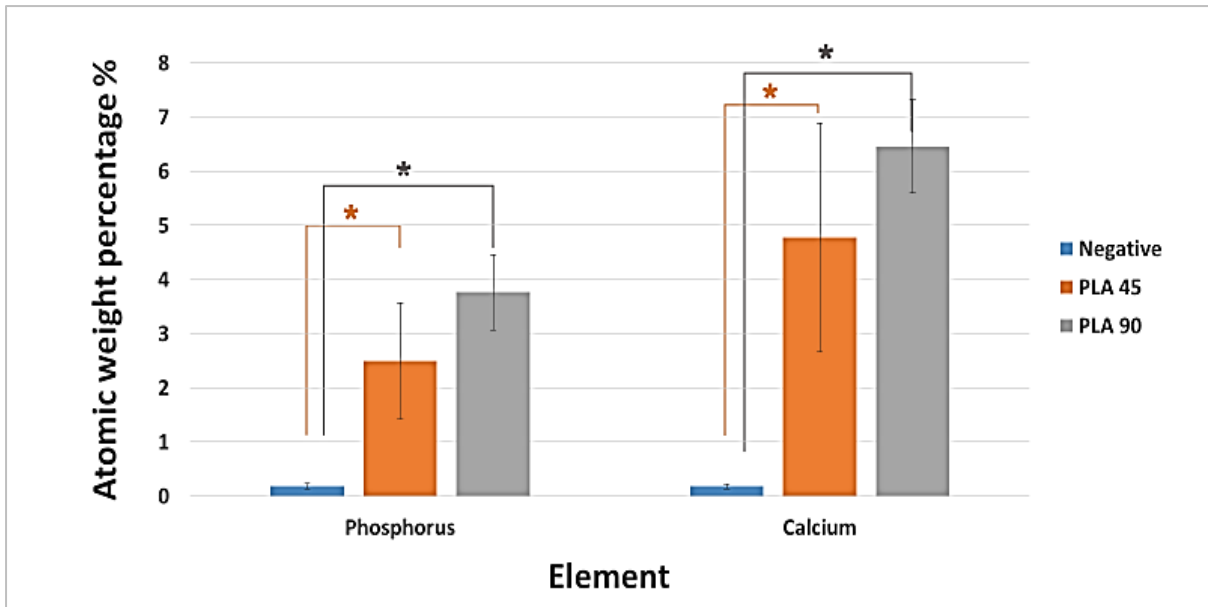
Figure 5-11: Comparison of Ca and P atomic weight percentages between areas of possible mineral deposits within 3D printed PLA constructs after 4 weeks of osteo-inductive culture in vitro.

125
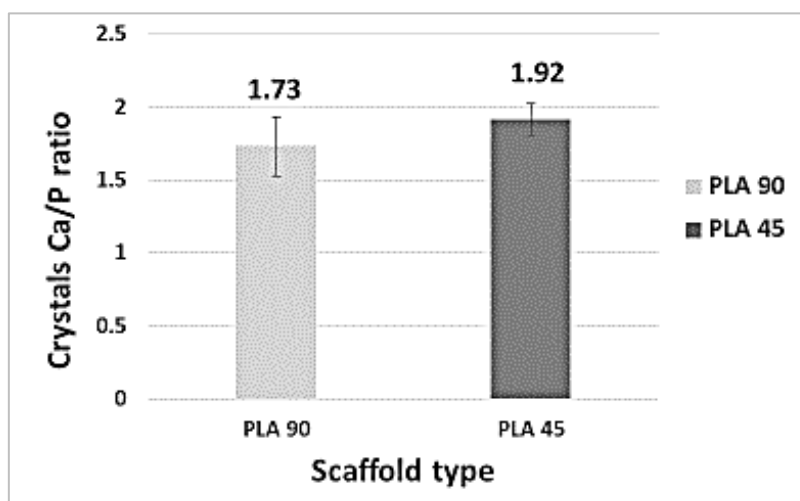
Figure 5-12: Comparison of Ca/ P ratio in crystal deposits found within neo-matrix formed within 3D printed PLA constructs after 4 weeks of osteo-inductive culture *in vitro* (n=3, mean± SD). No significant difference was detected between the two groups (p>0.05)

5.4.5.3. Von Kossa histology staining

Positive Von Kossa staining was detected within histological sections of both PLA groups regardless of fibre angle after 5 weeks of osteo-inductive culture. Staining appeared as black deposits seen within the neo-matrix. (Figure 5-14).

5.4.6. Effect of PLA fibre angle on newly formed tissue growth and histological appearance within PLA constructs *in vitro*

Von Kossa-haematoxylin-safranin red histological staining of constructs after 5 weeks in osteo-inductive culture revealed high cellular growth surrounded by well-established connective tissue formation in both PLA groups with no apparent differences between them (Figure 5-13).
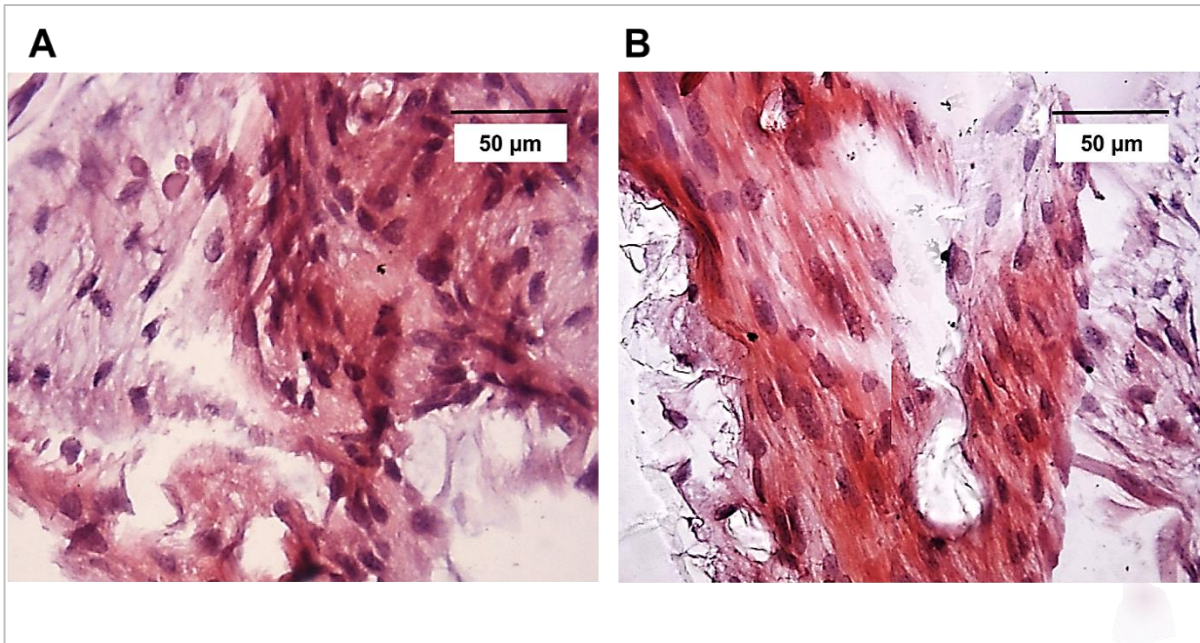
Figure 5-13: Histological appearance (Von Kossa-haematoxylin-safranin red staining) of 3D printed PLA constructs after 5 weeks in osteo-inductive culture *in vitro*, showing obvious hDPSCs growth and extracellular matrix formation in all constructs regardless of fibre angle. A: PLA 90°. B: PLA 45°.
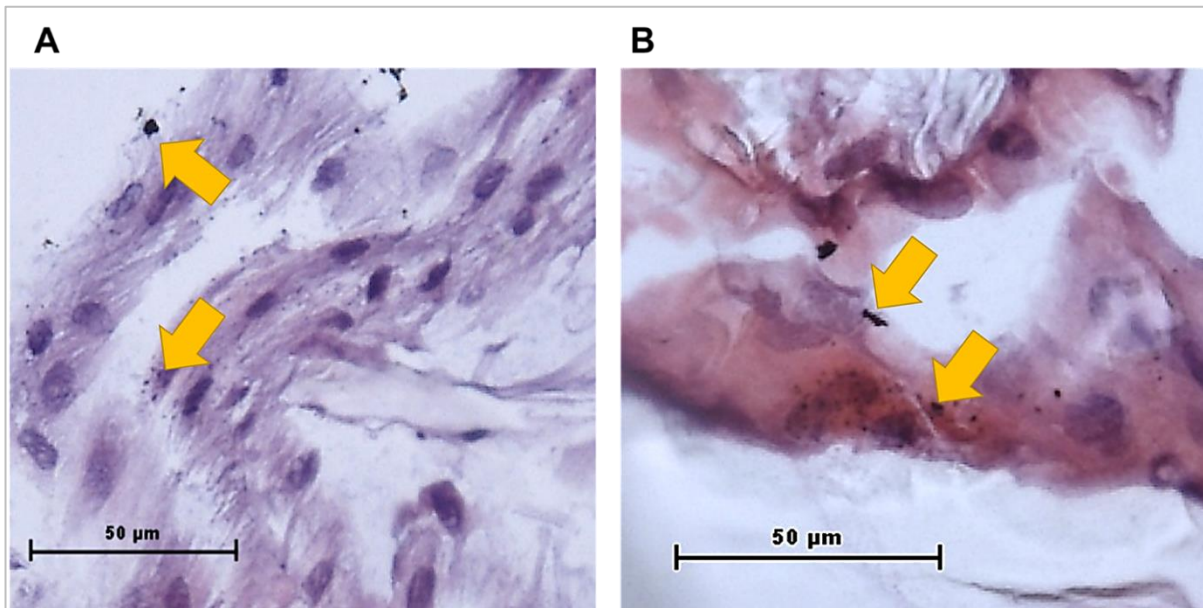
Figure 5-14: Histological appearance at high magnification (Von Kossa-haematoxylin-safranin red staining) of 3D printed PLA constructs after 5 weeks in osteo-inductive culture *in vitro* showing positive Von Kossa staining seen as black mineral deposits (arrows) within the newly formed matrix of both PLA groups. A: PLA 90°. B: PLA 45°.

5.4.7. Effect of fibre angle on hDPSCs expression of osteogenic markers *in vitro* determined by histochemical staining and IHC

5.4.7.1. ALP staining

PLA constructs of both groups showed intense positive ALP staining after 3 weeks in osteo-inductive culture irrespective of PLA fibre angle (Figure 5-15).
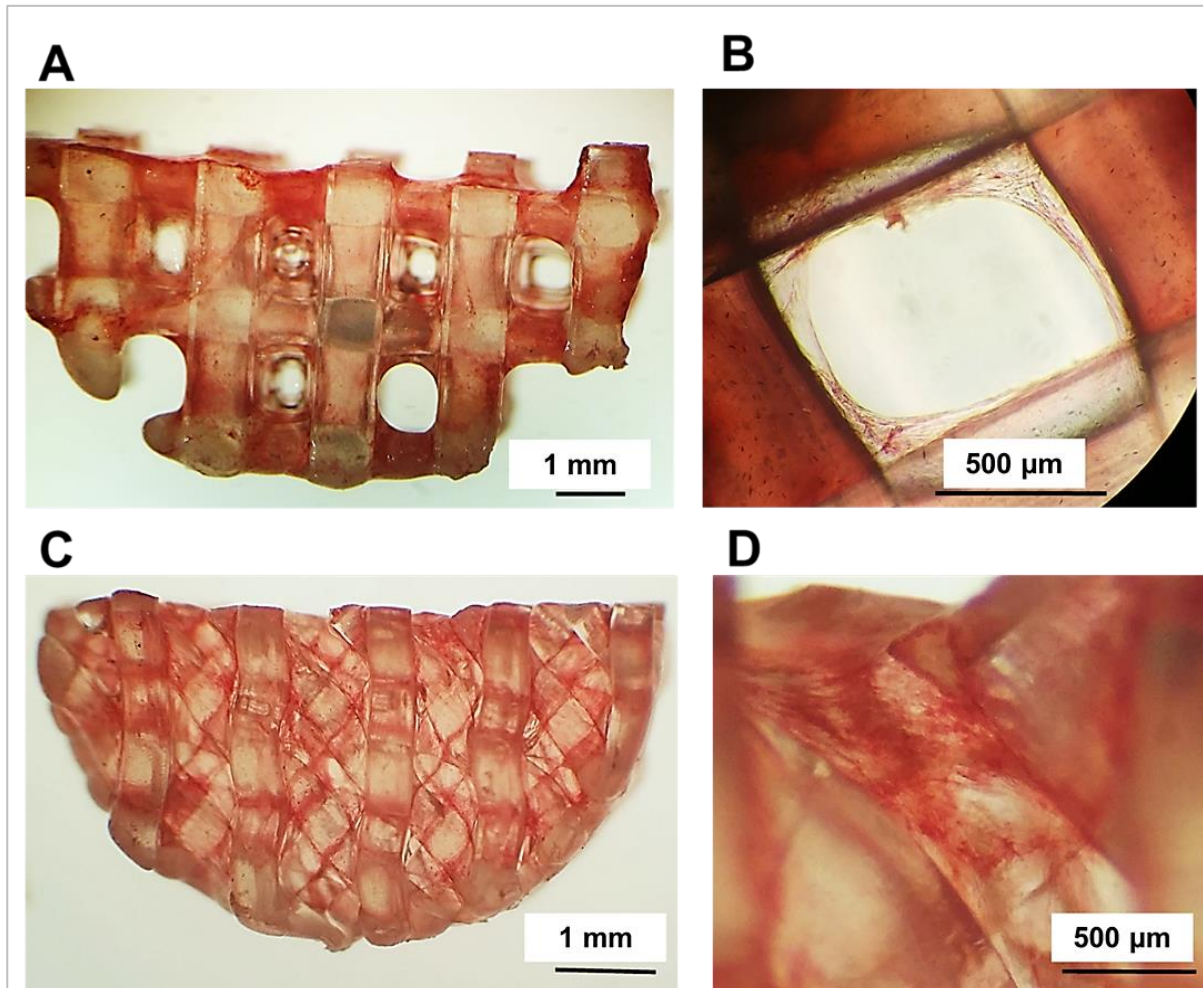
Figure 5-15: Stereomicroscopy images for ALP stained 3D printed PLA constructs after 3 weeks in osteo-inductive culture. Both PLA groups showed strongly positive reaction (pink-red) to ALP stain regardless of scaffold fibre angle. A: PLA 90°. B: PLA 90° at higher magnification. C: PLA 45°. D: PLA 45° at higher magnification.

5.4.7.2. IHC detection of bone markers

IHC was used to determine the expression of bone markers in 3D printed PLA-hDPSC constructs after 5 weeks in osteo-inductive culture. Positive reactivity was seen using anti-Col-I, OPN and OCN antibodies within different areas within the newly formed matrix of both PLA groups, with no particular distribution pattern. IHC staining, especially for Col-I and OCN were observably distributed over wider areas within the newly formed ECM in the PLA 45° group compared to PLA 90° in some regions (Figure 5-16).
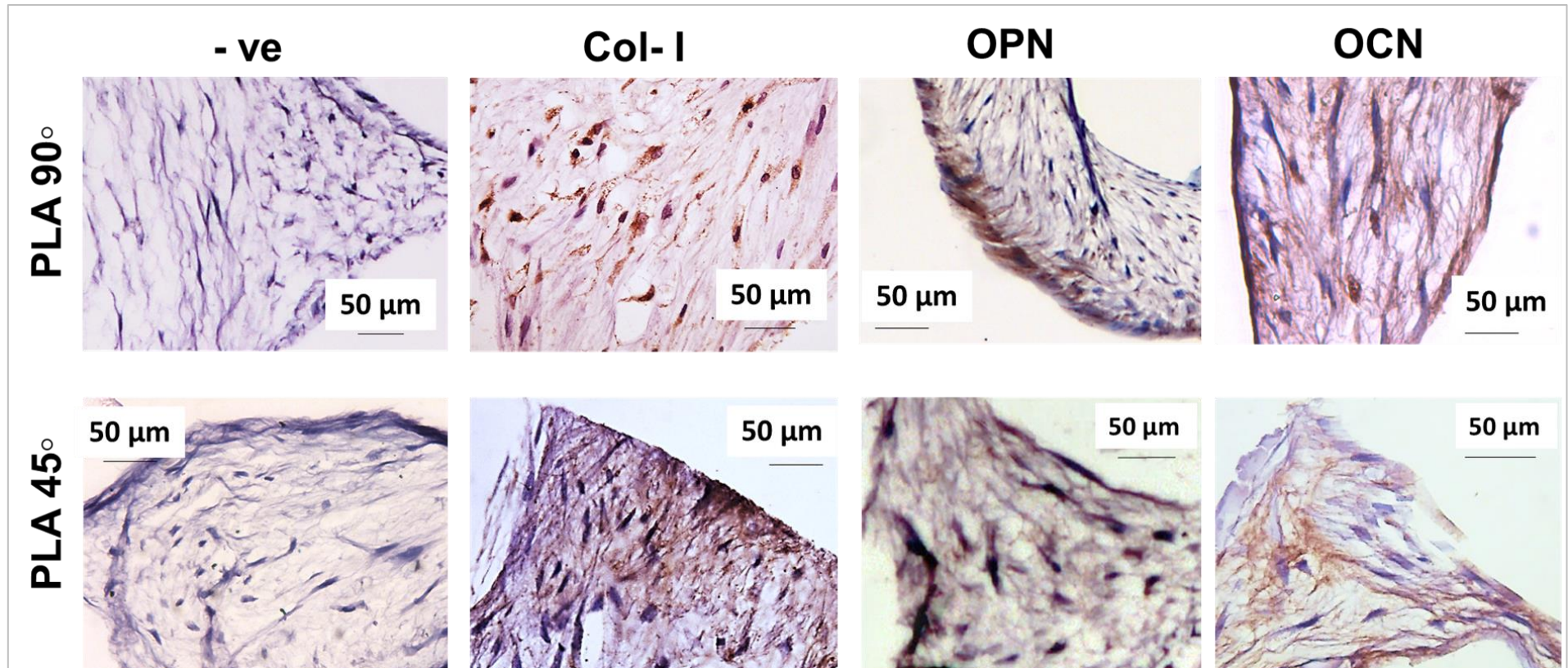
Figure 5-16: IHC for 3D printed PLA-hDPSC constructs after 5 weeks in osteo-inductive culture *in vitro* using anti- Col-I, OPN and OCN antibodies. Top row: PLA 90° constructs showing positive reaction (seen as brown staining) against anti-Col-I, OPN and OCN antibodies. Bottom row: PLA 45° constructs showing positive reaction against anti- Col-I, OPN and OCN antibodies. Expression of Col-I and OCN seemed to be distributed over wider areas than those seen within PLA 90° group.

5.4.8. Effect of PLA scaffold fibre angle on hDPSCs growth, osteogenic differentiation and mineralisation *in vivo*

5.4.8.1. SEM and EDS analysis for *in vivo* 3D printed PLA constructs

Eight weeks after *in vivo* intraperitoneal implantation of 3D printed PLA constructs, SEM images showed that the constructs implanted immediately after cell seeding showed only a small amount of neo-tissue formation in both PLA groups (Figure 5-17 A and B) with sparse mineral deposits detected under high magnification only in the 45° PLA samples (Figure 5-18 A and B).

For constructs that were pre-cultured *in vitro* in osteo-inductive culture for 8 weeks prior to implantation in the animal model, SEM showed dense tissue formation in both PLA 90° and 45° constructs, covering most of the scaffold surface (Figure 5-17 C and D). Obvious mineral deposits were detected within both groups, but these deposits seemed to be more obvious in the PLA 45° samples compared to the PLA 90° group (Figure 5-18 C and D). EDS elemental mapping showed a widespread distribution of Ca and P within the mineral deposits in the newly formed tissue of both PLA groups regardless of scaffold fibre angle (Figure 5-19).
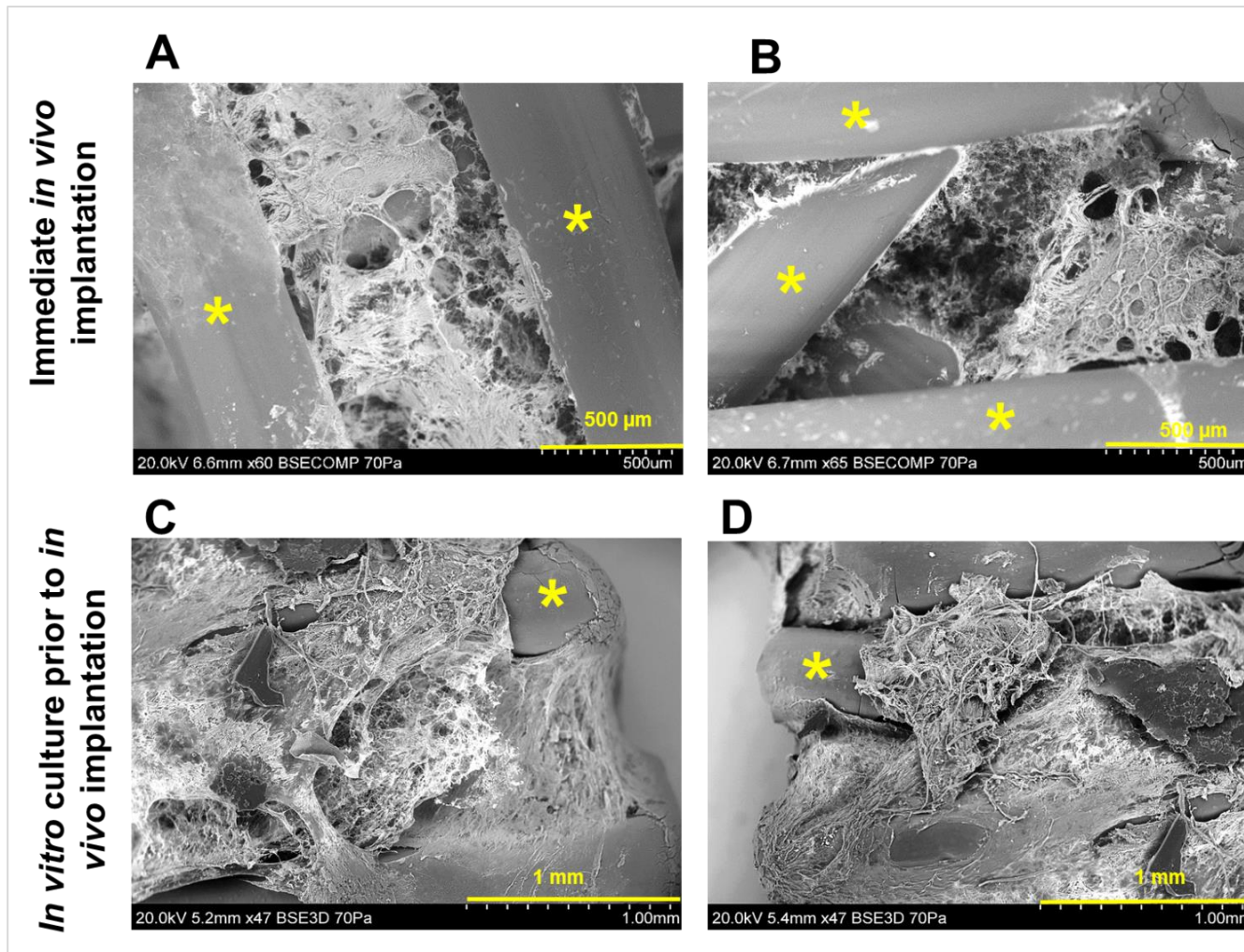
Figure 5-17: SEM imaging of 3D printed PLA-hDPSC constructs retrieved following 8 weeks in DCs *in vivo* showing new tissue formation.
A and B: Less tissue was detected in constructs that were immediately implanted in DCs after seeding regardless of scaffold fibre angle. C and D: Obvious tissue formation was detected in constructs pre-cultured *in vitro* for 8 weeks in osteo-inductive culture prior to implantation in mice regardless of scaffold fibre angle (yellow * represents scaffold fibre).
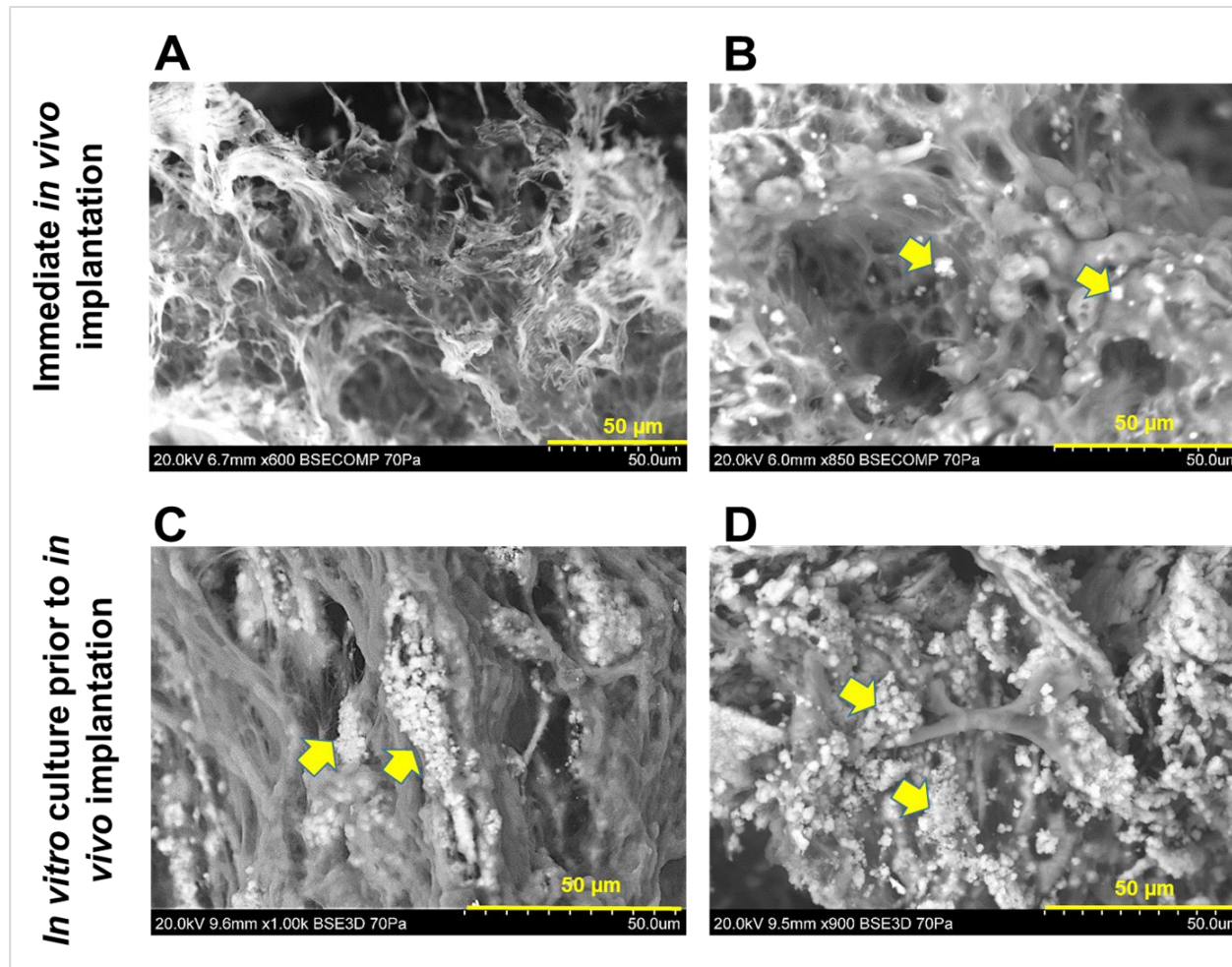
Figure 5-18: SEM imaging of 3D printed PLA-hDPSC constructs retrieved following 8 weeks in DCs *in vivo* showing mineral deposition within the constructs. A: No deposits could be detected in PLA 90° constructs that were immediately implanted *in vivo* after seeding. B: A few scattered mineral deposits could be seen in PLA 45° constructs implanted immediately after seeding (arrows). C: PLA 90° constructs pre-cultured *in vitro* for 8 weeks in osteo-inductive culture prior to *in vivo* implantation showed mineral deposits in clusters. D: PLA 45° constructs pre- cultured *in vitro* prior to *in vivo* implantation showed a greater abundance of mineral deposits (arrows) in comparison with the PLA 90° group.
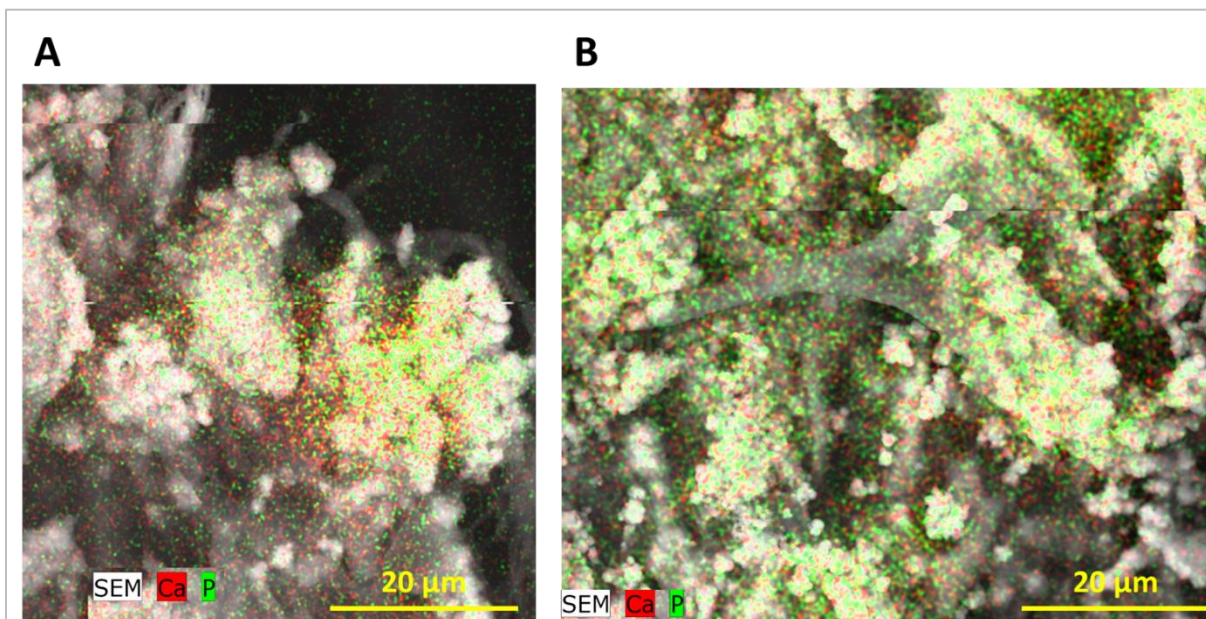
Figure 5-19: EDS elemental mapping of areas of mineral deposits within 3D printed PLA constructs retrieved from DCs after 8 weeks of implantation *in vivo*. Constructs were pre-incubated for 8 weeks in osteo-inductive medium prior to implantation. Mineral deposits seen on constructs from both PLA groups showed pseudo colouring with red and green channels, corresponding to Ca and P respectively. A: PLA 90°. B: PLA 45°

5.4.8.2. Histology of *in vivo* 3D printed PLA-hDPSC constructs using AB-SR and Von Kossa stains

Upon histological sectioning of 3D printed PLA constructs that had been immediately implanted *in vivo* after seeding and retrieved 8 weeks after implantation in the animal model, insufficient tissue could be collected on microscope slides from both PLA groups to permit histological examination (i.e. no evaluation could be carried out).

For 3D printed PLA-hDPSC constructs that were pre-cultured in osteo-inductive conditions for 8 weeks *in vitro* prior to implantation for 8 weeks in the animal model, AB-SR histological staining showed dense tissue surrounding both PLA 90° and 45° scaffolds, which was positive for AB stain within the new ECM in some regions (Figure 5-20). Positive staining with Von Kossa mineral stain was also detected in both PLA groups. However, the black stained deposits were found to be more abundantly distributed within the new matrix of PLA 45°

constructs. Mineral deposits seen in PLA 90° samples were obviously fewer in number and only seen as a thin "frame" lining the PLA fibres that formed the square scaffold pore. In addition, the black deposits were larger in the PLA 45° constructs compared to those seen within PLA 90° constructs (Figure 5-19).
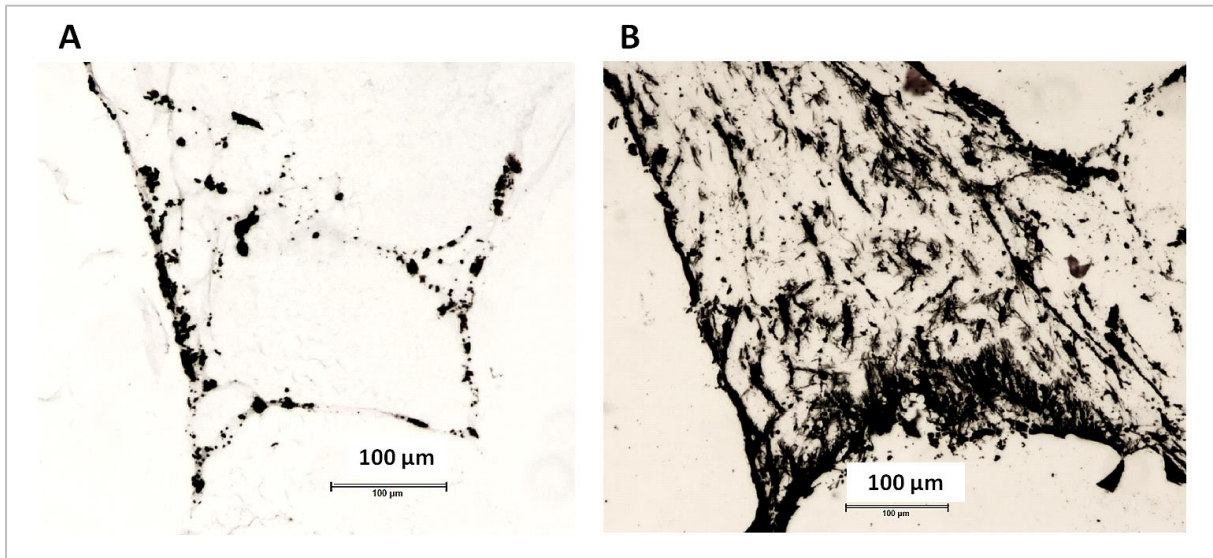
Figure 5-20: Von Kossa staining for 3D printed PLA-hDPSC constructs retrieved from DCs after 8 weeks of implantation *in vivo*. Constructs were pre-incubated for 8 weeks in osteo-inductive medium prior to implantation. A: PLA 90° constructs showed positively stained black deposits distributed as a thin "frame" lining the PLA fibres that form the square scaffold pore. B: In contrast, PLA 45° constructs showed a greater amount and wider distribution of positively stained material, with the black (presumed mineral) deposits themselves being larger than those seen within PLA 90° constructs.

5.4.8.3. IHC analysis for *in vivo* 3D printed PLA-hDPSC constructs

For 3D printed PLA-hDPSC constructs that had been immediately implanted *in vivo* after seeding and retrieved 8 weeks after implantation in the animal model, insufficient tissue was collected on slides for constructs from both PLA groups for IHC analysis where implantation had occurred immediately after seeding. For 3D printed PLA constructs that were pre-cultured *in vitro* in osteo-inductive conditions for 8 weeks prior to implantation for 8 weeks in the animal model, IHC examination showed positive reactivity to anti- Col-I, OPN and OCN osteogenic marker antibodies for constructs in both PLA groups, with no particular pattern of positive stain distribution apparent. No noticeable

difference in staining intensity was detected between the two groups; however,

PLA 45° constructs showed a wider distribution of the bone markers compared

to PLA 90° (Figure 5-21).
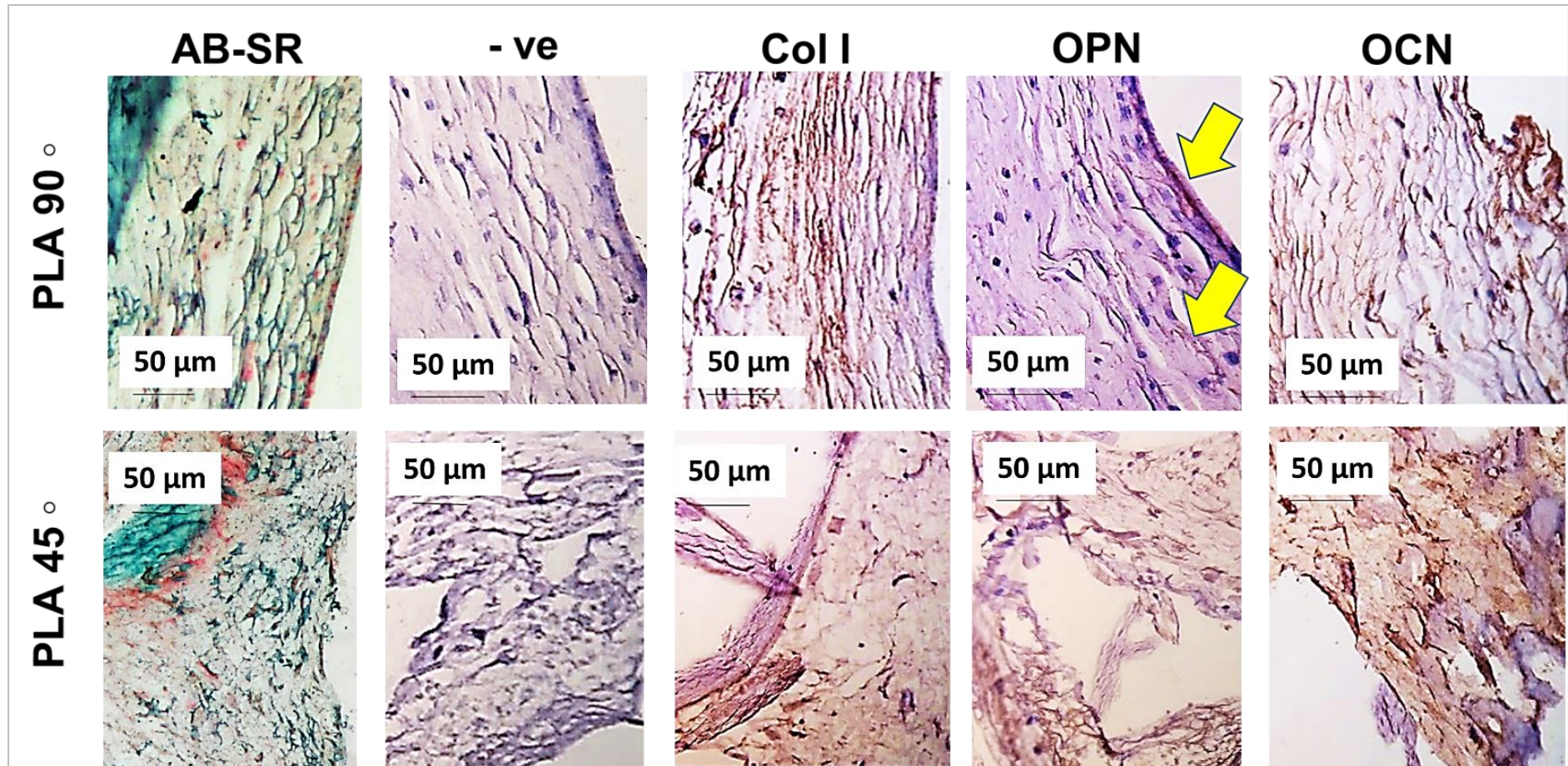
Figure 5-21: Histology (AB-SR stain) and IHC (Col-I, OPN and OCN antibodies) for 3D printed PLA-hDPSC constructs retrieved from DCs after 8 weeks of implantation *in vivo*. Constructs were pre-incubated for 8 weeks in osteo-inductive medium prior to implantation. Top row: PLA 90° constructs showed dense tissue formation with some areas stained positive to AB within the ECM. Positive reactivity (seen as brown staining) against anti- Col-I, OPN (yellow arrows) and OCN antibodies was detected within the constructs. Bottom row: PLA 45° constructs showed dense tissue formation with some areas staining positive for AB within the ECM. Positive reactivity (seen as brown staining) against anti-Col-I, OPN and OCN antibodies, which apparently seemed to be more widely distributed than that seen within PLA 90° group was evident in some areas.

5.5. Discussion

In this thesis, PLA 90° scaffold was used to represent the classic design, creating uniform box-shaped macropores that were evenly distributed within the scaffold. Scaffolds of this kind have been frequently used elsewhere as a control model compared to other suggested layouts that were evaluated (Burg *et al.*, 2000; Hutmacher *et al.*, 2001; Yilgor *et al.*, 2008; Sobral *et al.*, 2011; Domingos *et al.*, 2013; Berner *et al.*, 2014) and were used similarly here. However, there has been a recent tendency in research towards production of 3D printed scaffolds with a gradient in pore sizes and geometries generated by an offset layer stacking aimed to increase scaffold efficiency in supporting cellular attachment and proliferation (Burg *et al.*, 2000). To the author's best knowledge, no previous work has described the combination of PLA 45° 3D printing layout with hDPSCs primary cultures for bone tissue regeneration.

The choice of a scaffold seeding technique, whether static or dynamic needs to be considered carefully depending on scaffold material and geometry (Melchels *et al.*, 2010). In this work, preliminary trials (data not shown) using dynamic seeding showed few hDPSCs attached to scaffold surfaces at the end of the seeding procedure compared to static seeding, with clumping of cells into larger lumps. This may be due to a continuous washing off of attached cells from the relatively smooth PLA fibre surfaces as a result of the continually circulating medium during dynamic culture, with the scaffold itself floating and continuously moving inside the seeding chamber. This concurs with what has been reported previously in the literature in that increased agitation during dynamic seeding can cause accelerated shear forces across the scaffold that adversely affect cellular attachment by washing off the newly adherent cells (Burg *et al.*, 2000; Alvarez-Barreto *et al.*, 2007).

5.5.1. Increased hDPSCs attachment on PLA 45° compared to PLA 90° *in vitro*

Results of this study showed that the PLA 45° scaffolds supported greater hDPSCs adhesion compared to PLA 90° after 4 hours of static seeding. This may be attributed to both the presence of offset between scaffold layers and the overall reduced medium flow throughout the scaffold during the cell seeding process (Woodfield *et al.*, 2004). It has been previously suggested by Yilgor *et al.* (2008) that the offset pattern would provide higher available fibre surface area on the top of the scaffold, where the fibres would act as a trap to the cells falling by gravity during static seeding. In contrast, where the offset is absent (as in case of PLA 90° scaffolds), there is an increased likelihood of cells passing through the scaffold without having the chance to attach anywhere; as they would face a clear path through the open pores all the way down to the bottom of the well, where they would mostly settle (Yilgor *et al.*, 2008; Sobral *et al.*, 2011). Another aspect to consider is the regulation of cell suspension permeability within the scaffold guided by the geometrical orientation of scaffold fibres. The PLA 90° used in this study is considered to be highly permeable compared to 45° PLA (Sobral *et al.*, 2011), where there is a decrease in pore size from the surface layer towards the middle of the scaffold (500, 250 and 90 mm^2 respectively as demonstrated in table 5-1). This size gradient will restrain medium flow through the scaffold, supporting superior cell attachment to the fibre surfaces and junction sites (Sobral *et al.*, 2011). The study by Impens *et al.* (2010) also supported the latter view, concluding that decreasing scaffold permeability significantly increased seeding efficiency by enhancing cellular attachment.

5.5.2. Enhanced hDPSCs growth and pore bridging detected within PLA 45° constructs *in vitro and in vivo*

Cellular growth and colonisation within porous matrices are greatly influenced by how fluently cells can bridge pores and spread inside the scaffold. One factor to consider in this respect is pore size, as too large a pore compared to cell spanning capability will make it more difficult for cells to spread and form networks throughout the scaffold (Lawrence and Madihally, 2008). During cellular attachment, larger pores will support cells to attach only to a single strut at a time and in this case, cells will continue growing as monolayers on the fibre surface, until they form enough ECM to support their further spread into the empty central space of the pore, then increasing the overall time required for them to bridge the gap (Lawrence and Madihally, 2008). In contrast, with small pores where fibres are closer together, multiple contact points will be available for the cell to attach (Domingos *et al.*, 2013). However, previous studies have suggested that larger pores would provide more open spaces for cells to grow and ensure unrestricted diffusion of oxygen and nutrients, especially to the central parts of the scaffold, thus supporting enhanced cellular growth (Van Bael *et al.*, 2012; Berner *et al.*, 2014). In this context, a combination of both smaller and larger pores within the same scaffold design, rather than a mono-pore architecture, offers a promising approach to consider. This could be one reason behind PLA 45° showing superior support to hDPSCs growth and more rapid pore bridging and closure compared to PLA 90°, as the former enclosed generally smaller pores with a gradient pore size distribution from larger at the surface to smaller towards the middle of the scaffold; which in turn could create a funnel effect that helps deeper invasion of cells inside the scaffold structure (Sobral *et al.*, 2011). However, Domingos *et al.* (2013) disagree with this view, as they suggested that smaller pores should be incorporated at the scaffold surface and gradually get larger towards the centre of the scaffold to provide better

oxygen and nutrient supply to the deeper parts of the construct. It is thought to be essential to take into consideration that the overall porosity of the scaffold is also contributory to this outcome, apart from pore size (Hutmacher *et al.*, 2001). For that reason, future investigations would be valuable to quantify and compare the overall porosity percentage of the two PLA designs used in this study.

Another architectural factor affecting cells ability to bridge and close scaffold pores is pore geometry. It has been reported that pores with sharper angles are generally more rapidly occupied by newly formed tissue than pores of similar overall size but with wider angles (Uebersax et al., 2006; Lee et al., 2008). This was explained by the decreased distance generated between two struts towards the corner of a pore, creating an initiation region where cells could quickly start bridging (Rumpler *et al.*, 2008). This phenomenon was clearly observed in the PLA constructs used in the current study, where pore bridging was observably superior in the narrow corners of PLA 45° pores compared to the broader pores of PLA 90° after 3 weeks of culture *in vitro*. Also, the rotation of stacking angle between PLA 45° scaffold layers created a more complex 3D pore geometry with an increased number of angles within the same pore. The greater the number of corners within a pore, the more areas that can be bridged (Knychala *et al.*, 2013). In contrast to this hypothesis, several studies in the literature imply that cellular bridging behaviour is a purely down to pore size, regardless of its geometry (Shor *et al.*, 2007; Lee *et al.*, 2008; Van Bael *et al.*, 2009; Van Bael *et al.*, 2012). The differences in pore occlusion seen in these reported studies could be attributed to the different types of cells used in each of them as maximal spanning distance could presumably be variable from one cell type to the other.

Kommareddy *et al.* (2010) showed that the tissue growth in 3D scaffolds follows two stages; the first stage is guided by cell-material interactions that are strongly

dependent on the polymer material. In the later stage of growth, cells start to grow within their own matrix resulting in 3D tissue amplification, which is controlled by the pore size and geometry rather than scaffold material properties. Previous studies also demonstrated that cellular growth in 3D structures followed a curvature-driven mechanism, where the highest initial tissue growth was observed in corners with increased curvature. (Rumpler *et al.*, 2008; Knychala *et al.*, 2013). The latter studies also suggested that this accelerated growth would gradually decrease as the neo tissue progressively filled the pore, reaching a mechanical equilibrium. This was reflected in the results of this thesis, as cellular bridging progressed more in PLA 45° constructs after 3 weeks of culture *in vitro* compared to the PLA 90° group; apparently newly formed, highly viable cell sheets were then seen to cover all constructs regardless of PLA fibre angle used after week 4 of culture, although a few pores were still seen to be open when the PLA 90° constructs were viewed laterally. It is important to note that the estimation of cellular growth in this project was qualitative, so future DNA quantification assays could be considered to accurately compare cellular growth rate within the constructs of the two designs of PLA used here.

With regard to the evaluation of *in vivo* growth of hDPSCs on 3D printed PLA scaffolds, PLA constructs that were implanted *in vivo* immediately after seeding showed deficient cellular growth, as scant tissue could be detected by SEM within the constructs after 8 weeks of *in vivo* culture. The author suggests that this could be related to the cell seeding density used, or it could be a specific phenomenon related to the particular use of the DC *in vivo* model. It is known that for any construct to act successfully *in vivo*, high cell densities are required to ensure adequate tissue formation within the 3D scaffolds, especially in DCs where a gradual decrease in oxygen and nutrient diffusion occurs as mouse fibrous tissues and debris collectively accumulate on the

outside of the chamber filter (Breivik *et al.*, 1971). Also, trials to increase the seeding density for PLA scaffolds in this study beyond that applied *in vitro* (2×10^5 cell/sample) led to clumping and/or stratification of the seeded cells overlying one another and then all finally peeling off the smooth polymer surface. It was also suggested by Vunjak-Novakovic and Radisic (2004) that this could be caused by the general characteristics of PLA material, such as relatively solid polymer fibres that limit cells' ability to ingress within the scaffold material itself. This could result in a shortage in the number of cells required to produce adequate tissue *in vivo* (Galban and Locke, 1999; Sobral *et al.*, 2011). In addition, the choice of diffusion chamber model for use in this project was based on different reasons and this will be discussed later in ***Chapter 7*** of this thesis. In contrast, the current results showed that the PLA constructs pre-cultured *in vitro* before *in vivo* implantation demonstrated hugely increased amounts of tissue formed within DC. Again, this pre-culture period could be a specific need related to the cell density used and/or DC model, as discussed above. More realistic understanding to the *in vivo* constructs' behaviour could be achieved with the future use of an actual bone defect *in vivo* model.

No obvious difference was detected in tissue growth within constructs of the two PLA designs pre-cultured *in vitro* and examined after 8 weeks of *in vivo* implantation. Roosa *et al.* (2010) found that in 3D printed polymer scaffolds, pore size differences can have a time-dependent effect on the *in vivo* regenerated bone tissue, as differences could be detected after 4 weeks of *in vivo* culture but not after 8 weeks, at this time all the constructs seemed to have similar bone growth regardless of the pore size used. Miao and Sun (2010) explained this by suggesting that fast initial bone growth rate into the pore spaces gradually slows down with maturation and remodelling of the bone.

5.5.3. HDPSCs osteogenic differentiation on 3D printed PLA scaffolds *in vitro* and *in vivo*

The results of this project showed that both PLA 90° and 45° designs supported osteogenic differentiation of hDPSCs *in vitro.* Constructs from both groups were strongly stained positive for ALP, an early marker of osteogenesis (Cowles *et al.*, 1998), after 3 weeks of osteo-inductive culture. In addition, the newly formed tissue within the two groups of constructs positively expressed 3 other known bone markers; Col-I, OPN and OCN as detected by IHC (Hauschka *et al.*, 1983; Cowles *et al.*, 1998; Seibel *et al.*, 2006) after 5 weeks in osteo-inductive culture. PLA 45° constructs showed stronger reactivity against Col-I and OCN antibodies compared to PLA 90°constructs. This could be attributed to the greater cellular attachment and growth within PLA 45° constructs compared to PLA 90°, with the greater stimuli generated by more cell-scaffold and cell-cell interactions at an earlier stage that potentially accelerated osteogenic differentiation (Van Bael *et al.*, 2012). This finding, however, conflicts with a number of previous studies reporting the potential of 3D printed polymer scaffolds to support osteogenic differentiation *in vitro* regardless of scaffold design (Lee *et al.*, 2008; Van Bael *et al.*, 2012). It is important to note that the methods to evaluate osteo-differentiation used in this project were all qualitative; so for a more accurate analysis, future quantitative measures like histomorphometry or polymerase chain reaction (qPCR) could be carried out to compare bone marker expression levels between the two 3D printed PLA designs used.

The results of this study showed that both PLA 45° and PLA 90° scaffolds supported osteogenesis within the newly formed ECM after 8 weeks of *in vivo* culture, with PLA 45° showing more widely distributed reactivity against antibodies for the bone markers Col-I, OPN and OCN in IHC compared to the PLA 90° group, confirming the results obtained *in vitro* above. It is important to keep in mind that it is still unknown whether

the positive AB staining detected within the newly formed tissue within constructs implanted *in vivo* reflected chondrogenic differentiation or was an indicator for an early form of osteogenesis. This might require a more detailed IHC analysis to detect the presence of reactivity against antibodies for Col-II, a marker for chondrogenesis. It would also be interesting to determine the presence of any dentinogenesis (using specific IHC markers like dentine sialophosphoprotein), which would also give a positive reaction for the bone markers seen here.

Different studies have investigated the effect of polymer scaffold geometrical design on bone formation *in vivo*. It has been reported that overall scaffold porosity and pore size have the most considerable influence on bone tissue formation within *in vivo* polymer scaffolds (Van Tienen *et al.*, 2002; Karageorgiou and Kaplan, 2005). Others, contrastly, stated that there is a limited effect of pore size on bone formation *in vivo* (Fisher *et al.*, 2002; Schek *et al.*, 2006). In a study by Berner *et al.* (2014), it was found that 3D printed polymer scaffolds with larger homogenous cubic pores showed superior bone formation in calverial bone defects than a similar scaffold with smaller polygonal pores at different sizes. This could be due to the more efficient invasion of scaffold larger pores by the neighbouring bone ingrowth, as well as more effective oxygen and nutrient supply lead by more open space provided by larger pores. Other studies have emphasised the fact that combining both small and larger pores within the same 3D printed scaffold design might increase the overall quality of the scaffold in supporting bone regeneration, thus simulating a more natural bone environment (Karageorgiou and Kaplan, 2005; Miao and Sun, 2010; Van Bael *et al.*, 2012). It has been stated that for bone ingrowth to occur in a 3D scaffold *in vivo*, a minimum pore size of around 100 µm is required for cell migration and nutrient diffusion, while pore sizes above 300 µm are recommended to promote new bone formation and tissue

vascularisation (Sobral *et al.*, 2011). Thus, porous biomaterials with uniform shape and distribution of porosities would show functional limitations during bone regeneration when compared to graded/gradient porosity designs (Simske *et al.*, 1997; Miao and Sun, 2010).

5.5.4. Matrix mineralisation within 3D printed PLA constructs *in vitro* and *in vivo*

Investigations to detect evidence of mineralisation within the constructs following incubation *in vitro* in the current study confirmed the presence of matrix mineral deposits regardless of construct fibre angle. SEM imaging of both groups showed the presence of rod-like mineralised crystal clusters in different areas within the constructs. A number of studies reported the formation of different forms of mineral within newly formed tissue matrix, including rod-like crystals, as reflective of the surrounding solution pH and mineral ion content (Ho *et al.*, 2006; Lin *et al.*, 2014; Shi *et al.*, 2015). The deposits found within PLA constructs in the current study are likely to be a form of calcium phosphate mineral aggregates (not merely crystal precipitations from the immersing solutions) as EDS analysis showed that the main mineral content within these crystals was Ca and P (Lawlor, 2016). Biological hydroxyapatite formed in bone presents as nanoscale rod-like or plate-like crystals with a thickness of a few nanometers and tens of nanometers long (Lin *et al.*, 2014; Okada and Matsumoto, 2015). However, although the mean molar ratio of Ca/ P value ratio of the crystals formed in this study was close, it was still higher than that expected for hydroxyapatite crystals, which is 1.67 (Masson *et al.*, 2017), suggesting calcium-rich accretions (or phosphate poor). Von Kossa histochemical staining supported the presence of mineral deposits within the neo matrix of both PLA construct groups. Many previous studies agreed with these results in that 3D printed polymer scaffolds

146

have the potential to support neo matrix mineralisation *in vitro* (Cartmell *et al*., 2004; Ho *et al*., 2006; Davies *et al*., 2015; Shi *et al*., 2015).

Although no obvious difference in *in vitro* mineralisation was detected, the prolonged *in vivo* culture could provide a good approach to evaluate the effect of PLA fibre angle on longer-term mineralisation potential of the ECM formed within 3D printed PLA constructs *in vivo*, as most mineralisation studies usually require extended culture times and a change of culture conditions (Newton *et al*., 2012). In the work of this thesis, SEM imaging showed densely distributed mineral deposits within the ECM of PLA 45° constructs that were much more abundant than those seen within PLA 90° constructs after 8 weeks of *in vivo* culture. EDS image mapping showed that these deposits were mainly composed of Ca and P; however, it was difficult to obtain consistent quantification of these minerals by EDS because of their extended, random spread within the matrices of the two PLA groups constructs examined. Von Kossa staining confirmed the SEM/ EDS results, interestingly showing heavy accumulations of large black deposits within the ECM of PLA 45° constructs compared to the PLA 90° group, where smaller black deposits were seen as a thin frame lining the square-shaped scaffold macropore.

Many studies have reported that matrix mineralisation mediated by stromal cells during their osteogenic differentiation on biodegradable polymer scaffolds was seen to be running along the fibre periphery. In this zone, initial cellular spreading occurred covering the whole fibre surface until confluent. Then, subsequent differentiation and neo-matrix mineralisation started to take place within these initial cellular layers possibly earlier than the later formed tissue within the scaffold pore (Ishaug *et al*., 1997; Ishaug-Riley *et al*., 1998; Cartmell *et al*., 2004). This could explain the mineralisation pattern that was detected in the current study for PLA constructs after

implantation *in vivo*. Mineral deposits ran along the intersected PLA fibres forming the square pore framework of PLA 90° constructs, presenting as a thin square lining of minerals, while within PLA 45° constructs, deposits were spread along the offset overlapping PLA fibres extending through the whole pore, producing a dense mineral deposition pattern. In respect of the difference in mineral deposit size seen within the two construct types with Von Kossa staining in this thesis, Ho *et al.* (2006) suggested that increased black spot size with Von Kossa stain indicates a higher degree of mineralisation activity, while the larger area of black spots spread reflects that more cells have been involved in matrix mineralisation. It is also important to consider that the general increase in hDPSCs attachment and growth within PLA 45° constructs compared to PLA 90° could possibly dictate earlier overall differentiation, so more advanced matrix mineralisation might take place within the same period of culture. This assumption is supported by the increased expression of osteogenic markers seen using IHC within PLA 45° constructs compared to the same analysis of PLA 90° constructs at the end of the *in vivo* implantation period. In this respect, OCN is of especial importance, as it is usually produced later in the osteoblast differentiation pathway prior to and during mineralisation (Fanburg *et al.*, 1997).

5.6. Conclusion

This study showed that 45° angled PLA 3D printed scaffolds enhanced hDPSCs attachment, cellular bridging and possible mineralisation both *in vitro* and *in vivo* compared to the 90° angled design, illustrating the importance of fibre geometry in influencing cell behaviour and the potential use of this kind of 3D printed scaffold to enhance bone tissue regeneration.

CHAPTER SIX

Effect of combining Self-Assembling Peptide P$_{11}$-4 with 3D printed PLA scaffolds on hDPSCs attachment, growth and osteogenic differentiation *in vitro* and *in vivo*

Chapter 6. Effect of combining Self-Assembling Peptide P$_{11}$-4 with 3D printed PLA scaffolds on hDPSCs attachment, growth and osteogenic differentiation *in vitro* and *in vivo*

6.1. Introduction

Synthetic polymers like polylactic acid (PLA) are mechanically strong with excellent manufacturer control over a wide range of porosity and degradability characteristics (Li and Ma, 2004; Serra *et al*, 2014). Their use as matrices for BTE became even more tempting after the introduction of scaffold 3D printing fabrication technology, providing more precise control over scaffold shape and internal structure geometry (Liu *et al*, 2008; Serra *et al*, 2013; Li *et al*, 2014; Holmes *et al*, 2015). However, PLA as a raw material is criticised for being relatively hydrophobic and chemically inert so has no reactive side-chain groups on its surface (Burg *et al*., 1999, Farah *et al*., 2016). This would give lower chances for cellular affinity, which is a major factor for any material to be successfully used as a scaffold for tissue regeneration (Rasal *et al*., 2010).

Different techniques have been adopted to enhance PLA scaffolds' surface wettability and cellular adhesion. These include direct surface coating with extracellular proteins, like fibronectin and laminin (Serra *et al*., 2013, Rasal *et al*., 2010), UV\ozone photo-grafting and nitrogen, oxygen or helium plasma treatments (Jacobs *et al*., 2012, Rasal *et al*., 2010, de Valence *et al*., 2013) (please see more details in *1.5.5.1.4.3*). More recently, various nanophase materials were combined with PLA scaffold in an attempt to create a nano environment that can upgrade cellular behaviour and function within the scaffold, rather than simply modifying its surface (Eid *et al*., 2001, Chen *et al*., 2006, Gelain *et al*., 2007).

Self-assembled peptides (SAPs) applications in tissue engineering were recently highlighted for their superiority in providing a real 3D environment that can homogeneously incorporate cells, growth factors, and other bioactive compounds

(Hosseinkhani *et al.*, 2006). This technology can generate nano scaled supramolecular structures with a fibrillar diameter in the lowest size range found in natural ECM collagen (Wu *et al.*, 2012), with scaffold formation being initiated spontaneously under physiological conditions without the need for chemical solvents (Gelain *et al.*, 2007). SAP P_{11}-4 in particularl is gaining attention with the field of mineralised tissues engineering including bone and teeth, caries treatment, and management of bone deteriorating conditions, such as osteoarthritis (Bell *et al.*, 2006, Brunton *et al.*, 2013). SAP can work as a template for the nucleation and growth of inorganic materials, mainly due to its ability to increase mineral gain by nucleating hydroxyapatite *de novo* (Kirkham *et al.*, 2007, Boden *et al.*, 2015). However, like other hydrogels, one major disadvantage of the use of SAPs as scaffolds for bone tissue regeneration is its weak mechanical properties, making its use limited in load-bearing areas (Fedorovich *et al.*, 2007). Incorporating the gel within a more rigid material frame could significantly enhance its potential use for bone repair.

To our knowledge, no previous work had been conducted to combine 3D printed PLA scaffolds with SAP P_{11}-4 gel for use in bone tissue regeneration. This combination has great potential for use as a scaffold for BTE. It could hypothetically provide a hybrid micro-nano scale structure composed of a biodegradable, highly porous 3D PLA framework that has excellent mechanical properties and can be printed to match any bone defect shape; enriched with a self-assembled, nanostructured, highly cell-friendly extracellular matrix-like hydrogel that has the potential to nucleate hydroxyapatite crystals *de novo* and promote mineralisation. It would also have a significant advantage in that its production would be a relatively cost-effective, uncomplicated, straight forward procedure compared to other existing methods, as will be discussed later.

6.2. Aims of the chapter

This chapter aimed to evaluate the effect of using PLA 45°/ SAP P_{11}-4 combination as a scaffold for enhancing hDPSCs attachment, growth and osteogenic differentiation for BTE both *in vitro* and *in vivo.*

6.3. Materials and methods

6.3.1. Preparing P_{11}-4 gels

P_{11}-4 peptide powder was purchased from Credentis AG (Windisch, Switzerland). Peptide quality control was undertaken via High Performance Liquid Chromatography (HPLC) and mass spectrometry, indicating a peptide purity of over 98%. The freeze-dried peptide was stored at -20° C before use. The peptide was sterilised in its dry state before gel preparation using gamma irradiation at 25 KGray (Xiros, Leeds, UK). To prepare the gel, freeze-dried P_{11}-4 peptide was dissolved in plain α-MEM to a concentration of 30 mg/mL. Ammonia solution was added to raise the pH to aid dissolution by ensuring that the peptide was in the monomeric state. The solution was vortexed and sonicated as necessary to ensure complete peptide dissolution. Using the phenol red indicator present in α-MEM, the pH of the monomeric peptide solution was then adjusted by the addition of 1 M HCl until a rose-pink colour was seen (pH 7.4). Before use in experiments, gelation was allowed to occur for a minimum of 3 hours. All procedures were carried out at room temperature.

6.3.2. Seeding hDPSCs on PLA 45° scaffolds

Eight 3D printed PLA 45° scaffolds were prepared and sterilised as described earlier in *3.3.7.1.* These scaffolds were then divided into 2 groups (n=4), one contained PLA 45°scaffolds that were seeded with a suspension of hDPSCs mixed with SAP P_{11}-4 (PLA 45°/SAP P_{11}-4 constructs); while the other acted as a control group, where hDPSCs were seeded on PLA 45° scaffolds alone in the absence of SAPs.

To prepare PLA 45°/SAP P$_{11}$-4 constructs, 500 µL of the prepared SAP gel (from **6.4.1)** was heated on a hot plate and vortexed to induce disassembly (no particular temperature was applied, the sample was heated until full disassembly). The disassembled gel was then diluted with 500 µL of plain medium (giving a final SAP concentration of 15 mg/mL) and kept in a 37° C water bath until use. A CMFDA live-cell marker-labelled hDPSCs cell suspension was prepared to provide 2×10^5 cells in 100 µL of suspension (as was described in **3.3.7.2**). To seed each individual PLA 45° scaffold, 100 µL of SAP P$_{11}$-4 disassembled gel was mixed thoroughly with 100 µL cell suspension, giving a final P$_{11}$-4 working concentration of 7.5 mg/mL. Two hundred microliters of the final cell-disassembled gel mix were injected with a pipette all over and through PLA 45°scaffolds placed at the bottom of a tilted tube to keep the cell-disassembled gel mixture in place until fully gelated (assembled) all around the PLA fibres. Control group PLA 45° scaffolds were seeded with P4 hDPSCs at 2×10^5 cell/sample. The full procedure for this was described in **3.3.7.2.** Constructs from both groups were then incubated for 4 hours at 37° C, 5% CO_2 for later assessment. HDPSCs from all the 3 donors were collectively used with cell passages ≤ 5 to reduce the possible effects of primary culture ageing (Park *et al.*, 2005, Turinetto *et al.*, 2016). Different time points were selected for different investigations; with each time point optimised to best detect and/or monitor hDPSCs ongoing growth and expression of variable osteogenic differentiation markers throughout the 5 weeks of *in vitro* culture. Figure (6-1) below summarises PLA 45° seeding method with and without SAP P$_{11}$-4.
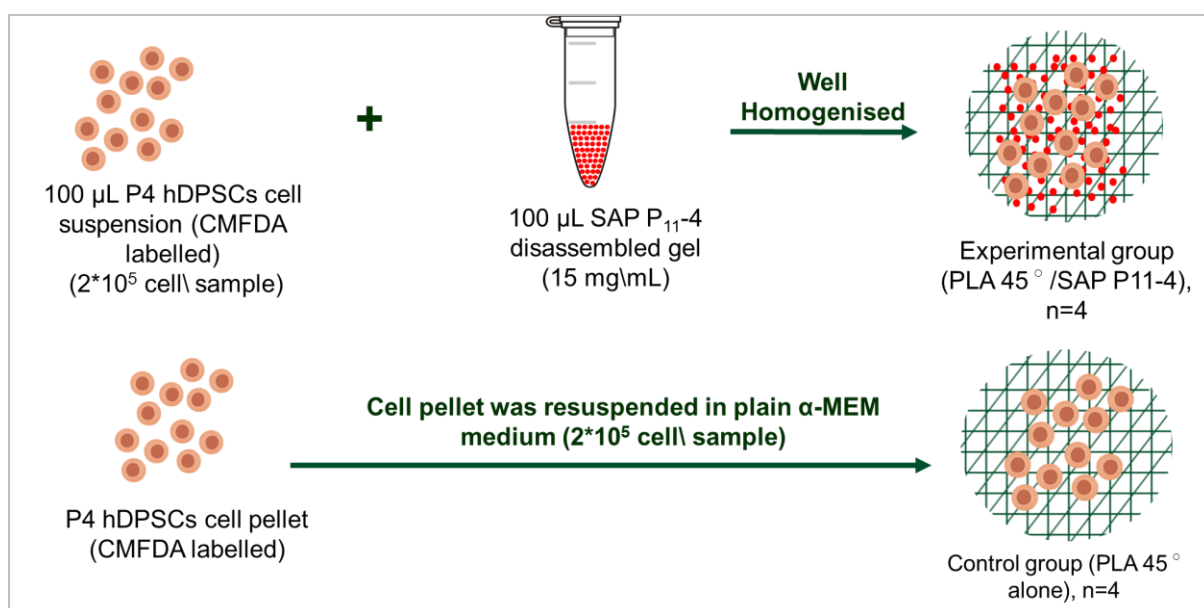
Figure 6-1: Method for seeding hDPSCs on 3D printed PLA 45° scaffold with and without SAP P_{11}-4 gel. For experimental PLA 45°/SAP P_{11}-4 group (n=4), the cell suspension was thoroughly mixed with P_{11}-4 disassembled gel (2*10⁵ cell / sample) before being injected all around the PLA fibres. For control group (n=4), hDPSCs were seeded on scaffolds by direct static seeding (2*10⁵ cell / sample)

6.3.3. Evaluation of hDPSCs attachment on PLA 45°control and PLA 45°/SAP P_{11}-4 scaffolds *in vitro*

Four hours after seeding (Figure 6-1), all constructs (PLA 45° control and PLA 45°/SAP P_{11}-4) were examined using the fluorescence microscope to check the level of cellular attachment in each group. For constructs with SAP, a minimal amount of cell-gel mix was left in the tube after removing the construct following seeding. This was topped up to 1 mL using a plain medium, vortexed to disassemble the SAP gel, then re-suspended into 5 mL Bijou tubes (Star Lab, Blake lands, UK) to obtain a single-cell suspension before cell counting (as described in **3.3.5**). For PLA 45° control group, the number of unattached cells remaining after seeding was counted as described in **3.3.5** and subtracted from the original number of cells seeded in order to indirectly compute the number of attached cells on each scaffold. All of the constructs were then cultured in an osteo-inductive medium at 37° C for up to 5 weeks. Special care was

155

given to the constructs with SAPs during regular medium changes so as not to disturb the gel.

6.3.4. Determination of *in vitro* metabolic activity of hDPSCs on PLA 45° control and PLA 45°/SAP P$_{11}$-4 scaffolds using an Alamar blue assay

In order to monitor hDPSCs metabolic activity on 3D PLA scaffolds with and without SAPs, an Alamar blue metabolic activity assay was performed on 3 constructs from each group at days 1, 14 and 21 of culture (Rampersad, 2012). The protocol used to perform the assay was as described by the manufacturer's instructions. At each time point, Alamar blue reagent (Thermo-fisher Scientific, Loughborough, UK) was added at a concentration of 10 µL/100 µL of medium to each sample well (for 24 well plates, 50 µL of Alamar blue was added to the 500 µL of medium per well). Medium alone was used as a blank control to which the same concentration and volume of Alamar blue reagent was added. The plate was then incubated, protected from light, at 37°C with 5 % CO2 and assessed after 24 hours. At the time of assessment, 100 µL of the medium from each well, including the blank, was transferred into wells of a 96 flat-bottom well plate (n=3). The absorbance values of the solution were obtained using a microplate reader at 570 nm wavelength. The medium for the constructs was then replaced with fresh osteo-inductive medium (0.5 mL/well) and the samples were re-incubated at 37° C, 5 % CO2 for up to 5 weeks.

6.3.5. Evaluation of hDPSCs cell viability and growth on PLA 45°/SAP P$_{11}$-4 and PLA 45° scaffolds control using CMFDA/ EDH-1 cell viability markers

After 4 weeks in osteo-inductive culture, one construct from each group (PLA 45°/SAP P$_{11}$-4 and PLA 45° control) was labelled with live/dead markers (CMFDA/EHD1) to check cellular growth and viability on the scaffolds (as described in *3.3.8*). The labelled

constructs were then fixed (as described in **3.3.9.3.**) before being examined under a fluorescent microscope as described previously (please see **3.3.9.2** for details).

6.3.6. Evaluation of newly formed ECM in PLA 45° control and PLA 45°/SAP P₁₁-4 constructs using SEM

The fixed samples from **6.3.5** above were used for SEM imaging to examine cellular growth and any new tissue formation in both groups after 4 weeks in osteo-inductive culture (as described in **3.3.9.3**).

6.3.7. Histological examination of *in vitro* PLA 45°control and PLA 45°/SAP P₁₁-4 constructs

Histological evaluation was conducted on PLA 45°/SAP P₁₁-4 and PLA 45° control constructs (n=3) 5 weeks after osteo-inductive culture for detailed detection of any possible differences in cellular growth and pattern of the newly formed matrix associated with the presence of SAP. Haematoxylin-eosin (H-E) and Alcian blue- Van Giessen (AB-VG) stains were used for histological examination (**3.5.2.1, 3.5.2.2** and **3.5.2.3**).

6.3.8. IHC evaluation of PLA 45° control and PLA 45°/SAP P₁₁-4

To evaluate possible osteo-inductive differentiation within the new matrix of PLA 45°/SAP P₁₁-4 and PLA 45° control constructs, IHC analysis was performed on the same constructs described in **section 6.3.7** above in order to detect any expression of osteo-inductive markers including Col-I, OPN and OCN (full details are given in **3.6**).

6.3.9. *In vivo* evaluation of hDPSCs growth on PLA 45° control and PLA 45°/SAP P₁₁-4 scaffolds

HDPSCs (P5) were seeded onto 45° PLA scaffolds with and without SAP P₁₁-4 (from **6.3.2**) at a density of (2×10^5 cell/sample) (n=3). All the constructs were then cultured

in plain for 6 hours and then placed in diffusion chambers (DC) and implanted intraperitoneally in CD1 nude mice (as described in **3.4.1**). After 7 weeks, the mice were euthanised using schedule-1 procedures and the chambers were retrieved from the peritoneum cavities (please see **3.4.2**) and fixed with 10% NBF for 24 hours prior to be further assessed.

6.3.9.1. Macroscopic inspection of *in vivo* PLA 45° control and PLA 45°/SAP P_{11}-4 constructs

The retrieved constructs from **6.3.9** above were examined by eye to note any obvious differences in tissue growth between the constructs in both groups.

6.3.9.2. SEM imaging of *in vivo* PLA 45° control and PLA 45°/SAP P_{11}-4 constructs

The retrieved constructs from **6.3.9** were analysed using environmental SEM to investigate cellular growth and the pattern of any neo-tissue, as described in **3.3.9.3.**

6.3.9.3. Histological examination of *in vivo* PLA 45° control and PLA 45°/SAP P_{11}-4 constructs

Retrieved constructs were processed using a tissue processor, then embedded and sectioned for histological examination using H-E and AB-VG stains to assess cellular growth and characterize any newly formed matrix as described in **3.5.2.1, 3.5.2.2** and **3.5.2.3.**

6.3.9.4. IHC analysis of *in vivo* PLA 45° control and PLA 45°/SAP P_{11}-4 constructs

After tissue processing, the embedded constructs prepared as described in **6.3.9.3** above were used for IHC analysis to evaluate the expression of Col-I,

OPN and OCN osteogenic markers within the newly formed matrix (full

description for the procedure is given in *3.6.*).

6.4. Results

6.4.1. Effect of SAP P_{11}-4 on hDPSCs attachment to PLA 45° scaffolds *in vitro*

After 4 hours of seeding with hDPSCs, fluorescent microscopic imaging showed a high number of viable cells attached to or within both PLA 45°/SAP P_{11}-4 and PLA 45° control constructs. However, different patterns of cellular attachment could be seen when the two groups were compared. For the PLA 45°/SAP P_{11}-4 constructs, large numbers of viable cells could be seen attached to the scaffold surface and in between the scaffold fibres. Cells appeared round in morphology, non-spreading and seemingly "captured" within the SAP P_{11}-4 gel (Figure 6-2 A). In contrast, for PLA 45° control constructs, the cells were seen attached along the surfaces of the PLA fibres, and some had already started spreading (Figure 6-2 B).
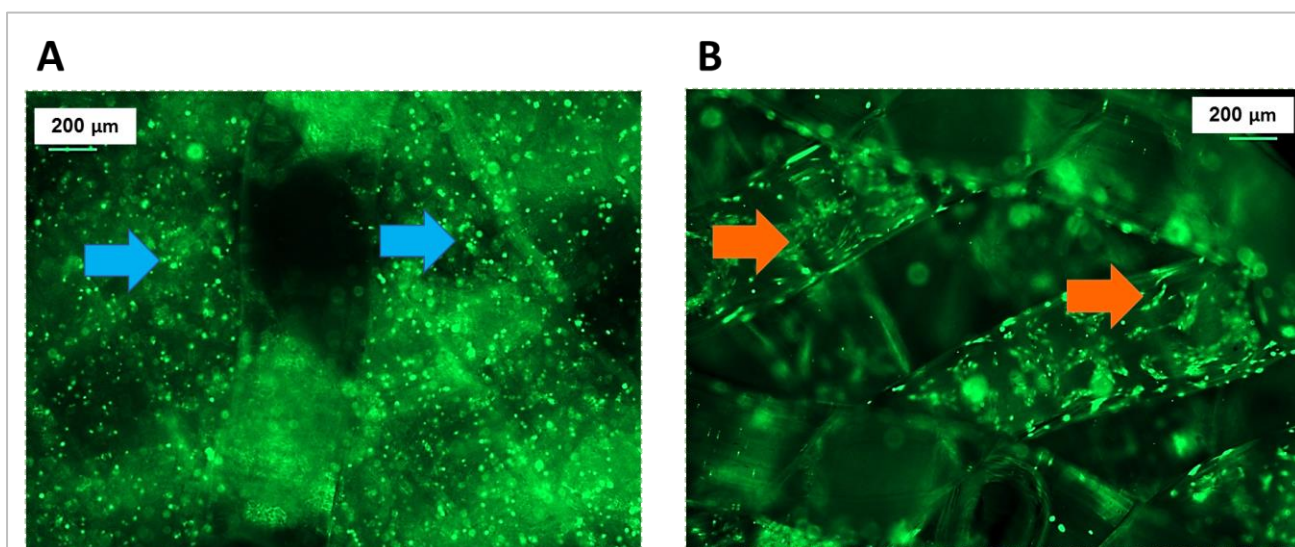
Figure 6-2: CMFDA labelled hDPSCs on PLA 45°/SAP P_{11}-4 and PLA 45° control scaffolds 4 hours after static seeding. A: PLA 45°/SAP P_{11}-4 showing large numbers of viable, spherical cells (blue arrows) apparently captured within the gel and distributed all around and in between PLA fibres. B: PLA 45° control constructs showing viable hDPSCs, some of which already started spreading (orange arrows), attached to PLA fibre surfaces.

Indirect HCM cell counting (n=3) revealed that the number of cells attached on PLA 45°/SAP P_{11}-4 constructs was significantly higher compared to that on PLA 45° control scaffolds ($p < 0.05$) (Figure 6-3).
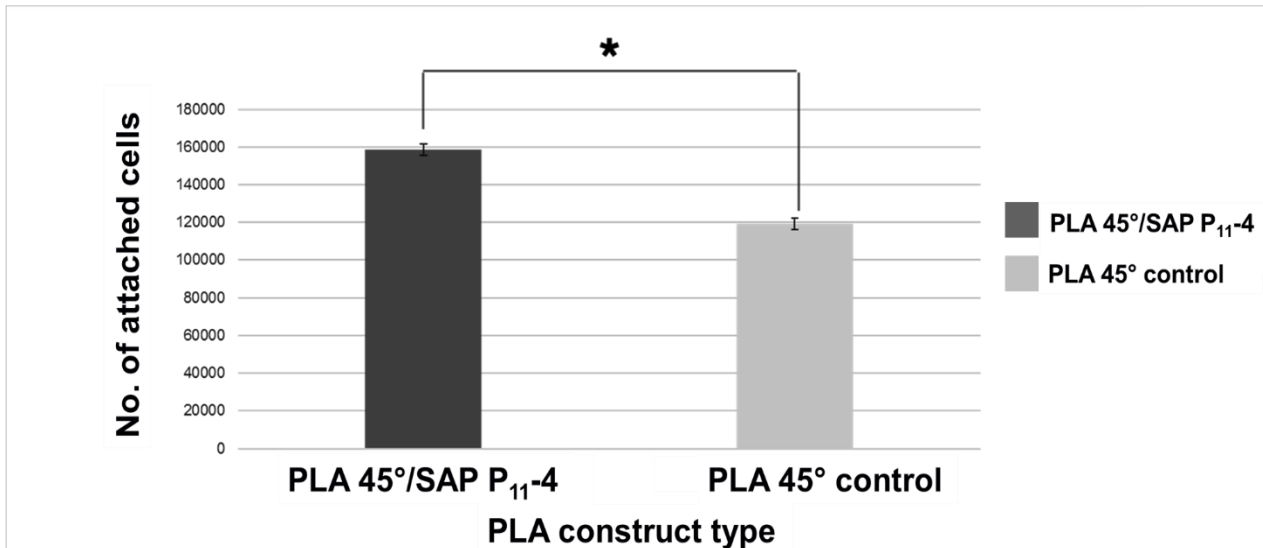
Figure 6-3: Comparison of number of hDPSCs attached to PLA 45°/SAP P_{11}-4 and PLA 45° control scaffolds 4 hours after seeding. The number of cells attached to PLA 45°/SAP P_{11}-4 constructs was significantly higher compared with PLA 45° controls (*$p < 0.05$) (n=3, mean ±SD).

6.4.2. Effect of SAP P_{11}-4 on the metabolic activity of hDPSCs within PLA 45° scaffolds *in vitro*

Generally, Alamar blue assays showed that hDPSCs on both constructs (PLA 45° control group and PLA 45°/SAP P_{11}-4) showed significant increased metabolic activity at day 14 of osteo-inductive culture compared to that of day 1 ($p < 0.05$ for both groups). Regarding the difference between the two groups, metabolic activity of hDPSCs on PLA PLA 45°/SAP P_{11}-4 was higher than that of PLA 45° control constructs at all the 3 tested culture time points in osteo-inductive culture, with statistical significance detected between the metabolic activity of the two groups on day 14 after culture ($p < 0.05$) (Figure 6-4).
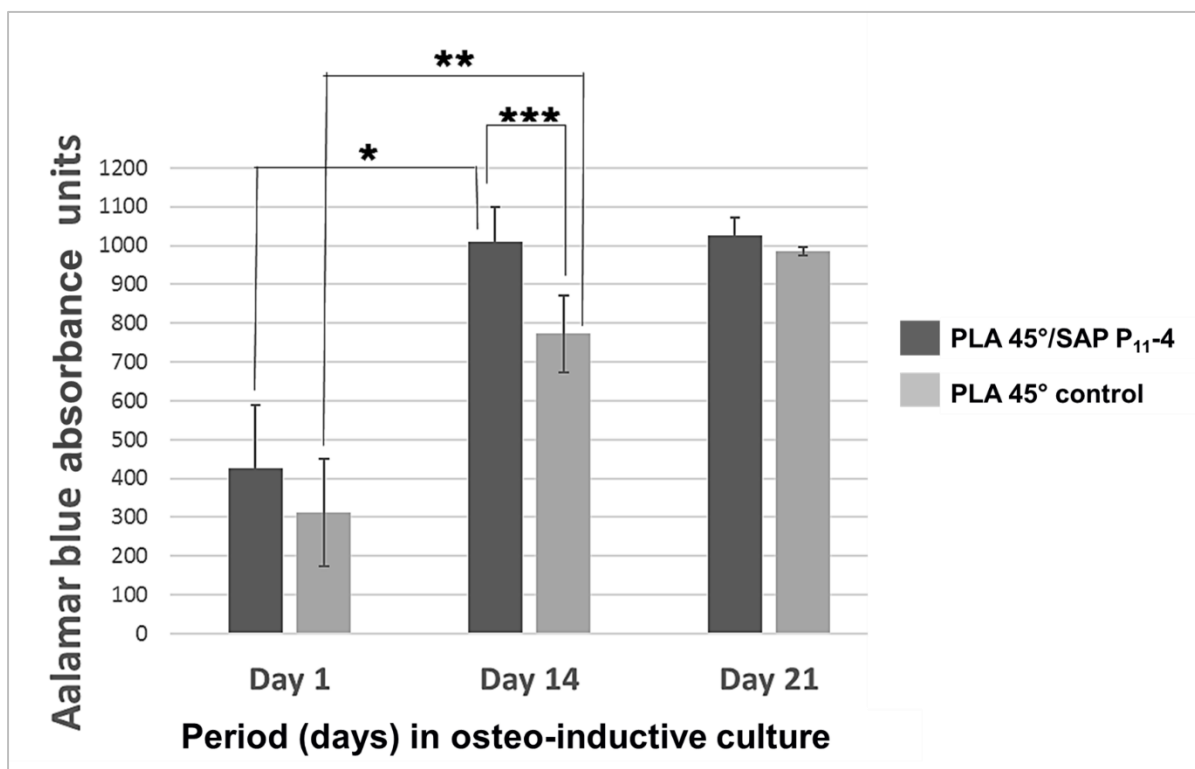
Figure 6-4: Comparison of metabolic activity using Alamar blue assays for hDPSCs on PLA 45°/SAP P$_{11}$-4 and PLA 45° control scaffolds at 1, 14 and 21 days after osteo-inductive culture. HDPSCs showed significantly higher metabolic activity on to PLA 45°/SAP P$_{11}$-4 and PLA 45° control scaffolds on day 14 after culture compared to corresponding day 1 of both groups (*p<0.05 for PLA 45°/SAP P$_{11}$-4 group, n=3, mean ± STD; **p<0.05, n=3, mean ± STD for PLA 45° control). HDPSCs in general increased their metabolic activity within PLA 45°/SAP P$_{11}$-4 compared to PLA 45° control scaffolds which was statistically significant at day 14 of osteo-inductive culture (*** p<0.05, n=3, mean ± STD).
.

6.4.3. Effect of SAP P$_{11}$-4 on viability, pore bridging and growth of hDPSCs on PLA 45° scaffolds *in vitro*

After 4 weeks of osteo-inductive culture, live\dead cell tracker staining of the constructs showed that almost all cells seen on the constructs from both groups were viable and had apparently proliferated considerably with only occasional dead cells seen as red labelled "dots" within the new matrix. Widespread sheets of cells could be seen in all constructs regardless of SAP P$_{11}$-4 incorporation. These appeared to cover the scaffold surfaces without leaving visibly open pores (Figure 6-5).
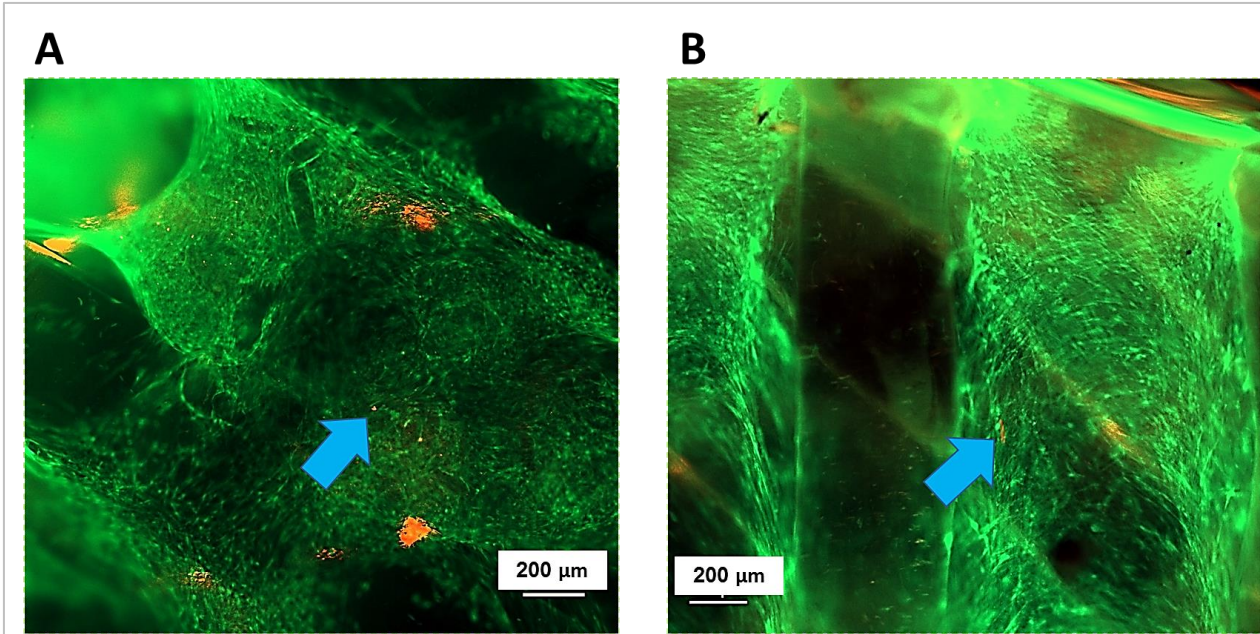
Figure 6-5: Live\ Dead cell labelling of hDPSCs in PLA 45° SAP P$_{11}$-4 and PLA 45° control constructs after 4 weeks in osteo-inductive culture. A: PLA 45°/SAP P$_{11}$-4 group and B: PLA 45° control group both showed dense sheets of viable cells (labelled green) with a few dead cells (blue arrows) scattered within the new matrix.

6.4.4. Effect of SAP P$_{11}$-4 on hDPSCs growth, cellular bridging and pattern of the newly formed ECM on PLA 45° scaffolds *in vitro*

After 4 weeks in osteo-inductive culture, SEM imaging showed that all inter-fibrillar gaps within the PLA 45°scaffolds in both groups were bridged with what appeared to be new tissue. However, a distinct difference in the appearance of these newly formed cell sheets was detected when comparing PLA 45°/SAP P$_{11}$-4 with PLA 45° control constructs. Cell sheets within the PLA 45°/SAP P$_{11}$-4 constructs appeared "flakier", were denser and had a coarser-looking surface when compared to similar features formed in constructs with PLA 45° (Figure 6-6).

163
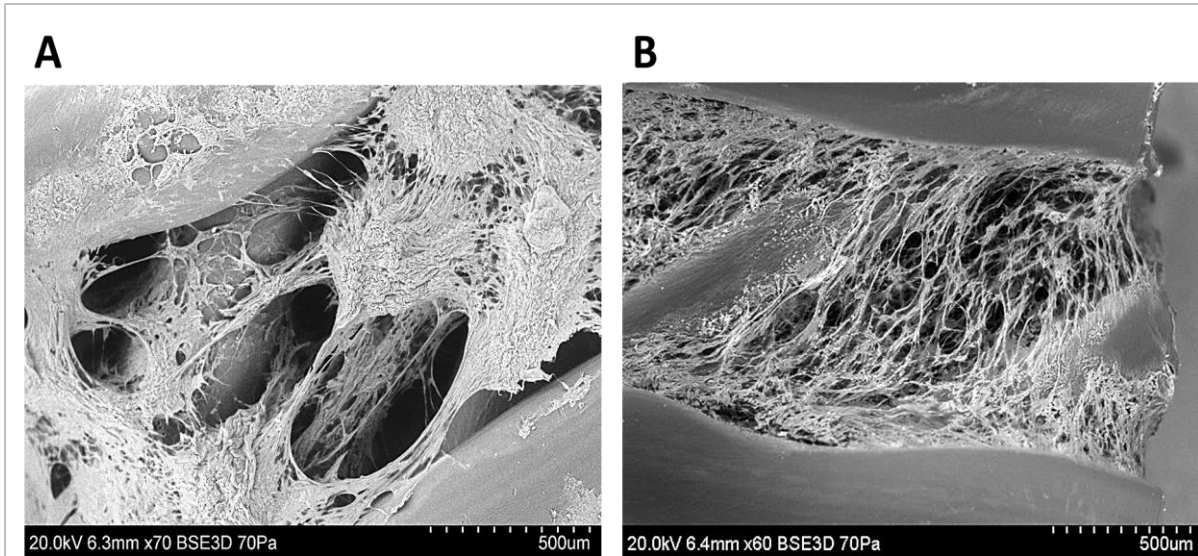
Figure 6-6: SEM imaging for hDPSCs on PLA 45° /SAP P$_{11}$-4 and PLA 45° control constructs after 4 weeks in osteo-inductive culture. A: PLA 45°/SAP P$_{11}$-4 constructs showed "flaky" sheets of newly formed matrix within the scaffold pores that looked dense and had a coarse appearance. B: Loosely textured cell sheets formed within the pores of PLA 45° control constructs.

6.4.5. Effect of SAP P$_{11}$-4 on the histological appearance of the newly formed matrix in PLA 45° scaffolds *in vitro*

Histological examination of the PLA 45°/SAP P$_{11}$-4 and PLA 45° control constructs after 5 weeks in osteo-inductive culture revealed two completely different types of newly formed tissue. H-E staining of 45°/SAP P$_{11}$-4 constructs revealed the formation of a dense tissue including multiple round-oval structures of different sizes (ranging from 20 µm to 200 µm in maximum diameter) seen throughout the matrix. High magnification examination of the oval structures within the 45°/SAP P$_{11}$-4 constructs showed that they were filled with eosinophilic material that had a fibrillar structure. A row of single, fibroblast-like, cells was seen surrounding the periphery of these oval structures (Figure 6-7). The tissue in between the structures consisted of loose connective tissue with cells that ranged from narrow spindle to broad flat cells with a prominent nucleus (Figure 6-8). When AB-VG stain was used on sections of PLA 45°/SAP P$_{11}$-4 constructs, some of the oval structures were stained bright pink, while

164

others showed a gradient of blue to pink hue stained variably from blue to pink in different regions (Figure 6-9 A and B). In contrast, H-E staining of PLA 45° control constructs showed the formation of what appeared to be a loose connective tissue, with spindle-shaped cells scattered throughout (Figure 6-7 B). When using AB-VG stain, most of the loose matrix material was stained with a pink hue (Figure 6-9 C).
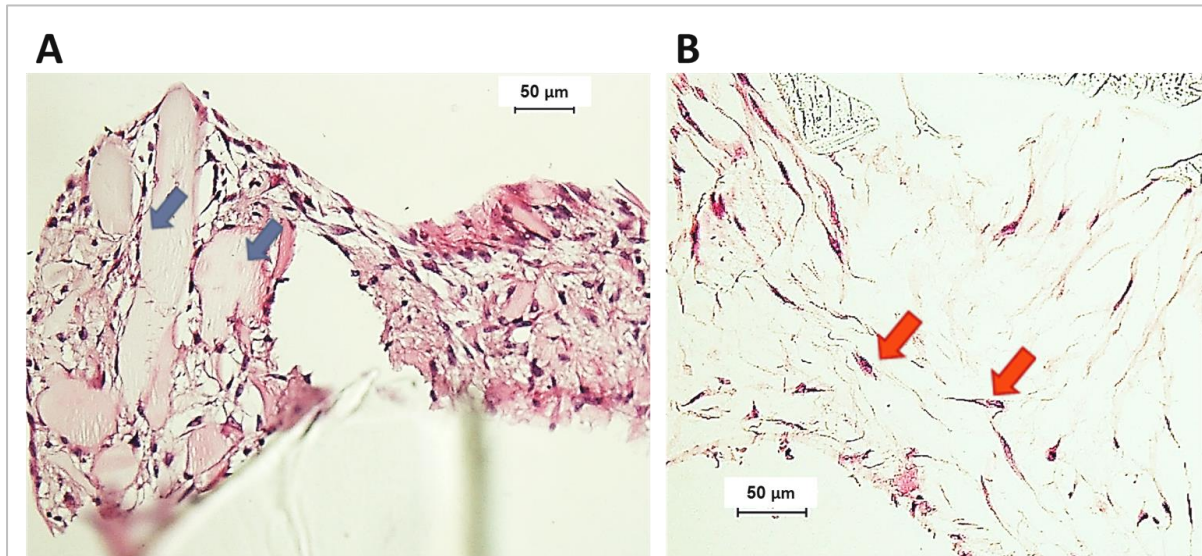
Figure 6-7: Histological H-E stained sections of hDPSCs within PLA scaffolds with and without SAP P$_{11}$-4, 5 weeks after culture in osteo-inductive medium. A: PLA 45°/SAP P$_{11}$-4 constructs showed multiple oval structures of variable sizes (blue arrows) spreading throughout the newly formed dense matrix. B: PLA 45° control constructs showed the formation of loose connective tissue with fibroblast-like cells scattered within (orange arrows).
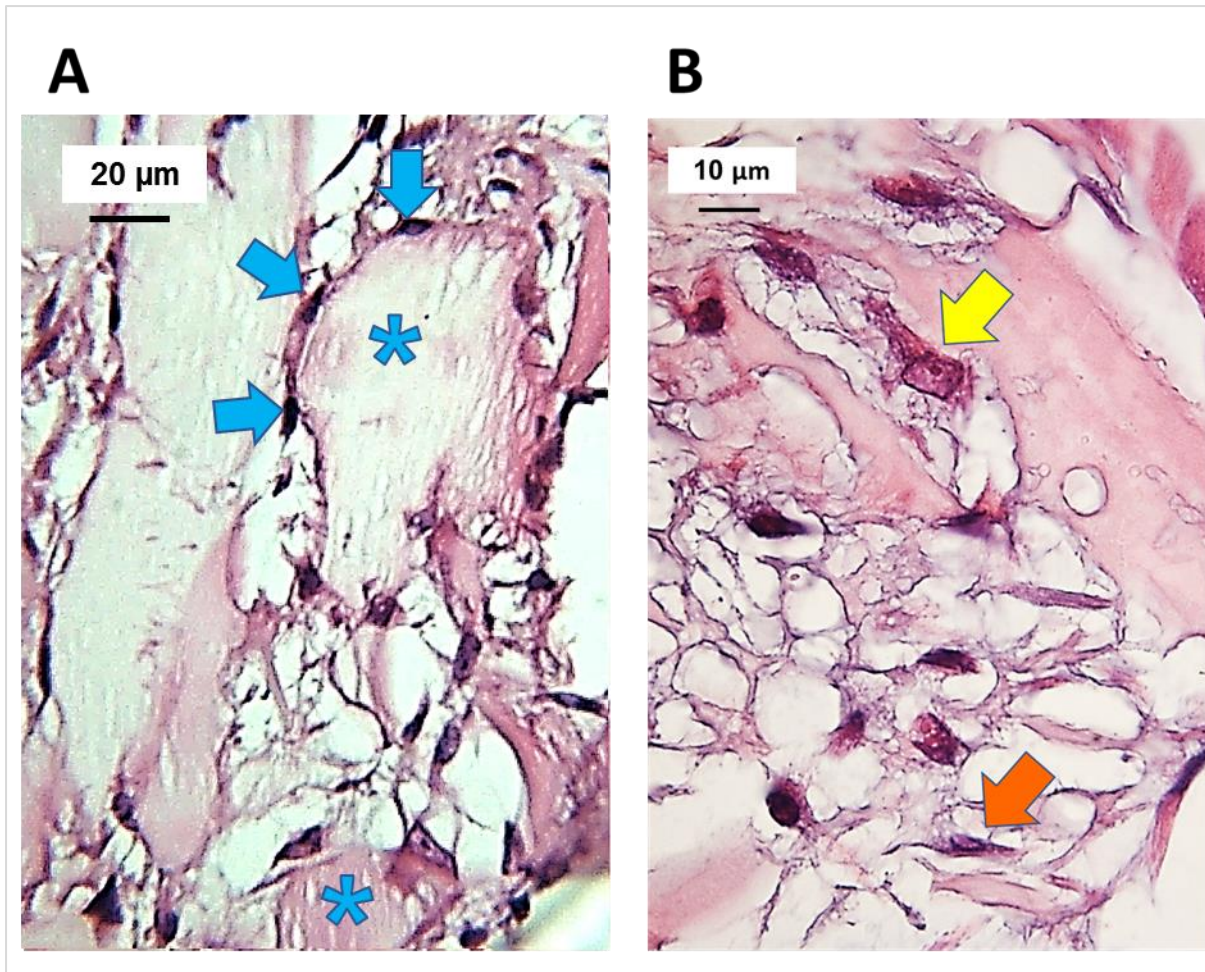
Figure 6-8: High magnification of extracellular matrix formed within PLA 45°/SAP P$_{11}$-4 *in vitro* constructs after 5 weeks in osteo-inductive culture (histology H-E stain). A: Fibrillar, eosinophilic material (defined on the image by the blue stars) was seen inside the oval structures within the matrix. A single line of fibroblast-like cells was seen surrounding the oval structures (blue arrows). B: Higher magnification showing loose connective tissue in between the oval structures, containing cells that range from spindle (orange arrow) to a more flat, broad morphology (yellow arrow).
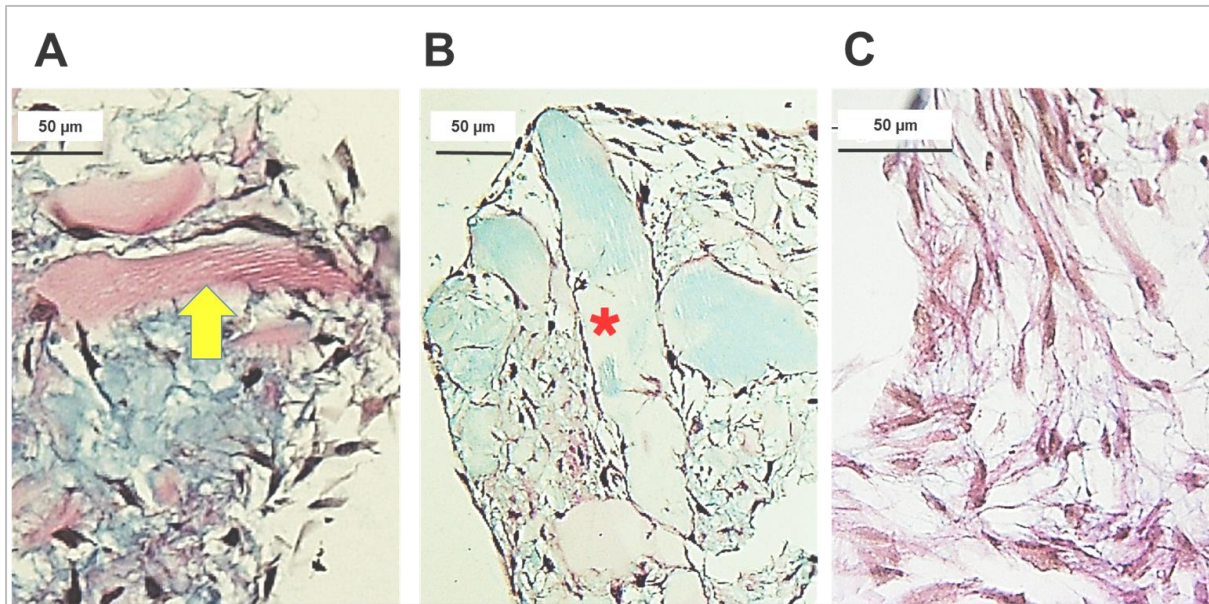
Figure 6-9: Histology (AB- VG staining) for *in vitro* hDPSCs within PLA 45°/ P$_{11}$-45 and PLA 45° control constructs 5 weeks after osteo-inductive culture. A: PLA-SAP P$_{11}$-4 group, some oval structures were stained bright pink that could indicate collagenous matrix (yellow arrow). B: Other oval structures within the same construct had a gradient of blue (acidic matrix) to light pink colour (marked on the image with red star). C: Connective tissue within PLA 45° control constructs showed a pink hue as it was negative to AB stain.

6.4.6. Effect of SAP P$_{11}$-4 on osteogenic differentiation of hDPSCs on PLA 45° scaffolds *in vitro*

After 5 weeks in osteo-inductive culture *in vitro*, the immunohistochemistry (IHC) examination showed that both PLA 45° control and PLA 45°/SAP P$_{11}$-4 constructs were stained positively for osteo-inductive markers (Col-I, OPN and OCN). For the PLA 45°/SAP P$_{11}$-4 group, the oval structures described above showed strong reactivity against antibodies to all 3 markers (Figure 6-10), with the loose tissue in between the structures showing less intense or even no immunostaining in some areas (Figure 6-11). In contrast, the control, PLA 45° control constructs showed areas of positive reactivity with a variable distribution within the loose, new connective tissue matrix for all the 3 osteogenic markers investigated (Figure 6-10).
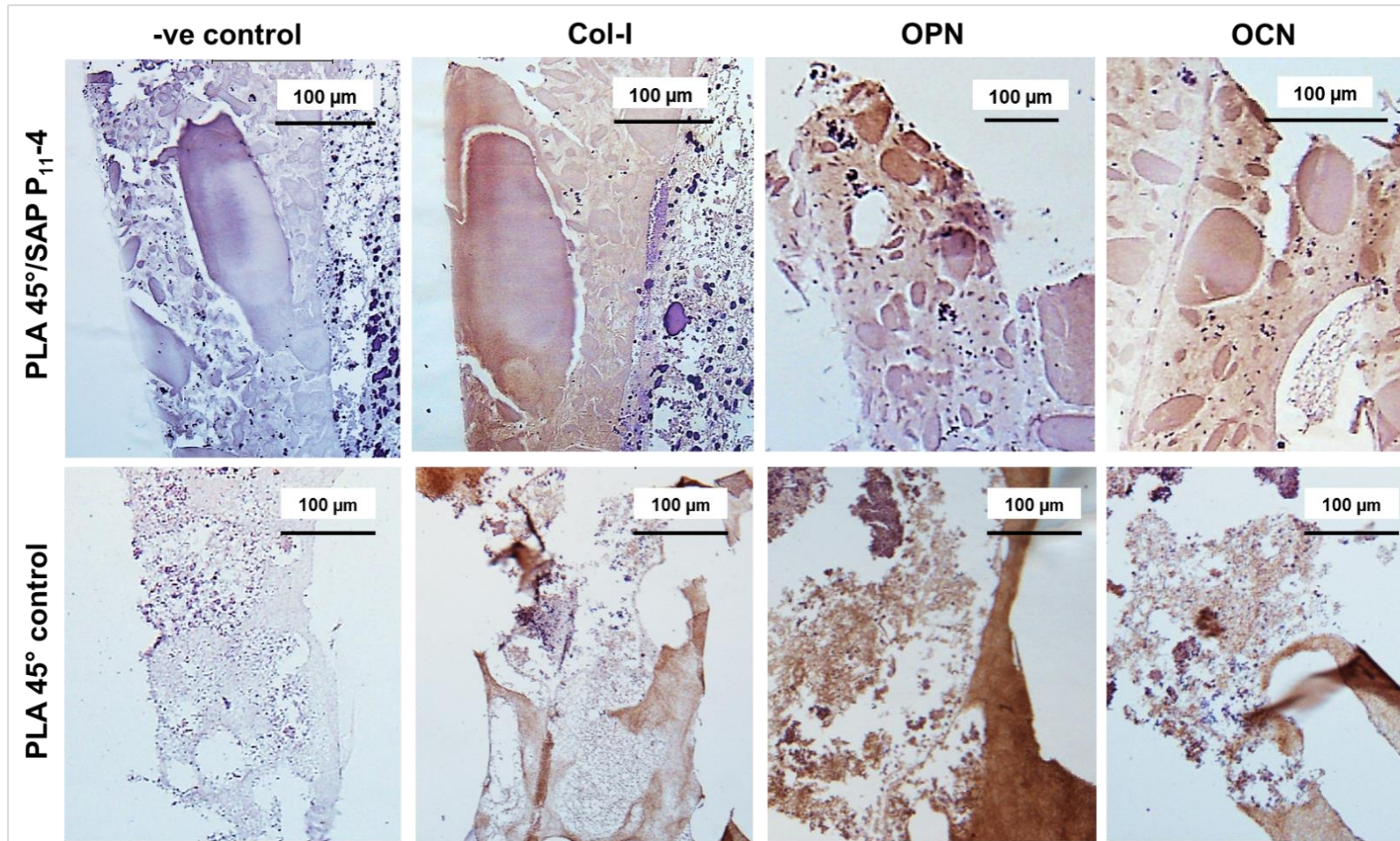
Figure 6-10: IHC (Col-I, OPN and OCN) for hDPSCs within PLA 45°/SAP P$_{11}$-4 and PLA 45° control scaffolds after 5 weeks in osteo-inductive culture *in vitro*. Top row: In PLA 45°/SAP P$_{11}$-4 constructs, the oval structures showed strongly positive immunostaining (brown colour) for each of Col-I, OPN and OCN markers. Bottom row: PLA 45° control constructs. Positive reactivity can be seen as brown staining in scattered areas within the loosely formed connective tissue for all the markers used (Col-I, OPN and OCN).
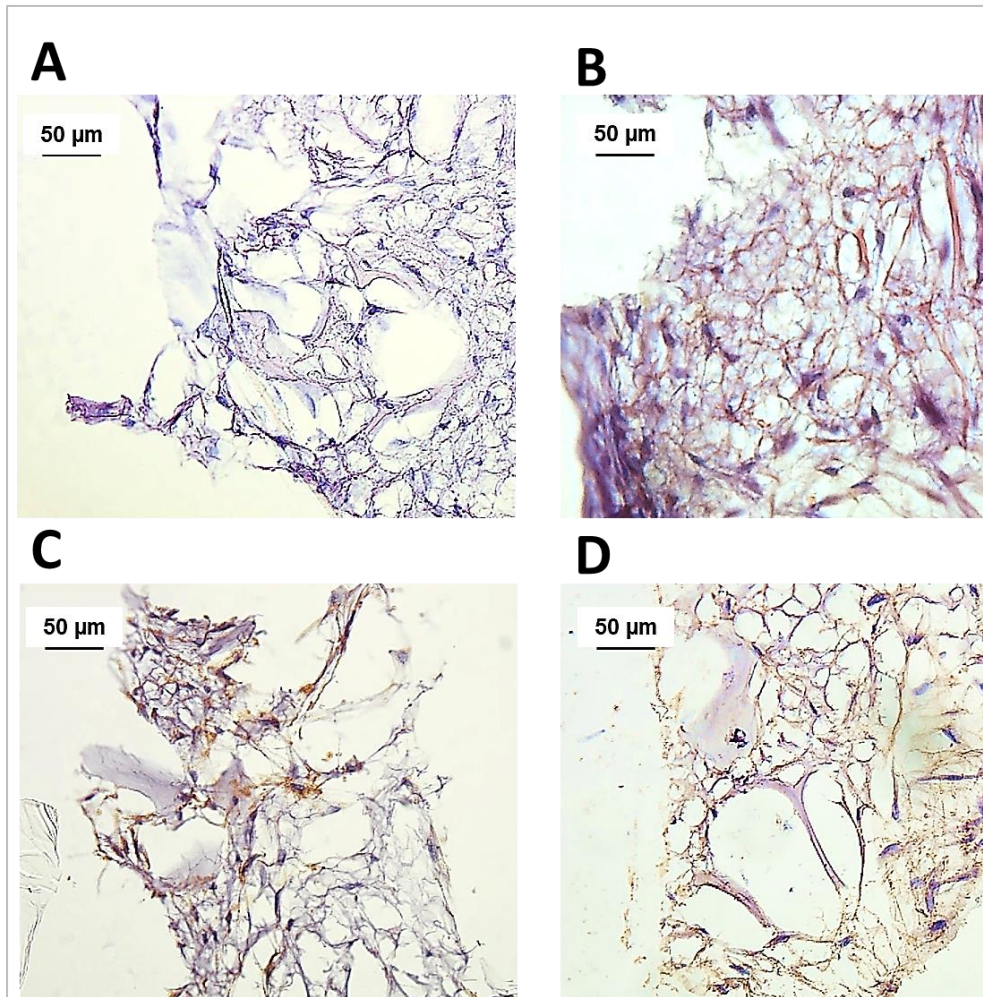
Figure 6-11: IHC (Col-I, OPN and OCN) for hDPSCs within PLA 45°/SAP P_{11}-4 after 5 weeks in osteo-inductive culture *in vitro* showing positive expression (brown stain) of the 3 used osteogenic markers within the connective tissues in between the oval structures. A: Negative control. B: Col- I. C: OPN. D: OCN

6.4.7. Effect of SAP P$_{11}$-4 on hDPSCs growth and osteogenic differentiation on PLA 45° scaffolds incubated in DCs *in vivo*

6.4.7.1. Macroscopic inspection of the retrieved DCs

After 7 weeks of implantation intraperitoneally in nude mice, the DCs containing PLA 45°/ SAP P$_{11}$-4 and PLA 45° control constructs were retrieved as described previously (please see *3.4.2.*). Visual inspection of the retrieved DCs showed that PLA 45°/ SAP P$_{11}$-4 constructs had apparent extensive tissue formation that had caused expansion of the plastic chamber ring and bulging of the two sealing membranes of the DC. In contrast, DCs containing the constructs of PLA 45° control appeared almost the same as their original form before *in vivo* implantation (Figure 6-12).
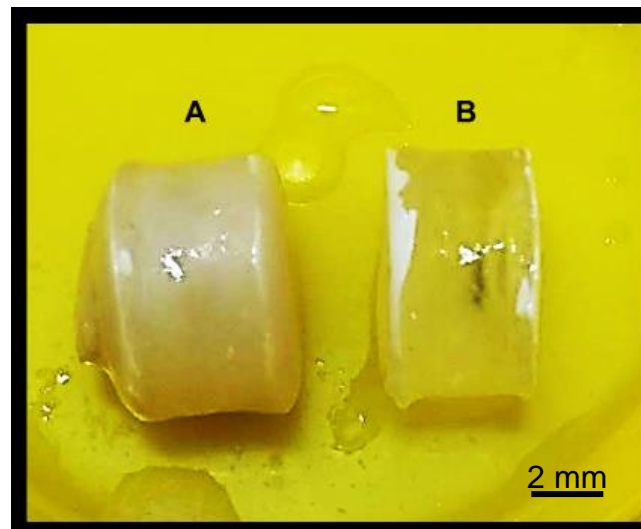
Figure 6-12: Macroscopic appearance of DCs containing hDPSCs on PLA 45°/SAP P$_{11}$-4 and PLA 45° control constructs retrieved from nude mice 7 weeks after intraperitoneal implantation. A: Chambers with PLA 45°/SAP P$_{11}$-4 constructs showed obvious interior tissue formation that had caused expansion of the chamber plastic ring and bulging of the sealing membranes. B: DCs containing PLA 45° control constructs showed minimal tissue growth on visual inspection

170

6.4.7.2. SEM imaging of hDPSCs constructs on PLA 45°/SAP P$_{11}$-4 and PLA 45° control scaffolds incubated in DCs *in vivo*

SEM imaging of the retrieved constructs 7 weeks after implantation *in vivo* revealed major differences in the pattern of new tissue formation between PLA 45°/SAP P$_{11}$-4 and PLA 45° control constructs. ECM in PLA 45°/SAP P$_{11}$-4 constructs showed a complex arrangement of newly formed tissue in a multilocular, soap-bubble with variably sized pores. In addition, what appeared to be obvious mineral deposits could be detected everywhere within the matrix (Figure 6-13 A and B). Control PLA 45° constructs showed the presence of connective tissue sheets, filling the spaces in between the PLA fibres, with some apparent mineral deposits detected within the neo-matrix material (Figure 6-13 C and D).
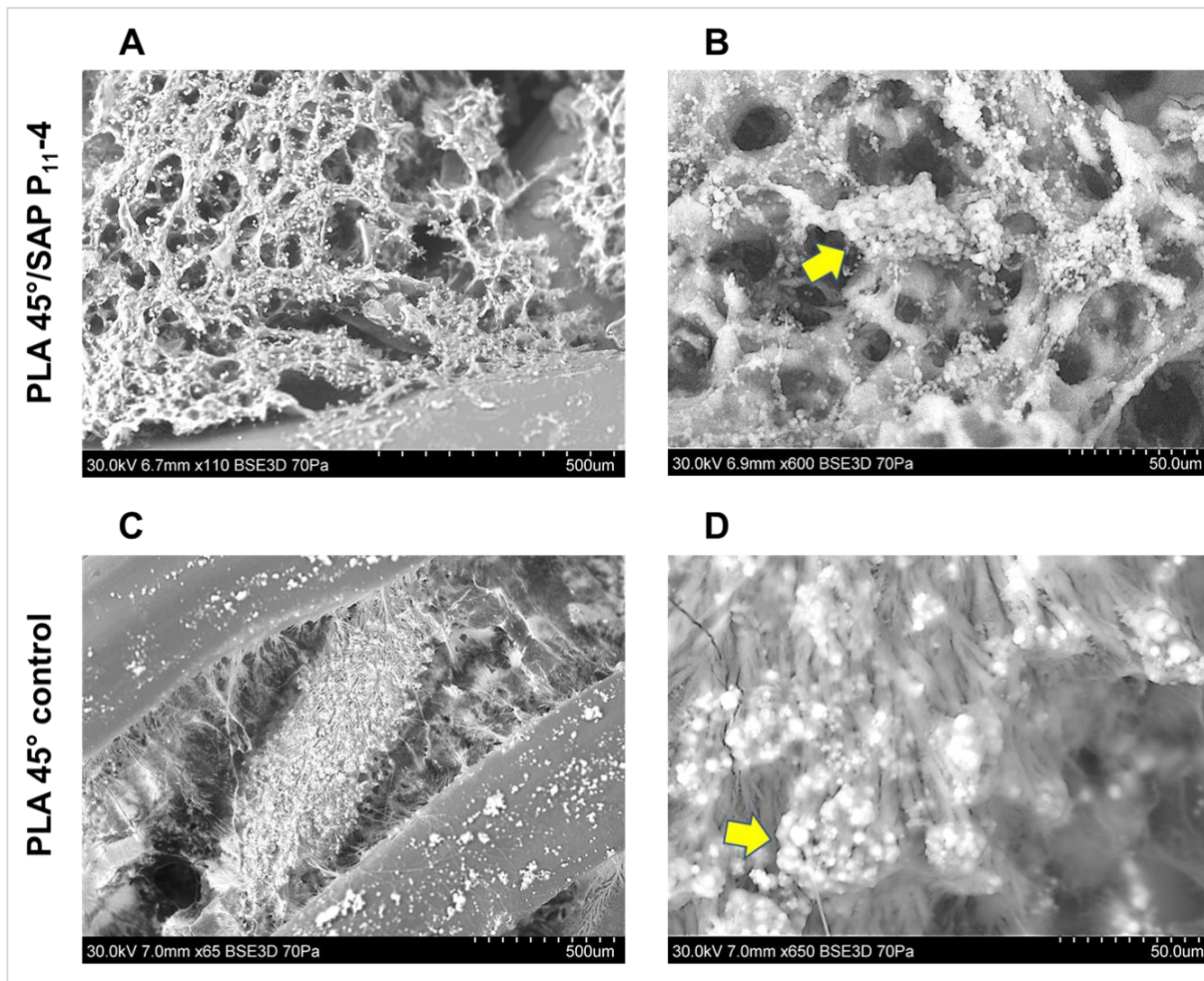
Figure 6-13: SEM of hDPSCs constructs on PLA 45°/SAP P$_{11}$-4 and PLA 45° control constructs retrieved from DCs 7 weeks after implantation *in vivo*. A: PLA 45°/SAP P$_{11}$-4 constructs showed the formation of a highly organised extracellular matrix with a honey-comb appearance. B: Higher magnification showed the presence of clusters of apparently mineral deposit (arrow). C: PLA 45° control constructs showed scanty loose connective tissue formed in between PLA fibres in the absence of SAP P$_{11}$-4. D: Few possible mineral deposits were detected within the new matrix in the absence of SAP P$_{11}$-4 (arrow).

6.4.7.3. Histological appearance of hDPSCs constructs on PLA 45°/SAP P$_{11}$-4 and PLA 45° control scaffolds incubated in DCs *in vivo*

H-E staining of the retrieved constructs after 7 weeks *in vivo* showed that for PLA 45°/SAP P$_{11}$-4 constructs, multiple oval-shaped structures of variable sizes, filled with eosinophilic fibrillar material could be seen within the newly formed tissue directly surrounding the PLA scaffold fibres. Prominent purple nuclei could be seen distributed within the interstitial matrix in between the oval features (Figure 6-14 A and B). Multiple, small round bodies of about 10 μm in diameter could

172

also be seen scattered throughout the matrix, having an eosinophilic centre and encircled by a ring of deeply purple-stained cuboidal or rounded cells (Figure 6-14 C). AB-VG staining showed positive AB staining within the interstitial matrix in between the oval structures, while the structures themselves were stained red, with some showing a gradient of red-blue colour (red arrows) (Figure 6-15 A). Also, the material within the small round bodies examined under high magnification revealed that they were stained with a mixed red- blue with AB-VG stain (Figure 6-15 B).

Considerable amounts of granuloma-like tissue could also be seen surrounding the exterior of these constructs, with a dense connective tissue that formed an outer capsule, followed by an inner connective tissue zone with marked cellularity. Signs of necrosis could be noticed towards the centre of the DC, represented by acellular zones of an amorphous matrix material, with pools of what appeared to be nuclear debris seen as deep-purple stained areas (Figure 6-16 A). With AB-VG staining, the outer cell-rich zones were stained bright pink, while the necrotic areas showed a faint pink hue. (Fig 6-16 B).

PLA 45° control constructs (control group) showed the formation of a small amount of loose connective tissue in between the PLA fibres, with dark purple stained structures noticed within the connective tissue that could possibly be nuclear material debris (Figure 6-14 D). No other salient features were noted. No clear AB-VG staining on sections could be obtained for these samples.
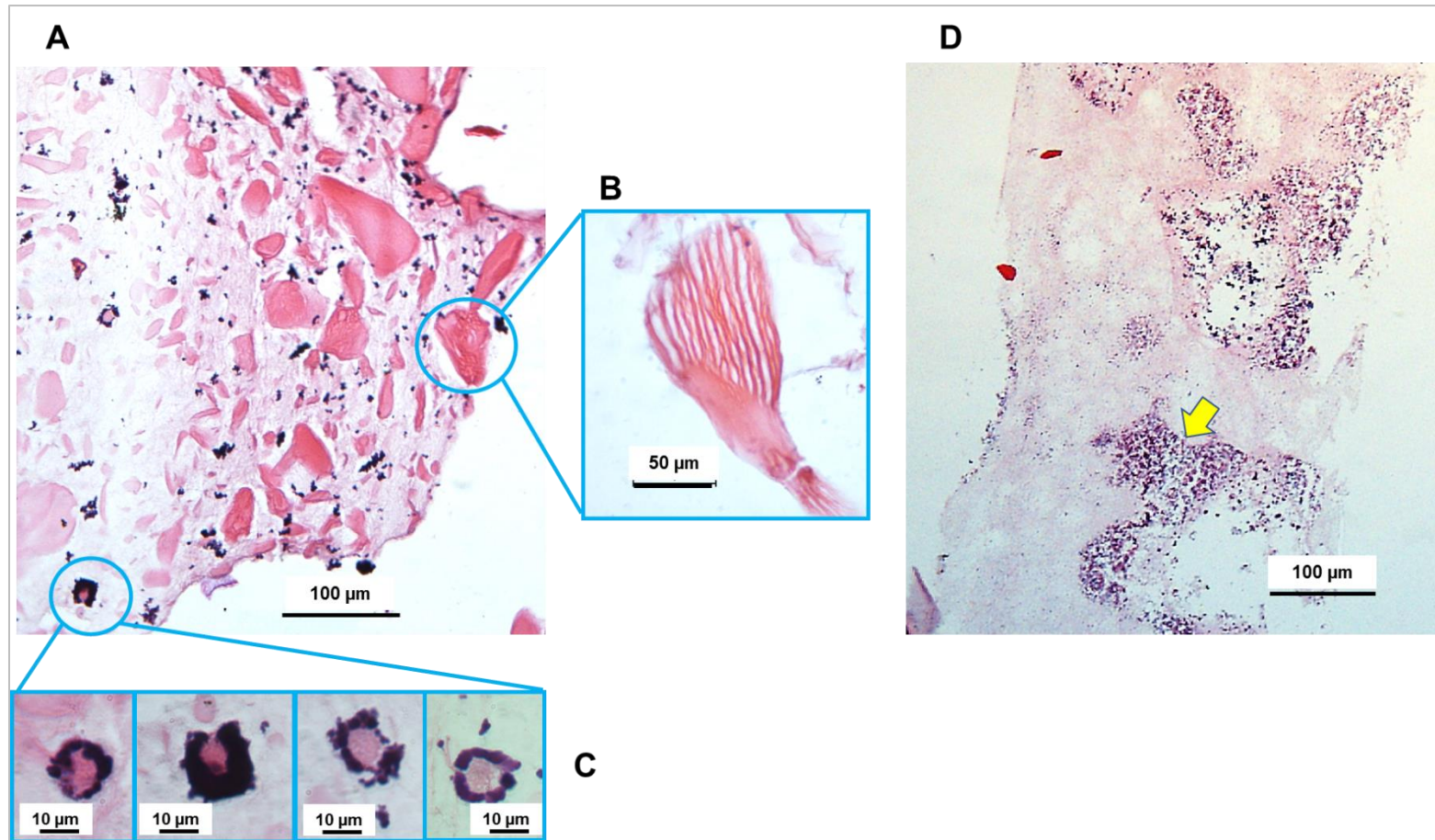
Figure 6-14: H-E histological staining of hDPSCs constructs of PLA 45°/SAP P$_{11}$-4 and PLA 45° control scaffolds in DCs retrieved from nude mice after 7 weeks of *in vivo* implantation. A: Constructs containing SAP showed the formation of multiple round-oval structures within newly formed connective tissue directly surrounding PLA. B: Higher magnification of the oval structures described in (A) showing the eosinophilic fibrillar texture. C: Multiple small spherical structures could also be seen within the connective tissue in between the oval structures. These spherical structures had an eosinophilic centre surrounded by a ring of deep- purple cells. D: Loose connective tissue was detected within the control constructs in the absence of SAP, with pools of what could possibly be necrotic nuclear debris (arrow) towards the centre of the newly formed tissue within the construct.
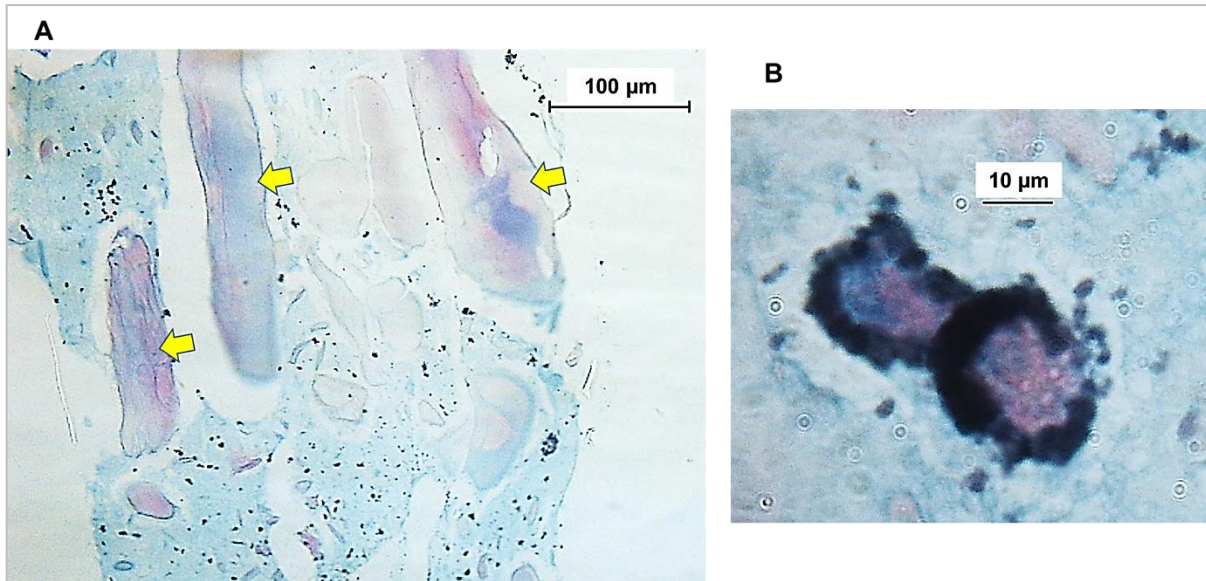
Figure 6-15: AB-VG histological staining of PLA 45°/SAP P$_{11}$-4 constructs retrieved from nude mice 7 weeks after implantation *in vivo*. A: Positive blue AB stain was seen within the interstitial matrix in between the oval structures indicating the formation of acidic matrix, while the structures themselves were stained red, with some showing gradient red- blue colour (arrows) which corresponds to a gradient collagenous-acidic matrix respectively. B: High magnification demonstrated that the material within the round bodies were stained a mixed red- blue with AB-VG stain.
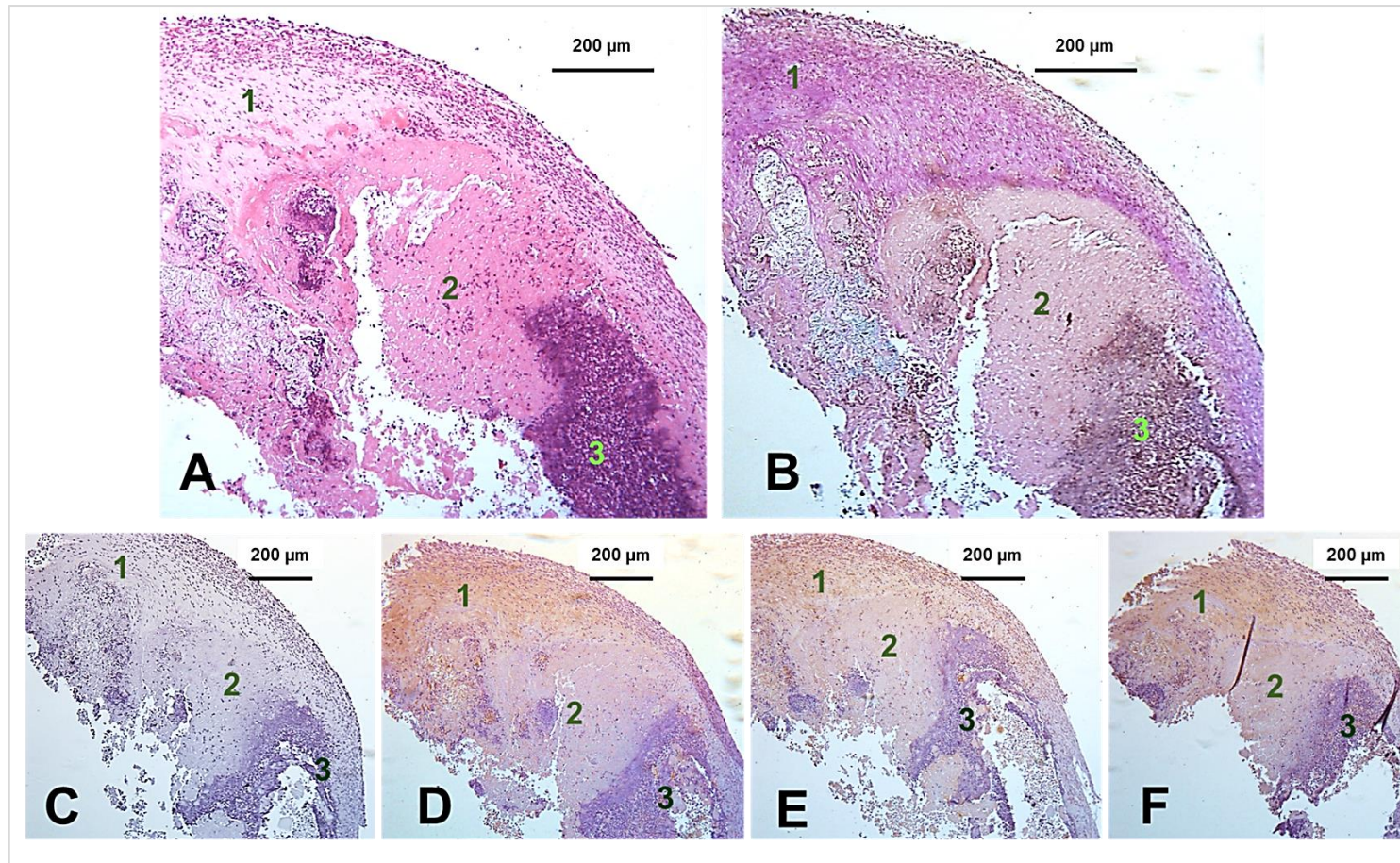
Figure 6-16: Histology (H-E and AB-VG) and IHC (Col-I, OPN and OCN) of connective tissue outgrowth surrounding PLA 45°/SAP P$_{11}$-4 constructs inside the retrieved diffusion chambers 7 weeks after *in vivo* implantation in nude mice. A: H-E staining showing an outer, capsule-like, cell rich layer (labelled,1 in the image) followed by a necrotic, cell free zone (labelled 2 in the image) then finally a zone of necrotic nuclear debris (labelled 3 in the image) could be seen towards the centre of the DC. B: AB-VG stain showed bright pink staining, with a small area stained blue within zone 1. Zone 3 showed concentrated dark grey Wiegart nuclear stain. C: IHC negative control. D: Col-I immunostaining. Zone 1 was strongly positive, zone 2 was weakly positive and zone 3 was negative. E: OPN immunostaining. Zone 1 was positive, zone 2 was weakly positive and zone 3 negative. F: OCN immunostaining showing almost similar reactivity pattern to OPN.

6.4.7.4. IHC of hDPSCs constructs on PLA 45°/SAP P$_{11}$-4 and PLA 45° control scaffolds incubated in DCs *in vivo*

After 7 weeks *in vivo* implantation, IHC staining showed clear and strong reactivity for all the 3 osteogenic markers. This was especially noticeable within the oval structures present in the matrix formed directly surrounding PLA fibres (Figure 6-17). Positive reactivity was also seen within granulomatous tissue surrounding the whole scaffold, with the strongest reactivity for all markers towards the peripheral, capsule-like layer of newly formed tissue. This then started to reduce towards the necrotic tissue zone at the centre of the DC, becoming entirely negative close to the area of nuclear-debris material (Figure 6-16 C, D, E and F). Control PLA 45° constructs showed positive reactivity for all 3 markers within the loosely formed matrix but with no discernible pattern (Figure 6-17).
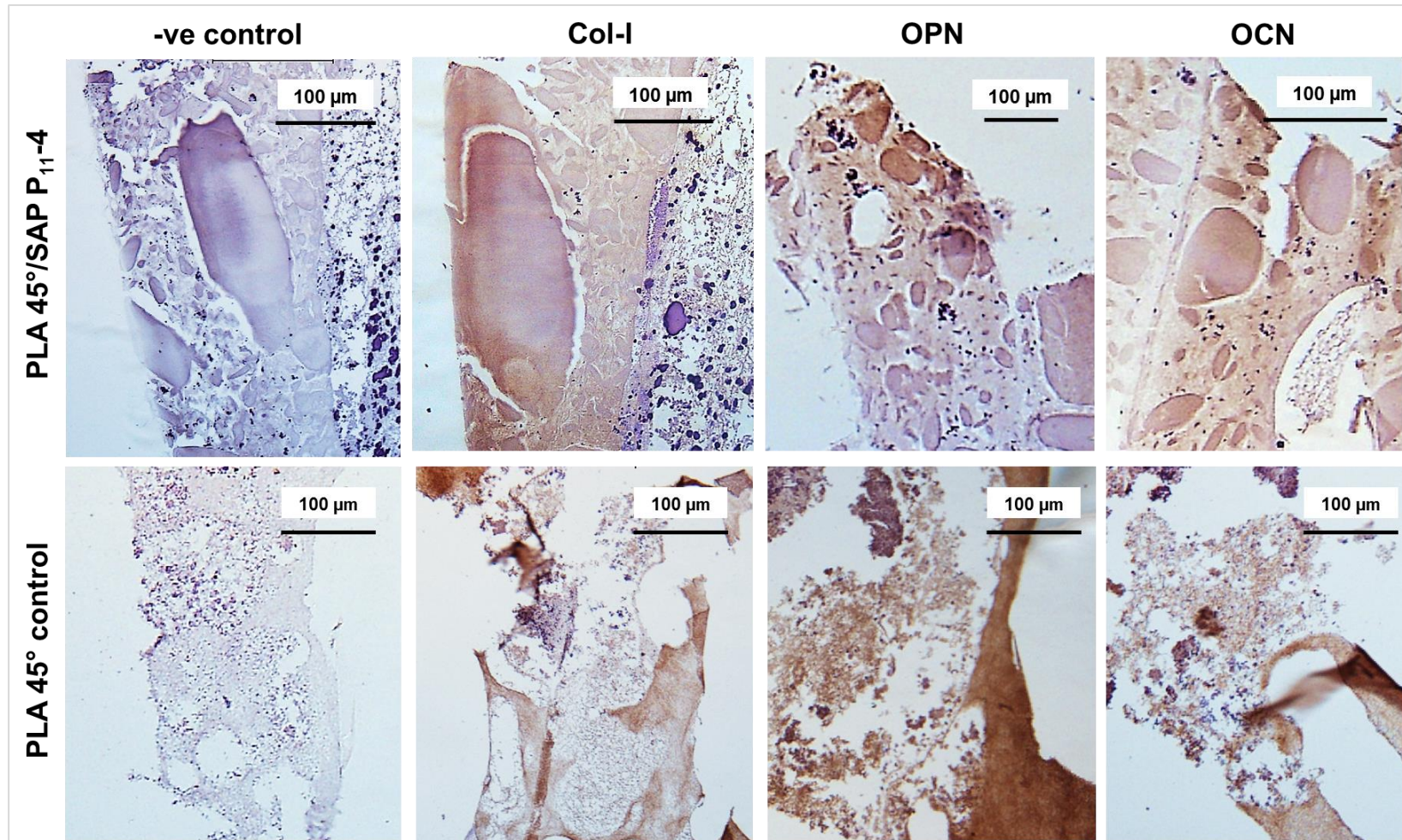
Figure 6-17: IHC (Col-I, OPN and OCN) for hDPSCs within PLA 45°/SAP P$_{11}$-4 and PLA 45° control scaffolds retrieved from nude mice 7 weeks after DC implantation *in vivo.* **Top row: PLA 45°/SAP P$_{11}$-4 constructs demonstrating the strong brown positive immunostaining for each of Col-I, OPN and OCN markers within the oval structures, while connective tissues in between showed variable distribution of positive immunostaining for all the 3 markers. Bottom row: PLA 45° control constructs. Positive reactivity can be seen as brown staining in scattered areas within the loosely formed connective tissue for all the used markers (Col-I, OPN and OCN).**

6.5. Discussion

Three-dimensional printed PLA scaffolds (Xu *et al.*, 2010, Bose *et al.*, 2013, Asa'ad *et al.*, 2016) and SAP P_{11}-4 (Burke, 2011, Saha *et al.*, 2019) have both been used individually as scaffold materials for bone tissue regeneration. In this study, the choice of combining the two materials aimed to hypothetically blend the advantages of both technologies in a way that they would complement the drawbacks of each other for promoting bone tissue regeneration, as was demonstrated in the literature review (***Chapter 1***), and will be discussed in general discussion (***Chapter 7***) of this thesis.

In this study, the choice of a PLA 45° scaffold design, rather than the 90° PLA scaffolds, to be combined with SAP P_{11}-4, was based on the results of ***Chapter 5***, as 3D printed PLA 45° scaffold design showed better support for hDPSCs attachment, growth and osteo-inductive potential both *in vitro* and *in vivo* compared to PLA 90° design. This was also supported in the literature by several authors, who reported the superiority of narrower 3D printed scaffolds angles in supporting cellular growth and scaffolds gap bridging as was discussed in ***5.5.2.***

6.5.1. SAP P_{11}-4 enhanced cell attachment compared to PLA 45° control *in vitro*

The results reported here showed that by adding SAP P_{11}-4 to cell suspensions prior to seeding on PLA 45° scaffolds significantly increased cellular content within the construct 4 hours later compared to cells seeded directly on to PLA 45° scaffolds without SAP. One possible explanation for this could be that by injecting SAP-cell suspension all around the PLA 45° sample, it would increase the chance for greater cell attachment on the PLA fibres within the scaffold from all directions, as well as capturing cells within the larger macro-pores in between the fibres (Vunjak-Novakovic and Radisic, 2004, Kretsinger *et al.*, 2005). In contrast, for PLA 45° control scaffolds where static seeding was used, the suspended cells landing by gravity would be

limited to the superficial PLA fibres of the scaffold with only limited numbers gaining access inside the top pores and to a lesser extent to attach on the scaffold sides (Yilgor *et al.*, 2008). Moreover, the smaller volume of SAP-cell suspension (200 µL) that was used to seed PLA 45°/SAP P$_{11}$-4 constructs could have helped to concentrate the cells all around the scaffolds, compared to the larger volume used for seeding PLA 45° control scaffolds (1mL / sample) (Radisic *et al.*, 2003, Vunjak-Novakovic and Radisic, 2004).

Addressing the biology behind this observation is also of great importance. An artificial replacement of ECM represented by the scaffold material should ideally closely simulate the structure of native ECM in order to actively take its role in supporting cellular attachment, migration and proliferation (Vasita and Katti, 2006, Hosseinkhani *et al.*, 2006). Self- assembly can generate small-diameter nanofibers in the lowest end of the size range of natural bone ECM building blocks (Hosseinkhani *et al.*, 2006, Wu *et al.*, 2012, Boden *et al.*, 2015). Apart from that, this nano fibrillar architecture exhibits unique surface topography, chemistry and energy offered by the significant increase in surface area and roughness compared to conventional or micron structured materials. This, in turn, would mediate more specific protein adsorption (like fibronectin, vitronectin and laminin) to further enhance cellular adhesion and bioactivity (Zhang and Webster, 2009). Several studies have supported the fact that vitronectin (a plasma protein that is well known to encourage osteoblast adhesion) showed much higher adsorption on nano phased scaffold surfaces leading to a significant increase in osteoblast adhesion (Webster *et al.*, 1999, Webster *et al.*, 2000, Webster *et al.*, 2001, Gutwein and Webster, 2004). In addition, SAPs are designed to have at least one bioactive domain after assembly, so can be further decorated with specific bioactive sequences like the arginine–glycine–aspartic acid (RGD) sequence which is

a highly conserved sequence found in many cell adhesion proteins. Integrin receptors found on cell membrane specifically recognize the RGD sequence, permitting cells to bind to their ECM environment (Nuttelman *et al.*, 2005, Boden *et al.*, 2015). In the case of SAP P_{11}-4 however, there was no consensus cell attachment sequence included (Boden *et al.*, 2015).

It is also worth taking into account that despite the advances in 3D printing of synthetic polymers to produce high porosity scaffolds aiming to culture cells in a 3D environment, these porosities are formed by microfibers that have relatively large diameters compared to cell size. The PLA 45 ° scaffold used in this study had a fibre strut diameter of 500 μm size, which is much larger than hDPSCs size (30–60 μm) (Lopez-Cazaux *et al.*, 2006, Haratizadeh *et al.*, 2017), so the cells would still exhibit attachment behaviour to a 2D rather than a 3D culture. In order to culture cells in an actual 3D environment, the cells need to be fully enclosed within the surrounding scaffold material in a way where they can contact and communicate with ECM in three dimensions, much like the native environment (Gelain *et al.*, 2007, Woo *et al.*, 2003).

6.5.2. Cellular morphology and viability within PLA 45°/SAP P_{11}-4 constructs *in vitro*

Despite the fact that the PLA 45° scaffold fibres used in this study were surface plasma-treated, which is proven to increase cellular affinity, surface roughness and area to eventually increase protein adsorption (Jacobs *et al.*, 2012, Rasal *et al.*, 2010); this modification still did not exceed the 2D concept especially on flat polymer surfaces (rather than pores joints and corners) where cells will attach and interact with scaffold material only on one side (Woo *et al.*, 2003, Shah *et al.*, 2011). Consequently, the growing cells would often undergo morphological changes, as this type of culture confines cells to a planar environment and restricts the more complex morphologies

observed *in vivo* (Gelain *et al.*, 2006, Tibbitt and Anseth, 2009). This is the reason why cells appear flattened and seem to be more spread on rigid substrates, such as plastic polymers, but are more cuboidal or round on malleable ECM-like gels. It is reasonable to suggest that the malleable SAP gels would act more like the natural ECM in maintaining cytoskeletal tensions, keeping cells in a rounded morphology, while rigid materials such as plastic cannot (Watt, 1986). The results of this study clearly reflected this, as hDPSCs were seen to be flattened on bare PLA fibre surfaces 4 hours after seeding but showed a more rounded shape within constructs containing SAP P_{11}-4 gel for the same period, consistent with previous observations where cells retain round morphologies within malleable materials (DiPersio *et al.*, 1991, Zhang *et al.*, 1995). Re *et al.* (1994) reported that when anchorage-dependent cells remain rounded within their surroundings, they fail to organize actin microfilaments required for their spreading and eventually undergo rapid apoptosis within hours of culture because a minimal degree of shape change is required for cells in order to survive. This was not the case in this study, as the majority of hDPSCs were proven to be viable and highly proliferating within the PLA 45°/SAP P_{11}-4 constructs for the whole culture period (5 weeks) as will be discussed later. Dikovsky *et al.* (2006) suggested that in hydrogel scaffolds, cells which are initially round beginning to have elongated filopodea within 24 hours upon spreading within the hydrogels. Gelain *et al.* (2006) proved that initially, round neural cells formed long cellular processes within SAP scaffold hydrogels when monitored for 14 days after culture.   The results of the current study cannot add a great deal to this point as further tracking of changes in cellular morphology were not followed. Live/dead cell fluorescent labelling requires multiple media changes and scaffold washing, raising concerns that frequent agitation could disturb the assembled SAP scaffold within the PLA template. The Alamar blue metabolic activity assay was

182

therefore used to monitor hDPSCs activity within the PLA 45°/SAP P_{11}-4 constructs during the first 3 weeks in osteo-inductive culture. Although this method is not the optimal way to track cellular activity, it offered a simple technique (Rampersad, 2012) with minimal mechanical disturbance to the gel. The assay showed a high level of cellular metabolic activity for hDPSCs within PLA 45°/SAP P_{11}-4 constructs at 7, 14 and 21 days of an osteo-inductive culture that tended to be higher than that seen for cells in control constructs of PLA 45° alone although statistical significance was seen only at day14 of culture. This suggests higher growth rates for hDPSCs within PLA 45°/SAP P_{11}-4 construct compared to cells on PLA 45° control, though the latter "catch up" after 21 days in culture. However, it is not possible to know whether this observation was merely attributable to the higher cellular attachment levels encountered on PLA 45°/SAP P_{11}-4 constructs, as the assay was not normalised against DNA content or cell number counting. Nevertheless, live\dead fluorescence imaging showed that most of the hDPSCs were viable with only a scanty of dead cells after 4 weeks in osteo-inductive culture in both PLA 45°/SAP P_{11}-4 and PLA 45° control constructs. Different studies have reported that SAP P_{11}-4 gel is highly biocompatible and supports cellular viability (Burke, 2011, Kyle *et al.*, 2012, Ravichandran *et al.*, 2014, Boden *et al.*, 2015, Saha *et al.*, 2019). Likewise, in a study by Wu *et al.* (2012), SAP Beta11B scaffold (that was designed after P_{11}-4 SAP polymer), showed that most of the encapsulated pre-osteoblast cells within the hydrogel were viable 1 week after culture.

6.5.3. SAP P_{11}-4 enhanced cellular growth in PLA 45°/SAP P_{11}-4 constructs compared to PLA 45° control construct *in vitro*

In tissue engineering, cell-scaffold adhesion paves the way to downstream events such as cellular migration, growth and function (Woo *et al.*, 2003). Higher levels of

cellular growth were noticed *in vitro* for PLA 45°/SAP P_{11}-4 constructs seen by SEM imaging after 4 weeks in osteo-inductive culture compared to those formed on control constructs containing PLA 45° alone. The newly formed matrix on the PLA 45°/SAP P_{11}-4 constructs also seemed to be much denser, with a coarse, flaky appearance. In common with other hydrogels, SAPs are highly hydrated materials, contain mainly the aqueous phase (Nuttelman *et al.*, 2005, Fedorovich *et al.*, 2007). They are formed with a very low peptide concentration (0.01 volume fraction of peptide and 0.99 volume fraction of solvent (Boden *et al.*, 2015). This will give the encapsulated cells within the gels a lot of space to grow and communicate with each other; with nutrients, oxygen, and various metabolites being almost freely diffusible in and out of the gel network (Fedorovich *et al.*, 2007). In addition, there is an interstitial spacing between the fibrils of forming the gel matrix allowing gas and nutrient exchange with the gel surface until a new tissue matrix is formed. Furthermore, the ability of the SAP to freely remodel (by breaking and reforming) enables it as a scaffold to be gradually replaced by a cell-formed matrix as a response to growing tissue expansion (Boden *et al.*, 2015). This scenario is in sharp contrast to what is predicted to happen on scaffolds made up by PLA 45° alone. The pores created within the 3D printed scaffold are large compared to cell size and are about 1,000– 10,000 times larger than the size of nano biomolecules, including hormones, proteins and growth factors. Consequently, an extra time and effort are required for the unsupported cells to bridge and fill these gaps, with the essential bio-regulating molecules quickly diffusing away within the sizeable empty pore (Gelain *et al.*, 2006, Gelain *et al.*, 2007). This lack of sustained, free diffusion of growth factors to cell surface receptors within the scaffold matrix can greatly affect the intracellular signalling pathways which are of such importance in defining subsequent cellular behaviour, including growth and differentiation (Das and

Zouani, 2014). The coarse, flaky appearance of newly formed cell sheets within PLA 45°/SAP P_{11}-4 constructs could be a reflection of the high cellular growth guided by the rough, nano fibrillar topography of the interwoven SAP P_{11}-4 nanofibrils (Figure 6-18). Again, this is different from the smooth cell sheets suspended in space to bridge the gap between bare PLA fibres.
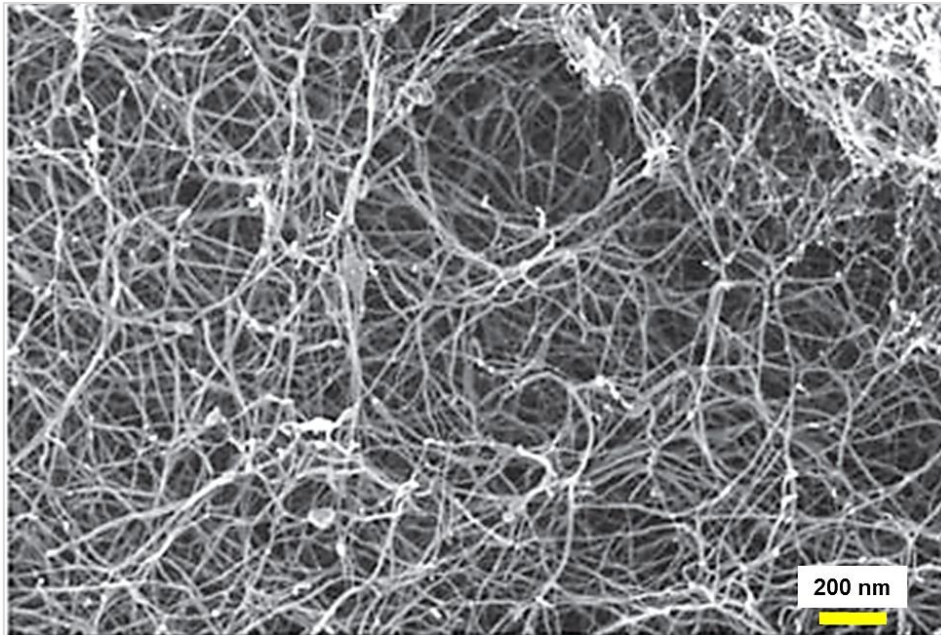
Figure 6-18: SEM structure of the cell-free assembled SAP P_{11}-4 gel (ethanol dried-gold coated) (Kyle *et al.*, 2012)

6.5.4. Histological and IHC analysis of PLA 45°/SAP P_{11}-4° and PLA 45° control constructs following osteo-inductive culture *in vitro*

After 5 weeks of osteo-inductive culture, the results described above were confirmed with histological examination, as observably greater amounts of more dense tissue were formed within PLA 45°/SAP P_{11}-4 constructs compared to those with PLA 45° alone. The presence of acellular oval structures within the newly formed matrix could suggest neo-matrix deposition, especially given the fibrillar pattern these structures showed. Similar structures were described by Burke (2011) when using P_{11}-4 gel for the repair of cranial bone defects in rabbits. Burke's study suggested that these oval structures were most likely to be the SAP gel material itself within the defect, as it was

seen after 3 days of *in vivo* implantation, and showed blue staining with AB stain which normally binds to negatively charged acidic molecules, such as SAP P_{11}-4, (Steedman, 1950, Ovchinnikov, 2009, Boden *et al.*, 2015). However, although the histological nature of the tissue formed within PLA 45°/SAP P_{11}-4 constructs in this study is not fully understood, there are clues to suggest that the fibrillar, acellular structures are more likely to be new matrix tissue rather than simply remnants of SAP P_{11}-4 gel. First of all, most of these structures showed intense positive VG red staining, which usually has a high affinity to collagenous connective tissue (Puchtler and Sweat, 1964). Noticeably, some of these structures showed light blue or blue-pink gradient hue with AB-VG stains. As discussed earlier, the ability of the SAP gel to gradually degrade and be replaced by newly formed ECM may explain this finding, or this could be a sign of chondrogenic activity within the formed tissue (Ovchinnikov, 2009). In addition, the oval structures were detected after 5 weeks of culture, a period where the SAP gel would be very likely to fully degraded. Burke's results (2011) found no histological evidence of the SAP P_{11}-4 gel after 10 days post-implantation *in vivo*. More importantly, these oval structures showed strong positive immunostaining against 3 main osteogenic markers; Col- I, OPN and OCN. In a similar way, the interstitial connective tissue formed was also positive to AB stain and IHC osteogenic markers (mainly Col-I and OCN). In addition, in a study conducted by (Kyle *et al.*, 2012), SAP P_{11}-4 was highly degraded when examined histologically 14 days after *in vitro culture* with primary human dermal fibroblasts (Figure 6-19). However, it was not investigated whether the assembled gel alone would show any reactivity against Col-I, OPN and OCN antibodies by itself without the cells included, though P_{11}-4 carries no consensus sequences with any of these molecules and there was no sign of non-specific antibody binding in the negative controls. Further investigations need to be carried out in the

future to decode these findings, for example, using more specific immunostaining to detect the presence of SAP P_{11}-4 remnants, IHC on PLA 45°/SAP P_{11}-4 scaffolds without hDPSCs to detect reactivity against the bone markers used, or IHC to detect the presence of cartilage proteins within the newly formed matrix. More thorough IHC investigations are also required in order to detect possible dentinogenesis (as opposed to osteogenesis) that might be occurring within the constructs, as to this point, the IHC markers used (Col-I and OCN) could give positive reactivity in both bone and dentine (Wang *et al.*, 2011).
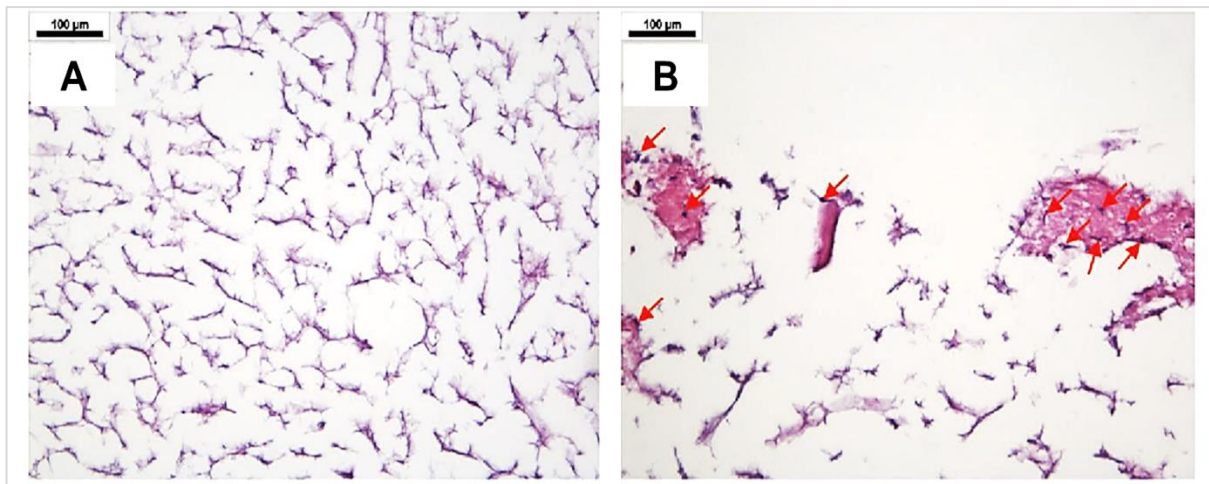
Figure 6-19: Histology (H-E) for SAP P_{11}-4 gel. A: histological appearance of cell- free SAP P_{11}-4. B: SAP P_{11}-4 showing degradation 14 days after *in vitro* culture with primary human dermal fibroblasts (arrows show neo tissue growth) (Kyle *et al.,* 2012)

6.5.5. The effect of SAP P_{11}-4 on cellular growth and neo-ECM formed within *in vivo* constructs

The *in vivo* results obtained in this chapter showed that newly formed tissue was remarkably increased in DCs containing PLA 45°/SAP P_{11}-4 constructs when inspected in comparison with the hDPSCs on PLA 45° control scaffolds 7 weeks after implantation, causing the chamber walls to detectably distend. This is consistent with the preceding *in vitro* findings described above, where a considerable increase in cellular growth was encountered in constructs containing SAP P_{11}-4 gel. Moreover, the "soap-bubble" or alternatively called "honeycomb" appearance of the newly formed

matrix within PLA 45°/SAP P_{11}-4 *in vivo* constructs seen by SEM was very interesting. Although the guiding processes to form this complex architecture within the ECM in the SAP occupied pores is yet not fully understood, it is of note that a honeycomb matrix configuration is frequently associated with osteogenesis in the literature, in respect of its similarities with the developing trabecular bone pattern (Sikavitsas *et al.*, 2001, Salgado *et al.*, 2004). However, it could equally be simply produced by voids left after SAP gel degradation within the cell sheets (though it was not apparent previously in the *in vitro* constructs). It would require further work to elucidate the significance and origin of this architectural feature.

6.5.6. Possible signs of ECM mineralisation detected within *in vivo* constructs

SEM imaging of *in vivo* samples showed increased size and amount of aggregates that are presumed to represent mineral deposition within PLA 45°/SAP P_{11}-4 constructs compared to those in the control group and may be related to P_{11}-4's proven ability to nucleate hydroxyapatite mineral *de novo* (Kirkham *et al.*, 2007). Using *in silico* modelling, Saha *et al.* (2019) suggested that the assembled SAP P_{11}-4 fibrils are capable of nucleating hydroxyapatite mineral through negatively charged domains binding calcium ions, creating a nucleus for hydroxyapatite formation under physiological conditions. The results presented here still require a more thorough characterisation of these presumed mineralised deposits, including EDS analysis and histological staining for mineral both *in vitro* and *in vivo*.

6.5.7. The effect of SAP P_{11}-4 on histogenesis and expression of bone markers in PLA 45° constructs implanted *in vivo*

Histological sections of constructs retrieved after implantation in DCs *in vivo* showed excessive growth of new tissue inside the DC in the PLA 45°/SAP P_{11}-4 constructs compared to that of PLA control constructs, represented by densely formed connective

tissue within the SAP occupied spaces and even outgrowing as a thick capsule outside the scaffold. Cellular necrosis at the centre of the DC reflects this high growth rate, as it hurdled nutrients and oxygen perfusion from outside the chamber towards the centre. This assumption is supported by a Volkmer *et al.* (2008) study, giving evidence that enclosed 3D cultures are associated with oxygen gradient that considerably drops towards the centre of the construct, causing subsequent inconsistent tissue quality and cellular death in central regions of the scaffold, but not in its periphery. The accumulation of mouse peritoneal cells and fibrin-like material outside the DC filter would probably lead to progressive loss of the filter's efficiency to diffuse nutrients and waste products into and out of the construct (Breivik *et al.*, 1971). Consequently, it is most likely that cellular necrosis in the centre of the DC occurred after good initial growth, and even differentiation of hDPSCs within the chamber, supported by the fact that the tissue outgrowth periphery was still showing cellular activity and positive reaction against IHC bone markers which gradually faded away towards the necrotic centre.

Another aspect of histological similarity of the *in vivo* with the *in vitro* findings was the presence of acellular, fibrillar oval structures within the newly formed tissue of the PLA 45°/SAP P_{11}-4 constructs. This supports suggestions that these are more likely to be a form of ECM deposition rather than P_{11}-4 gel residues, given that all control constructs containing the SAP gel alone showed complete dissolution of the gels inside their DCs by the end of the 7th week of the *in vivo* culture. When constructs were stained with AB-VG, the oval structures showed variably bluish to pink gradient colouration, with the interstitial matrix being mainly blue and therefore positive for the AB stain. Again, this could indicate gradual replacement of the SAP P_{11}-4 gel by neo-ECM formation, or it could be symptomatic of bone-like tissue analogue, as was

discussed in **6.6.4**, especially as the new matrix showed strong positive reactivity with antibodies directed against Col-I, OPN and OCN osteogenic markers. However, although OPN and OCN are known osteogenic markers (Hauschka *et al.*, 1989, Rickard *et al.*, 1994), there is still a possibility for false positives, especially when considering the strong expression seen in the samples here. OPN is present in almost all body fluids and is abundantly secreted by MSCs in culture (Chen *et al.*, 2014). The anti-OPN antibodies used in this study was theoretically human OPN specific; therefore, any OPN detected should be from the hDPSCs within the constructs rather than from the mouse host. OCN is a highly soluble protein, so its diffusion into the DCs may result in a false-positive reactivity that is not actually associated with the expression of OCN by hDPSCs (Fanburg *et al.*, 1997). Also, both OPN and OCN have a high affinity for Ca++ ions and hydroxyapatite crystals (Fanburg *et al.*, 1997, Sodek *et al.*, 2000), so the positive reaction seen in the recovered DCs could possibly reflect the ability of SAP P_{11}-4 to nucleate minerals *de novo* when bound to circulating OPN/OCP from the host animal circulation. Future investigations need to be addressed including the use of anti- SAP P_{11}-4 antibodies to check for residual SAP gel and anti-Col-II antibodies to detect any cartilage formation in addition to IHC and histochemical studies on PLA-SAP P_{11}-4 scaffolds in the absence of hDPSCs, mineralisation assays such as EDS and Von Kossa staining, and using actual *in vivo* bone defects to investigate constructs' ability for bone regeneration.

The presence of the round eosinophilic bodies encircled with darkly purple-stained cellular ring within the new matrix was another interesting histological finding within the PLA 45°/SAP P_{11}-4 constructs recovered after implantation *in vivo.* Although not yet clear in nature, these oval-round bodies exhibited some characteristics that could be related to early osteogenesis. Here, cuboidal darkly stained active osteoblasts form

groups called ossification centres and start laying down bone matrix in a spongy bone pattern. Some osteoblasts become trapped within this matrix to turn into osteocytes (Junqueira and Mescher, 2013). Many of these centres of ossification enlarge until they coalesce; then eventual maturation occurs to produce an outer compact bone and interior spongy bone (Berkovitz, 2017). This could be, to a certain extent, supported by this study's SEM results, where sponge-like honeycomb-patterned ECM was seen within PLA 45°/SAP P_{11}-4 constructs that had been implanted *in vivo*. Dental pulp cells originate from the maxillofacial flat bones of the skeleton, and could, therefore, undergo a type of intramembranous ossification when induced (Alkaisi *et al.*, 2013). However, this was not supported by the parallel histological findings showing a clear AB positively stained ECM, which is more suggestive of endochondral ossification. Besides, some positive blue AB stain was detected inside the round bodies' matrix. Possibly, this could fit to a certain extent to what Ashton *et al.* (1980) stated about rabbit marrow stromal cells osteogenic behaviour in DC. Interestingly, he found that osteogenic tissue differentiation within DC could give rise into two forms; formation of bone tissue in a fibrous layer surrounding cartilage and/or intramembranous bone formed without cartilage formation. Longer culture time might be required in the future to closely monitor any possible enlargement of those osteoid-like structures and detect the presence of osteocytes within their matrix. It is also of importance to include IHC analysis to detect angiogenesis, as these round bodies could be a sign of angiogenesis (Gerber and Ferrara, 2000). However, there was no evidence of red blood cells within these bodies, as the lumen was filled with matrix material instead. Figure (6-20) compares the morphology of the detected round bodies within PLA 45°/SAP P_{11}-4 *in vivo* constructs with intramembranous centres of ossification found in the literature.
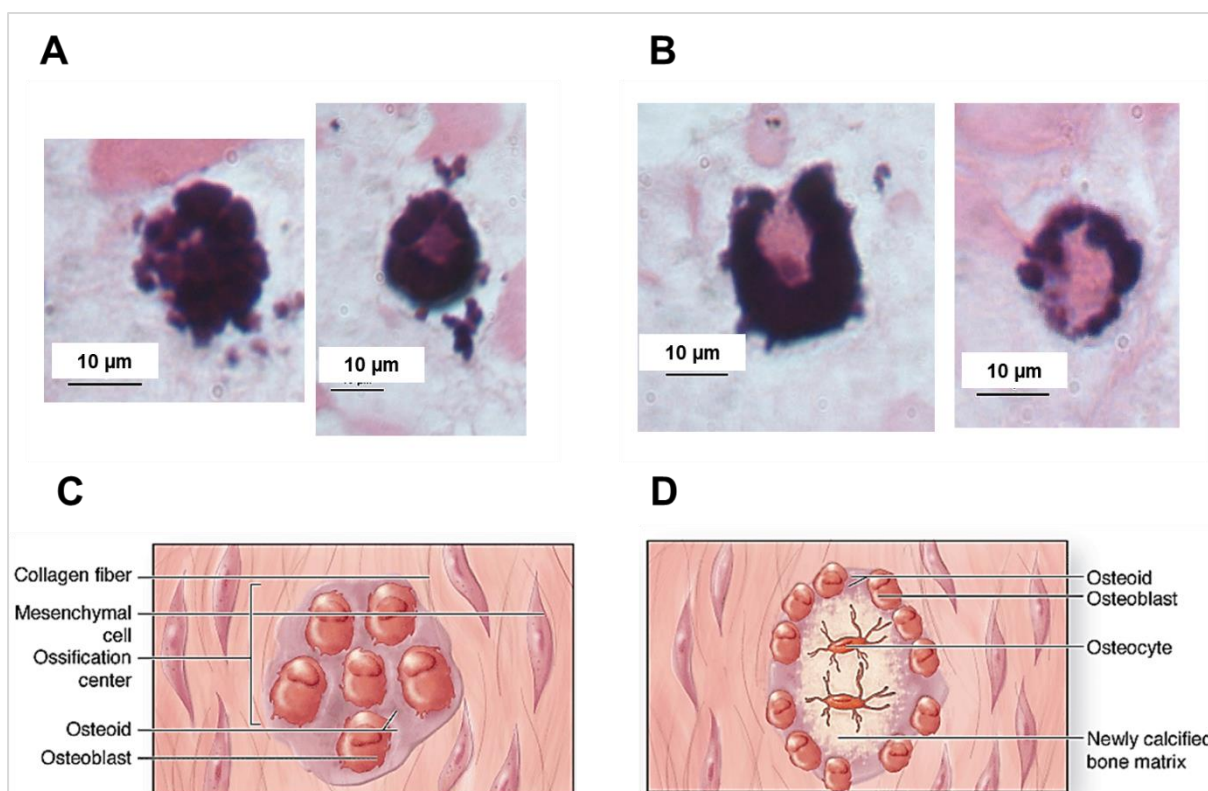
Figure 6-20: Comparison between the morphology of the round bodies detected within PLA 45°/SAP P$_{11}$-4 constructs in DCs after 7 weeks *in vivo* with intramembranous centres of ossification found in literature. A: A group of darkly purple stained cells round up to form distinctive bodies within the matrix of PLA 45°/SAP P$_{11}$-4 constructs. B: Similar characteristics are seen in literature describing ossification centres within the mesenchyme (Junqueira and Mescher, 2013). C: Some of the round bodies in PLA 45°/SAP P$_{11}$-4 constructs appeared as a ring of dark purple cells enclosing an eosinophilic centre. D: Osteoid description in literature showing some similarities (Junqueira and Mescher, 2013)

6.5.8. PLA 45°/SAP P$_{11}$-4 scaffolds potential to support osteogenesis

Human mesenchymal stem cells, including hDPSCs, have the capacity to differentiate into multiple cell lineages (Pittenger *et al.*, 1999). Tibbitt and Anseth (2009) suggested that a cell can no longer be regarded as an isolated being defined by its genome, but must be studied in the setting of the surrounding dynamic, extracellular environment that controls intracellular signalling cascades which eventually alter gene and protein expression (Birgersdotter *et al.*, 2005). Cellular choice of differentiation fate is thought to be governed by commands from the surrounding stem cell niche. These commands

192

can be broadly classified into biochemical cues resulting from the combined effects of available growth factors within the environment; and physical cues directed by the surrounding ECM topographic features and stiffness (Engler *et al.*, 2006, Discher *et al.*, 2009). Growth factors, whether insoluble or ECM bound form (Das and Zouani, 2014) would be more readily available to cells enclosed within SAP gels compared to those in large, empty 3D printed PLA 45° macro-pores, as the gel itself would act as a medium to transport such factors. Moreover, as shown by this work's results, the addition of SAP gels to PLA scaffolds would help maintain a high density of cells within the confined spaces of the PLA 45° scaffold macro-pores, bringing cells into closer proximity (Radisic *et al.*, 2003). Possibly this will increase the chance for cell-cell biochemical signalling to take place which is a key component of the cell niche, the microenvironment that regulates cell survival and differentiation (Discher *et al.*, 2009). In a study by Xue *et al.* (2013), mesenchymal stem cells (MSCs) seeded at high densities in 3D cultures were found to upregulate osteogenic genes. Similarly, limiting the degree of cell-cell contacts between MSCs was found to inhibit their adipogenic, osteogenic, and chondrogenic differentiation (Tang *et al.*, 2010, Wang *et al.*, 2013, Cao *et al.*, 2015).

Physical properties of the scaffold are known to have a major impact on cellular differentiation cues. Stiffness is one parameter to consider. In a landmark paper by Engler *et al.* (2006), evidence was provided that in the absence of growth factors, matrix stiffness can specify the lineage to which MSCs would differentiate, whether into neurons, myoblasts, or osteoblasts. In another study by Mao *et al.* (2016), it was demonstrated that both scaffold stiffness and cell density were important for osteo-inductive differentiation, as gels with a higher modulus of elasticity produced more elevated levels of ALP activity than softer gels with similar cell seeding density. It was

also suggested that MSCs would rather be driven through osteogenic cues on materials with a high modulus of elasticity rather than softer surfaces, which are more likely to produce muscle or fat cells (Xue *et al.*, 2013). In respect of gels, assembled SAP gels are known to have a high modulus of elasticity at 10 mg/mL (Boden *et al.*, 2015). The SAP gel stiffness was found to be most affected by the peptide sequence, followed by peptide concentration and surrounding buffer composition (Koch *et al.*, 2018). For SAP P_{11}-4 at a concentration between 10-30 mg/ ml, stiffness was found to have a range of (2–4.6 kPa) in Tris NaCl buffer with an ionic strength of 140 mM and a final pH of 7.2 (Koch *et al.*, 2018). Huebsch *et al.* (2010) reported that this could be within the minimal gel stiffness range to support osteogenesis. This disagrees with (Guvendiren and Burdick, 2012), who reported that matrix stiffness around 3 kPa would promote adipogenic differentiation. However, Yin and Li (2006) explained that in physiological conditions, MSCs reside in the bone marrow, which is soft and has the stiffness resembling adipose tissues. Mao *et al.* (2016) also found that higher ALP production (which is an early protein marker for osteogenesis) is guided by both substrate modulus and cell-cell interactions within the matrix; as single MSCs produced little ALP, regardless of the material modulus. They also found that in substrates with high modulus, only cells experiencing direct cell-cell contact produced significant amounts of ALP. To some extent, this could explain the high expression of osteogenic markers within the PLA 45°/SAP P_{11}-4 constructs in the current project, driven by the high hDPSCs intercellular contact when contained within the SAP gel. Nano topography, on the other hand, also plays an important role in affecting cellular differentiation cues (Kim *et al.*, 2011). It was reported that nano pits and nanotubes were found to stimulate osteogenic differentiation of MSCs in the absence of osteo-inductive media (Dalby *et al.*, 2007, Oh *et al.*, 2009). Likewise, Sjöström *et al.* (2009)

reported skeletal differentiation of MSCs was maximal on 15 nm nanopillars. It was also found that osteoblast ALP activity and ECM secretion on carbon nanofibers increased dramatically with decreasing fibre diameter in the range of 60–200 nm (Hosseinkhani *et al.*, 2006). However, this disagrees with other studies suggesting that nano topography is not sufficient to guide osteogenic differentiation on its own, but works synergistically with the growth factors in the culture medium (You *et al.*, 2010). Nuttelman *et al.* (2004) showed that encapsulating MSCs in hydrogel with no differentiation induction cues dramatically decreased their viability with culture time.

6.6. Conclusion

Based on the data reported in this chapter, it is concluded that even though 3D printed PLA microfibers provide a biocompatible extracellular environment, they are still far from simulating natural nanoscale ECM. Incorporating SAP P$_{11}$-4 into 3D printed PLA enhanced hDPSCs attachment, new tissue formation and osteogenesis both *in vitro* and *in vivo*, illustrating the potential use of this novel combination for enhanced bone tissue engineering.

CHAPTER SEVEN

General discussion, future work and conclusion

Chapter 7.   General discussion, future work and conclusion

This chapter will discuss the overall outcomes of this project and how they would fit within the context of the current literature, addressing any clinical translation issues whenever relevant and highlighting the final conclusions and suggestions for possible future work.

The choice of dental pulp tissue isolated from third molar teeth as a cell source for BTE in this project offered several advantages. They provided relatively rapid proliferation rate and were easily accessible, as sound third molars were frequently available from the tissue bank as they are routinely removed from young patients due to dental arch lack of space issues causing them to be partially or fully impacted (Nakajima *et al.*, 2018). Being the last tooth to develop within the adult dental arch and obtained from young donors, privileged third molars are thought to have the youngest adult pulp as a dental tissue source (Zhang *et al.*, 2006). This increased its potential to express stem cell activity that can be recruited for regeneration research (Zhang *et al.*, 2006). This was clearly reflected in the results of ***Chapter 4*** of the current thesis, where the potency of hDPSCs primary cultures obtained from third molars of different donors was successfully induced and characterised via the trilineage differentiation method, in line with what was concluded in previous studies (Jo *et al.*, 2007, Nuti *et al.*, 2016, Zhou *et al.*, 2018, Zhu *et al.*, 2018). Being able to demonstrate this capability was of great importance to ensure appropriate cell source quality of the different donors before using this hDPSCs source for further experiments. The International Society for Cellular Therapy (ISCT), proposed a set of standard criteria to encourage a more uniform characterisation of MSCs among investigators. This included a combined demonstration of MSC plastic-adherence, expression of specific stem cell surface markers with the absence of certain other cell markers and the potential for

multilineage differentiation *in vitro* (Dominici *et al.*, 2006) as was discussed in **Chapter 4**. However, this approach is not always practical as it involves prolonged and laborious characterisation work and requires modification as new knowledge unfolds; therefore, it is generally used where it is employed to standardise stem cells' characteristics from different donors before their application in a clinical trial (Dominici *et al.*, 2006, Pamphilon *et al.*, 2013).

In this project, the osteogenic potential of hDPSCs was evaluated in a step by step manner, from monolayers to 3D cultures. It was first demonstrated that hDPSCs from the 3 different donors could respond to osteogenic cues when cultured in monolayers *in vitro*, agreeing with several studies in the literature (Zhang *et al*, 2006; d'Aquino *et al*, 2008; Morad *et al*, 2013). Generally, *in vitro* evaluation of BTE potential of cells cultured on flat 2D substrates is consistently still in use, as it offers an easy approach to monitoring and understanding fundamental biological events associated with cell culture which are more difficult to measure and control within multifaceted 3D culture conditions (Kim *et al.*, 2012). However, monolayer cultures alone do not reflect the complexity found in 3D microenvironments (Kim *et al.*, 2012). Extensive experimental evidence suggests that cell behaviour is extremely different in 3D matrices versus flat 2D culture substrates (Cukierman *et al.*, 2001, Yamada and Cukierman, 2007). This is attributed to the rigid, inert surface of cell culture vessels where cells in monolayers adhere and migrate on a 2D surface, as only a part of the cell surface can interact with neighbouring cells or be exposed to the culture medium. This is in sharp contrast to the 3D *in vivo* environment, where the cell fully interacts with its surrounding extracellular matrix and with the membranes of neighbouring cells (Cukierman *et al.*, 2001). In addition, transport processes in 3D culture are significantly different from those in 2D, as cytokines, chemokines, and growth factors follow gradient diffusion

systems, playing a pivotal role in cell signalling and development. This is in contrast to monolayer cultures, where biochemical molecules quickly diffuse in the medium across the culture vessel (Gelain *et al.*, 2007). For these reasons, the assessment of hDPSCs' behaviour in this project was then taken to the next level above 2D culture and their osteogenic behaviour was evaluated in a 3D matrix culture setting.

Three dimensional *in vitro* models bridge the gap between 2D cell cultures and *in vivo* animal systems, as mimicking specific tissues *in vitro* facilitates close-up monitoring of miscellaneous cellular and biological events within the constructs in a more nature-representative manner prior to *in vivo* evaluation (Yamada and Cukierman, 2007). It was demonstrated in the current project that hDPSCs had the potential to superiorly support formation of bone-like tissue when cultured on 3D matrices that were fabricated by 3D printing of PLA fibres, in a (0°/45°/90°/135°) offset layout (PLA 45°) compared to the conventional (0°/90°) printing layout (PLA 90°) as was demonstrated in ***Chapter 5***. To the best of the author's knowledge, no previous work has been reported in the literature describing the combination of 3D printed PLA 45° with hDPSCs primary cultures for bone tissue regeneration, although a number of previous studies on different materials and/or cells recommended the use of similar 3D printed designs in supporting cellular attachment, growth and differentiation (Yilgor *et al.*, 2008, Sobral *et al.*, 2011, Lee *et al.*, 2012, Van Bael *et al.*, 2012, Domingos *et al.*, 2013). The results of the current study also proved that this scaffold design could generate a gradient of pore sizes within the range approximating to that found in the natural bone environment. Complex pore geometries and narrower fibre angles were seen to favour improved hDPSCs attachment, growth and osteogenic differentiation, as was discussed in ***Chapter 5***.

In vivo evaluation of 3D printed PLA 45° constructs showed good potential of this design to support bone-like tissue formation using hDPSCs *in vivo*. HDPSCs in PLA 45° constructs showed superior ability to support neo-tissue mineralisation compared to hDPSCs on PLA 90° negative control group. As was discussed in ***Chapter 5***, this could be attributed to the potential of narrower fibre angles and the offset struts layout of the PLA 45° design encouraging faster cellular bridging and growth, ending up with accelerated osteo-differentiation and mineral deposition by the end of the culture period compared to the control group. The hDPSCs-PLA 45° constructs were therefore used in subsequent *in vivo* experiments. However, the main problem encountered during the *in vivo* work was the failure of these scaffolds to support cellular growth sufficient for construct survival inside the diffusion chamber (DC) when they were immediately implanted intraperitoneally after seeding. The resulting strategy, therefore, required a prolonged *in vitro* culture prior to *in vivo* implantation to overcome this problem. If prior *in vitro* culture were to be necessary, then this could create a major limitation in future clinical translation, as long *ex vivo* culture periods can result in cellular ageing which significantly impairs their proliferation and differentiation potential (Park *et al.*, 2005, Turinetto *et al.*, 2016), together with possibilities of changes to cell genotype (Kretlow *et al.*, 2008, Liu and Tang, 2016).

The results obtained here might, however, be related to many aspects. Inadequate polymer scaffold seeding density could be one reason; however trails to increase cell density and/ or use dynamic seeding did not give the desired result, as was discussed in ***Chapter 5***. Another possibility could be donor-related cell growth issues. This was, however, not very likely to be the case as the donors used for this particular experiment were checked in advance and previously proved to have adequate growth and differentiation capacities (as discussed in ***Chapter 4***). The use of the DC as an *in vivo*

model could also attribute to this outcome, as it has been previously suggested that the chamber filter pores might become occluded with time by fibrinous debris from the surrounding peritoneal environment that gradually accumulates on the chamber surface. This would reduce oxygen and nutrients transport to the inside of the chamber (Breivik *et al.*, 1971). Mikos *et al.* (1993) reported that initial dependence on diffusion for nutrient-waste exchange in *in vivo* work might significantly limit cellular growth, viability, and histogenesis within the implants. Despite this, the DC model was of great value as an *in vivo* model of choice in the current project. Their use was justified by several previous studies that adopted a similar model for *in vivo* evaluation of bone tissue regeneration using skeletally derived cell populations to resolve the problems of host versus donor reaction (Ashton *et al.*, 1980, Partridge *et al.*, 2002, Yang *et al.*, 2003, Yang *et al.*, 2004). As human cells were used in the current study, it was essential to select an immune-deficient animal model (e.g. athymic mice or rats) to avoid provoking graft rejection reactions against the implanted constructs (Belizário, 2009). DCs provided the required isolation of the hDPSCs within the constructs from the surrounding mouse cells in a way that cannot be provided by other *in vivo* models such as subcutaneous implantation (Jones and Yang, 2011). Actual bone defects, however, represent the best model to evaluate *in vivo* responses to tissue regeneration constructs (Pearce *et al.*, 2007). It is important to consider the future evaluation of the proposed 3D printed constructs' *in vivo* performance in actual bone in order to predict its potential for future clinical application better. However, as the size of 3D printed PLA scaffolds used in the current study were relatively large, it was not practical to fit them in an induced bone defect in nude mice. Smaller PLA discs with a reduced thickness could be printed in the future (preserving the size and geometry of the current pores) to give the opportunity of implanting the proposed

constructs in cranial bone defects in nude mice or rats calvaria. Likewise, cranial bone defects in larger animal models (like rabbits) could be used for future *in vivo* evaluation; with the 3D printed PLA scaffolds seeded with cells isolated from that particular species (this would require preliminary *in vitro* cell characterisation and osteogenic induction optimisation), or the cell-free scaffold could be used as a bone graft to eliminate the risk of graft rejection.

Taking a step forward from what had previously been reported in the literature, the inert nature of PLA fibres led to the idea of combining 3D printed PLA 45° (after proving its efficiency both *in vitro* and *in vivo*) with a nanophase material aiming to enhance its surface chemistry and create a synthetic nano analogue for biological extracellular matrices that would hopefully be more favourable for cells (Hosseinkhani, 2006; Horii *et al*, 2007; Semino, 2008; Nisbet *et al*, 2012). In this project, the choice of a self-assembling peptide (SAP P_{11}-4) to be combined with 3D printed PLA was based on its previous successful outcomes as a scaffold for BTE on its own (Burke, 2011, Saha *et al*., 2019). However, these studies reported that a major limitation of using this SAP alone was that it is "mechanically weak". The mechanical weakness of a scaffold can be an issue in supporting bone defects during healing, especially in load-bearing areas (Semino, 2008). The following previous studies have suggested incorporation of additional rigid scaffold elements to support the weak gels during bone regeneration; however, a number of limitations were spotted in the designs suggested by these studies.

 Nakahara *et al*. (2010) used a 3D printed polyether-ether-ketone polymer cage to support the contained RAD-16-I (PuraMatrix™) SAP gel to be used as a combined scaffold for segmental bone defect healing in rats. However, the proposed cage served

merely as an outer shell, with no internal polymer elements to support the gelatinous core or aid in the osteo-induction.

Likewise, Wu *et al*. (2011) mixed N-(2-hydroxypropyl) methacrylamide (HPMA) copolymer with a complementary β-sheet Beta11A peptide conjugated as grafts to form a self-assembled gel in physiological pH. The conjugated scaffold fabrication procedure was extremely complicated involving strong chemical solvents, with the resultant scaffold mechanical properties still an issue.

Gharaei *et al*. (2016) attempted to enhance self-assembling peptide mechanical properties as a scaffold for TE via the introduction of a special electro-spun nano/micro scaffold combination of poly (ε-caprolactone) and SAP P_{11}-8 fibres. However, discontinuities in the fibril-based nano-network were experienced during the electrospinning process due to the high velocity. In addition, technical limitation and the use of chemical solvents during the process would hinder the *in situ* assembly of this scaffold for future clinical application; especially if cells are planned to be involved. In addition, the general disadvantages of electro-spinning scaffold fabrication versus 3D printing are still to be considered (please see *1.7.1.2*).

Heo *et al*. (2017) suggested a different design, where a 3D printed PLA framework was used to support an injected methacrylated gelatine (GelMA) hydrogel core, reinforced with gold nanoparticles to provide nanoscale structure. However, the PLA was 3D printed in a classic 0/90° layout and the gel used required photo-initiation to harden. Also, the fabrication of the gold nanoparticles required a prolonged laboratory procedure; not to mention the additional steps involved in conjugating the particles with the hydrogel. In addition, incorporation of cells within the scaffold could not be carried out directly during scaffold assembly due to the harsh chemicals used during scaffold fabrication.

The novel PLA 45°/SAP P_{11}-4 scaffold constructs used in the present study suggested a new approach to deal with the limitations addressed above. It offered a double-action outcome by blending the advantages of both 3D printing and SAPs technologies into one scaffold unit in a way that would complement the drawbacks of each other. PLA provided an excellent biocompatible, rigid, biodegradable and highly porous template to support the fragile SAP gel during bone regeneration, with the possibility of 3D printing controlling scaffold pore size and geometry in order to meet the physiological needs of the engineered bone tissue (Wahl *et al*, 2007; Liu *et al*, 2008; Serra *et al*, 2013; Liu *et al*, 2014). Additionally, the incorporation of SAP did more than merely coat PLA fibres and improve its inert surface chemistry; it also aimed to fill in the relatively large macro-pores within the 3D printed scaffold. Radisic *et al*. (2003) reported that inoculating gel–cell into a polymer scaffold followed by the immediate establishment of perfusion of culture medium through the construct can be utilised to generate high initial densities of viable cells. This, in turn, will maximize the utilisation of donor cells, provide a uniform spatial distribution of attached cells and ensure high initial construct cellularity to enhance the rate of tissue development. The gel will also act as a supporting vehicle to the growing cells and a reservoir medium for signalling growth factors transport inter-cellularly (Vunjak-Novakovic and Radisic, 2004). Incorporating self-assembling peptides had been utilised by many studies in the literature to improve the biological properties of otherwise weakly bioactive scaffolds such as ceramics, porous titanium and polycaprolactone, thus broadening their applications for bone tissue engineering applications (Sargeant *et al*., 2008, Andukuri *et al*., 2011, Wu *et al*., 2012). Nano-scale dimensions of SAP P_{11}-4 was also of great importance in enhancing the osteogenic process; which (on assembly) provides its own nanostructure. A great deal of research had been reported in previous literature to

address the positive role of nano-structuring enhancing bone regeneration process as was thoroughly discussed in the discussion section of **Chapter 6** of this thesis. Also, the results of **Chapter 6** of this thesis clearly showed the promising superiority of PLA 45°/SAP P_{11}-4 combinations in supporting hDPSCs attachment, growth and osteogenic differentiation *in vitro* compared to PLA 45° control group. In addition, this novel combination produces a gradient within the same scaffold entity; with structural hierarchy from the nanoscale to the macroscale within the same scaffold entity in respect of dimension scale, and form a rigid, solid framework to compliant highly hydrated gel core in respect of stiffness. This, indeed, is much more representative of what we see in natural bone rather than any of the materials in isolation, providing a more "natural" physiological cellular environment (Sant *et al.*, 2010). Thinking along this direction opens up another aspect of interest for future investigation, as this gradient can provide an advanced function of spatial control over directed cell migration, in contrast to the random migration that occurs in uniformly structured microenvironments (Rao *et al.*, 2012). This could be produced by providing both durotaxis (cell migration along variable material stiffness gradient) and topotaxis (cell migration along a gradient in variable surface topography scale) (Kim *et al.*, 2012, Rao *et al.*, 2012).

Some rheological measurements had already been undertaken *in vitro* on the assembled SAP gels to determine its stiffness. Koch *et al.* (2018) reported that P_{11}-4 stiffness had a range of (2–4.6 kPa) at a concentration between 10-30 mg/ml in Tris NaCl buffer with an ionic strength of 140 mM and a final pH of 7.2, as was discussed in **6.5.8**. This study involved a detailed rheological assessment of SAP gels degradation rate and mechanical properties, taking into account different SAP peptide sequences in a range of peptide concentrations and buffer compositions. This study

also tried to investigate the stability of SAP gels under the effect of enzymatic and bacterial exposure trying to simulate their responses within an inflammatory natural environment. A central issue with this study was that it did not directly compare the SAP stiffness and/or degradation values soaked within the same buffer at different time points. In addition, it tested the effect on one individual variable at a time on a given property of SAP gel. This could be applicable *in vitro* as all of these variables are under control, with the possibility to measure each parameter solely without being affected by the others. However, a similar approach could be quite challenging when trying to measure *in vivo* settings. The spatial/temporal variability in SAP stiffness driven by variability in its degradation depending on the environment pH, surrounding ionic concentration and mechanical agitation is expected during different stages of bone healing; adding to this the inability to measure the individual effect of each of those factors on the gel mechanical properties separated from the others within a dynamic, living environment. (Carrick *et al.*, 2007, Aggeli *et al.*, 2001, Davies *et al.*, 2006, Boden *et al.*, 2015). The possible variability in SAP stiffness *in vivo* could have a direct effect on cellular differentiation within the gel, as reported by Guvendiren and Burdick (2012). In the latter study, hydrogels based on methacrylated hyaluronic acid (MeHA) were used to demonstrate the effect of temporal gel stiffening on MSCs differentiation. It showed that the cells gradually changed their differentiation potential from adipogenic to osteogenic and this corresponded to scaffold stiffening by photo-polymerisation at different time points for up to 7 days, demonstrating MSCs response to matrix dynamic stiffness.

From a technical point of view, the novel combination of PLA 45° with SAP P_{11}-4 was advantageous compared to previously described nanophase coatings for polymer-based scaffolds (Liao *et al.*, 2004, Wu *et al.*, 2011, Zakaria *et al.*, 2013, Heo *et al.*,

2017). The scaffold combination described in this thesis was reproducible, relatively easy to assemble with no need for harsh chemical treatments, adding to that the ability of SAP molecules to spontaneously assemble into well-organised structures with literally no additional manipulation required and with hDPSCs already directly included without the need for an extra step to seed the scaffold. From a clinical application point of view, this could reduce the overall time and cost required for scaffold production, with the extra bonus of the possibility of performing the PLA 45°/SAP P_{11}-4 combination procedure *in situ* (Boden *et al.*, 2015); especially with P_{11}-4 already being licensed for clinical use and commercially produced to good manufacturing practice (GMP) for the treatment of early enamel carious lesions (Brunton *et al.*, 2013, Ravichandran *et al.*, 2014). This could be supported by the interesting outcomes of the *in vivo* evaluation of PLA 45°/SAP P_{11}-4 scaffolds described in this thesis, as they showed significant enhancement of hDPSCs growth and possible osteogenic differentiation compared to PLA 45° control constructs even when implanted immediately after seeding. However, this extensive cellular growth inside a sealed DC was one possible explanation behind what looked like necrotic tissue that was detected towards the centre of the chamber, as was reported by previous studies (Breivik *et al.*, 1971, Volkmer *et al.*, 2008). Future evaluation of these constructs needs to be carried out in actual bone defects to provide more information about their actual performance within a more realistic setting.

It's worth to keep in mind that the superiority for using SAP P_{11}-4 in particular for BTE rises from its unique ability to be able to nucleate hydroxyapatite crystals *de novo* which can potentially make a huge difference to bone construct mineralisation outcomes (Firth *et al*, 2006, Kirkham *et al* 2007, Nisbet & Williams, 2012). Unfortunately, limited time availability restricted the scope of the current thesis to cover

mineralisation evaluation procedures for the proposed novel combination constructs. This is an aspect of research that needs to be considered for future plans.

Cell-free SAP P_{11}-4 gels were previously used as scaffold materials to promote regeneration of bone in rabbit calvarial defects, showing high potential to promote new bone formation (Burke, 2011). In this study, hDPSCs were incorporated as a stem cell source within the scaffold. Encapsulating stem cells within the nano-phase SAP gel has been previously shown to synergise tissue regeneration processes with their self-renewal and immunomodulatory properties similar to that of native tissue (Horii *et al.*, 2007, Wu *et al.*, 2011). However, one *in vivo* study that combined SAP P_{11}-4 with hDPSCs for regeneration of cranial bone defects in rats showed that addition of hDPSCs to SAP P_{11}-4 constructs failed to outperform in bone repair compared to P_{11}-4 alone, referring to the possibility of SAP gel disintegration and metabolism by the included hDPSCs (Saha *et al.*, 2019). This, however, is in contrast to the work undertaken by Kyle *et al.* (2012) who reported that SAP P_{11}-4 significantly supported the proliferation of primary human dermal fibroblasts over 21 days of *in vitro* culture. This divergence in outcomes could be attributed to differences in the seeding technique, culture periods and the *in vivo* study models used. In the current project, hDPSCs were mixed as a cell suspension with disassembled P_{11}-4 before being injected around the PLA 45° scaffold fibres (Boden *et al.*, 2015) rather than mixing the freeze-dried P_{11}-4 to a pre-prepared cell suspension, as was used by (Saha *et al.*, 2019). The choice for the technique used here was made on the basis of maximising cellular viability by reducing potential chemical harm to the cells resulting from adjusting the pH of the SAP P_{11}-4 solution to the required level prior to mixing with the cell suspension. In addition, this technique facilitated flexible handling of gel disassembly (by sonication and heating on a hot plate) producing a more reliable

single-cell suspension without risking cells viability by overheating. Saha's study did not track the fate of the hDPSCs after implantation to determine whether they initially survived seeding or not. Secondly, it would be unreliable to compare the response of constructs used without SAPs in Saha's study with the study model used here, as the constructs used *in vivo* here were contained within a chamber isolating them from direct contact with surrounding *in vivo* cellular events. They were also not implanted into actual bone defects where presumably all the native inflammatory and osteo-inductive cytokines would take an active role in orchestrating the bone regeneration process. Given that the *in vitro* and DC *in vivo* results here both indicated that PLA 45°/SAP P_{11}-4 scaffolds potentially support hDPSCs osteogenesis, testing *in vivo* with a real bone defect design needs to be considered in the future.

Limitations and future work

With respect to the current project, several points could be taken into consideration to be further investigated in future work; the following are some suggestions:

- Mechanical characterisation of the used 3D printed PLA scaffolds could be performed to investigate the effect of PLA fibre angle on the mechanical properties and degradation rate of the printed polymer scaffold.

- In this project, histochemical staining and IHC were of great value in comparing qualitative differences among constructs of different experiments (PLA 45° vs PLA 90°, and PLA 45° with and without SAP P_{11}-4). However, adopting quantitative *in vitro* analysis procedures in the future would provide a more accurate way of comparison among the groups in regard to DNA quantification assays to assess cellular growth rate, histomorphometry and/ or PCR to compare bone marker expression levels among the used scaffold designs.

- Full *in vivo* assessment of (PLA 45° vs PLA 90°, and PLA 45° with and without SAP P_{11}-4) constructs is required (with and without hDPSCs included), using more representative natural bone defect model (like cranial bone defects) to assess the implanted constructs responses in a realistic living environment. This might require the fabrication of smaller scale PLA discs with reduced thickness saving current pores size and geometry to fit in nude mice cranial bone defects. Larger animal models, like rabbits, could also be considered after preliminary optimisation work for their autologous cells to be used for scaffold seeding.

- More detailed future IHC assessment for PLA 45°/SAP P_{11}-4 constructs including anti SAP P_{11}-4 antibody, anti-Col-II antibody to detect chondrogenesis or dentine specific IHC markers to detect possible dentinogenesis (like dentine sialophosphoprotein and dentin matrix protein) both *in vitro* and *in vivo.*

- A detailed assessment of potential ECM mineralisation within *in vitro* and *in vivo* PLA 45°/SAP P_{11}-4 constructs using EDS analysis and Von Kossa histology staining, including negative PLA 45°/SAP P_{11}-4 controls without cells added both *in vitro* and *in vivo.*

Towards clinical translation

Regarding cell-based BTE research in general, several limitations are still present towards clinical therapeutic translation; related to cell source, biomaterials and current pre-clinical *in vivo* models. The majority of promising clinical trials found in the literature involving MSCs in regenerative therapy for bone and cartilage repair used bone marrow-derived stem cells as a primary cell source (Marquez-Curtis *et al.*, 2015). However, some drawbacks associated with the invasiveness of the sampling procedure, the possible morbidity at the sampling site and the low output of the cell-sorting procedure lead to the quest for alternative cell sources from multiple

anatomical locations, including dental tissues (Machado *et al.*, 2012). Few clinical trials could be found in the literature demonstrating the successful use of hDPSCs based therapies in bone regeneration, mainly associated with dentoalveolar bone repair (d'Aquino *et al.*, 2009, Machado *et al.*, 2012, Giuliani *et al.*, 2013, Sheth *et al.*, 2017). Despite the ongoing trials, it is important to keep in mind that regenerative therapy based on stem cells is still hurdled with limitations towards its actual clinical application in bone repair. The rare being of MSCs cells in various mesenchymal tissues would necessitate prolonged *ex vivo* expansion in order to obtain an adequate number of cells for clinical therapy (Kim and Park, 2017). Repetitive cell passages in *in vitro* culture conditions prior to clinical installation can cause cellular genetic alteration (Kretlow *et al.*, 2008, Liu and Tang, 2016) and likely evoke cellular ageing which significantly impairs their proliferation and differentiation potential (Park *et al.*, 2005, Turinetto *et al.*, 2016). Other concerns associated with stem cell therapy in the clinic include immunogenicity against allogenic animal contaminants from cell culture (like FBS) (Bueno and Glowacki, 2009), and the inability to track the therapeutic cells to assess the risk of tumorigenicity (Goldring *et al.*, 2011). A recent field of interest in research is keen to develop methods that can adjust MSCs properties aiming to create the ideal stem cell model for regenerative purposes via tailoring their DNA or genetic profile to control their differentiation, prolonging their life span or reprogramming them to become pluripotent (Baksh *et al.*, 2004, Vitale *et al.*, 2011). The clinical application of these strategies, however, is still a concern in regards to genetic stability and carcinogenic transformation of the final product (Ben-David and Benvenisty, 2011, Goldring *et al.*, 2011).

From biomaterial point of view, clinical translation of 3D printing in scaffold-based BTE strategies is still limited, despite the expanded fields of application in medicine and the

intensive published research work that has been achieved in that area in the last two decades (Liu *et al.*, 2013). This is likely to evolve in the soon future as the requited equipment for 3D printing becomes more affordable, and printing software is made more accessible. Another critical limitation of BTE is the construct scalability. This is to engineer a bone graft with clinically relevant size, yet maintaining sufficient oxygen and nutrients supply throughout the construct, which if not appropriately secured, will result in cultured cells loss of function or even death after implantation (Fedorovich *et al.*, 2011). Strategies to enhance construct vascularisation are widely investigated, including the incorporation of interconnected micro-channels into the construct to assist vascularisation and cellular ingrowth. However, one limitation of this is the reduction of space available for cell seeding (Bueno and Glowacki, 2009).

Considering currently available designs of bone scaffolds, laboratory simulation for the natural bone structure is a bit primitive; as most of 3D printed bone scaffold models adopt the strategy of the uniformly distributed porosity throughout the whole construct, whereas the natural bone does not have a uniform porosity size or distribution. It has a dense outer cortex that gradually grades towards the spongy, highly porous core (Bose *et al.*, 2012). However, gradient porosity distribution from scaffold periphery towards the centre is challenging to be achieved using the current 3D printing modalities due to challenges including non-uniform material shrinkage during the printing process and difficulty to ensure mechanical integrity and pores interconnectivity (Bose *et al.*, 2012, Bose *et al.*, 2013). Also, further progress in 3D printing technologies is required to improve the printing resolution without sacrificing shape, strength and handleability of scaffolds. In order to achieve nanoscale printed scaffold constructs, there is a challenge in creating small features that would survive the fabrication process; as with the current technology, it is difficult to fabricate more

robust structures without increasing dimensions to certain limits (Colasante *et al.*, 2016, Chia and Wu, 2015).

Likewise, the possibility to achieve programmed spatial/ temporal disassembly of biomimetic gels, like SAPs and consequently controlling their mechanical stiffness as a response to different pH and environmental ionic strength would greatly contribute to their use in skeletal tissue repair and provide a better understanding of the effect of its mechanical properties on *in vivo* bone regeneration process (Guvendiren and Burdick, 2012, Das and Zouani, 2014, Koch *et al.*, 2018).

With regard to animal testing of stem cell products, to date, a major issue for pre-clinical evaluation of engineered bone constructs is the immunological response of testing human cells in an animal model. To overcome this problem, immunosuppressive agents or immune-deficient animal models (mice or rats) are likely to be used (Goldring *et al.*, 2011). Despite their unquestionably valuable contribution in pre-clinical stem cell research, mice and rats, however, show dissimilarities with human body settings in terms of bone size and structure compared to other models like pigs or dogs (La Noce *et al.*, 2014); not to mention that the immune-deficient model approach might conceal any possible immune response that might occur naturally in real patients undergoing cell-based therapy (Goldring *et al.*, 2011). In addition, longer follow-up studies of the therapy are not possible, as the timeline analysis of the tested therapy is limited to the lifespan of the animal which is much shorter compared with the lifespan of a human patient (Kilborn *et al.*, 2002, Goldring *et al.*, 2011). Progress has been made with the introduction of humanised mice models, in which a mouse gene is replaced by either a human gene, genomic sequence or regulatory element aiming to mimic the physiological conditions of a functionally human microenvironment (Goldring *et al.*, 2011). Methods to humanise

the bone for implantation in immunocompromised mouse models have been adopted in studying bone malignancies; however, their clinical translation is not yet clear (Reinisch *et al.*, 2016, Martine *et al.*, 2017, Quent *et al.*, 2018). Bone tissue engineering and regenerative medicine techniques can also utilise this model to generate as much human-like bone as possible within the murine host (McGovern *et al.*, 2018).

Conclusions

The current project demonstrated the ability of hDPSCs to commit to osteogenic differentiation cue both *in vitro* and *in vivo*. This confirms their being good candidates as an adult cell source for bone tissue engineering studies. However, their future use in clinical application is still in its early stages. On the other hand, 3D printed scaffold architecture and fibre layout were shown to have a significant effect on BTE outcomes when used with hDPSCs; both *in vitro* and *in vivo*. This suggests the importance to consider scaffold 3D printing layout as an essential factor in future designing of 3D printed PLA as scaffolds for BTE. With the advancement of 3D printing technology, adopting 3D printing strategies that more closely simulate natural bone structure, based on non-uniform size and distribution of scaffold pores and taking scaffold resolution to the nano level would be a pivotal aspect to be further developed. In addition, it was demonstrated by this project that the marriage between 3D printing and SAPs technologies gave birth to unique scaffold entity with gradient nano- micro scale dimensions and a naturally inspired gradient in matrix stiffness; suggesting a solution to overcome SAP gel weakness in supporting bone defects and helped to enhance PLA surface characteristics. Controlling SAP gel stiffness and disintegration under *in vivo* conditions would open the horizon for additional promising possibilities toward future clinical applications in BTE.

REFERENCES

References

AGGELI, A., BELL, M., BODEN, N., KEEN, J., MCLEISH, T., NYRKOVA, I., RADFORD, S. & SEMENOV, A. 1997. Engineering of peptide β-sheet nano-tapes. Journal of Materials Chemistry, 7, 1135-1145.

AGGELI, A., NYRKOVA, I., BELL, M., HARDING, R., CARRICK, L., MCLEISH, T. C., SEMENOV, A. N. & BODEN, N. 2001. Hierarchical self-assembly of chiral rod-like molecules as a model for peptide β-sheet tapes, ribbons, fibrils, and fibres. Proceedings of the National Academy of Sciences, 98, 11857-11862.

ALBERTS, B., WILSON, J. & HUNT, T. 2008. Molecular Biology of the Cell (Garland Science, New York). USA. 1601p.

ALFORD, A., KOZLOFF, K. & HANKENSON, K. 2015. Extracellular matrix networks in bone remodelling. The international journal of biochemistry & cell biology, 65, 20-31.

ALKAISI, A., ISMAIL, A., MUTUM, S., AHMAD, Z., MASUDI, S. & RAZAK, N. 2013. Transplantation of human dental pulp stem cells: enhance bone consolidation in mandibular distraction osteogenesis. Journal of Oral and Maxillofacial Surgery, 71, 1758. e1-1758. e13.

ALRAIES, A. 2013. Characterisation of clonal dental pulp progenitors and the effects of *in vitro* expansion and hydrogen peroxide. Cardiff University.

ALSULAIMANI, R., AJLAN, S., ALDAHMASH, A., ALNABAHEEN, M. & ASHRI, N. 2016. Isolation of dental pulp stem cells from a single donor and characterization of their ability to differentiate after 2 years of cryopreservation. J Saudi medical journal, 37, 551.

ALVAREZ-BARRETO, J., LINEHAN, S., SHAMBAUGH, R. & SIKAVITSAS, V. 2007. Flow Perfusion Improves Seeding of Tissue Engineering Scaffolds with Different Architectures. Annals of Biomedical Engineering, 35, 429-442.

ANDUKURI, A., KUSHWAHA, M., TAMBRALLI, A., ANDERSON, J., DEAN, D., BERRY, J., SOHN, Y., YOON, Y., BROTT, B. & JUN, H. 2011. A hybrid biomimetic nano-matrix composed of electro-spun polycaprolactone and

bioactive peptide amphiphiles for cardiovascular implants. Acta biomaterialia, 7, 225-233.

ANUSAKSATHIEN, O. & GIANNOBILE, W. 2002. Growth factor delivery to re-engineer periodontal tissues. Current pharmaceutical biotechnology, 3, 129-139.

ARNETT, T. 2003. Regulation of bone cell function by acid–base balance. Proceedings of the Nutrition Society, 62, 511-520.

ASA'AD, F., PAGNI, G., PILIPCHUK, S., GIANNI, A., GIANNOBILE, W. & RASPERINI, G. 2016. 3D-Printed Scaffolds and Biomaterials: Review of Alveolar Bone Augmentation and Periodontal Regeneration Applications. Int J Dent, 2016, 1239842.

ASHTON, B., ALLEN, T., HOWLETT, C., EAGLESOM, C., HATTORI, A. & OWEN, M. 1980. Formation of bone and cartilage by marrow stromal cells in diffusion chambers *in vivo*. Clinical orthopaedics and related research, 294-307.

AURAS, R., HARTE, B. & SELKE, S. 2004. An overview of polylactides as packaging materials. Macromolecular bioscience, 4, 835-864.

BAKSH, D., SONG, L. & TUAN, R. 2004. Adult mesenchymal stem cells: characterization, differentiation, and application in cell and gene therapy. J Journal of cellular molecular medicine, 8, 301-316.

BANCROFT, G., SIKAVITSAS, V. & MIKOS, A. 2003. Design of a flow perfusion bioreactor system for bone tissue-engineering applications. J Journal of Biomedical Materials Research: An Official Journal of the Society for Biomaterials, The Japanese Society for Biomaterials, 9, 549-554.

BANDYOPADHYAY, A., BOSE, S. & DAS, S. 2015. 3D printing of biomaterials. MRS bulletin, 40, 108-115.

BAUER, T. & MUSCHLER, G. 2000. Bone Graft Materials: An Overview of the Basic Science. Clinical Orthopaedics and Related Research, 371, 10-27.

BEANE, O., FONSECA, V., COOPER, L., KOREN, G. & DARLING, E. 2014. Impact of aging on the regenerative properties of bone marrow-, muscle-, and adipose-derived mesenchymal stem/stromal cells. PloS one, 9, e115963.

BELIZÁRIO, J. 2009. Immunodeficient mouse models: an overview. The open immunology journal, 2.

BELL, C., CARRICK, L., KATTA, J., JIN, Z., INGHAM, E., AGGELI, A., BODEN, N., WAIGH, T. & FISHER, J. 2006. Self-assembling peptides as injectable lubricants for osteoarthritis. Journal of Biomedical Materials Research Part A: An Official Journal of the Society for Biomaterials, The Japanese Society for Biomaterials, and The Australian Society for Biomaterials and the Korean Society for Biomaterials, 78, 236-246.

BELLOWS, C., AUBIN, J. & HEERSCHE, J. 1991. Initiation and progression of mineralization of bone nodules formed *in vitro*: the role of alkaline phosphatase and organic phosphate. J Bone mineral, 14, 27-40.

BEN-DAVID, U. & BENVENISTY, N. 2011. The tumorigenicity of human embryonic and induced pluripotent stem cells. Nature Reviews Cancer, 11, 268.

BERKOVITZ, B. 2017. Oral Anatomy, Histology and Embryology E-Book, Elsevier Health Sciences. Pp: 237-265.

BERNABE, P., MELO, L., CINTRA, L., GOMES-FILHO, J., DEZAN, E., J & NAGATA, M. 2012. Bone healing in critical-size defects treated with either bone graft, membrane, or a combination of both materials: a histological and histometric study in rat tibiae. Clin Oral Implants Res, 23, 384-8.

BERNARDI, L., LUISI, S., FERNANDES, R., DALBERTO, T., VALENTIM, L., CHIES, J., FOSSATI, A. & PRANKE, P. 2011. The isolation of stem cells from human deciduous teeth pulp is related to the physiological process of resorption. Journal of endodontics, 37, 973-979.

BERNER, A., WOODRUFF, M., LAM, C., ARAFAT, M., SAIFZADEH, S., STECK, R., REN, J., NERLICH, M., EKAPUTRA, A. & GIBSON, I. 2014. Effects of scaffold architecture on cranial bone healing. International journal of oral and maxillofacial surgery, 43, 506-513.

BERTHIAUME, F., MAGUIRE, T. & YARMUSH, M. 2011. Tissue engineering and regenerative medicine: history, progress, and challenges. Annual Review of Chemistry Biomolecular Engineering, 2, 403-30.

BIRGERSDOTTER, A., SANDBERG, R. & ERNBERG, I. Gene expression perturbation *in vitro*—a growing case for three-dimensional (3D) culture systems. Seminars in cancer biology, 2005. Elsevier, 405-412.

BLOKHUIS, T. & ARTS, J. 2011. Bioactive and osteo-inductive bone graft substitutes: definitions, facts and myths. Injury, 42, S26-S29.

BODEN, N., AGGELI, A., INGHAM, E. & KIRKHAM, J. 2015. Beta sheet tapes ribbons in tissue engineering. Google Patents.

BOLAN, M. & DE CARVALHO ROCHA, M. 2007. Histopathologic study of physiological and pathological resorptions in human primary teeth. Oral Surgery, Oral Medicine, Oral Pathology, Oral Radiology, and Endodontology, 104, 680-685.

BOLANDER, M. 1992. Regulation of fracture repair by growth factors. Proceedings of the Society for Experimental Biology and Medicine, 200, 165-170.

BÖNECKER, M., MANTESSO, A., DE ARAUJO, N. & ARAUJO, V. 2009. Expression of proteins in the extracellular matrix of pulp tissue in human primary teeth during physiologic root resorption. Quintessence International, 40.

BONEWALD, L., HARRIS, S., ROSSER, J., DALLAS, M., DALLAS, S., CAMACHO, N., BOYAN, B. & BOSKEY, A. 2003. Von Kossa staining alone is not sufficient to confirm that mineralization *in vitro* represents bone formation. Calcified tissue international, 72, 537-547.

BOSE, S., DARSELL, J., KINTNER, M., HOSICK, H. & BANDYOPADHYAY, A. 2003. Pore size and pore volume effects on alumina and TCP ceramic scaffolds. Materials Science and Engineering: C, 23, 479-486.

BOSE, S., ROY, M. & BANDYOPADHYAY, A. 2012. Recent advances in bone tissue engineering scaffolds. Trends Biotechnology, 30, 546-54.

BOSE, S., VAHABZADEH, S. & BANDYOPADHYAY, A. 2013. Bone tissue engineering using 3D printing. Materials Today, 16, 496-504.

BOSKEY, A. 1989. Non-collagenous matrix proteins and their role in mineralization. Bone, 6, 111-123.

BREIVIK, H., BENESTAD, H. & BØYUM, A. 1971. Diffusion chamber and spleen colony assay of murine haematopoietic stem cells. Journal of cellular physiology, 78, 65-72.

BRUNTON, P., DAVIES, R., BURKE, J., SMITH, A., AGGELI, A., BROOKES, S. & KIRKHAM, J. 2013. Treatment of early caries lesions using biomimetic self-assembling peptides–a clinical safety trial. British dental journal, 215, E6.

BRYDONE, A., MEEK, D. & MACLAINE, S. 2010. Bone grafting, orthopaedic biomaterials, and the clinical need for bone engineering. Proceedings of the Institution of Mechanical Engineers, Part H: Journal of Engineering in Medicine, 224, 1329-1343.

BUCKWALTER, J., GLIMCHER, M., COOPER, R. & RECKER, R. 1995. Bone biology. Journal of Bone Joint Surgery Am, 77, 1256-1275.

BUENO, E. & GLOWACKI, J. 2009. Cell-free and cell-based approaches for bone regeneration. J Nature Reviews Rheumatology, 5, 685.

BURG, K., HOLDER, J., CULBERSON, C., BEILER, R., GREENE, K., LOEBSACK, A., ROLAND, W., EISELT, P., MOONEY, D. & HALBERSTADT, C. 2000. Comparative study of seeding methods for three-dimensional polymeric scaffolds. Journal of biomedical materials research, 51, 642-649.

BURG, K., HOLDER, W., CULBERSON, C., BEILER, R., GREENE, K., LOEBSACK, A., ROLAND, W., MOONEY, D. & HALBERSTADT, C. 1999. Parameters affecting cellular adhesion to polylactide films. Journal of Biomaterials Science, Polymer Edition, 10, 147-161.

BURKE, J. 2011. In situ engineering of skeletal tissues using self-assembled biomimetic scaffolds. University of Leeds.

CALORI, G., MAZZA, E., COLOMBO, M. & RIPAMONTI, C. 2011. The use of bone-graft substitutes in large bone defects: any specific needs? Injury, 42 Suppl 2, S56-63.

CAMACHO-FERNÁNDEZ, C., HERVÁS, D., RIVAS-SENDRA, A., MARÍN, M. & SEGUÍ-SIMARRO, J. 2018. Comparison of six different methods to calculate cell densities. J Plant methods, 14, 30.

CAO, B., LI, Z., PENG, R. & DING, J. 2015. Effects of cell–cell contact and oxygen tension on chondrogenic differentiation of stem cells. Biomaterials, 64, 21-32.

CAPLAN, A. I. 2005. Mesenchymal stem cells: cell–based reconstructive therapy in orthopedics. Tissue engineering, 11, 1198-1211.

CARRICK, L. M., AGGELI, A., BODEN, N., FISHER, J., INGHAM, E. & WAIGH, T. A. J. T. 2007. Effect of ionic strength on the self-assembly, morphology and gelation of pH responsive β-sheet tape-forming peptides. 63, 7457-7467.

CARTMELL, S., HUYNH, K., LIN, A., NAGARAJA, S. & GULDBERG, R. 2004. Quantitative microcomputed tomography analysis of mineralization within three-dimensional scaffolds *in vitro*. Journal of Biomedical Materials Research Part A: An Official Journal of the Society for Biomaterials, The Japanese Society for Biomaterials, and The Australian Society for Biomaterials and the Korean Society for Biomaterials, 69, 97-104.

CECI, M., MIRANDO, M., BELTRAMI, R., CHIESA, M., COLOMBO, M. & POGGIO, C. 2016. Effect of self-assembling peptide P11-4 on enamel erosion: AFM and SEM studies. Scanning, 38, 344-351.

CHADIPIRALLA, K., YOCHIM, J.M., BAHULEYAN, B., HUANG, C.Y.C., GARCIA-GODOY, F., MURRAY, P.E. AND STELNICKI, E.J., 2010. Osteogenic differentiation of stem cells derived from human periodontal ligaments and pulp of human exfoliated deciduous teeth. Cell and tissue research, 340(2), 323-333.

CHEN, Q., SHOU, P., ZHANG, L., XU, C., ZHENG, C., HAN, Y., LI, W., HUANG, Y., ZHANG, X. & SHAO, C. 2014. An osteopontin-integrin interaction plays a critical role in directing adipogenesis and osteogenesis by mesenchymal stem cells. Stem Cells, 32, 327-337.

CHEN Q. 2012 Progress and challenges in biomaterials used for bone tissue engineering: bioactive glasses and elastomeric composites. Progress in Biomaterials, 1, 2-22.

CHEN, Y., MAK, A. F., WANG, M., LI, J. & WONG, M. 2006. PLLA scaffolds with biomimetic apatite coating and biomimetic apatite/collagen composite coating to

enhance osteoblast-like cells attachment and activity. Surface and Coatings Technology, 201, 575-580.

CHENG, Y., DENG, S., CHEN, P. & RUAN, R. 2009. Polylactic acid (PLA) synthesis and modifications: a review. Frontiers of chemistry in China, 4, 259-264.

CHEUNG, H.-Y., LAU, K.-T., LU, T.-P. & HUI, D. 2007. A critical review on polymer-based bio-engineered materials for scaffold development. Composites Part B: Engineering, 38, 291-300.

CHIA, H. N. & WU, B. M. 2015. Recent advances in 3D printing of biomaterials. Journal Biological Engineering, 9, 4.

COELHO, M. & FERNANDES, M.H. 2000. Human bone cell cultures in biocompatibility testing. Part II: effect of ascorbic acid, B-glycerophosphate and dexamethasone on osteoblastic differentiation. Biomaterials 21 ,1095-1102.

COLASANTE, C., SANFORD, Z., GARFEIN, E. & TEPPER, O. 2016. Current Trends in 3D Printing, Bioprosthetics, and Tissue Engineering in Plastic and Reconstructive Surgery. Current Surgery Reports, 4(2), 6.

COUBLE, M.-L., FARGES, J.-C., BLEICHER, F., PERRAT-MABILLON, B., BOUDEULLE, M. & MAGLOIRE, H. 2000. Odontoblast differentiation of human dental pulp cells in explant cultures. Calcified Tissue International, 66, 129-138.

COWLES, E., DEROME, M., PASTIZZO, G., BRAILEY, L. & GRONOWICZ, G. J. C. T. I. 1998. Mineralization and the expression of matrix proteins during *in vivo* bone development. 62, 74-82.

CUI, Q., WANG, G.-J. & BALIAN, G. 1997. Steroid-induced adipogenesis in a pluripotential cell line from bone marrow. JBJS, 79, 1054-63.

CUKIERMAN, E., PANKOV, R., STEVENS, D. R. & YAMADA, K. M. 2001. Taking cell-matrix adhesions to the third dimension. Science, 294, 1708-1712.

COOK, S, SALKELD, S, BRINKER, M, WOLFE, M & RUEGER, D. 1998. Use of an Osteoinductive Biomaterial (rhOP-1) in Healing Large Segmental Bone Defects. Journal of Orthopaedic Trauma, 12 407-412.

D'AQUINO, R., DE ROSA, A., LANZA, V., TIRINO, V., LAINO, L., GRAZIANO, A., DESIDERIO, V., LAINO, G. & PAPACCIO, G. 2009. Human mandible bone defect repair by the grafting of dental pulp stem/progenitor cells and collagen sponge bio-complexes. Eur Cell Mater, 18, 75-83.

D'AQUINO, R., PAPACCIO, G., LAINO, G. & GRAZIANO, A. 2008. Dental pulp stem cells: a promising tool for bone regeneration. Stem cell reviews, 4, 21-26.

DABROWSKI, B., SWIESZKOWSKI, W., GODLINSKI, D. & KURZYDLOWSKI, K. J. 2010. Highly porous titanium scaffolds for orthopaedic applications. Journal of Biomedical Materials Research Part B: Applied Biomaterials, 95, 53-61.

DAI, J. & RABIE, A. J. J. O. D. R. 2007. VEGF: an essential mediator of both angiogenesis and endochondral ossification. 86, 937-950.

DAI, J., WANG, J., LU, J., ZOU, D., SUN, H., DONG, Y., YU, H., ZHANG, L., YANG, T. & ZHANG, X. 2012. The effect of co-culturing costal chondrocytes and dental pulp stem cells combined with exogenous FGF9 protein on chondrogenesis and ossification in engineered cartilage. Biomaterials, 33, 7699-7711.

DALBY, M. J., GADEGAARD, N., TARE, R., ANDAR, A., RIEHLE, M. O., HERZYK, P., WILKINSON, C. D. & OREFFO, R. O. 2007. The control of human mesenchymal cell differentiation using nanoscale symmetry and disorder. Nature materials, 6, 997.

DALTOE, F. P., MENDONCA, P. P., MANTESSO, A. & DEBONI, M. C. Z. 2014. Can SHED or DPSCs be used to repair/regenerate non-dental tissues? A systematic review of *in vivo* studies. Brazilian oral research, 28, 1-7.

DANIELS, F., TER HAAR ROMENY, B. M., RUBBENS, M. & VAN ASSEN, H. Quantification of collagen orientation in 3D engineered tissue. 3rd Kuala Lumpur International Conference on Biomedical Engineering 2006, 2007. Springer, 282-286.

DAS, R. K. & ZOUANI, O. F. 2014. A review of the effects of the cell environment physicochemical nanoarchitecture on stem cell commitment. Biomaterials, 35, 5278-5293.

DATTA, H., NG, W., WALKER, J., TUCK, S. & VARANASI, S. 2008. The cell biology of bone metabolism. Journal of clinical pathology, 61, 577-587.

DAVIES, O., COOPER, P., SHELTON, R., SMITH, A., SCHEVEN, B. J. J. O. B. & METABOLISM, M. 2015. A comparison of the *in vitro* mineralisation and dentinogenic potential of mesenchymal stem cells derived from adipose tissue, bone marrow and dental pulp. 33, 371-382.

DAVIES, R., AGGELI, A., BEEVERS, A., BODEN, N., CARRICK, L., FISHWICK, C., MCLEISH, T., NYRKOVA, I. & SEMENOV, A. 2006. Self-assembling β-sheet tape forming peptides. Supramolecular Chemistry, 18, 435-443.

DE VALENCE, S., TILLE, J.-C., CHAABANE, C., GURNY, R., BOCHATON-PIALLAT, M., WALPOTH, B. & MÖLLER, M. 2013. Plasma treatment for improving cell biocompatibility of a biodegradable polymer scaffold for vascular graft applications. European Journal of Pharmaceutics and Biopharmaceutics, 85, 78-86.

DEHNE, T., KARLSSON, C., RINGE, J., SITTINGER, M. & LINDAHL, A. 2009. Chondrogenic differentiation potential of osteoarthritic chondrocytes and their possible use in matrix-associated autologous chondrocyte transplantation. Arthritis research & therapy, 11, R133.

DENHARDT, D. T., NODA, M., O'REGAN, A. W., PAVLIN, D. & BERMAN, J. S. J. T. J. O. C. I. 2001. Osteopontin as a means to cope with environmental insults: regulation of inflammation, tissue remodeling, and cell survival. 107, 1055-1061.

DETELA, G., BAIN, O. W., KIM, H. W., WILLIAMS, D. J., MASON, C., MATHUR, A. & WALL, I. B. 2018. Donor variability in growth kinetics of healthy hMSCs using manual processing: considerations for manufacture of cell therapies. Biotechnology journal, 13, 1700085.

DIKOVSKY, D., BIANCO-PELED, H. & SELIKTAR, D. 2006. The effect of structural alterations of PEG-fibrinogen hydrogel scaffolds on 3-D cellular morphology and cellular migration. Biomaterials, 27, 1496-1506.

DIMITRIOU, R., MATALIOTAKIS, G. I., CALORI, G. M. & GIANNOUDIS, P. V. 2012. The role of barrier membranes for guided bone regeneration and restoration of

large bone defects: current experimental and clinical evidence. BMC Med, 10, 81.

DIMITRIOU, R., TSIRIDIS, E. & GIANNOUDIS, P. V. 2005. Current concepts of molecular aspects of bone healing. Injury, 36, 1392-1404.

DIPERSIO, C., JACKSON, D. & ZARET, K. 1991. The extracellular matrix coordinately modulates liver transcription factors and hepatocyte morphology. Molecular and Cellular Biology, 11, 4405-4414.

DISCHER, D., MOONEY, D. & ZANDSTRA, P. 2009. Growth factors, matrices, and forces combine and control stem cells. Science, 324, 1673-1677.

DJOUAD, F., GUERIT, D., MARIE, M., TOUPET, K., JORGENSEN, C. & NOEL, D. 2012. Mesenchymal stem cells: New insights into bone regenerative applications. Journal of biomaterials and tissue engineering, 2, 14-28.

DŁUGOŃ, E., NIEMIEC, W., FRĄCZEK-SZCZYPTA, A., JELEŃ, P., SITARZ, M. & BŁAŻEWICZ, M. 2014. Spectroscopic studies of electrophoretically deposited hybrid HAp/CNT coatings on titanium. Spectrochimica Acta Part A: Molecular and Biomolecular Spectroscopy, 133, 872-875.

DOMINGOS, M., INTRANUOVO, F., RUSSO, T., DE SANTIS, R., GLORIA, A., AMBROSIO, L., CIURANA, J. & BARTOLO, P. 2013. The first systematic analysis of 3D rapid prototyped poly (ε-caprolactone) scaffolds manufactured through BioCell printing: the effect of pore size and geometry on compressive mechanical behaviour and *in vitro* hMSC viability. Biofabrication, 5, 045004.

DOMINICI, M., LE BLANC, K., MUELLER, I., SLAPER-CORTENBACH, I., MARINI, F., KRAUSE, D., DEANS, R., KEATING, A., PROCKOP, D. & HORWITZ, E. 2006. Minimal criteria for defining multipotent mesenchymal stromal cells. The International Society for Cellular Therapy position statement. Journal Cytotherapy, 8, 315-317.

DRUKKER, M., KATCHMAN, H., KATZ, G., EVEN-TOV FRIEDMAN, S., SHEZEN, E., HORNSTEIN, E., MANDELBOIM, O., REISNER, Y. & BENVENISTY, N. 2006. Human embryonic stem cells and their differentiated derivatives are less susceptible to immune rejection than adult cells. Stem cells, 24, 221-229.

DRUMRIGHT, R., GRUBER, P. & HENTON, D. 2000. Polylactic acid technology. Advanced materials, 12, 1841-1846.

DUCY, P., ZHANG, R., GEOFFROY, V., RIDALL, A. & KARSENTY, G. 1997. Osf2/Cbfa1: a transcriptional activator of osteoblast differentiation. Journal of Cell Biology, 89, 747-754.

DUNN, C. A., JIN, Q., TABA, M., JR., FRANCESCHI, R. T., BRUCE RUTHERFORD, R. & GIANNOBILE, W. V. 2005. BMP gene delivery for alveolar bone engineering at dental implant defects. Molecular Therapy, 11, 294-9.

EID, K., CHEN, E., GRIFFITH, L. & GLOWACKI, J. 2001. Effect of RGD coating on osteo-compatibility of PLGA-polymer disks in a rat tibial wound. Journal of biomedical materials research, 57, 224-231.

EIJKEN, M., KOEDAM, M., VAN DRIEL, M., BUURMAN, C.J., POLS, H.A. & VAN LEEUWEN, J.P., 2006. The essential role of glucocorticoids for proper human osteoblast differentiation and matrix mineralization. Molecular and cellular endocrinology, 248(1-2), 87-93.

EINHORN, T. 1998. The cell and molecular biology of fracture healing. J Clinical Orthopaedics Related Research®

355, S7-S21.

EL HAJ, A. & CARTMELL, S., PART H: JOURNAL OF ENGINEERING IN MEDICINE 2010. Bioreactors for bone tissue engineering. 224, 1523-1532.

EL-GENDY, R. 2010. Bone tissue engineering using dental pulp stem cells. University of Leeds.

ELLURU, V. & RAMESH, D. 2012. Stem cell therapy: Dental aspects. Journal of Indian Academy in Oral Medicine Radiology, 24, 45:50.

EL-SAYED, K. 2010. Isolation and Characterization of Multipotent Postnatal Stem Cells from the Alveolar Bone and Gingival Cervical Margin. Ph.D Dissertation. School of Medicine the Christian-Albrechts-University of Kiel, 17-18.

ENGLER, A. J., SEN, S., SWEENEY, H. L. & DISCHER, D. E. 2006. Matrix elasticity directs stem cell lineage specification. Cell, 126, 677-689.

FONTANA, F, ROCCHIETTA, I, DELLAVIA, C' NEVINS, M & SIMION, M. 2008. Biocompatibility and manageability of a new fixable bone graft for the treatment of localised bone defects: preliminary study in a dog model. Int. J. Periodontics. Restorative. Dent., 28, 601-607.

FANBURG, J. C., ROSENBERG, A. E., WEAVER, D. L., LESLIE, K. O., MANN, K. G., TAATJES, D. J. & TRACY, R. P. 1997. Osteocalcin and osteonectin immunoreactivity in the diagnosis of osteosarcoma. American journal of clinical pathology, 108, 464-473.

FARAH, S., ANDERSON, D. G. & LANGER, R. 2016. Physical and mechanical properties of PLA, and their functions in widespread applications - A comprehensive review. Advanced Drug Delivery Review, 107, 367-392.

FARRÉ-GUASCH, E., WOLFF, J., HELDER, M. N., SCHULTEN, E. A., FOROUZANFAR, T. & KLEIN-NULEND, J. 2015. Application of additive manufacturing in oral and maxillofacial surgery. Journal of Oral and Maxillofacial Surgery, 73, 2408-2418.

FEDOROVICH, N. E., ALBLAS, J., DE WIJN, J. R., HENNINK, W. E., VERBOUT, A. J. & DHERT, W. J. 2007. Hydrogels as extracellular matrices for skeletal tissue engineering: state-of-the-art and novel application in organ printing. Tissue engineering, 13, 1905-1925.

FEDOROVICH, N. E., ALBLAS, J., HENNINK, W. E., ÖNER, F. C. & DHERT, W. J. 2011. Organ printing: the future of bone regeneration? Trends in biotechnology, 29, 601-606.

FERNANDEZ-YAGUE, M. A., ABBAH, S. A., MCNAMARA, L., ZEUGOLIS, D. I., PANDIT, A. & BIGGS, M. J. 2015. Biomimetic approaches in bone tissue engineering: Integrating biological and physicomechanical strategies. Advanced Drug Deliver Review, 84, 1-29.

FIRTH, A., AGGELI, A., BURKE, J. L., YANG, X. & KIRKHAM, J. 2006. Biomimetic self-assembling peptides as injectable scaffolds for hard tissue engineering.

FISHER, J. P., VEHOF, J. W., DEAN, D., VAN DER WAERDEN, J. P. C., HOLLAND, T. A., MIKOS, A. G., JANSEN, J. A. J. J. O. B. M. R. A. O. J. O. T. S. F. B., THE

JAPANESE SOCIETY FOR BIOMATERIALS,, BIOMATERIALS, T. A. S. F. & BIOMATERIALS, T. K. S. F. 2002. Soft and hard tissue response to photo-cross linked poly (propylene fumarate) scaffolds in a rabbit model. 59, 547-556.

FRATZL, P. 2003. Cellulose and collagen: from fibres to tissues. J Current opinion in colloid and interface science, 8, 32-39.

FRIEDRICHS, J. 2009. Analyzing interactions between cells and extracellular matrix by atomic force microscopy. Doctoral Dissertation. Verlag nicht ermittelbar.

FROSCH, K.-H. & STÜRMER, K. M. 2006. Metallic biomaterials in skeletal repair. European Journal of Trauma, 32, 149-159.

GAGGL, A., SCHULTES, G. & KARCHER, H. 1999a. Distraction implants: a new operative technique for alveolar ridge augmentation. Joural Craniomaxillofacial Surgery 27, 214–221.

GAGGL, A., SCHULTES, G. & KARCHER, H. 1999b. Distraction implants—a new possibility for augmentative treatment of the edentulous atrophic mandible: case report. Br J Oral Maxillofacial Surgery, 37, 481–485.

GALBAN, C. J. & LOCKE, B. R. 1999. Effects of spatial variation of cells and nutrient and product concentrations coupled with product inhibition on cell growth in a polymer scaffold. 64, 633-643.

GAZIT, E. 2007. Self-assembled peptide nanostructures: the design of molecular building blocks and their technological utilization. Chemical Society Reviews, 36, 1263-1269.

GELAIN, F., BOTTAI, D., VESCOVI, A. & ZHANG, S. 2006. Designer self-assembling peptide nanofiber scaffolds for adult mouse neural stem cell 3-dimensional cultures. PloS one, 1, e119.

GELAIN, F., HORII, A. & ZHANG, S. 2007. Designer self-assembling peptide scaffolds for 3-d tissue cell cultures and regenerative medicine. Macromol Biosci, 7, 544-51.

GERBER, H.-P. & FERRARA, N. 2000. Angiogenesis and bone growth. Trends in cardiovascular medicine, 10, 223-228.

GERSHON, D. 2003. Stem-cell research. Nature, 422, 928.

GHARAEI, R., TRONCI, G., DAVIES, R. P., GOSWAMI, P. & RUSSELL, S. J. 2016. An investigation into the nano-/micro-architecture of electro-spun poly (ε-caprolactone) and self-assembling peptide fibers. MRS Advances, 1, 711-716.

GIANNOUDIS, P. V., DINOPOULOS, H. & TSIRIDIS, E. 2005. Bone substitutes: an update. Injury, 36 Suppl 3, S20-7.

GIBSON, I. 2006. Rapid prototyping: from product development to medicine and beyond. Virtual and Physical Prototyping, 1, 31-42.

GIOVENTU, S., ANDRIOLO, G., BONINO, F., FRASCA, S., LAZZARI, L., MONTELATICI, E., SANTORO, F. & REBULLA, P. 2012. A novel method for banking dental pulp stem cells. Transfus Apher Sci, 47, 199-206.

GIULIANI, A., MANESCU, A., LANGER, M., RUSTICHELLI, F., DESIDERIO, V., PAINO, F., DE ROSA, A., LAINO, L., D'AQUINO, R. & TIRINO, V. 2013. Three years after transplants in human mandibles, histological and in-line holotomography revealed that stem cells regenerated a compact rather than a spongy bone: Biological and clinical implications. Stem cells translational medicine, 2, 316-324.

GOLDRING, C. E., DUFFY, P. A., BENVENISTY, N., ANDREWS, P. W., BEN-DAVID, U., EAKINS, R., FRENCH, N., HANLEY, N. A., KELLY, L. & KITTERINGHAM, N. R. 2011. Assessing the safety of stem cell therapeutics. Cell stem cell, 8, 618-628.

GRAZIANO, A., D'AQUINO, R., ANGELIS, M. G. C. D., DE FRANCESCO, F., GIORDANO, A., LAINO, G., PIATTELLI, A., TRAINI, T., DE ROSA, A. & PAPACCIO, G. 2008. Scaffold's surface geometry significantly affects human stem cell bone tissue engineering. Journal of cellular physiology, 214, 166-172.

GREGORY, C.A., GUNN, W.G., PEISTER, A. & PROCKOP, D.J. 2004. An Alizarin red-based assay of mineralization by adherent cells in culture: comparison with cetylpyridinium chloride extraction. Analytical biochemistry, 329(1), 77-84.

GRIFFITHL, L. & NAUGHTON, G. 2002. Tissue Engineering-Current and Challenges Expanding Opportunity. Science. 8, 295, 1009-1014.

GRONTHOS, S., BRAHIM, J., LI, W., FISHER, L., CHERMAN, N., BOYDE, A., DENBESTEN, P., ROBEY, P. G. & SHI, S. 2002. Stem cell properties of human dental pulp stem cells. 81, 531-535.

GRONTHOS, S., MANKANI, M., BRAHIM, J., ROBEY, P. G. & SHI, S. 2000. Postnatal human dental pulp stem cells (DPSCs) *in vitro* and *in vivo*. Proc Natl Acad Sci U S A, 97, 13625-30.

GROSS, B. C., ERKAL, J. L., LOCKWOOD, S. Y., CHEN, C. & SPENCE, D. M. 2014. Evaluation of 3D printing and its potential impact on biotechnology and the chemical sciences. ACS Publications.

GUGALA, Z., LINDSEY, R. W. & GOGOLEWSKI, S. 2007. New Approaches in the Treatment of Critical-Size Segmental Defects in Long Bones. Macromolecular Symposia, 253, 147-161.

GUNDBERG, C. M. 2003. Matrix proteins. Osteoporosis international, 14, 37-42.

GUNDLE, R. & BERSFORD, J.N. 1995. The Isolation and Culture of Cells from Explants of Human Trabecular Bone. Calcified Tissue Int 56, S8-S10.

GUPTA, B., REVAGADE, N. & HILBORN, J. 2007. Poly (lactic acid) fiber: an overview. Progress in polymer science, 32, 455-482.

GUTWEIN, L. G. & WEBSTER, T. J. 2004. Increased viable osteoblast density in the presence of nanophase compared to conventional alumina and titania particles. Biomaterials, 25, 4175-4183.

GUVENDIREN, M. & BURDICK, J. 2012. Stiffening hydrogels to probe short-and long-term cellular responses to dynamic mechanics. 3, 792.

HALLMAN, M., LUNDGREN, S. & SENNERBY, L. 2001. Histologic analysis of clinical biopsies taken 6 months and 3 years after maxillary sinus floor augmentation with 80% bovine hidroxyapatite and 20% autogenous bone mixed with fibren glue. Clinical Implantology Dentistry Related Research. 3, 87-96

HARATIZADEH, S., NAZM BOJNORDI, M., DARABI, S., KARIMI, N., NAGHIKHANI, M., GHASEMI HAMIDABADI, H. & SEIFI, M. 2017. Condition medium of cerebrospinal fluid and retinoic acid induces the trans-differentiation of human

dental pulp stem cells into neuroglia and neural like cells. Anatomy & cell biology, 50, 107-114.

HARDWICK, R., HAYES, B. & FLYNN, C. 1995. Devices for dentoalveolar regeneration: an up-to-date literature review.. Journal Periodontology 66, 495-505.

HARRISON, C. & ALLEN, T. J. D. 1979. Cell surface morphology after trypsinisation depends on initial cell shape. 15, 61-66.

HASEGAWA, S., NEO, M., TAMURA, J., FUJIBAYASHI, S., TAKEMOTO, M., SHIKINAMI, Y., OKAZAKI, K. & NAKAMURA, T. 2007. *In vivo* evaluation of a porous hydroxyapatite/poly-DL-lactide composite for bone tissue engineering. J Biomed Mater Res A, 81, 930-8.

HAUSCHKA, P., FRENKEL, J., DEMUTH, R. & GUNDBERG, C. J. J. O. B. C. 1983. Presence of osteocalcin and related higher molecular weight 4-carboxyglutamic acid-containing proteins in developing bone. 258, 176-182.

HAUSCHKA, P. V., LIAN, J. B., COLE, D. & GUNDBERG, C. M. 1989. Osteocalcin and matrix Gla protein: vitamin K-dependent proteins in bone. Physiological reviews, 69, 990-1047.

HEGAB AF, S. M. 2012. Distraction Osteogenesis of the Maxillofacial Skeleton: Biomechanics and Clinical Implications. Dentistry, 01, 509.

HEMATTI, P. J. C. 2012. Mesenchymal stromal cells and fibroblasts: a case of mistaken identity? 14, 516-521.

HEO, D. N., CASTRO, N. J., LEE, S. J., NOH, H., ZHU, W. & ZHANG, L. G. 2017. Enhanced bone tissue regeneration using a 3D printed microstructure incorporated with a hybrid nano hydrogel. Nanoscale, 9, 5055-5062.

HIDDING, F., LAZAR, J. & ZÖLLER, E. 1999. Initial outcome of vertical distraction osteogenesis of the atrophic alveolar ridge. Mund-, Kiefer-und Gesichtschirurgie: MKG, 3, S79-83. [Suppl 1], S79–S83.

HILKENS, P., GERVOIS, P., FANTON, Y., VANORMELINGEN, J., MARTENS, W., STRUYS, T., POLITIS, C., LAMBRICHTS, I. & BRONCKAERS, A. 2013. Effect

of isolation methodology on stem cell properties and multilineage differentiation potential of human dental pulp stem cells. Cell Tissue Res, 353, 65-78.

HILL, C. 2013. Adult Permanent (Extracted) Teeth as a Source of Dental Pulp-Derived Mesenchymal Stem Cells (DPSC): A Pilot Study. Master of Science - Oral Biology, University of Nevada, Las Vegas.

HO, M., HOU, L., TU, C., HSIEH, H., LAI, J., CHEN, W. & WANG, D. 2006. Promotion of cell affinity of porous PLLA scaffolds by immobilization of RGD peptides via plasma treatment. J Macromolecular bioscience, 6, 90-98.

HOEMANN, C.D., EL-GABALAWY, H. & MCKEE, M.D., 2009. *In vitro* osteogenesis assays: influence of the primary cell source on alkaline phosphatase activity and mineralization. Pathologie Biologie, 57(4), 318-323.

HOLMES, B., ZHU, W., LI, J., LEE, J. D. & ZHANG, L. G. 2015. Development of novel three-dimensional printed scaffolds for osteochondral regeneration. Tissue Engineering Part A, 21, 403-15.

HORII, A., WANG, X., GELAIN, F. & ZHANG, S. 2007. Biological designer self-assembling peptide nanofiber scaffolds significantly enhance osteoblast proliferation, differentiation and 3-D migration. PloS one, 2, e190.

HOSSEINKHANI, H., HOSSEINKHANI, M., TIAN, F., KOBAYASHI, H. & TABATA, Y. 2006. Osteogenic differentiation of mesenchymal stem cells in self-assembled peptide-amphiphile nanofibers. Biomaterials, 27, 4079-4086.

HUANG, A. H. C., CHEN, Y. K., LIN, L. M., SHIEH, T. Y. & CHAN, A. W. S. 2008. Isolation and characterization of dental pulp stem cells from a supernumerary tooth. Journal of Oral Pathology & Medicine, 37, 571-574.

HUANG, G.-J., GRONTHOS, S. & SHI, S. 2009. Mesenchymal stem cells derived from dental tissues vs. those from other sources: their biology and role in regenerative medicine. 88, 792-806.

HUANG, G. T.-J., SONOYAMA, W., CHEN, J. & PARK, S. H. 2006. *In vitro* characterization of human dental pulp cells: various isolation methods and culturing environments. Cell and tissue research, 324, 225.

HUEBSCH, N., ARANY, P. R., MAO, A. S., SHVARTSMAN, D., ALI, O. A., BENCHERIF, S. A., RIVERA-FELICIANO, J. & MOONEY, D. J. 2010. Harnessing traction-mediated manipulation of the cell/matrix interface to control stem-cell fate. Nature materials, 9, 518.

HUGHES, D. & MEHMET, H. 2003. Cell proliferation and apoptosis, Taylor & Francis.

HUGHES, F. J., TURNER, W., BELIBASAKIS, G. & MARTUSCELLI, G. 2006. Effects of growth factors and cytokines on osteoblast differentiation. Periodontology 2000, 41, 48-72.

HUNTER, G. K. & GOLDBERG, H. 1993. Nucleation of hydroxyapatite by bone sialoprotein. 90, 8562-8565.

HUTMACHER, D. W., SCHANTZ, T., ZEIN, I., NG, K. W., TEOH, S. H. & TAN, K. C. 2001. Mechanical properties and cell cultural response of polycaprolactone scaffolds designed and fabricated via fused deposition modelling. Journal of Biomedical Materials Research: An Official Journal of the Society for Biomaterials, the Japanese Society for Biomaterials, and The Australian Society for Biomaterials and the Korean Society for Biomaterials, 55, 203-216.

IKADA, Y. 2006. Challenges in tissue engineering. J R Soc Interface, 3, 589-601.

IM, G.-I., SHIN, Y.-W. & LEE, K.-B. 2005. Do adipose tissue-derived mesenchymal stem cells have the same osteogenic and chondrogenic potential as bone marrow-derived cells? Osteoarthritis and cartilage, 13, 845-853.

IMPENS, S., CHEN, Y., MULLENS, S., LUYTEN, F. & SCHROOTEN, J. J. T. E. P. C. M. 2010. Controlled cell-seeding methodologies: a first step toward clinically relevant bone tissue engineering strategies. 16, 1575-1583.

ISHAUG, S. L., CRANE, G. M., MILLER, M. J., YASKO, A. W., YASZEMSKI, M. J., MIKOS, A. G. & BIOMATERIALS, T. J. S. F. 1997. Bone formation by three-dimensional stromal osteoblast culture in biodegradable polymer scaffolds. J Journal of Biomedical Materials Research: An Official Journal of the Society for Biomaterials, 36, 17-28.

ISHAUG-RILEY, S. L., CRANE-KRUGER, G. M., YASZEMSKI, M. J. & MIKOS, A. G. 1998. Three-dimensional culture of rat calvarial osteoblasts in porous biodegradable polymers. Biomaterials, 19, 1405-1412.

ISHIDA, Y. & HEERSCHE, J.N., 1998. Glucocorticoid-induced osteoporosis: both *in vivo* and *in vitro* concentrations of glucocorticoids higher than physiological levels attenuate osteoblast differentiation. Journal of Bone and Mineral Research, 13(12), 1822-1826.

ITAYA, T., KAGAMI, H., OKADA, K., YAMAWAKI, A., NARITA, Y., INOUE, M., SUMITA, Y. AND UEDA, M., 2009. Characteristic changes of periodontal ligament-derived cells during passage. Journal of periodontal research, 44(4), pp.425-433.

ITO, K., YAMADA, Y., NAKAMURA, S. & UEDA, M. 2011. Osteogenic Potential of Effective Bone Engineering Using Dental Pulp Stem Cells, Bone Marrow Stem Cells, and Periosteal Cells for Osseointegration of Dental Implants. INT J ORAL MAXILLOFAC IMPLANTS, 26, 947–954.

IWATA, T., YAMATO, M., ZHANG, Z., MUKOBATA, S., WASHIO, K., ANDO, T., FEIJEN, J., OKANO, T. & ISHIKAWA, I., 2010. Validation of human periodontal ligament-derived cells as a reliable source for cytotherapeutic use. Journal of Clinical Periodontology, 37(12), pp.1088-1099.

JABLONSKI-MOMENI, A., KORBMACHER-STEINER, H., HEINZEL-GUTENBRUNNER, M., JABLONSKI, B., JAQUET, W. & BOTTENBERG, P. 2019. Randomised in situ clinical trial investigating self-assembling peptide matrix P11-4 in the prevention of artificial caries lesions. Scientific reports, 9, 269.

JACKSON, S. 1957. The fine structure of developing bone in the embryonic fowl. 146, 270-280.

JACOBS, T., MORENT, R., DE GEYTER, N., DUBRUEL, P. & LEYS, C. 2012. Plasma surface modification of biomedical polymers: influence on cell-material interaction. Plasma Chemistry and Plasma Processing, 32, 1039-1073.

JAHAN-TIGH, R. R., RYAN, C., OBERMOSER, G. & SCHWARZENBERGER, K. J. T. J. O. I. D. 2012. Flow cytometry. 132, e1.

JI, J., SUN, W., WANG, W., MUNYOMBWE, T. & YANG, X. 2014. The effect of mechanical loading on osteogenesis of human dental pulp stromal cells in a novel *in vitro* model. J Cell tissue research, 358, 123-133.

JO, Y.-Y., LEE, H.-J., KOOK, S.-Y., CHOUNG, H.-W., PARK, J.-Y., CHUNG, J.-H., CHOUNG, Y.-H., KIM, E.-S., YANG, H.-C. & CHOUNG, P.-H. 2007. Isolation and characterization of postnatal stem cells from human dental tissues. Tissue engineering, 13, 767-773.

JOHNSTONE, B., HERING, T. M., CAPLAN, A. I., GOLDBERG, V. M. & YOO, J. U. 1998. *In vitro* chondrogenesis of bone marrow-derived mesenchymal progenitor cells. Experimental cell research, 238, 265-272.

JONES, E. & YANG, X. 2011. Mesenchymal stem cells and bone regeneration: current status. Injury, 42, 562-568.

JØRGENSEN, N.R., HENRIKSEN, Z., SØRENSEN, O.H. & CIVITELLI, R., 2004. Dexamethasone, BMP-2, and 1, 25-dihydroxyvitamin D enhance a more differentiated osteoblast phenotype: validation of an *in vitro* model for human bone marrow-derived primary osteoblasts. Steroids, 69(4), 219-226.

JUNQUEIRA, L. C., CARNEIRO, J. & KELLEY, R. O. 2003. Basic histology: text & atlas, McGraw-Hill New York.

JUNQUEIRA, L. C. & MESCHER, A. L. 2013. Junqueira's basic histology: text & atlas/Anthony L. Mescher, New York [etc.]: McGraw-Hill Medical.

KALFAS, I. H. 2001. Principles of bone healing. Neurosurgical focus, 10, 1-4.

KANG, I., LEE, B.-C., CHOI, S. W., LEE, J. Y., KIM, J.-J., KIM, B.-E., KIM, D.-H., LEE, S. E., SHIN, N. & SEO, Y. 2018. Donor-dependent variation of human umbilical cord blood mesenchymal stem cells in response to hypoxic preconditioning and amelioration of limb ischemia. Experimental & molecular medicine, 50, 35.

KARAGEORGIOU, V. & KAPLAN, D. J. B. 2005. Porosity of 3D biomaterial scaffolds and osteogenesis. 26, 5474-5491.

KAWASHIMA, N. 2012. Characterisation of dental pulp stem cells: a new horizon for tissue regeneration? Archive of Oral Biology, 57, 1439-58.

KE, T., SUN, S. X. & SEIB, P. 2003. Blending of poly (lactic acid) and starches containing varying amylose content. Journal of applied polymer science, 89, 3639-3646.

KEYHAN, S., GHANEAN, S., NAVABAZAM, A., KHOJASTEH, A. & IRANAQ, M. 2016. Three-dimensional printing: a novel technology for use in oral and maxillofacial operations. A Textbook of Advanced Oral and Maxillofacial Surgery Volume 3. IntechOpen.

KHAJEH, S., RAZBAN, V., TALAEI-KHOZANI, T., SOLEIMANI, M., ASADI-GOLSHAN, R., DEHGHANI, F., RAMEZANI, A. & MOSTAFAVI-POUR, Z. 2018. Enhanced chondrogenic differentiation of dental pulp-derived mesenchymal stem cells in 3D pellet culture system: effect of mimicking hypoxia. Biologia, 73, 715-726.

KHANNA-JAIN, R. 2012. Growth and Differentiation of Human Dental Pulp Stem Cells Maintained in Fetal Bovine Serum, Human Serum and Serum-free/Xeno-free Culture Media. Journal of Stem Cell Research & Therapy. 02(04).

KHANNA-JAIN, R., VUORINEN, A., SÁNDOR, G.K., SUURONEN, R. & MIETTINEN, S., 2010. Vitamin D3 metabolites induce osteogenic differentiation in human dental pulp and human dental follicle cells. The Journal of steroid biochemistry and molecular biology, 122(4), 133-141.

KILBORN, S. H., TRUDEL, G. & UHTHOFF, H. 2002. Review of growth plate closure compared with age at sexual maturity and lifespan in laboratory animals. Journal of the American Association for Laboratory Animal Science, 41, 21-26.

KIM, D.-H., BEEBE, D. J. & LEVCHENKO, A. 2011. Micro-and nanoengineering for stem cell biology: the promise with a caution. Trends in biotechnology, 29, 399-408.

KIM, D.-H., PROVENZANO, P. P., SMITH, C. L. & LEVCHENKO, A. 2012. Matrix nano-topography as a regulator of cell function. Journal of Cell Biology, 197, 351-360.

KIM, H. J. & PARK, J.-S. 2017. Usage of human mesenchymal stem cells in cell-based therapy: advantages and disadvantages. J Development reproduction, 21, 1.

KIM, H. W., LEE, E. J., JUN, I. K., KIM, H. E. & KNOWLES, J. C. 2005. Degradation and drug release of phosphate glass/polycaprolactone biological composites for hard-tissue regeneration. Journal of Biomedical Materials Research Part B: Applied Biomaterials, 75, 34-41.

KIM, J. M., KIM, J., KIM, Y. H., KIM, K. T., RYU, S. H., LEE, T. G. & SUH, P. G. 2013. Comparative secretome analysis of human bone marrow-derived mesenchymal stem cells during osteogenesis. Journal of cellular physiology, 228, 216-224.

KIM, M., ERICKSON, I. E., HUANG, A. H., GARRITY, S. T., MAUCK, R. L. & STEINBERG, D. R. 2018. Donor variation and optimization of human mesenchymal stem cell chondrogenesis in hyaluronic acid. Tissue Engineering Part A, 24, 1693-1703.

KIRKHAM, J., FIRTH, A., VERNALS, D., BODEN, N., ROBINSON, C., SHORE, R., BROOKES, S. & AGGELI, A. 2007. Self-assembling peptide scaffolds promote enamel remineralization. Journal of dental research, 86, 426-430.

KLEIN, G. T., LU, Y. & WANG, M. Y. 2013. 3D printing and neurosurgery—ready for prime time? World neurosurgery, 80, 233-235.

KLEINMAN, H. K., PHILP, D. & HOFFMAN, M. P. 2003. Role of the extracellular matrix in morphogenesis. Current Opinion in Biotechnology, 14, 526-532.

KNYCHALA, J., BOUROPOULOS, N., CATT, C., KATSAMENIS, O., PLEASE, C. & SENGERS, B. J. A. O. B. E. 2013. Pore geometry regulates early stage human bone marrow cell tissue formation and organisation. 41, 917-930.

KOCH, F., MÜLLER, M., KÖNIG, F., MEYER, N., GATTLEN, J., PIELES, U., PETERS, K., KREIKEMEYER, B., MATHES, S. & SAXER, S. 2018. Mechanical characteristics of beta sheet-forming peptide hydrogels are dependent on peptide sequence, concentration and buffer composition. Royal Society open science, 5, 171562.

KOMMAREDDY, K. P., LANGE, C., RUMPLER, M., DUNLOP, J. W., MANJUBALA, I., CUI, J., KRATZ, K., LENDLEIN, A. & FRATZL, P. J. B. 2010. Two stages in three-dimensional *in vitro* growth of tissue generated by osteoblast-like cells. 5, 45-52.

KOYAMA, N., OKUBO, Y., NAKAO, K. & BESSHO, K. 2009. Evaluation of pluripotency in human dental pulp cells. Journal of Oral and Maxillofacial Surgery, 67, 501-506.

KRETLOW, J. D., JIN, Y.-Q., LIU, W., ZHANG, W. J., HONG, T.-H., ZHOU, G., BAGGETT, L. S., MIKOS, A. G. & CAO, Y. 2008. Donor age and cell passage affects differentiation potential of murine bone marrow-derived stem cells. BMC cell biology, 9, 60.

KRETLOW, J. D., YOUNG, S., KLOUDA, L., WONG, M. & MIKOS, A. G. 2009. Injectable biomaterials for regenerating complex craniofacial tissues. Adv Mater, 21, 3368-93.

KRETSINGER, J. K., HAINES, L. A., OZBAS, B., POCHAN, D. J. & SCHNEIDER, J. P. 2005. Cytocompatibility of self-assembled β-hairpin peptide hydrogel surfaces. Biomaterials, 26, 5177-5186.

KUBO, Y., KAIDZU, S., NAKAJIMA, I., TAKENOUCHI, K. & NAKAMURA, F. 2000. Organization of extracellular matrix components during differentiation of adipocytes in long-term culture. *In vitro* Cellular & Developmental Biology-Animal, 36, 38-44.

KYLE, S., FELTON, S. H., MCPHERSON, M. J., AGGELI, A. & INGHAM, E. 2012. Rational Molecular Design of Complementary Self-Assembling Peptide Hydrogels. Advanced healthcare materials, 1, 640-645.

LA NOCE, M., PAINO, F., SPINA, A., NADDEO, P., MONTELLA, R., DESIDERIO, V., DE ROSA, A., PAPACCIO, G., TIRINO, V. & LAINO, L. 2014. Dental pulp stem cells: state of the art and suggestions for a true translation of research into therapy. J Journal of dentistry, 42, 761-768.

LAINO, G., GRAZIANO, A., D'AQUINO, R., PIROZZI, G., LANZA, V., VALIANTE, S., DE ROSA, A., NARO, F., VIVARELLI, E. & PAPACCIO, G. 2006. An approachable human adult stem cell source for hard-tissue engineering. J Cell Physiology, 206, 693-701.

LANGENBACH, F. & HANDSCHEL, J. 2013. Effects of dexamethasone, ascorbic acid and β-glycerophosphate on the osteogenic differentiation of stem cells *in vitro*. Stem cell research & therapy, 4, 117.

LANGER, R. & VACANTI, J. P. 1993. R tic l e. Science, 260, 14.

LANZA, R., LANGER, R. & VACANTI, J. P. 2011. Principles of tissue engineering, Academic press.

LATINOAMERICANO, P. R. E. 2010. Chondrogenic Differentiation of Bone Marrow Mesenchymal Stem Cells. First Successful Latin-American Report. Int. J. Morphology, 28, 749-754.

LAWLOR, L. M. 2016. The Effect of HDAC Inhibitor MI192 on Stem Cell Behaviour-The Potential of Utilising MI192 for Bone Tissue Engineering. University of Leeds.

LAWRENCE, B. J. & MADIHALLY, S. V. 2008. Cell colonization in degradable 3D porous matrices. Cell adhesion & migration, 2, 9-16.

LEE, J., CUDDIHY, M. J. & KOTOV, N. 2008. Three-dimensional cell culture matrices: state of the art. 14, 61-86.

LEE, J. S., CHA, H. D., SHIM, J. H., JUNG, J. W., KIM, J. Y. & CHO, D. W. 2012. Effect of pore architecture and stacking direction on mechanical properties of solid freeform fabrication-based scaffold for bone tissue engineering. Journal of Biomedical Materials Research Part A, 100, 1846-1853.

LEE, M., DUNN, J. C. & WU, B. M. 2005 a. Scaffold fabrication by indirect three-dimensional printing. Biomaterials, 26, 4281-4289.

LEE, S., AN, S., KANG, T. H., KIM, K. H., CHANG, N. H., KANG, S., KWAK, C. K. & PARK, H.-S. 2011. Comparison of mesenchymal-like stem/progenitor cells derived from supernumerary teeth with stem cells from human exfoliated deciduous teeth. Regenerative medicine, 6, 689-699.

LEE, S. B., KIM, Y. H., CHONG, M. S., HONG, S. H. & LEE, Y. M. 2005 b. Study of gelatin-containing artificial skin V: fabrication of gelatin scaffolds using a salt-leaching method. Biomaterials, 26, 1961-1968.

LEGEROS, R. Z. 2002. Properties of osteoconductive biomaterials: calcium phosphates. Clinical orthopaedics and related research, 395, 81-98.

LEVI, B. & LONGAKER, M. T. 2011. Concise review: adipose-derived stromal cells for skeletal regenerative medicine. Stem cells, 29, 576-582.

LI, J., HSU, Y., LUO, E., KHADKA, A. & HU, J. 2011. Computer-aided design and manufacturing and rapid prototyped nanoscale hydroxyapatite/polyamide (n-HA/PA) construction for condylar defect caused by mandibular angle ostectomy. Aesthetic plastic surgery, 35, 636-640.

LI, J. J., KAPLAN, D. L. & ZREIQAT, H. 2014. Scaffold-based regeneration of skeletal tissues to meet clinical challenges. J. Mater. Chem. B, 2, 7272-7306.

LIAO, S., CUI, F., ZHANG, W. & FENG, Q. 2004. Hierarchically biomimetic bone scaffold materials: nano-HA/collagen/PLA composite. Journal of Biomedical Materials Research Part B: Applied Biomaterials: An Official Journal of The Society for Biomaterials, The Japanese Society for Biomaterials, and The Australian Society for Biomaterials and the Korean Society for Biomaterials, 69, 158-165.

LIN, K., WU, C. & CHANG, J. 2014. Advances in synthesis of calcium phosphate crystals with controlled size and shape. J Acta biomaterialia, 10, 4071-4102.

LIU, C. Z., XIA, Z. D., HAN, Z. W., HULLEY, P. A., TRIFFITT, J. T. & CZERNUSZKA, J. T. 2008. Novel 3D collagen scaffolds fabricated by indirect printing technique for tissue engineering. Journal of Biomedical Material Research B Applied Biomaterls, 85, 519-28.

LIU, H, WANG, D. S., SU, F., WU, X., SHI, Z. P., LV, Y. & WANG, J. Z. 2011. Reconstruction of alveolar bone defects using bone morphogenetic protein 2 mediated rabbit dental pulp stem cells seeded on nano-hydroxyapatite/collagen/poly(L-lactide). Tissue Engineering Part A, 17, 2417-33.

LIU, X. & MA, P. 2004. Polymeric scaffolds for bone tissue engineering. Annals of biomedical engineering, 32, 477-486.

LIU, Y., LIM, J. & TEOH, S. H. 2013. Review: development of clinically relevant scaffolds for vascularised bone tissue engineering. Biotechnology Advances, 31, 688-705.

LIU, Y. & TANG, S. C. 2016. Recent progress in stem cell therapy for diabetic nephropathy. Kidney Diseases, 2, 20-27.

LOH, Q. L. & CHOONG, C. 2013. Three-dimensional scaffolds for tissue engineering applications: role of porosity and pore size. Tissue Engineering Part B Rev, 19, 485-502.

LOPES, M. S., JARDINI, A. & MACIEL FILHO, R. 2012. Poly (lactic acid) production for tissue engineering applications. Procedia Engineering, 42, 1402-1413.

LOPEZ-CAZAUX, S., BLUTEAU, G., MAGNE, D., LIEUBEAU, B., GUICHEUX, J. & ALLIOT-LICHT, B. 2006. Culture medium modulates the behaviour of human dental pulp-derived cells. Eur Cell Mater, 11, 35-42.

LV, F., TUAN, R. S., CHEUNG, K. M. & LEUNG, V. Y. J. S. C. 2014. Concise review: the surface markers and identity of human mesenchymal stem cells. 32, 1408-1419.

MA, H., DAVIS, R. H. & BOWMAN, C. N. 2000. A novel sequential photoinduced living graft polymerization. Macromolecules, 33, 331-335.

MA, J. L., PAN, J. L., TAN, B. S. & CUI, F. Z. 2009. Determination of critical size defect of minipig mandible. J Tissue Engineering and Regenerative Medicine, 3, 615-22.

MA, P. 2004. Scaffolds for tissue fabrication. Materials today, 7, 30-40.

MACHADO, E., FERNANDES, M. H. & DE SOUSA GOMES, P. 2012. Dental stem cells for craniofacial tissue engineering. Oral surgery, oral medicine, oral pathology and oral radiology, 113, 728-733.

MAHAJAN, A., KASHYAP, D., SINGH, B., KUMAR, A. & POONAM 2013. Scope of distraction osteogenesis in dentistry – a mini review. Journal of Regenerative Medicine and Tissue Engineering, 2, 3.

MANGANO, C., DE ROSA, A., DESIDERIO, V., D'AQUINO, R., PIATTELLI, A., DE FRANCESCO, F., TIRINO, V., MANGANO, F. & PAPACCIO, G. 2010. The osteoblastic differentiation of dental pulp stem cells and bone formation on different titanium surface textures. Biomaterials, 31, 3543-3551.

MAO, A. S., SHIN, J.-W. & MOONEY, D. J. 2016. Effects of substrate stiffness and cell-cell contact on mesenchymal stem cell differentiation. Biomaterials, 98, 184-191.

MARKS, J., C, S., POPOFF, S. N. & ANATOMY, J. A. J. O. 1988. Bone cell biology: the regulation of development, structure, and function in the skeleton. 183, 1-44.

MARQUEZ-CURTIS, L. A., JANOWSKA-WIECZOREK, A., MCGANN, L. E. & ELLIOTT, J. A. 2015. Mesenchymal stromal cells derived from various tissues: biological, clinical and cryopreservation aspects. J Cryobiology, 71, 181-197.

MARRO, A., BANDUKWALA, T. & MAK, W. 2016. Three-dimensional printing and medical imaging: a review of the methods and applications. Current problems in diagnostic radiology, 45, 2-9.

MARTIN, I., WENDT, D. & HEBERER, M. 2004. The role of bioreactors in tissue engineering. Trends Biotechnology, 22, 80-6.

MARTINE, L. C., HOLZAPFEL, B. M., MCGOVERN, J. A., WAGNER, F., QUENT, V. M., HESAMI, P., WUNNER, F. M., VAQUETTE, C., DE-JUAN-PARDO, E. M. & BROWN, T. D. J. N. P. 2017. Engineering a humanized bone organ model in mice to study bone metastases. 12, 639.

MASSON, J.-D., THIBAUDON, M., BÉLEC, L. & CRÉPEAUX, G. 2017. Calcium phosphate: a substitute for aluminum adjuvants? J Expert review of vaccines, 16, 289-299.

MATHOULIN, C., GRAS, M. & ROUKOS, S. 2010. Vascularized bone grafting from the volar distal radius for carpal bones reconstruction. 29, S65-76.

MAUDE, S., INGHAM, E. & AGGELI, A. 2013. Biomimetic self-assembling peptides as scaffolds for soft tissue engineering. Nanomedicine, 8, 823-847.

MCCAULEY, L. K. & SOMERMAN, M. J. 2012. Mineralized tissues in oral and craniofacial science: biological principles and clinical correlates, John Wiley & Sons.

MCGOVERN, J. A., GRIFFIN, M., HUTMACHER, D. & MECHANISMS 2018. Animal models for bone tissue engineering and modelling disease. 11, dmm033084.

MCKIBBIN, B. 1978. The biology of fracture healing in long bones. The Journal of bone joint surgery. British volume, 60, 150-162.

MEHRA, P., MINER, J., D'INNOCENZO, R. & NADERSHAH, M. 2011. Use of 3-d stereolithographic models in oral and maxillofacial surgery. Journal of maxillofacial and oral surgery, 10, 6-13.

MELCHELS, F. P., BARRADAS, A. M., VAN BLITTERSWIJK, C. A., DE BOER, J., FEIJEN, J. & GRIJPMA, D. W. J. A. B. 2010. Effects of the architecture of tissue engineering scaffolds on cell seeding and culturing. 6, 4208-4217.

MELCHELS, F. P., FEIJEN, J. & GRIJPMA, D. W. 2009. A poly (D, L-lactide) resin for the preparation of tissue engineering scaffolds by stereolithography. Biomaterials, 30, 3801-3809.

MIAO, X. & SUN, D. 2010. Graded/gradient porous biomaterials. Materials, 3, 26-47.

MIKOS, A. G., SARAKINOS, G., LYMAN, M. D., INGBER, D. E., VACANTI, J. P. & LANGER, R. 1993. Pre-vascularization of porous biodegradable polymers. Biotechnology and Bioengineering, 42, 716-723.

MIKOS, A. G. & TEMENOFF, J. S. 2000. Formation of highly porous biodegradable scaffolds for tissue engineering. Electronic Journal of Biotechnology, 3, 23-24.

MIURA, M., GRONTHOS, S., ZHAO, M., LU, B., FISHER, L. W., ROBEY, P. G. & SHI, S. 2003. SHED: stem cells from human exfoliated deciduous teeth. Proceedings of the National Academy of Sciences, 100, 5807-5812.

MIYAGI, S. P. H., KERKIS, I., DA COSTA MARANDUBA, C. M., GOMES, C. M., MARTINS, M. D. & MARQUES, M. M. 2010. Expression of extracellular matrix proteins in human dental pulp stem cells depends on the donor tooth conditions. Journal of endodontics, 36, 826-831.

MOBINI, S. & AYOUB, A. 2016. Bone Tissue Engineering in the Maxillofacial Region: The State-of-the-Art Practice and Future Prospects. Regeneration, Reconstruction & Restoration, 1, 8.

MODJARRAD, K. & EBNESAJJAD, S. 2013. Handbook of Polymer Applications in Medicine and Medical Devices, Elsevier.

MOHAMED-AHMED, S., FRISTAD, I., LIE, S. A., SULIMAN, S., MUSTAFA, K., VINDENES, H. & IDRIS, S. B. 2018. Adipose-derived and bone marrow mesenchymal stem cells: a donor-matched comparison. Stem cell research & therapy, 9, 168.

MONTEIRO, J., DAY, P., DUGGAL, M., MORGAN, C. & RODD, H. 2009. Pulpal status of human primary teeth with physiological root resorption. International journal of paediatric dentistry, 19, 16-25.

MORAD, G., KHEIRI, L. & KHOJASTEH, A. 2013. Dental pulp stem cells for *in vivo* bone regeneration: a systematic review of literature. Archive of Oral Biology, 58, 1818-27.

MOR-YOSSEF MOLDOVAN, L., LUSTIG, M., NAFTALY, A., MARDAMSHINA, M., GEIGER, T., GEFEN, A. & BENAYAHU, D. 2019. Cell shape alteration during adipogenesis is associated with coordinated matrix cues. J Journal of cellular physiology, 234, 3850-3863.

NAKAHARA, H., MISAWA, H., YOSHIDA, A., HAYASHI, T., TANAKA, M., FURUMATSU, T., TANAKA, N., KOBAYASHI, N. & OZAKI, T. 2010. Bone repair using a hybrid scaffold of self-assembling peptide PuraMatrix and polyetheretherketone cage in rats. Cell transplantation, 19, 791-797.

NAKAJIMA, K., KUNIMATSU, R., ANDO, K., ANDO, T., HAYASHI, Y., KIHARA, T., HIRAKI, T., TSUKA, Y., ABE, T. & KAKU, M. 2018. Comparison of the bone regeneration ability between stem cells from human exfoliated deciduous teeth, human dental pulp stem cells and human bone marrow mesenchymal stem cells. J Biochemical biophysical research communications, 497, 876-882.

NANCI, A. 2017. Ten Cate's Oral Histology-E-Book: Development, Structure, and Function, Elsevier Health Sciences.

NEUMANN, A. A. K., K. 2009. Biomaterials for craniofacial reconstruction. GMS Current Topics in Otorhinolaryngology - Head and Neck Surgery. 8, 1-17.

NEWTON, P., STAINES, K. A., SPEVAK, L., BOSKEY, A., TEIXEIRA, C., MACRAE, V., CANFIELD, A. & FARQUHARSON, C. 2012. Chondrogenic ATDC5 cells: An optimised model for rapid and physiological matrix mineralisation. 30, 1187-1193.

NIEMEYER, P., FECHNER, K., MILZ, S., RICHTER, W., SUEDKAMP, N. P., MEHLHORN, A. T., PEARCE, S. & KASTEN, P. 2010. Comparison of mesenchymal stem cells from bone marrow and adipose tissue for bone regeneration in a critical size defect of the sheep tibia and the influence of platelet-rich plasma. Biomaterials, 31, 3572-3579.

NISBET, D. R. & WILLIAMS, R. 2012. Self-assembled peptides: characterisation and *in vivo* response. 7, 2.

NISHI, M., MATSUMOTO, R., DONG, J. & UEMURA, T. 2012. Effects of implantation of three-dimensional engineered bone tissue with a vascular-like structure on repair of bone defects. Applied Surface Science, 262, 60-63.

NOVOSEL, E. C., KLEINHANS, C. & KLUGER, P. J. 2011. Vascularization is the key challenge in tissue engineering. Advanced Drug Delivery Review, 63, 300-11.

NUTI, N., CORALLO, C., CHAN, B., FERRARI, M., GERAMI-NAINI, B. & REPORTS 2016. Multipotent differentiation of human dental pulp stem cells: a literature review. J Stem Cell Reviews, 12, 511-523.

NUTTELMAN, C. R., TRIPODI, M. C. & ANSETH, K. S. 2004. *In vitro* osteogenic differentiation of human mesenchymal stem cells photo-encapsulated in PEG hydrogels. Journal of biomedical materials research Part A, 68, 773-782.

NUTTELMAN, C. R., TRIPODI, M. C. & ANSETH, K. S. 2005. Synthetic hydrogel niches that promote hMSC viability. Matrix biology, 24, 208-218.

OGDEN, K., ORDWAY, N., DIALLO, D., TILLAPAUGH-FAY, G. & ASLAN, C. Dimensional accuracy of 3D printed vertebra. Medical Imaging 2014: Image-Guided Procedures, Robotic Interventions, and Modelling, 2014. International Society for Optics and Photonics, 903629.

OH, I.-H., NOMURA, N., MASAHASHI, N. & HANADA, S. 2003. Mechanical properties of porous titanium compacts prepared by powder sintering. Scripta Materialia, 49, 1197-1202.

OH, S., BRAMMER, K. S., LI, Y. J., TENG, D., ENGLER, A. J., CHIEN, S. & JIN, S. 2009. Stem cell fate dictated solely by altered nanotube dimension. Proceedings of the National Academy of Sciences, 106, 2130-2135.

OKADA, M. & MATSUMOTO, T. 2015. Synthesis and modification of apatite nanoparticles for use in dental and medical applications. J Japanese Dental Science Review, 51, 85-95.

OLIVEIRA, P. T. D., ZALZAL, S. F., IRIE, K. & NANCI, A. 2003. Early expression of bone matrix proteins in osteogenic cell cultures. Journal of Histochemistry & Cytochemistry, 51, 633-641.

OLTRAMARI, P. V., DE LIMA NAVARRO, R., HENRIQUES, J. F., TAGA, R., CESTARI, T. M., CEOLIN, D. S., JANSON, G. & GRANJEIRO, J. M. 2007. Orthodontic movement in bone defects filled with xenogenic graft: an experimental study in minipigs. American Journal of Orthodontics and Dentofacial Orthopaedics, 131, 302 e10-7.

ORBAY, H., TOBITA, M. & MIZUNO, H. 2012. Mesenchymal stem cells isolated from adipose and other tissues: basic biological properties and clinical applications. Stem cells international, 2012.

OVCHINNIKOV, D. 2009. Alcian blue/alizarin red staining of cartilage and bone in mouse. Cold Spring Harbor Protocols, 2009, pdb. prot5170.

PAMPHILON, D., SELOGIE, E., MCKENNA, D., CANCELAS-PERES, J. A., SZCZEPIORKOWSKI, Z. M., SACHER, R., MCMANNIS, J., EICHLER, H., GARRITSEN, H. & TAKANASHI, M. J. C. 2013. Current practices and prospects for standardization of the hematopoietic colony-forming unit assay: a report by the cellular therapy team of the Biomedical Excellence for Safer Transfusion (BEST) Collaborative. 15, 255-262.

PARK, J.-S., KIM, H.-Y., KIM, H.-W., CHAE, G.-N., OH, H.-T., PARK, J.-Y., SHIM, H., SEO, M., SHIN, E.-Y. & KIM, E.-G. 2005. Increased caveolin-1, a cause for the

declined adipogenic potential of senescent human mesenchymal stem cells. Mechanisms of ageing and development, 126, 551-559.

PARTRIDGE, K., YANG, X., CLARKE, N. M., OKUBO, Y., BESSHO, K., SEBALD, W., HOWDLE, S. M., SHAKESHEFF, K. M., OREFFO, R. O. J. B. & COMMUNICATIONS, B. R. 2002. Adenoviral BMP-2 gene transfer in mesenchymal stem cells: *in vitro* and *in vivo* bone formation on biodegradable polymer scaffolds. 292, 144-152.

PAULING, L., COREY, R. B. & BRANSON, H. R. 1951. The structure of proteins: two hydrogen-bonded helical configurations of the polypeptide chain. Proceedings of the National Academy of Sciences, 37, 205-211.

PEARCE, A., RICHARDS, R., MILZ, S., SCHNEIDER, E. & PEARCE, S. J. E. C. M. 2007. Animal models for implant biomaterial research in bone: a review. 13, 1-10.

PELTTARI, K., STECK, E. & RICHTER, W. 2008. The use of mesenchymal stem cells for chondrogenesis. Injury, 39, 58-65.

PEREIRA, R., HALFORD, K., O'HARA, M., LEEPER, D., SOKOLOV, B., POLLARD, M., BAGASRA, O. & PROCKOP, D. 1995. Cultured adherent cells from marrow can serve as long-lasting precursor cells for bone, cartilage, and lung in irradiated mice. 92, 4857-4861.

PEREIRA, T., SILVA, M., OLIVEIRA, M., MAIA, I., SILVA, J., COSTA, M. & THIRÉ, R. 2012. Effect of process parameters on the properties of selective laser sintered Poly (3-hydroxybutyrate) scaffolds for bone tissue engineering: This paper analyzes how laser scan spacing and powder layer thickness affect the morphology and mechanical properties of SLS-made scaffolds by using a volume energy density function. Virtual and Physical Prototyping, 7, 275-285.

PETROVIC, V. & STEFANOVIC, V. 2009. Dental tissue—new source for stem cells. J The Scientific World Journal, 9, 1167-1177.

PETROVIC, V., ZIVKOVIC, P., PETROVIC, D. & STEFANOVIC, V. 2012. Craniofacial bone tissue engineering. Oral Surgery Oral Medicine Oral Pathology Oral Radiology, 114, e1-9.

PHINNEY, D. G., KOPEN, G., RIGHTER, W., WEBSTER, S., TREMAIN, N. & PROCKOP, D. J. 1999. Donor variation in the growth properties and osteogenic potential of human marrow stromal cells. Journal of cellular biochemistry, 75, 424-436.

PILBAUEROVÁ, N. & SUCHÁNEK, J. 2018. Cryopreservation of Dental Stem Cells. Acta medica (Hradec Kralove), 61, 1-7.

PITTENGER, M. F., MACKAY, A. M., BECK, S. C., JAISWAL, R. K., DOUGLAS, R., MOSCA, J. D., MOORMAN, M. A., SIMONETTI, D. W., CRAIG, S. & MARSHAK, D. R. 1999. Multilineage potential of adult human mesenchymal stem cells. Science, 284, 143-147.

PLACZEK, M. R., CHUNG, I.-M., MACEDO, H. M., ISMAIL, S., MORTERA BLANCO, T., LIM, M., MIN CHA, J., FAUZI, I., KANG, Y. & YEO, D. C. 2008. Stem cell bioprocessing: fundamentals and principles. Journal of the Royal Society interface, 6, 209-232.

POTDAR, P. D. & JETHMALANI, Y. D. 2015. Human dental pulp stem cells: Applications in future regenerative medicine. World journal of stem cells, 7, 839.

PROCKOP, D. J. & KIVIRIKKO, K. I. 1995. Collagens: molecular biology, diseases, and potentials for therapy. Annual review of biochemistry, 64, 403-434.

PUCHTLER, H. & SWEAT, F. 1964. Histochemical specifity of staining methods for connective tissue fibers: Resorcin-fuchsin and Van Gieson's picro-fuchsin. Histochemie, 4, 24-34.

QUENT, V., TAUBENBERGER, A., REICHERT, J., MARTINE, L., CLEMENTS, J., HUTMACHER, D., LOESSNER, D.. & MEDICINE, R. 2018. A humanised tissue-engineered bone model allows species-specific breast cancer-related bone metastasis *in vivo*. 12, 494-504.

RADISIC, M., EULOTH, M., YANG, L., LANGER, R., FREED, L. E. & VUNJAK-NOVAKOVIC, G. 2003. High-density seeding of myocyte cells for cardiac tissue engineering. Biotechnology and bioengineering, 82, 403-414.

RAMPERSAD, S. N. 2012. Multiple applications of Alamar Blue as an indicator of metabolic function and cellular health in cell viability bioassays. Sensors, 12, 12347-12360.

RAO, S. S., BENTIL, S., DEJESUS, J., LARISON, J., HISSONG, A., DUPAIX, R., SARKAR, A. & WINTER, J. O. 2012. Inherent interfacial mechanical gradients in 3D hydrogels influence tumour cell behaviours. PLoS One, 7, e35852.

RASAL, R. M., JANORKAR, A. V. & HIRT, D. E. 2010. Poly (lactic acid) modifications. Progress in polymer science, 35, 338-356.

RAVICHANDRAN, R., GRIFFITH, M. & PHOPASE, J. 2014. Applications of self-assembling peptide scaffolds in regenerative medicine: the way to the clinic. Journal of Materials Chemistry B, 2, 8466-8478.

RE, F., ZANETTI, A., SIRONI, M., POLENTARUTTI, N., LANFRANCONE, L., DEJANA, E. & COLOTTA, F. 1994. Inhibition of anchorage-dependent cell spreading triggers apoptosis in cultured human endothelial cells. The Journal of cell biology, 127, 537-546.

REDDI, A. H. 1981. Cell biology and biochemistry of endochondral bone development. J Collagen related research, 1, 209-226.

REGISTER, T., MCLEAN, F., LOW, M. & WUTHIER, R. J. J. O. B. C. 1986. Roles of alkaline phosphatase and labile internal mineral in matrix vesicle-mediated calcification. Effect of selective release of membrane-bound alkaline phosphatase and treatment with isosmotic pH 6 buffer. 261, 9354-9360.

REICH, C. M., RAABE, O., WENISCH, S., BRIDGER, P. S., KRAMER, M. & ARNHOLD, S. 2012. Isolation, culture and chondrogenic differentiation of canine adipose tissue-and bone marrow-derived mesenchymal stem cells–a comparative study. Veterinary research communications, 36, 139-148.

REINISCH, A., THOMAS, D., CORCES, M. R., ZHANG, X., GRATZINGER, D., HONG, W.-J., SCHALLMOSER, K., STRUNK, D. & MAJETI, R. J. N. M. 2016. A humanized bone marrow ossicle xenotransplantation model enables improved engraftment of healthy and leukemic human hematopoietic cells. 22, 812.

RICKARD, D., SULLIVAN, T., SHENKER, B., LEBOY, P. A. & KAZHDAN, I. 1994. Induction of rapid osteoblast differentiation in rat bone marrow stromal cell cultures by dexamethasone and BMP-2. Developmental biology, 161, 218-228.

ROBEY, P. G. 2000. Series Introduction: Stem cells near the century mark. The Journal of clinical investigation, 105, 1489-1491.

RODELLA, L. F., FAVERO, G. & LABANCA, M. 2011. Biomaterials in maxillofacial surgery: membranes and grafts. International journal of biomedical science: IJBS, 7, 81.

ROHNER, D., HUTMACHER, D. W., CHENG, T. K., OBERHOLZER, M. & HAMMER, B. 2003. *In vivo* efficacy of bone-marrow-coated polycaprolactone scaffolds for the reconstruction of orbital defects in the pig. Journal of Biomedical Materials Research Part B: Applied Biomaterials, 66, 574-580.

ROOSA, S.., KEMPPAINEN, J., MOFFITT, E., KREBSBACH, P. H. & HOLLISTER, S., . 2010. The pore size of polycaprolactone scaffolds has limited influence on bone regeneration in an *in vivo* model. The Japanese Society for Biomaterials, 92, 359-368.

ROSSO, F., MARINO, G., GIORDANO, A., BARBARISI, M., PARMEGGIANI, D. & BARBARISI, A. 2005. Smart materials as scaffolds for tissue engineering. Journal of cellular physiology, 203, 465-470.

ROZARIO, T. & DESIMONE, D. W. 2010. The extracellular matrix in development and morphogenesis: a dynamic view. Developments in Biology, 341, 126-40.

RUMPLER, M., WOESZ, A., DUNLOP, J. W., VAN DONGEN, J. T. & FRATZL, P. J. J. O. T. R. S. I. 2008. The effect of geometry on three-dimensional tissue growth. 5, 1173-1180.

SACHLOS, E. & CZERNUSZKA, J. 2003 Making tissue engineering scaffolds work. Review: the application of solid freeform fabrication technology the production of tissue engineering scaffolds. Eur Cells and Materials 5, 29-40.

SAHA, S., YANG, X. B., WIJAYATHUNGA, N., HARRIS, S., FEICHTINGER, G. A., DAVIES, R. P. W. & KIRKHAM, J. 2019. A biomimetic self-assembling peptide promotes bone regeneration *in vivo*: A rat cranial defect study. Bone.

SAIZ, E., ZIMMERMANN, E. A., LEE, J. S., WEGST, U. G. & TOMSIA, A. P. 2013. Perspectives on the role of nanotechnology in bone tissue engineering. Dent Mater, 29, 103-15.

SALGADO, A. J., COUTINHO, O. P. & REIS, R. L. 2004. Bone tissue engineering: state of the art and future trends. Macromolecular bioscience, 4, 743-765.

SALMON, C. R., TOMAZELA, D. M., RUIZ, K. G. S., FOSTER, B. L., LEME, A. F. P., SALLUM, E. A., SOMERMAN, M. J. & NOCITI JR, F. H. 2013. Proteomic analysis of human dental cementum and alveolar bone. Journal of proteomics, 91, 544-555.

SAMCHUKOV, M., COPE, J., HARPER, R. & ROSS, J. 1998. Biomechanical Considerations of Mandibular Lengthening and Widening by Gradual Distraction Using a Computer Model. Journal of Oral Maxillofacial Surgery, 56, 5 l-59.

SANCHEZ-RAMOS, J., SONG, S., CARDOZO-PELAEZ, F., HAZZI, C., STEDEFORD, T., WILLING, A., FREEMAN, T., SAPORTA, S., JANSSEN, W. & PATEL, N. J. E. N. 2000. Adult bone marrow stromal cells differentiate into neural cells *in vitro*. 164, 247-256.

SANDHU, S. & NAIR, M. 2009. Stem Cells: Potential Implications for tooth regeneration. People's Journal of Scientific Research, 2 41- 45.

SANT, S., HANCOCK, M. J., DONNELLY, J. P., IYER, D. & KHADEMHOSSEINI, A. 2010. Biomimetic gradient hydrogels for tissue engineering. The Canadian journal of chemical engineering, 88, 899-911.

SARGEANT, T. D., GULER, M. O., OPPENHEIMER, S. M., MATA, A., SATCHER, R. L., DUNAND, D. C. & STUPP, S. I. 2008. Hybrid bone implants: self-assembly of peptide amphiphile nanofibers within porous titanium. Biomaterials, 29, 161-171.

SARKAR, R. & BANERJEE, G. 2010. Ceramic based bio-medical implants. Interceram, 59, 98-102.

SCHEK, R. M., WILKE, E. N., HOLLISTER, S. J. & KREBSBACH, P. H. J. B. 2006. Combined use of designed scaffolds and adenoviral gene therapy for skeletal tissue engineering. 27, 1160-1166.

SCHENKE-LAYLAND, K. 2011. From tissue engineering to regenerative medicine-- the potential and the pitfalls. Advanced Drug Deliver Review, 63, 193-4.

SCHENKE-LAYLAND, K. & NEREM, R. M. 2011. *In vitro* human tissue models-- moving towards personalized regenerative medicine. Advanced Drug Deliver Review, 63, 195-6.

SCHLEE, M., SCHAD, T., KOCH, J. H., CATTIN, P. C. & RATHE, F. 2018. Clinical performance of self-assembling peptide P11-4 in the treatment of initial proximal carious lesions: A practice-based case series. Journal of investigative and clinical dentistry, 9, e12286.

SCHMIDMAIER, G., BAEHR, K., MOHR, S., KRETSCHMAR, M., BECK, S. & WILDEMANN, B. 2006. Biodegradable polylactide membranes for bone defect coverage: biocompatibility testing, radiological and histological evaluation in a sheep model. Clin Oral Implants Res, 17, 439-44.

SCHUBERT, C., VAN LANGEVELD, M. C. & DONOSO, L. A. 2013. Innovations in 3D printing: a 3D overview from optics to organs. British Journal of Ophthalmology, bjophthalmol-2013-304446.

SCHUGENS, C., MAQUET, V., GRANDFILS, C., JÉRÔME, R. & TEYSSIE, P. 1996. Polylactide macroporous biodegradable implants for cell transplantation. II. Preparation of polylactide foams by liquid-liquid phase separation. Journal of Biomedical Materials Research Part A, 30, 449-461.

SCOTT, J. E. 1995. Extracellular matrix, supramolecular organisation and shape. Journal of anatomy, 187, 259.

SEIBEL, M. J., ROBINS, S. P. & BILEZIKIAN, J. P. 2006. Dynamics of bone and cartilage metabolism: principles and clinical applications, Elsevier.

SEMINO, C. 2008. Self-assembling peptides: from bio-inspired materials to bone regeneration. Journal of dental research, 87, 606-616.

SEO, B., SONOYAMA, W., YAMAZA, T., COPPE, C., KIKUIRI, T., AKIYAMA, K., LEE, J. & SHI, S. 2008. SHED repair critical-size calvarial defects in mice. Oral diseases, 14, 428-434.

SERRA, T., MATEOS-TIMONEDA, M. A., PLANELL, J. A. & NAVARRO, M. 2013 a. 3D printed PLA-based scaffolds: a versatile tool in regenerative medicine. Organogenesis, 9, 239-44.

SERRA, T., ORTIZ-HERNANDEZ, M., ENGEL, E., PLANELL, J. A. & NAVARRO, M. 2014. Relevance of PEG in PLA-based blends for tissue engineering 3D-printed scaffolds. 38, 55-62.

SERRA, T., PLANELL, J. A. & NAVARRO, M. 2013 b. High-resolution PLA-based composite scaffolds via 3-D printing technology. Acta Biomaterial, 9, 5521-30.

SHAH, A., SHAH, S., MANI, G., WENKE, J. & AGRAWAL, M. 2011. Endothelial cell behaviour on gas-plasma-treated PLA surfaces: the roles of surface chemistry and roughness. Journal of tissue engineering and regenerative medicine, 5, 301-312.

SHARMA, S., SRIVASTAVA, D., GROVER, S. & SHARMA, V. 2014. Biomaterials in tooth tissue engineering: a review. J Clin Diagn Res, 8, 309-15.

SHETH, N., PARMAR, B., PATEL, H. & MAKWANA, K. 2017. Human mandible bone defect repair by the grafting of dental pulp stem/progenitor cells — a pilot study. International Journal of Oral and Maxillofacial Surgery, 46, 215.

SHI, H., GAN, Q., LIU, X., MA, Y., HU, J., YUAN, Y. & LIU, C. 2015. Poly (glycerol sebacate)-modified polylactic acid scaffolds with improved hydrophilicity, mechanical strength and bioactivity for bone tissue regeneration. J RSC Advances, 5, 79703-79714.

SHOR, L., GÜÇERI, S., WEN, X., GANDHI, M. & SUN, W. J. B. 2007. Fabrication of three-dimensional polycaprolactone/hydroxyapatite tissue scaffolds and osteoblast-scaffold interactions *in vitro*. 28, 5291-5297.

SIEGEL, G., KLUBA, T., HERMANUTZ-KLEIN, U., BIEBACK, K., NORTHOFF, H. & SCHÄFER, R. 2013. Phenotype, donor age and gender affect function of human bone marrow-derived mesenchymal stromal cells. BMC medicine, 11, 146.

SIKAVITSAS, V. I., BANCROFT, G. N. & MIKOS, A. 2002. Formation of three-dimensional cell/polymer constructs for bone tissue engineering in a spinner flask

and a rotating wall vessel bioreactor. The Japanese Society for Biomaterials 62, 136-148.

SIKAVITSAS, V. I., TEMENOFF, J. S. & MIKOS, A. G. 2001. Biomaterials and bone mechanotransduction. J Biomaterials, 22, 2581-2593.

SIMSKE, S. J., AYERS, R. A. & BATEMAN, T. Porous materials for bone engineering. Materials Science Forum, 1997. Trans Tech Publ, 151-182.

SJÖSTRÖM, T., DALBY, M. J., HART, A., TARE, R., OREFFO, R. O. & SU, B. 2009. Fabrication of pillar-like titania nanostructures on titanium and their interactions with human skeletal stem cells. Acta Biomaterialia, 5, 1433-1441.

SOBRAL, J. M., CARIDADE, S. G., SOUSA, R. A., MANO, J. F. & REIS, R. L. 2011. Three-dimensional plotted scaffolds with controlled pore size gradients: effect of scaffold geometry on mechanical performance and cell seeding efficiency. Acta biomaterialia, 7, 1009-1018.

SODEK, J., GANSS, B. & MCKEE, M. 2000. Osteopontin. Critical Reviews in Oral Biology & Medicine, 11, 279-303.

SOLHEIM, E. M. P., OVE TALSNES, TRINE BERG LARSEN, OLE J. KIRKEBY, EIRIK %J SCANDINAVIAN JOURNAL OF PLASTIC, SURGERY, R. & SURGERY, H. 2001. Revascularisation of fresh compared with demineralised bone grafts in rats. 35, 113-116.

STEEDMAN, H. 1950. Alcian blue 8GS: a new stain for mucin. Journal of Cell Science, 3, 477-479.

STREET, J., BAO, M., DEGUZMAN, L., BUNTING, S., PEALE, F. V., FERRARA, N., STEINMETZ, H., HOEFFEL, J., CLELAND, J. L. & DAUGHERTY, A. 2002. Vascular endothelial growth factor stimulates bone repair by promoting angiogenesis and bone turnover. Proceedings of the National Academy of Sciences, 99, 9656-9661.

SUCHANEK, J., SOUKUP, T., VISEK, B., IVANCAKOVA, R., KUCEROVA, L. & MOKRY, J. 2009. Dental pulp stem cells and their characterization. Biomedical Papers of the Medical Faculty of Palacky University in Olomouc, 153.

SWENNEN, G., SCHLIEPHAKE, H., DEMPF, R., SCHIERLE, H. & MALEVEZ, C. 2001. Craniofacial distraction osteogenesis: a review of the literature: Part 1: clinical studies. International Journal of Oral Maxillofacial Surgery, 30, 89-103.

TAKEBE, Y., TATEHARA, S., FUKUSHIMA, T., TOKUYAMA-TODA, R., YASUHARA, R., MISHIMA, K. & SATOMURA, K. 2017. Cryopreservation method for the effective collection of dental pulp stem cells. Tissue Engineering Part C: Methods, 23, 251-261.

TAKEMOTO, M., FUJIBAYASHI, S., NEO, M., SUZUKI, J., KOKUBO, T. & NAKAMURA, T. 2005. Mechanical properties and osteoconductivity of porous bioactive titanium. Biomaterials, 26, 6014-6023.

TANG, J., PENG, R. & DING, J. 2010. The regulation of stem cell differentiation by cell-cell contact on micropatterned material surfaces. Biomaterials, 31, 2470-2476.

TÉCLÈS, O., LAURENT, P., ZYGOURITSAS, S., BURGER, A.-S., CAMPS, J., DEJOU, J. & ABOUT, I. 2005. Activation of human dental pulp progenitor/stem cells in response to odontoblast injury. Archives of oral biology, 50, 103-108.

TIBBITT, M. W. & ANSETH, K. S. 2009. Hydrogels as extracellular matrix mimics for 3D cell culture. Biotechnology and bioengineering, 103, 655-663.

TIRINO, V., PAINO, F., DE ROSA, A. & PAPACCIO, G. 2012. Identification, Isolation, Characterization, and Banking of Human Dental Pulp Stem Cells. In: SINGH, S. R. (ed.) Somatic Stem Cells: Methods and Protocols. Totowa, NJ: Humana Press.

TOMANIN, R. & SCARPA, M. 2004. Why Do We Need New Gene Therapy Viral Vectors? Characteristics, Limitations and Future Perspectives of Viral Vector Transduction. Current Gene Therapy, 4, 357-372.

TOMLINSON, M. J., DENNIS, C., YANG, X. B. & KIRKHAM, J. 2015. Tissue non-specific alkaline phosphatase production by human dental pulp stromal cells is enhanced by high density cell culture. Cell and tissue research, 361, 529-540.

TOSOUNIDIS, T., KONTAKIS, G., NIKOLAOU, V., PAPATHANASSOPOULOS, A. & GIANNOUDIS, P. V. 2009. Fracture healing and bone repair: an update. Trauma, 11, 145-156.

TRAVASCIO, F. 2016. Composition and Function of the Extracellular Matrix in the Human Body, BoD–Books on Demand.

TSUKAMOTO, Y., FUKUTANI, S., SHIN-IKE, T., KUBOTA, T., SATO, S., SUZUKI, Y. & MORI, M. 1992. Mineralized nodule formation by cultures of human dental pulp-derived fibroblasts. Archives of oral biology, 37, 1045-1055.

TURINETTO, V., VITALE, E. & GIACHINO, C. 2016. Senescence in human mesenchymal stem cells: functional changes and implications in stem cell-based therapy. International journal of molecular sciences, 17, 1164.

UEBERSAX, L., HAGENMÜLLER, H., HOFMANN, S., GRUENBLATT, E., MÜLLER, R., VUNJAKNOVAKOVIC, G., KAPLAN, D. L., MERKLE, H. & MEINEL, L. J. T. E. 2006. Effect of scaffold design on bone morphology in vitro. 12, 3417-3429.

ULLAH, M., HAMOUDA, H., STICH, S., SITTINGER, M. & RINGE, J. J. B. O. A. 2012. A reliable protocol for the isolation of viable, chondrogenically differentiated human mesenchymal stem cells from high-density pellet cultures. 1, 297-305.

VACANTI, C. 2006. The history of tissue engineering. 10, 569-576.

VAN BAEL, S., CHAI, Y. C., TRUSCELLO, S., MOESEN, M., KERCKHOFS, G., VAN OOSTERWYCK, H., KRUTH, J.-P. & SCHROOTEN, J. J. A. B. 2012. The effect of pore geometry on the in vitro biological behavior of human periosteum-derived cells seeded on selective laser-melted Ti6Al4V bone scaffolds. 8, 2824-2834.

VAN BAEL, S., VANDENBROUCKE, B., KERCKHOFS, G., SCHROOTEN, J. & KRUTH, J.-P. Design and production of bone scaffolds with selective laser melting. TMS 2009, 2009.

VAN TIENEN, T. G., HEIJKANTS, R. G., BUMA, P., DE GROOT, J. H., PENNINGS, A. J. & VETH, R. 2002. Tissue ingrowth and degradation of two biodegradable porous polymers with different porosities and pore sizes. 23, 1731-1738.

VASANDAN, A. B., SHANKAR, S. R., PRASAD, P., SOWMYA JAHNAVI, V., BHONDE, R. R. & JYOTHI PRASANNA, S. 2014. Functional differences in mesenchymal stromal cells from human dental pulp and periodontal ligament. Journal of cellular and molecular medicine, 18, 344-354.

VASITA, R. & KATTI, D. S. 2006. Nanofibers and their applications in tissue engineering. International Journal of nanomedicine, 1(1),15.

VATER, C., KASTEN, P. & STIEHLER, M., 2011. Culture media for the differentiation of mesenchymal stromal cells. Acta biomaterialia, 7(2), 463-477.

VERMA, K., BAINS, R., BAINS, V. K., RAWTIYA, M., LOOMBA, K. & SRIVASTAVA, S. C. 2014. Therapeutic potential of dental pulp stem cells in regenerative medicine: An overview. Dental research journal, 11, 302.

VILLALONA, G. A., UDELSMAN, B., DUNCAN, D. R., MCGILLICUDDY, E., SAWH-MARTINEZ, R. F., HIBINO, N., PAINTER, C., MIRENSKY, T., ERICKSON, B. & SHINOKA, T. 2010. Cell-seeding techniques in vascular tissue engineering. 16, 341-350.

VITALE, A. M., WOLVETANG, E. & MACKAY-SIM, A. 2011. Induced pluripotent stem cells: a new technology to study human diseases. The international journal of biochemistry & cell biology, 43, 843-846.

VOLKMER, E., DROSSE, I., OTTO, S., STANGELMAYER, A., STENGELE, M., KALLUKALAM, B. C., MUTSCHLER, W. & SCHIEKER, M. 2008. Hypoxia in static and dynamic 3D culture systems for tissue engineering of bone. Tissue Engineering Part A, 14, 1331-1340.

VUNJAK-NOVAKOVIC, G. & RADISIC, M. 2004. Cell seeding of polymer scaffolds. Biopolymer Methods in Tissue Engineering. Springer.

WADDINGTON, R. J., ROBERTS, H. C., SUGARS, R. V., SCHONHERR, E. J. E. C. & MATERIALS 2003. Differential roles for small leucine-rich proteoglycans in bone formation. 6, 12-21.

WAGNER, W., WEIN, F., SECKINGER, A., FRANKHAUSER, M., WIRKNER, U., KRAUSE, U., BLAKE, J., SCHWAGER, C., ECKSTEIN, V. & ANSORGE, W. 2005. Comparative characteristics of mesenchymal stem cells from human bone marrow, adipose tissue, and umbilical cord blood. Experimental hematology, 33, 1402-1416.

WAHL, D. A., SACHLOS, E., LIU, C. & CZERNUSZKA, J. 2007. Controlling the processing of collagen-hydroxyapatite scaffolds for bone tissue engineering. 18, 201-209.

WALSH, S., JORDAN, G.R., JEFFERISS, C., STEWART, K. & BERESFORD, J.N., 2001. High concentrations of dexamethasone suppress the proliferation but not the differentiation or further maturation of human osteoblast precursors *in vitro*: relevance to glucocorticoid-induced osteoporosis. Rheumatology, 40(1), 74-83.

WAN, Y., WU, H., YU, A. & WEN, D. 2006. Biodegradable polylactide/chitosan blend membranes. Biomacromolecules, 7, 1362-1372.

WANG, X, SONG, W., KAWAZOE, N. & CHEN, G. 2013. The osteogenic differentiation of mesenchymal stem cells by controlled cell–cell interaction on micropatterned surfaces. Journal of Biomedical Materials Research Part A: An Official Journal of the Society for Biomaterials, the Japanese Society for Biomaterials, and The Australian Society for Biomaterials and the Korean Society for Biomaterials, 101, 3388-3395.

WANG, J., LIU, X. Y. & LUAN, B. 2008. Fabrication of Ti/polymer biocomposites for load-bearing implant applications. Journal of materials processing technology, 197, 428-433.

WANG, J., MA, H., JIN, X., HU, J., LIU, X., NI, L. & MA, P. X. 2011. The effect of scaffold architecture on odontogenic differentiation of human dental pulp stem cells. Biomaterials, 32, 7822-7830.

WANG, S., CUI, W. & BEI, J. 2005. Bulk and surface modifications of polylactide. Analytical and bioanalytical chemistry, 381, 547-556.

WARD, B. B., BROWN, S. E. & KREBSBACH, P. H. 2010. Bioengineering strategies for regeneration of craniofacial bone: a review of emerging technologies. Oral Dis, 16, 709-16.

WATT, F. M. 1986. The extracellular matrix and cell shape. Trends in Biochemical Sciences, 11, 482-485.

WEBSTER, T. J., ERGUN, C., DOREMUS, R. H., SIEGEL, R. W. & BIZIOS, R. 2000. Specific proteins mediate enhanced osteoblast adhesion on nanophase

WAHL, D. A., SACHLOS, E., LIU, C. & CZERNUSZKA, J. 2007. Controlling the processing of collagen-hydroxyapatite scaffolds for bone tissue engineering. 18, 201-209.

WALSH, S., JORDAN, G.R., JEFFERISS, C., STEWART, K. & BERESFORD, J.N., 2001. High concentrations of dexamethasone suppress the proliferation but not the differentiation or further maturation of human osteoblast precursors *in vitro*: relevance to glucocorticoid-induced osteoporosis. Rheumatology, 40(1), 74-83.

WAN, Y., WU, H., YU, A. & WEN, D. 2006. Biodegradable polylactide/chitosan blend membranes. Biomacromolecules, 7, 1362-1372.

WANG, X, SONG, W., KAWAZOE, N. & CHEN, G. 2013. The osteogenic differentiation of mesenchymal stem cells by controlled cell–cell interaction on micropatterned surfaces. Journal of Biomedical Materials Research Part A: An Official Journal of the Society for Biomaterials, the Japanese Society for Biomaterials, and The Australian Society for Biomaterials and the Korean Society for Biomaterials, 101, 3388-3395.

WANG, J., LIU, X. Y. & LUAN, B. 2008. Fabrication of Ti/polymer biocomposites for load-bearing implant applications. Journal of materials processing technology, 197, 428-433.

WANG, J., MA, H., JIN, X., HU, J., LIU, X., NI, L. & MA, P. X. 2011. The effect of scaffold architecture on odontogenic differentiation of human dental pulp stem cells. Biomaterials, 32, 7822-7830.

WANG, S., CUI, W. & BEI, J. 2005. Bulk and surface modifications of polylactide. Analytical and bioanalytical chemistry, 381, 547-556.

WARD, B. B., BROWN, S. E. & KREBSBACH, P. H. 2010. Bioengineering strategies for regeneration of craniofacial bone: a review of emerging technologies. Oral Dis, 16, 709-16.

WATT, F. M. 1986. The extracellular matrix and cell shape. Trends in Biochemical Sciences, 11, 482-485.

WEBSTER, T. J., ERGUN, C., DOREMUS, R. H., SIEGEL, R. W. & BIZIOS, R. 2000. Specific proteins mediate enhanced osteoblast adhesion on nanophase

ceramics. Journal of Biomedical Materials Research: An Official Journal of the Society for Biomaterials, the Japanese Society for Biomaterials, and The Australian Society for Biomaterials and the Korean Society for Biomaterials, 51, 475-483.

WEBSTER, T. J., SCHADLER, L. S., SIEGEL, R. W. & BIZIOS, R. 2001. Mechanisms of enhanced osteoblast adhesion on nanophase alumina involve vitronectin. Tissue engineering, 7, 291-301.

WEBSTER, T. J., SIEGEL, R. W. & BIZIOS, R. 1999. Osteoblast adhesion on nanophase ceramics. Biomaterials, 20, 1221-1227.

WEI, X., LING, J., WU, L., LIU, L. & XIAO, Y. 2007. Expression of mineralization markers in dental pulp cells. Journal of endodontics, 33, 703-708.

WEINER, S. & WAGNER, H. 1998. The material bone: structure-mechanical function relations. 28, 271-298.

WENZ, B., OESCH, B. & HORST, M. 2001. Analysis of the risk of transmitting bovine spongiform encephalopathy through bone grafts derived from bovine bone. Biomaterials, 22, 1599-1606.

WHITFORD, D. 2013. Proteins: structure and function, John Wiley & Sons.

WHITWORTH, S. 2018. Self-Assembling Peptide Nano-Apatite Hybrid Material for Dentine Mineralisation. University of Leeds.

WILLIAMS, J., ADEWUNMI, A., SCHEK, R., FLANAGAN, C., KREBSBACH, P., FEINBERG, S., HOLLISTER, S. & DAS, S. 2005. Bone tissue engineering using polycaprolactone scaffolds fabricated via selective laser sintering. Biomaterials, 26, 4817-4827.

WINDER, J. & BIBB, R. 2005. Medical rapid prototyping technologies: state of the art and current limitations for application in oral and maxillofacial surgery. Journal of oral and maxillofacial surgery, 63, 1006-1015.

WOO, K., CHEN, V. & MA, P. 2003. Nano-fibrous scaffolding architecture selectively enhances protein adsorption contributing to cell attachment. Journal of Biomedical Materials Research Part A: An Official Journal of the Society for

Biomaterials, the Japanese Society for Biomaterials, and The Australian Society for Biomaterials and the Korean Society for Biomaterials, 67, 531-537.

WOODARD, J., HILLDORE, A., LAN, S., PARK, C., MORGAN, A., EURELL, J., CLARK, S., WHEELER, M., JAMISON, R. & JOHNSON, A. 2007. The mechanical properties and osteoconductivity of hydroxyapatite bone scaffolds with multi-scale porosity. Biomaterials, 28, 45-54.

WOODFIELD, T., MALDA, J., DE WIJN, J., PETERS, F., RIESLE, J. & VAN BLITTERSWIJK, C. 2004. Design of porous scaffolds for cartilage tissue engineering using a three-dimensional fiber-deposition technique. Biomaterials, 25, 4149-4161.

WU, E., ZHANG, S. & HAUSER, C. 2012. Self-assembling peptides as cell-interactive scaffolds. Advanced functional materials, 22, 456-468.

WU, L., YANG, J. & KOPEČEK, J. 2011. Hybrid hydrogels self-assembled from graft copolymers containing complementary β-sheets as hydroxyapatite nucleation scaffolds. Biomaterials, 32, 5341-5353.

WU, S., LIU, X., YEUNG, K., LIU, C. & YANG, X. 2014. Biomimetic porous scaffolds for bone tissue engineering. Materials Science and Engineering: R: Reports, 80, 1-36.

XIONG, Z., YAN, Y., WANG, S., ZHANG, R. & ZHANG, C. 2002. Fabrication of porous scaffolds for bone tissue engineering via low-temperature deposition. Scripta Materialia, 46, 771-776.

XU, H., HAN, D., DONG, J., SHEN, G., CHAI, G., YU, Z., LANG, W. & AI, S. 2010. Rapid prototyped PGA/PLA scaffolds in the reconstruction of mandibular condyle bone defects. The international journal of medical robotics and computer assisted surgery, 6, 66-72.

XUE, R., LI, J., YEH, Y., YANG, L. & CHIEN, S. 2013. Effects of matrix elasticity and cell density on human mesenchymal stem cells differentiation. Journal of Orthopaedic Research, 31, 1360-1365.

YAMADA, K. M. & CUKIERMAN, E. 2007. Modelling tissue morphogenesis and cancer in 3D. Cell, 130, 601-610.

YAMADA, Y., NAKAMURA, S., ITO, K., KOHGO, T., HIBI, H., NAGASAKA, T. & UEDA, M. 2008. Injectable tissue-engineered bone using autogenous bone marrow-derived stromal cells for maxillary sinus augmentation: clinical application report from a 2-6-year follow-up. Tissue Engineering Part A, 14, 1699-707.

YAMADA, Y., NAKAMURA, S., ITO, K., SUGITO, T., YOSHIMI, R., NAGASAKA, T. & UEDA, M. 2010. A Feasibility of Useful Cell-Based Therapy by Bone Regeneration with Deciduous Tooth Stem Cells, Dental Pulp Stem Cells, or Bone-Marrow-Derived Mesenchymal Stem Cells for Clinical Study Using Tissue Engineering Technology. TISSUE ENGINEERING: Part A, 16, 1891-1900.

YAN, X.Z., BOTH, S.K., YANG, P.S., JANSEN, J.A., VAN DEN BEUCKEN, J.J. & YANG, F., 2014. Human periodontal ligament derived progenitor cells: effect of STRO-1 cell sorting and Wnt3a treatment on cell behaviour. BioMed research international, 2014.

YANG, X., BHATNAGAR, R., LI, S. & OREFFO, R. 2004 a. Biomimetic collagen scaffolds for human bone cell growth and differentiation. Tissue engineering, 10, 1148-1159.

YANG, X., HAN, G., PANG, X. & FAN, M. 2012. Chitosan/collagen scaffold containing bone morphogenetic protein-7 DNA supports dental pulp stem cell differentiation *in vitro* and *in vivo*. Journal of biomedical materials research Part A.

YANG, X., TARE, R., PARTRIDGE, K., ROACH, H., CLARKE, N., HOWDLE, S., SHAKESHEFF, K. & OREFFO, R. 2003. Induction of human osteoprogenitor chemotaxis, proliferation, differentiation, and bone formation by osteoblast stimulating factor-1/pleiotrophin: Osteoconductive biomimetic scaffolds for tissue engineering. J Journal of Bone Mineral Research, 18, 47-57.

YANG, X., VAN DER KRAAN, P., BIAN, Z., FAN, M., WALBOOMERS, X. & JANSEN, J. 2009. Mineralized tissue formation by BMP2-transfected pulp stem cells. Journal of dental research, 88, 1020-1025.

YANG, X., YUAN, M., LI, W. & ZHANG, G. 2004 b. Synthesis and properties of collagen/polylactic acid blends. Journal of applied polymer science, 94, 1670-1675.

YAZID, F., LUCHMAN, N., WAHAB, R. & ARIFFIN, S. Comparison of Characterization and Osteoblast Formation Between Human Dental Pulp Stem Cells (hDPSC) and Stem Cells from Deciduous Teeth (SHED). Proceedings of the Second International Conference on the Future of ASEAN (ICoFA) 2017–Volume 2, 2018. Springer, 605-614.

YEONG, W., CHUA, C., LEONG, K. & CHANDRASEKARAN, M. 2004. Rapid prototyping in tissue engineering: challenges and potential. Trends in biotechnology, 22, 643-652.

YILDIRIM, S., YAPAR, M., SERMET, U., SENER, K. & KUBAR, A. 2008. The role of dental pulp cells in resorption of deciduous teeth. Oral Surgery, Oral Medicine, Oral Pathology, Oral Radiology, and Endodontology, 105, 113-120.

YILGOR, P., SOUSA, R., REIS, R., HASIRCI, N. & HASIRCI, V. 3D plotted PCL scaffolds for stem cell based bone tissue engineering. Macromolecular symposia, 2008. Wiley Online Library, 92-99.

YIN, T. & LI, L. 2006. The stem cell niches in bone. J The Journal of clinical investigation, 116, 1195-1201.

YOU, M., KWAK, M., KIM, D., KIM, K., LEVCHENKO, A., KIM, D. & SUH, K. 2010. Synergistically enhanced osteogenic differentiation of human mesenchymal stem cells by culture on nanostructured surfaces with induction media. Biomacromolecules, 11, 1856-1862.

ZAKARIA, S., SHARIF ZEIN, S., OTHMAN, M., YANG, F. & JANSEN, J. 2013. Nanophase hydroxyapatite as a biomaterial in advanced hard tissue engineering: a review. Tissue Engineering Part B: Reviews, 19, 431-441.

ZHANG, L., SU, P., XU, C., YANG, J., YU, W. & HUANG, D. 2010. Chondrogenic differentiation of human mesenchymal stem cells: a comparison between micromass and pellet culture systems. Biotechnology letters, 32, 1339-1346.

ZHANG, L. & WEBSTER, T. 2009. Nanotechnology and nanomaterials: Promises for improved tissue regeneration. Nano Today, 4, 66-80.

ZHANG, S., HOLMES, T., DIPERSIO, C., HYNES, R., SU, X. & RICH, A. 1995. Self-complementary oligopeptide matrices support mammalian cell attachment. Biomaterials, 16, 1385-1393.

ZHANG, S., MARINI, D., HWANG, W. & SANTOSO, S. 2002. Design of nanostructured biological materials through self-assembly of peptides and proteins. Current opinion in chemical biology, 6, 865-871.

ZHANG, W., WALBOOMERS, X., SHI, S., FAN, M. & JANSEN, J. 2006. Multilineage differentiation potential of stem cells derived from human dental pulp after cryopreservation. J Tissue engineering, 12, 2813-2823.

ZHANG, Y., WU, C., WU, C., CHANG, J. & XIAO, Y. 2013. Bioactive inorganic and organic composite materials for bone regeneration and gene delivery. Advanced Bioactive Inorganic Materials for Bone Regeneration and Drug Delivery, 178-205.

ZHOU, M., LIU, N., SHI, S., LI, Y., ZHANG, Q., MA, Q., TIAN, T., MA, W., CAI, X. & LIN, Y. 2018. Effect of tetrahedral DNA nanostructures on proliferation and osteo/odontogenic differentiation of dental pulp stem cells via activation of the notch signalling pathway. J Nanomedicine: Nanotechnology, Biology, Medicine, 14, 1227-1236.

ZHU, L., MA, J., MU, R., ZHU, R., CHEN, F., WEI, X., SHI, X., ZANG, S. & JIN, L. 2018. Bone morphogenetic protein 7 promotes odontogenic differentiation of dental pulp stem cells *in vitro*. J Life sciences, 202, 175-181.

ZHU, Y., GAO, C., LIU, X., HE, T. & SHEN, J. 2004. Immobilization of bio-macromolecules onto aminolyzed poly (L-lactic acid) toward acceleration of endothelium regeneration. Tissue engineering, 10, 53-61.

ZUK, P., ZHU, M., MIZUNO, H., HUANG, J., FUTRELL, J., KATZ, A., BENHAIM, P., LORENZ, H. & HEDRICK, M. 2001. Multilineage cells from human adipose tissue: implications for cell-based therapies. Tissue engineering, 7, 211-228.

Appendix A: List of contributions and awards

1. Conference papers

- Effect of Fibre Angle of 3D Printed PLA Scaffolds on Human Dental Pulp Stromal Cells' Attachment, Growth and Osteogenic Differentiation *in vitro* and *in vivo*, R.F. Albannaa, J. Kirkham, J. Burke, C. Liu and X. Yang. 01-P150, 5th TERMIS World Congress, 2018, Kyoto, Japan (**poster presentation**).

- Novel 3D Printed PLA-SAPs Scaffold for Enhanced Bone Tissue Regeneration. R.F. Albannaa, J. Kirkham, R.P.W. Davies, J. Burke, C. Liu and X. Yang. 2018. J Dent Res J Dent Res Vol 97(B):1553. IADR/PER 96th General Session - 2018, London, UK (**oral presentation**).

- 3D Printed PLA scaffolds for bone tissue regeneration: Effect of scaffold fibre angle on attachment, growth and differentiation of human dental pulp stromal cells (hDPSCs) *in vitro* and *in vivo*. R.F. Albannaa, J. Kirkham, J. Burke, C. Liu and X. Yang. Bone and Enamel Tissue Science and Engineering (BETSE, 2017) meeting. Leeds University, UK (**poster presentation**).

- 3D Printed PLA scaffolds for bone tissue regeneration: Effect of scaffold structure on attachment and growth of human dental pulp stromal cells (hDPSCs). R.F. Albannaa, J. Kirkham, J. Burke, C. Liu and X. Yang. British Orthopaedics Research Society (BORS) Orthopaedic Proceedings. Vol. 98-B, No. SUPP-16- 2016. The University of Glasgow, UK (**oral presentation**).

- 3D Printed PLA scaffolds for bone tissue regeneration: Effect of scaffolds' structural difference on attachment and growth of human dental pulp stromal cells (hDPSCs). Rasha Albannaa, Jennifer Kirkham, Julie Burke, Chaozong Liu and Xuebin Yang. LIMM Postgraduate Research Symposium - 2016, Leeds University, UK (**poster presentation**).

- Effect of dexamethasone concentration on osteogenic differentiation of human dental pulp stromal cells *in vitro*. Rasha Albannaa, Jennifer Kirkham, Julie Burke, and Xuebin Yang. 17th annual meeting of biomaterials and tissue engineering group – 2015, York University, UK (**poster presentation**).

2. Awards

- Research image of the year (Leeds dental school research day 2019-Leeds, UK)

- 3rd poster prize (BETSE scientific meeting 2017- Leeds, UK)

- 2nd poster prize (LIMM symposium University of Leeds 2016- Leeds, UK)